

Early postmortem determination of porcine meat quality using Raman spectroscopy

Von der Universität Bayreuth
zur Erlangung des Grades eines
Doktors der Naturwissenschaften (Dr. rer. nat.)
genehmigte Abhandlung

von

Diplom-Physiker

Rico SCHEIER

aus Strausberg

1. Gutachter: Prof. Dr. Jürgen Köhler
2. Gutachter: Prof. Dr. Matthias Weiss

Tag der Einreichung: 23.01.2014

Tag des Kolloquiums: 16.05.2014

Bayreuth 2014
D703

Abstract

The chemical and structural composition of biological tissues can be non-invasively measured using Raman spectroscopy. The resulting Raman spectrum can be used for identification and quantification. In case of multi-component mixtures, this is complicated due to superimposing signals of individual compounds hence multivariate methods are mostly applied for the analysis of Raman spectra. However, these methods provide only little help to understand the physical and chemical processes causing the spectral alterations.

Therefore, the aim of this thesis was to determine the changes in the Raman spectra using the example of pork meat in the first hours after slaughter, to identify the underlying mechanisms and to evaluate the potential of early postmortem Raman spectra to predict important meat quality traits.

At first, pH and lactate concentration were chosen as indicators as they are known to correlate with the metabolic state of the muscle, which is again closely related to the resulting meat quality. Here, the pH value was shown to be calculable from only two vibrations of the Raman spectra assigned to the terminal phosphate moiety. More accurate predictions are possible with a multiple linear regression model based on signals of lactate, glycogen, creatine (Cr), phosphocreatine (PCr), ATP, IMP, the phosphate and carbonyl group or with a partial least squares regression model based on the whole spectrum. However, the determination of the lactate concentration is complicated due to superimposing signals of other metabolites. To quantify the contribution of individual components, the spectral alterations were simulated in the pre-rigor phase between 1 and 2 h and in the rigor phase between 2 and 8 h after slaughter. The simulation includes difference spectra of the energy metabolites PCr and Cr, glycogen and lactate, ATP and IMP as well as hydrogen and dihydrogen phosphate. Additionally, the Raman signals of α -helical proteins, phosphorylated sugars and the difference spectrum of oxy- and deoxymyoglobin add intensity to the observed alterations. The agreement between measured and simulated spectra proves that the Raman spectra indeed provide a detailed fingerprint of the metabolic state of the early postmortem muscle. In parallel, a portable Raman system with control software was developed and successfully tested in two field studies in commercial abattoirs. For the first time, the quality traits pH_{45} , pH_{24} , drip loss, color and shear force were predicted from Raman spectra measured only 1–2 h *post mortem*. Besides pH_{45} , these quality traits cannot currently be measured early postmortem and are only available 1–3 days after slaughter via partly invasive and time-consuming reference analysis. The promising predictions were confirmed for pH_{45} , pH_{24} and drip loss in a second study. In both studies, the PLSR models are mostly weighting Raman signals of the energy metabolites.

In this thesis, the potential of Raman spectroscopy was proven to rapidly and non-invasively determine important quality traits of pork meat based on early postmortem spectra. Thereby, signals of ubiquitous compounds of the postmortem metabolism are weighted by the prediction models. In future, Raman spectroscopy could therefore allow for an early assessment of quality traits of pork, but also other sorts of meat, at the slaughterline in abattoirs.

Zusammenfassung

Mit der Raman-Spektroskopie ist die chemische und strukturelle Zusammensetzung von biologischen Geweben nicht-invasiv messbar. Das Raman-Spektrum kann dabei zur Identifizierung und Quantifizierung dienen. Bei Gemischen ist dies allerdings durch die mehrdeutige Überlagerung von Signalen einzelner Stoffe erschwert. Vielfach werden deshalb statistische Auswerteverfahren zur Spektrenanalyse angewendet, welche jedoch kaum zum Verständnis der physikalischen und chemischen Zusammenhänge beitragen.

Ziel dieser Arbeit war es deshalb, Veränderungen in den Raman-Spektren am Beispiel von Schweinefleisch kurz nach der Schlachtung zu bestimmen und deren zugrundeliegende Mechanismen zu identifizieren. Zudem sollte geprüft werden, ob und wie technologisch wichtige Qualitätsparameter aus den früh-postmortalen Raman-Spektren von Fleisch vorhersagbar sind.

Als Indikatoren für den Stoffwechsellzustand des Muskels, der eng mit der Fleischqualität korreliert ist, wurden zunächst pH und Lactat-Konzentration gewählt. Der pH-Wert ist in diesem Fall mit den Raman-Peaks von nur zwei Schwingungen der Phosphatgruppe aus den Spektren berechenbar. Noch genauere Vorhersagen sind mit einem linearen Modell basierend auf ausgewählten Signalen von Lactat, Glycogen, Kreatin (Cr), Kreatinphosphat (PCr), ATP, IMP, der Phosphat- und Carbonyl-Gruppe sowie einem PLSR-Modell möglich. Die Vorhersage der Lactat-Konzentration aus den Raman-Spektren ist jedoch durch die Überlagerung von Signalen anderer Metabolite erschwert. Um die Beiträge der Einzelkomponenten zu ermitteln, wurden deshalb die spektralen Veränderungen im Schweinefleisch im Zeitraum zwischen 1 und 2 h sowie zwischen 2 und 8 h nach der Schlachtung simuliert. Die Simulation umfasst Differenzspektren der Energiemetabolite PCr und Cr, Glycogen und Lactat, ATP und IMP sowie Hydrogen- und Dihydrogenphosphat. Darüber hinaus tragen die Raman-Signale α -helikaler Proteine, phosphorylierter Zucker und das Differenzspektrum von Oxy- und Deoxymyoglobin zu den beobachteten Veränderungen bei. Die gute Übereinstimmung zwischen gemessenen und simulierten Spektren beweist, dass die Raman-Spektren eine detaillierte Momentaufnahme des frühpostmortalen Energiestoffwechsels im Muskel darstellen. Parallel zu diesen Studien wurde ein mobiles Raman-System konstruiert und erfolgreich während zwei Feldstudien in kommerziellen Schlachthöfen getestet. Die Raman-Spektren, die 1–2 h nach Schlachtung detektiert wurden, können dabei zur Vorhersage wichtiger Qualitätsparameter wie pH_{45} , pH_{24} , Tropfsaftverlust, Farbe und Scherkraft genutzt werden. Diese Parameter sind in der Regel früh-postmortal nicht verfügbar, sondern erst durch zum Teil invasive sowie arbeits- und zeitintensive Analysen 1–3 Tage nach der Schlachtung messbar. In einer zweiten Studie ist die Vorhersagbarkeit von pH_{45} , pH_{24} und Tropfsaftverlust aus den früh-postmortalen Raman-Spektren bestätigt und sogar noch verbessert worden. Die Korrelationen beruhen dabei hauptsächlich auf den zuvor identifizierten Signalen der Metabolite des Energiestoffwechsels.

Damit wird in dieser Arbeit erstmals das große Potential der Raman-Spektroskopie zur schnellen, nicht-invasiven und früh-postmortalen Bestimmung wichtiger Qualitätsparameter von Schweinefleisch offenbart. Da hierzu Signale universell vorkommender Metabolite des postmortalen Stoffwechsels genutzt werden, ist in Zukunft mit der Raman-Spektroskopie möglicherweise eine frühzeitige Qualitätssortierung von Schweinefleisch aber auch anderer Fleischsorten schon am Schlachtband realisierbar.

Contents

I. Introduction	7
1. Motivation	9
2. Theoretical Background	11
2.1. Raman Spectroscopy	11
2.1.1. Theory	11
2.1.2. Instrumentation	12
2.1.3. Application in Biological Systems	14
2.2. Meat	14
2.2.1. Muscle Structure, Composition and Contraction	14
2.2.2. Early Postmortem Metabolism	17
2.2.3. Technological Quality Traits	20
2.2.3.1. The pH Value	21
2.2.3.2. Drip Loss	22
2.2.3.3. Color	23
2.2.3.4. Shear Force	24
2.2.4. Classification of Meat Quality	25
2.2.5. Measurement of Quality Traits	26
2.2.5.1. The pH Value	26
2.2.5.2. Drip Loss	29
2.2.5.3. Color	32
2.2.5.4. Shear Force	35
3. Material & Methods	38
3.1. Meat Samples and Reference Measurements	38
3.2. Raman Setup	38
3.3. Software	43
3.4. Data Analysis	46
3.4.1. Baseline Correction	46
3.4.2. Principle Component Analysis	48
3.4.3. Partial Least Squares Regression	50
4. Results & Discussion	55
4.1. Spectroscopic Measurement of the pH Value	55
4.2. Early Postmortem Changes in Raman Spectra	60
4.3. Prediction of Quality Traits from Early Postmortem Raman Spectra	64
4.3.1. Field Study in the Chiller	64
4.3.2. Field Study at the Slaughterline	68
5. Conclusion & Outlook	78
Abbreviations	80

Bibliography	81
Acknowledgement	97
List of Publications	98
Erklärung	99
II. Publications	101
Measurement of the pH value in pork meat early postmortem by Raman spectroscopy	103
Identification of the early postmortem metabolic state of porcine <i>M. semimembranosus</i> using Raman spectroscopy	115
Early postmortem prediction of meat quality traits of porcine <i>semimembranosus</i> muscles using a portable Raman system	123

Part I.

Introduction

1. Motivation

As an emerging technique, Raman spectroscopy has lately received increasing attention by the scientific community. Although the Raman effect is known since the 1920's [1], the complicated, expensive and slow laboratory systems, which were still state of the art a decade ago, limited the field of application to basic research [2]. With the development of more advanced CCD detectors, (edge) filters and diode lasers, portable Raman systems became commercially available and expanded the application of Raman spectroscopy to security, cultural history, geology and life sciences [3].

“We must know – we will know!”

David Hilbert

In 2007, the project *FreshScan* was started to investigate spectroscopic concepts for the *in-situ* measurement of the microbiological spoilage on the surface of meat. At that time, an increasing awareness for meat quality had developed in the industrialized countries due to an increasing number of meat scandals. Especially spoiled meat received public attention. In this field, Raman spectroscopy proved its potential [4], and a hand-held device was already developed for fast and non-invasive Raman measurements in the laboratory [3]. First experiments in the framework of the project *FreshScan* indicated that lactate, an important compound of the early postmortem metabolism, could be measured with the Raman hand-held device. Besides, the lactate concentration is correlated with the pH, which is also known to be a reliable indicator for meat quality. Presently, the lactate concentration and the pH value of meat can still only be measured invasively although the need for on-line measurements of meat quality was already recognized in 1987 [5, 6]. Therefore, the measurement of quality traits received widespread attention by scientists which led to the evaluation of several, mainly spectroscopic techniques. Although some promising results were achieved, the investigated techniques lack either speed, non-invasiveness and/or accuracy which is why to date none of these methods is applied in commercial abattoirs.

Therefore, the applicability of Raman spectroscopy to measure the lactate concentration and/or the pH value will be investigated in this thesis. Basic research with reference spectra of pure components and spectral simulations should help to gain a better understanding of the early postmortem changes in the Raman spectra. To date, no complete understanding of the Raman spectra of early postmortem meat is accomplished [7]. In future, a deeper understanding of the Raman spectra will be helpful for the development and evaluation of chemometric models. In parallel, the Raman hand-held device already built in the project *FreshScan* has to be adapted and advanced to allow for measurements in abattoirs. For that purpose, a portable Raman system will be planned and constructed based on the aforementioned hand-held device. Additionally, the control software for the Raman system must be written to enable safe and convenient Raman measurements under real-life conditions in abattoirs even by untrained users. This will help to bring Raman spectroscopy one step closer to a commercial application in the meat industry. Using the portable system in a series of measurements in an abattoir, the potential of Raman spectroscopy to predict quality traits from early postmortem spectra will also be evaluated.

To date, only a preliminary study is published regarding the predictability of the water-holding capacity of pork meat from early postmortem Raman spectra [7]. Thus,

a completely new technique for the on-line assessment of objective quality traits of pork meat is investigated in this thesis. In future abattoirs, an automated and objective classification of meat quality shortly after slaughter could be realized using Raman spectroscopy. This would help to minimize losses to meat processors and to maximize meat quality for the consumer.

This thesis is organized as follows: Chapter 2 introduces the theoretical background. In section 2.1 Raman spectroscopy and its applications with biological tissues are described. In section 2.2, structure and function of muscle tissue (2.2.1) are outlined as well as the metabolic path which leads from muscle to meat (2.2.2). The definition of meat quality (2.2.3), a flowchart for the classification of meat (2.2.4) and the measurement of meat quality traits (2.2.5) are also introduced in this section. The reference analysis (section 3.1), the portable Raman system (section 3.2), its control software (section 3.3) and the applied data analyses (section 3.4) are briefly described in chapter 3. Chapter 4 gives a summary of the publication 1 to 3 and describes a series of measurements which confirms important findings of publication 3. In chapter 5, the main achievements of this work are summarized and a short outlook is provided to future applications of Raman spectroscopy in the meat industry and other fields.

2. Theoretical Background

In this chapter, the theoretical background of Raman spectroscopy is outlined, an introduction of relevant properties of meat is provided and the definition of meat quality and its measurement is discussed.

2.1. Raman Spectroscopy

This section is subdivided in a brief theoretical outline of Raman spectroscopy and is followed by a description of the typical instrumentation used for a Raman setup. The section ends with an overview of applications of Raman spectroscopy in biological systems.

2.1.1. Theory

In 1923, the Raman effect was predicted by Adolph Smekal [8]. It was experimentally proven in fluids by Raman and Krishnan in 1928 [1] and in the same year in solids by Landsberg and Mandelstam [9]. A detailed description of the Raman effect can be found in several publications [10, 11]. Thus, only a brief overview of the most significant properties of Raman spectroscopy will be given.

“The most exciting phrase to hear in science, the one that heralds the most discoveries, is not ‘Eureka!’ (I found it!) but ‘That’s funny...’”
Isaac Asimov

The Raman effect is an inelastic scattering process of photons with molecules or atomic lattices, i.e. energy is transferred between light and matter (see Fig. 2.1), unlike the much more likely elastic process, Rayleigh scattering, in which the wavelength of the incident light is unaltered. In general, an absorbed photon excites the material to a virtual electronic state which is unstable. In case of Rayleigh scattering, the photon is re-emitted with the same energy as it was absorbed. In case of Raman scattering, the photon has a different energy which corresponds to the energy required to excite the material to a higher (or lower) vibrational mode. Two outcomes can be observed: (1) Stokes Raman scattering in which the material absorbs energy, and the emitted photon has a lower energy and (2) anti-Stokes Raman scattering in which the material loses energy, and the emitted photon gains energy. The latter is highly unlikely for materials at ambient temperature. For instance, according to the Boltzmann distribution, at 25° C only 0.8 % of the phenylalanine molecules are excited to the ring-breathing vibration which leads to the Raman peak at 999 cm⁻¹. Hence, in general, Stokes Raman scattering is observed. Due to the small scattering cross section of ~10⁻³⁰ cm² [12], lasers are most commonly applied as light sources in Raman setups. For that matter, short wavelength lasers are advantageous due to a higher photon yield because the Raman scattering intensity is dependent on the 4th power of the frequency of the incident light ($I \propto \nu^4$). However, when dealing with biological samples fluorescence becomes an increasing problem with higher frequency (hence higher photon energy). This can easily be understood: A photon with low energy $h\nu_0$ is not able to excite the right-hand system in Fig. 2.1, and no fluorescence is observed. At the same time, the scattering cross-section of the fluorescence

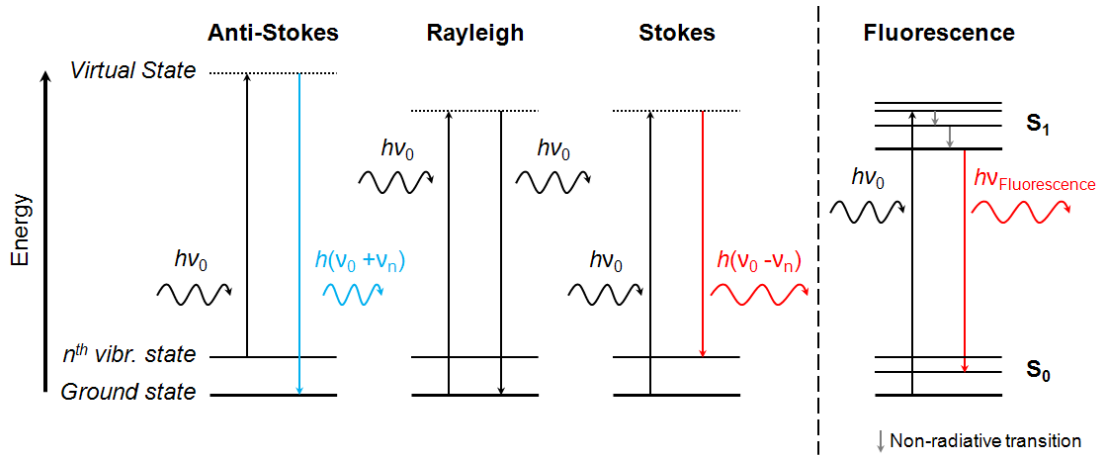


Figure 2.1.: Term scheme for Rayleigh and Raman (Stokes and Anti-Stokes) scattering and fluorescence.

process ($\sigma = 10^{-17} - 10^{-16} \text{ cm}^2$) is many magnitudes larger than the cross-section for Raman scattering [13].

Raman spectroscopy is closely related to infrared (IR) spectroscopy in the wavelength range $2.5\text{--}25 \mu\text{m}$ ($4000\text{--}400 \text{ cm}^{-1}$)¹. Both yield similar, but complementary, information about the molecular structure. While a change in the molecular polarizability α with respect to the vibrational coordinate is required for a molecule to exhibit Raman scattering:

$$\left(\frac{\partial\alpha}{\partial q}\right)_0 \neq 0, \quad (2.1)$$

the selection rule of IR spectroscopy is determined by a change of the dipole moment μ :

$$\left(\frac{\partial\mu}{\partial q}\right)_0 \neq 0 \quad (2.2)$$

In centrosymmetric molecules, this contrasting feature allows to analyze transitions which are not IR active via Raman spectroscopy and *vice versa*.

Raman spectroscopy can provide high resolution spectroscopic fingerprints reflecting the composition and structure of biological matter *independently* of the water content and is, therefore, well suited for investigations with meat.

2.1.2. Instrumentation

In 1928, C. V. Raman was using the sunlight as the light source in his experiment applying a narrow band photographic filter to create monochromatic light. Today, lasers are considered the ideal light sources for Raman setups due to their monochromatic light, low beam divergence and high output power. In case of Raman investigations with biological tissue, which frequently reveal high fluorescence background, 785 nm is the most common wavelength for measurements, and even infrared lasers (1064 nm) are in use.

Either way, if the laser light is scattered by the sample, only a small fraction is scattered inelastically. For instance, the Rayleigh scattering cross section of the nitrogen molecule N_2 is $\sigma = 5.1 \cdot 10^{-27} \text{ cm}^2$ [14] while the Raman cross section is only $\sigma = 5.5 \cdot 10^{-31} \text{ cm}^2$

¹In the, commonly used, NIR wavelength range $0.8\text{--}2.5 \mu\text{m}$, overtones and harmonic vibrations are excited.

[12]. In case of vibrations of biological molecules, the difference is even larger. To suppress the Rayleigh scattered light, edge filters are commonly used. These filters are reflective to a certain wavelength and become transparent beyond that wavelength (Stokes). Hence, edge filters are characterized by their cut-on (or cut-off) wavelength, which defines the wavelength at which the filter transmits 50 % of the incident light. The second most important parameter is the transition width, which defines the steepness of the transition between the region of transmission and reflection. Another important parameter is the reflective index because the filters main function is the suppression of the laser line. Therefore, an ideal edge filter for Raman setups (Stokes) would have 100 % reflectivity at the laser wavelength and a very steep transition to 100 % transmittance at higher wavelengths. In reality, the transition width of ultra-steep 785 nm edge filter is, for example, around 4 nm which enables to measure Raman shifts of approximately 70 cm^{-1} .

Beyond the edge filter, only Raman and fluorescence light are present in the setup but all wavelengths are still combined in one beam. Hence, a dispersive element, most commonly a diffraction grating, is used to split and diffract the light according to its wavelength. Today, mostly holographic gratings are in use, which are created from holographic interference patterns using photolithographic techniques. Besides, Fourier transform spectrometer are in use in which a interferogram is created by a moving mirror and a Fourier transform is applied to reconstruct the actual spectrum.

For the light detection, charged coupled devices (CCD) are applied, which are silicon-based integrated circuits consisting of a dense matrix of photodiodes that operate by converting light energy into an electronic charge. The most important quality parameter of a CCD is its quantum efficiency, which is defined as the number of electron-hole pairs created and successfully read out by the device for each incoming photon. Modern CCDs can reach over 90 % quantum efficiency. The optimal spectral range depends amongst others on the architecture of the CCD, but beyond 750 nm the sensitivity of most detectors decline rapidly [15]. In principle, photodiodes comprise three layers: A transparent conductor on an isolator on a semiconductor material (doped silicon). By applying a voltage, a potential well is formed in the semiconductor next to the isolator. Incident photons excite electrons from the conduction band to the valence band via the photoelectric effect, and the excited electrons will be trapped in the potential well. Here, statistical variation in the arrival rate of photons lead to the so-called photon or shot noise [16]. Besides, electrons may jump into the well via thermic excitation causing thermic, dark or detector noise, which is why CCDs are most commonly cooled. As a shutter blocks the light from the CCD, the electrons are stepwise moved to an adjacent pixel. At the edge of the CCD, the charge is amplified, transferred to an electronic system and submitted to a computer, which can display and save the data. During the process of converting the CCD charge to a digital signal, read-out noise is added to the existing noise.

For presentation of Raman data, the relative wavenumber ω (not the wavelength λ) is used as the x-coordinate:

$$\Delta\omega = \frac{1}{\lambda_0} - \frac{1}{\lambda_1} \quad (2.3)$$

As the inverse of the wavelength, the wavenumber is proportional to the energy. In this context, *relative* means difference between incident laser λ_0 and scattered Raman light λ_1 . Therefore, independently of the laser, all Raman peaks have the same wavenumber, and Raman spectra of different setups can easily be compared. In addition, Raman spectra are comparable to IR spectra which are also presented in wavenumbers.

2.1.3. Application in Biological Systems

Raman spectroscopy was already applied in meat science and several other biological systems which are related to this work. A brief overview of this work is given in this section.

Raman spectroscopy has already proven to be a sensitive probe of the secondary structure of proteins (α -helix, β -sheet, random coil) [17–19]. The amide I modes around 1650 cm^{-1} , the amide III modes between 1225 and 1310 cm^{-1} and the carbon-carbon stretching modes of the protein backbone at 1155 cm^{-1} can be used as indicators. Additionally, α -helical proteins exhibit signals at 900 , 935 , 1305 , 1445 and 1650 cm^{-1} [20, 21]. Myosin, as the most important protein in muscle cells (see section 2.2.1), was already investigated using Raman spectroscopy in the late 1970's [22, 23]. Further assignments to Raman signals of meat can be found in numerous studies and are summarized in Tab. 2.1 [18, 24–28]. Also, fat is known to be an excellent Raman scatterer and its assignments are well-known [29–35]. An overview of the assignments is given in Tab. 2.1. Interestingly, Raman spectroscopy was also shown to be sensitive for pH-induced conformational changes in amino acids [36, 37], poly-amino acids [38, 39] and the protein transferrin [40]. In addition, the pH value is reflected in Raman spectra by two strong vibrations of the terminal phosphate moiety at 980 and 1080 cm^{-1} [41, 42]. The latter is shifted to higher wavenumbers in case of two (1105 cm^{-1}) or three (1120 cm^{-1}) phosphate groups due to coupling of the polyphosphate chain [41, 43]. This becomes relevant in context of this thesis due to the universal occurrence of phosphorylated compounds in the metabolism of muscle cells, called metabolites and the early postmortem pH fall in the muscle cell. In addition, Raman spectroscopy proved its potential to provide useful information about meat quality traits such as water-holding capacity [7], shear force (tenderness) [44–46], cooking temperature [47], microbiological spoilage [4] and sensory quality [48].

2.2. Meat

Meat is defined as all parts of slaughtered or slayed warm-blooded animals which are determined for human consumption [49] or simply as animal flesh that is eaten as food [50].

2.2.1. Muscle Structure, Composition and Contraction

The main component of muscle tissue is water (74–76 %), which is found within the

- myofibrils,
- between the myofibrils,
- between the myofibrils and the cell membrane (sarcolemma),
- between muscle cells and
- between muscle bundles (groups of muscle cells).

The remaining fourth of the muscle's mass comprise proteins (20–25 %), connective tissue (<1 %), fat (in lean meat 1–5 %) and minerals (<1 %) [51–55].

Its organizational structure and top-down hierarchy is presented in Fig. 2.2. The muscle is sheathed by a tough layer of connective tissue called the epimysium and is composed of several fiber bundles or fascicles (sheathed by the perimysium) which consist

Table 2.1.: Overview of assignments to characteristic vibrations of myosin and fat.

	Peak position / cm^{-1}	Assignment	Reference
Myosin	720	Adenine	[27]
	750–760	Tryptophan	[28]
	827–834	Tyrosine	[28]
	850–860	Tyrosine	[28]
	900–901	C-C skeletal stretching	[22]
	934–944	C-C skeletal stretching	[28]
	1000–1006	Phenylalanine	[28]
	1030–1033	Phenylalanine	[22]
	1040–1120	C-N and C-C skeletal stretching	[22]
	1127–1130	C-N stretching	[24]
	1156	C-C stretching, COH deformation	[27]
	1172–1175	Tyrosine	[24]
	1205–1209	Phenylalanine, tyrosine	[22]
	1225–1250	Amid III (β -pleated and random coil)	[22]
	1265–1278	Amid III (α -helix)	[28]
	1301–1309	Amid III (α -helix)	[28]
	1316–1322	Tryptophan, C-H deformation	[27]
	1339–1342	Tryptophan, C-H deformation	[28]
	1395	symmetric CH_3 deformation	[27]
	1447–1451	CH_3 , CH_2 , CH bending	[22]
	1460–1483	CH_3 , CH_2 bending	[28]
	1553–1554	Tryptophan	[28]
	1605–1618	Tryptophan, phenylalanine, tyrosine	[28]
1645–1658	Amid I (α -helix), OH bending (water)	[22, 28]	
1660–1665	Amid I (random coil)	[28]	
1665–1680	Amid I (β -pleated)	[28]	
Fat	727	=C-H deformation (in plane)	[30]
	800–920	C-C, C-O stretching, CH_3 rocking	[32]
	970–972	=C-H deformation (out-of-plane)	[33]
	1060–1068	aliphatic C-C stretching (out-of-plane)	[32]
	1076–1090	aliphatic C-C stretching (out-of-phase)	[34]
	1119–1129	aliphatic C-C stretching	[33]
	1263–1266	symmetric =C-H rocking	[33]
	1295–1306	CH_2 torsion (in-phase)	[34]
	1368	symmetric CH_3 deformation	[33]
	1436–1443	symmetric CH_2 deformation	[33]
	1455–1460	CH_2 deformation	[35]
	1650–1670	C=C stretching	[34]
	1730–1750	C=O stretching in esters	[32]

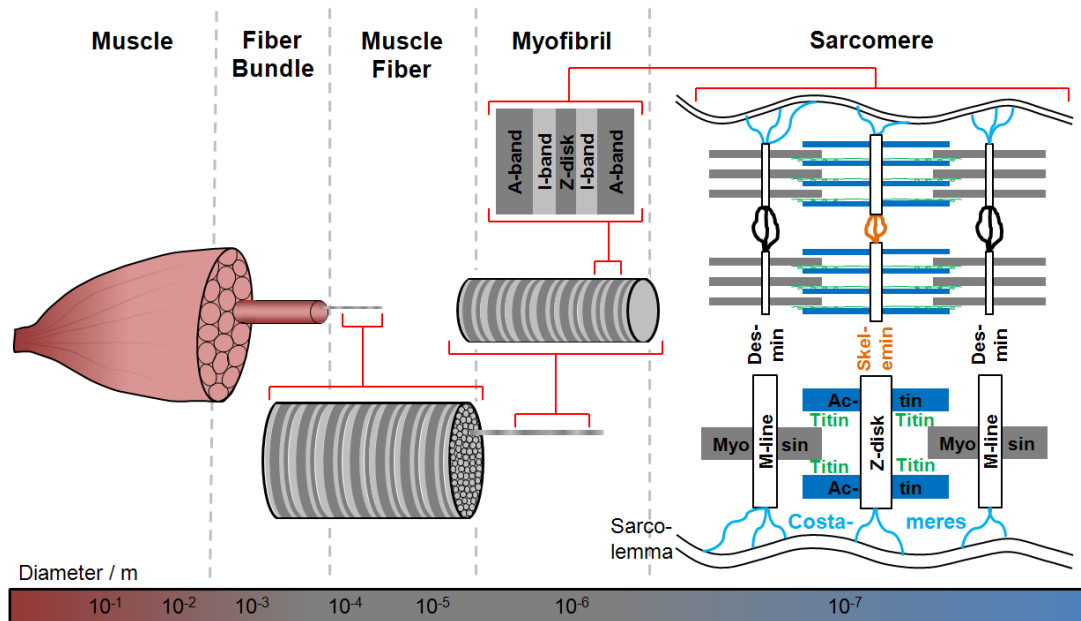


Figure 2.2.: Schematic representation of the organizational structure of the muscle.

of single muscle fibers (sheated by the endomysium). The muscle fibers have a length of up to 400 mm but only a diameter of 0.01–0.1 mm. Each muscle fiber is composed of thousands of myofibrils, and the myofibrils themselves are bundles of protein filaments.

The myofibrils are organized in repeating units called sarcomers, which can be spotted using a polarizing microscope. Thereby, two distinct areas appear, the anisotropic A-band and the isotropic I-band. The latter is crossed by the dark Z-disk while the paler M-line can be found in the A-band. Its appearance is a result of the different protein composition. While the A-band (thick filaments) is mainly composed of one basic protein, myosin, the I-band (thin filaments) is made up of the basic structural protein actin and the two regulatory proteins troponin and tropomyosin. Together, myosin and actin account for 80% of the weight of the contractile tissue. Besides, the Z-disk is mainly constituted of alpha-actinin and the giant protein titin, which extends into the M-line and binds to myosin. Another giant protein, nebulin is known to extend over the whole I-band. Its main function is to anchor the thin filaments into the Z-disk [56]. Intermediate filaments such as skelemin and desmin run perpendicular to the length of the muscle fiber and keep the three-dimensional shape of the sarcomere and myofibrils. On the other hand, costameric proteins (costameres) such as filamin, dystrophin, vinculin and talin fix the position of the myofibrils relative to the sarcolemma and interact possibly even with the endomysium layer outside the sarcolemma. These proteins also extend into the muscle cell where they encircle the myofibrils at the Z-disk and run from myofibril to myofibril to link adjacent Z-disks and M-lines laterally [57]. Both, intermediate filaments and costameres, have become a source of much interest as it appears that the degradation of these proteins during postmortem aging may play a major role in the tenderization of the muscle [58].

The muscle's basic function is to provide mechanical energy hence contraction by converting chemical energy. This is realized on the molecular level by interaction of myosin with actin. As a first step, an action potential from the central nervous system is sent via an axon to the muscle cell triggering a calcium ion (Ca^{2+}) flux into the muscle cell. Then, the Ca^{2+} ions bind with troponin-C molecules, which are regularly dispersed throughout the tropomyosin protein. This protein is covering the actin binding sites

for the myosin heads. Due to the binding with the Ca^{2+} ions, a conformational shift of troponin-C is caused which moves the tropomyosin filaments and thereby reveals the binding sites for myosin. Now, the myosin head will bind to the actin filament to form an actomyosin complex. ADP and inorganic phosphate (P_i), which were bound to the myosin head, can be released. This changes the angle of the myosin head from 90° to 50° , and further to 45° as P_i and ADP are released, respectively. This pulls the Z-disks towards each other, thus shortening the I-band (not the A-band [59]) and contracting the muscle by about 4–5 nm. The myosin head still remains attached to actin until a new ATP binds to it. This releases the actin-myosin bonding and returns the myosin head back to its 90° -formation. Repeated contractions can shorten the sarcomere from about 2.7 to 1.5 μm and the muscle up to 30 % [58].

2.2.2. Early Postmortem Metabolism

The quality of muscle foods relies heavily on the process of the muscle to meat conversion. Antemortem and postmortem changes affect quality traits such as tenderness, juiciness and color. Hence, it is necessary to introduce the basic, metabolic processes which occur early postmortem in the muscle cell.

“Dead is when the chemists take over the subject.”

Arthur L. Schawlow

As the animal is slaughtered, the cell’s metabolism has to shift from aerobic to anaerobic. Without oxygen supply, the muscle has only limited options to produce energy and hence regenerate ATP (see Fig. 2.3). This can be done by using [60]:

1. the short term storage of phosphocreatine (PCr) which accumulates adenosine diphosphate (ADP) and creatine (Cr),
2. two ADP via the adenylate kinase reaction which accumulates adenosine monophosphate (AMP) or
3. the long term storage of glycogen via the glycolytic pathway at the end of which lactate and H^+ ions are accumulated.

It is noteworthy that triphosphates like inosine (ITP) and guanosine triphosphate (GTP) may also produce energy via breakdown to di- and monophosphates, and glycerol 3-phosphate can enter the glycolytic pathway, but due to the small concentration of those metabolites [61–63], they only play a minor role in the regeneration of ATP. Shortly after slaughter, the PCr storage is mainly exploited for ATP regeneration by transferring the phosphate group from PCr to ADP. Thus, creatine is accumulated. The PCr storage consists of up to 20–30 mmol/kg [64, 65] but is depleted within 1–2 h after slaughter. Additionally, up to 70–100 mmol/kg glycogen [61, 64, 66] can supply the muscle cell with energy up to eight or more hours after slaughter². Thereby, glycogen is metabolized to pyruvate (glycolysis) which can be separated in two phases. In the *investment phase*, glycogen is split into glucose and phosphorylated to glucose 6-phosphate (G6P), rearranged into fructose 6-phosphate (F6P) and again phosphorylated to fructose 1,6-bisphosphate (F-1,6-P) which overall consumes two ATP molecules. As F-1,6-P is split into dihydroxyacetone phosphate (DHAP) and glyceraldehyde 3-phosphate (GA3P) and DHAP is further metabolized to GA3P the investment phase ends, and the *pay-off phase* begins. Firstly, GA3P is dehydrogenated and P_i is

²Interestingly, porcine longissimus muscle was shown to only metabolizes 35–40 mmol/kg of its glycogen storage [67].

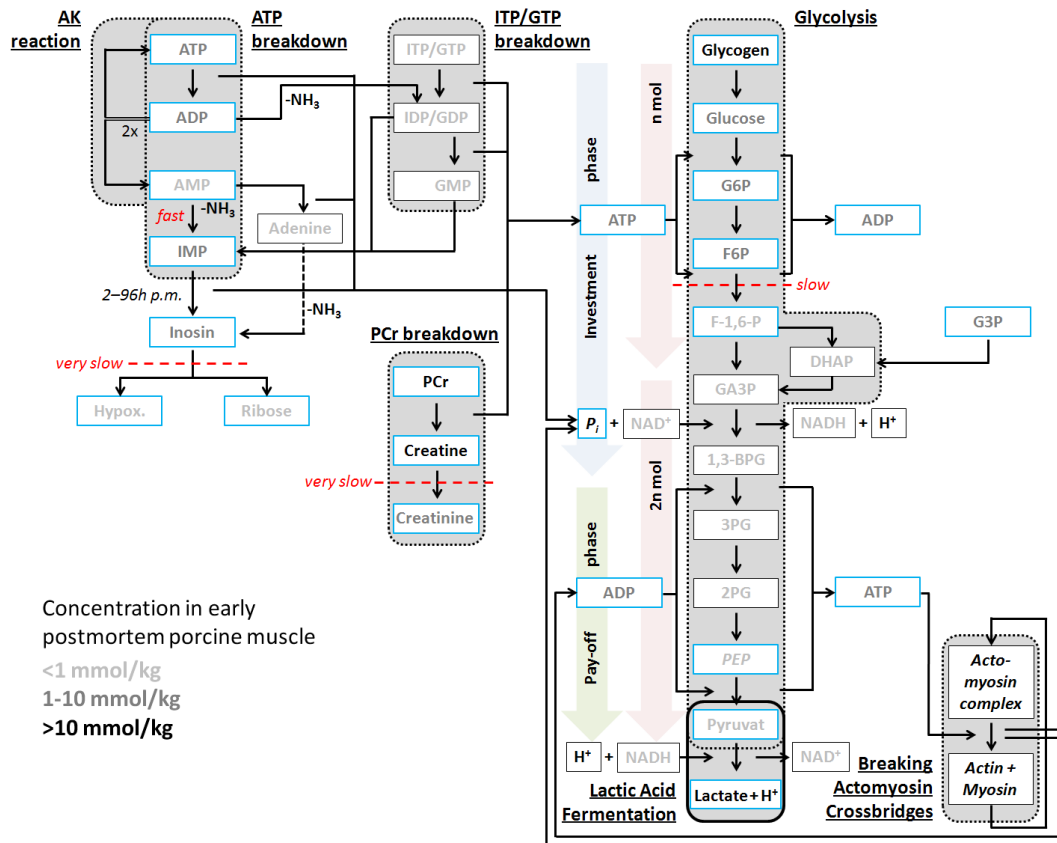


Figure 2.3.: Overview of the early postmortem metabolism in the muscle cell. Raman spectra of metabolites in blue frames were measured in this thesis.

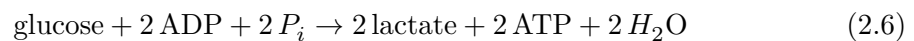
added to form 1,3-bisphosphoglycerate (1,3-BPG). In this step, the H^+ ion is formed as NAD^+ is reduced, and NADH is produced, i.e. in this step the acid is formed, which eventually leads to the pH fall from 7.2 in the living pig muscle to 5.3–5.5 in pork meat. In the next step, one of the phosphate groups of 1,3-BPG is used to form ATP while 3-phosphoglycerate (3PG) is formed. In the next steps, 2-phosphoglycerate (2PG) and phosphoenolpyruvate (PEP) are formed. In the final step of the pay-off phase, ADP is phosphorylated to ATP via the formation of pyruvate from PEP. To sum up, the overall process of glycolysis is:



With only small amounts of NAD^+ in the muscle cell, the glycolysis would stop rapidly. Therefore, NADH has to be oxidized back to NAD^+ . Without oxygen supply, the muscle cell realizes this by lactic acid fermentation. In this process, pyruvate is converted to lactate (which is the conjugated base of lactic acid):



Combining equation 2.4 and 2.5 yields:



which sums up the ATP regeneration via glycolysis and lactic acid fermentation.

The ATP produced during glycolysis and via breakdown of PCr is mainly used to break the acto-myosin cross-bridges and to keep the muscle in the relaxed state, but

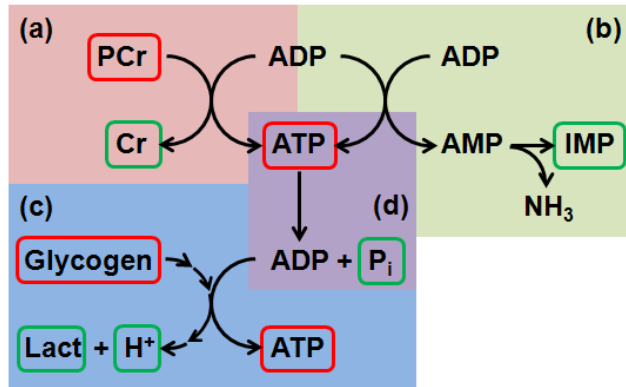


Figure 2.4.: Simplified early postmortem metabolism in the muscle cell with (a) breakdown of phosphocreatine (PCr) to creatine (Cr), (b) two adenosine diphosphate (ADP) forming adenosine tri- (ATP) and monophosphate (AMP) with subsequent deamination to inosine monophosphate (IMP), (c) glycolysis in which glycogen is degraded to pyruvate, which is finally reduced to lactate (Lact) and H^+ ions to recycle NAD^+ , which consumes ADP and inorganic phosphate (P_i), and (d) ATP hydrolysis to break actomyosin bonds. Framed metabolites are depleted (red) or accumulated (green) in the early postmortem muscle cell.

also to fuel active transport and to maintain ion gradients [60]. Thereby, ADP and P_i are formed. When the glycogen storage is completely depleted or the ultimate pH of 5.3–5.5 is reached, the ATP regeneration via the adenylate kinase (AK) reaction ($ADP + ADP \rightarrow ATP + AMP^3$) comes also to halt, and the muscle will enter the *rigor mortis*. The beginning of this state is characterized by the formation of actomyosin cross-bridges stiffening the muscle. The end of *rigor mortis* is less clearly defined as the muscle is gradually tenderizing due to proteolysis (see section 2.2.3.4). In pork muscle, the tenderizing in *M. longissimus dorsi* takes about five days [68]. In this time frame, creatine is also metabolized to creatinine and IMP to inosine which is subsequently split into hypoxanthine and ribose [69].

In summary, PCr, glycogen and ATP are depleted in the early postmortem muscle while Cr, lactate, H^+ , IMP and P_i are accumulated (see Fig. 2.4).

These general metabolic steps occur in every muscle cell after slaughter, but large variations can be observed between different animals regarding velocity and extent of postmortem metabolism. If the metabolic activity is elevated, the rate of acidification is high and the muscle's pH can fall to its minimum in less than one hour while the carcass is still warm. High temperature and low pH are known to cause protein denaturation [70, 71] and defects of the cell membrane [72], which lead to meat with pale color, soft texture and low water-holding capacity (WHC). This condition is described as pale, soft and exudative (PSE) meat and was firstly introduced in the 1960's [73]. The condition may be caused by the typical scalding of the carcasses or by high antemortem muscle activity but is mostly a result of accelerated metabolism [66]. PSE occurs, if the animal is exposed to perimortem stress, and the anaerobic metabolism based on glycolysis is triggered before slaughter. PSE meat is known to give reduced yield hence is undesired by meat processors for most applications [70]. For instance, cooked hams manufactured from severe PSE pork meat can result in up to 50 % financial loss [74]. Thus, effort was put into preventing the occurrence of PSE. However, modern pig breeds with high lean

³Once formed, AMP is quickly converted to inosine monophosphate (IMP).

meat content seem to be susceptible for stress which is why PSE meat is still a problem.

In contrary to PSE, reduced metabolic activity can also be observed in the early postmortem muscle. Very early experimental findings in the 1870's using rats and rabbits revealed that this condition is caused by the limited formation of lactate [6, 75]. This deviation can be found in animals which were exposed to chronic or long term stress before slaughtering which led to the depletion of stored glycogen [70]. Without glycogen, no glycolytic acidification occurs. Thus, these muscles have a higher ultimate pH and develop a more rapid onset of *rigor mortis*. The high ultimate pH leads to a greater absorbance than normal. Thus, more incident light than normal is trapped within the meat rather than being reflected which results in a darker than normal appearance [6]. The high pH causes relatively little denaturation of proteins which leads to firm texture and high WHC [76]. This quality deviation is commonly known as dark, firm and dry (DFD) meat. It is also known for its short shelf-life due the higher than normal pH which leads to a faster microbial spoilage [77]. As PSE, DFD is undesired by most meat processors, but unlike PSE it became a minor problem as today's animals are treated more carefully during the preslaughter handling. However, the DFD deviation can *occasionally* be observed while milder forms *regularly* occur even in modern abattoirs [70, 78].

2.2.3. Technological Quality Traits

Quality is a perceptual, conditional and subjective attribute which makes it hard to define. For most consumers, quality is the *superiority* of something in comparison to something else of the same category. It may also be defined as *fitness for purpose*.

“Uncontrolled variation is the enemy of quality.”

Edward Deming

As for the general term, *meat* quality is a somewhat subjective term, but there are objective measurements which are helpful to define meat quality. In general, it is a complex and multivariate property influenced by multiple interacting factors (see Fig. 2.5). These include *intrinsic parameters* such as breed, genotype, sex, muscle fiber type and oxidative capacity of the muscle [79] and *external parameters* such as climate, temperature, feeding, dietary, fasting, training, preslaughter handling (stress), stunning, slaughter method, postmortem electrical stimulation, chilling and storage conditions. These conditions influence the *early postmortem metabolism* of the muscle cells, which is indicated by the rate of glycolysis, the enzymatic activity and protein denaturation. Several techniques and methods were developed to obtain objective information about the early postmortem conditions in the muscle [80]. These information or *quality traits* are pH, concentration of lactate and other metabolites, drip and cooking loss, meat color, shear force, lean meat content, electrical impedance or conductivity, fat composition and many more. In opposite to the technological quality traits, subjective parameters can be obtained by either trained panelists or untrained consumers. Here, categories such as taste, tenderness, juiciness, palatability and chewiness can be found. These are to some degree correlated to the objective measurements although a prediction is difficult and contradictory correlations were reported in the literature (see the discussion of shear force and tenderness in section 2.2.3.4).

In the following sections, only objective parameters will be discussed which are established in meat science, i.e. pH, drip loss, color and shear force. Firstly, the importance of the parameter for meat quality and its relationship to the early postmortem metabolism is discussed. Then, a classification chart, based on pH, drip loss and L* value, is introduced. In section 2.2.5, the physical principles of the reference methods to measure these quality traits are shortly discussed and alternative measuring techniques are evaluated.

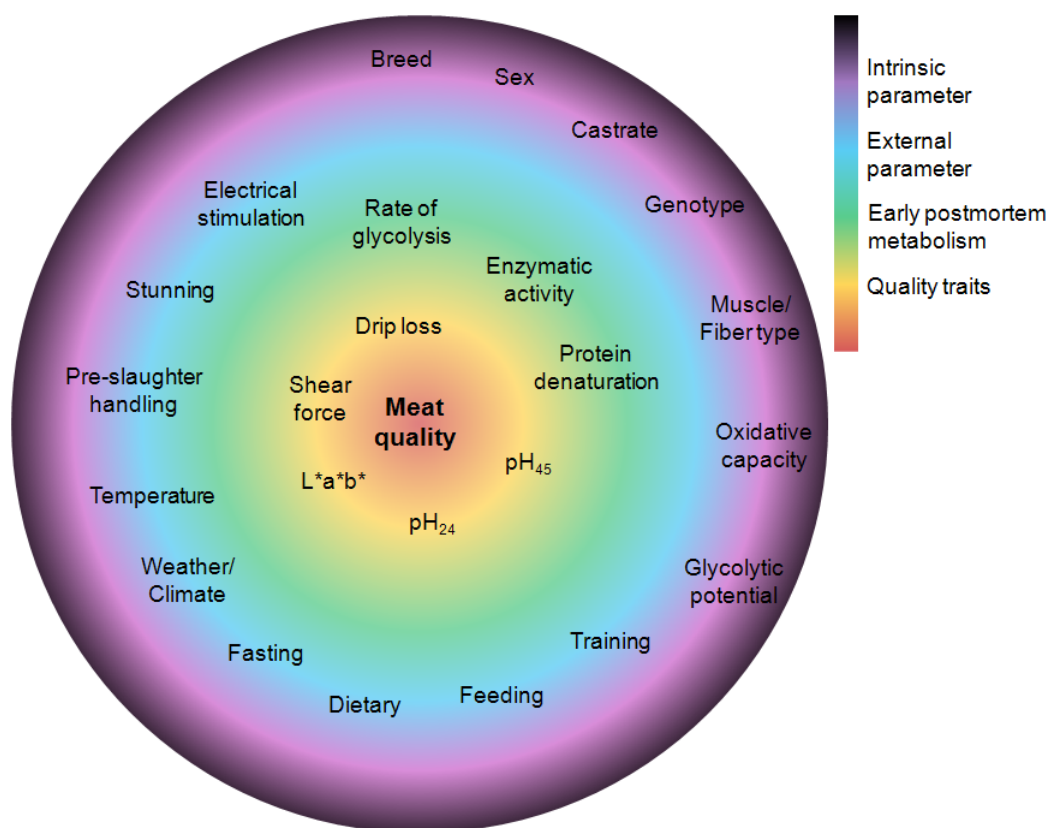


Figure 2.5.: Overview of factors determining meat quality.

2.2.3.1. The pH Value

The pH value has been shown to be the best among the known predictors of technological yield and the accuracy and precision is better than that of many other examined techniques [81]. Two pH values are commonly used for classification of pork in the meat industry [58, 82–85]:

1. The *early postmortem* pH (pH_{45}) most often measured 45 min p.m. is indicative for PSE meat and
2. the *ultimate* pH (pH_u or pH_{24}) measured 24 h p.m. helps to detect the DFD deviation.

In 1959, an early measurement of the pH of the LD muscle of split pork carcasses was proposed to diagnose potential PSE quality [82]. At this time, the earliest measurement that could be conducted at the slaughterline was at 45 min p.m., which is why the pH_{45} became the most commonly used early postmortem pH value. The same study proposed a threshold value of 6.2 for the discrimination between normal and PSE pork, but also stated that this value only applies for the majority of white muscles with ultimate pH values in the range from 5.4 to 5.8 pH-units. In red muscles with normal pH_u values above 6.2, the PSE condition rarely appears. In later studies, threshold values of $pH_{45} < 6.0$ [83, 84] or even < 5.8 [85] were considered as critical values below which PSE meat develops. At the same time, it was stated that pH measurements alone might not be reliable predictors of PSE [5], but to date, no suitable, non-invasive surrogate or auxiliary technique is known. For instance, only a weakly correlation ($r = -0.17$) between pH_{45} and reflectance was found [86]. However, internal light scattering and

electrical conductivity measurements, in combination with pH_{45} and pH_{24} were shown to allow for an accurate quality classification in normal, slightly PSE, slightly DFD, PSE and DFD pork meat [87].

The velocity of early postmortem acidification was shown to be dependent on breed, genotype, stunning method and muscle fiber type [6, 58]. A linear relationship between pH fall and lactate formation was reported by Bendall [88]. In the same study, the author found an exponential relationship between muscle pH and phosphocreatine levels.

The glycolytic potential (GP) affected ultimate pH in pork loin [89]. The GP is the sum of the concentrations of glycogen, G6P, glucose and lactate [90]. At the same time, a curvilinear relationship between muscle glycogen content and pH_u was reported between 7.2 and 5.7, but below 5.7 distinct variations were observed [64]. Accordingly, at low pH values the variations in residual glycogen concentration in three porcine muscles were found to be enormous (10–83 mmol/kg) and independent of ultimate pH [91]. Interestingly, loin pH_u ($N = 4560$) varied significantly with month of slaughter, which might be explained by the weather, changing slaughtering rates and variable resting periods before slaughter [92]. Finally, ultimate pH may be useful to predict cooking loss. In one study, pH_u was highly correlated ($r = -0.94$) with cooking loss of veal LD muscles ($N = 12$) [93]. In contrary, a correlation between cooking loss and pH_u of only $r = -0.04$ was reported for Japanese black steers ($N = 11$) in a second study [94]. However, both studies comprise only few samples which makes it difficult to draw a final conclusion.

2.2.3.2. Drip Loss

Drip loss is defined as the weight loss via exudate during the first days after slaughter. Therefore, it is of high economical interest due to reduced processing yields [74].

Three “kinds” of water can be distinguished within the muscle: Bound, entrapped (or immobilized) and free water [58, 95]. *Free water* is held within the muscle only by weak capillary force while *bound water* is closely bound to muscle proteins. Therefore, its amount is changed very little in post-rigor muscles [96]. However, free and bound water only make up less than a tenth of the total water in the muscle. On the other hand, *entrapped water* is also held within the muscle structure, but it is not as closely bound to protein as bound water [95, 97]. It is mostly affected by the early postmortem metabolic processes in the muscle and dependent on alteration (degradation) of the muscle’s cell structure and lowering of the pH. The latter is of importance due to the isoelectric point (pI) of the major structural proteins of the muscle, especially myosin (pI = 5.4) [95]. If the pH reached the isoelectric point, the number of positive and negative charges on the proteins are equal. The minimum charge causes a reduction of the water holding capacity. As the net charge of the proteins approach zero, the repulsive force between the proteins is reduced allowing the myofibrils to pack more closely. This is confirmed by a study using x-ray diffraction measurements at 45 min p.m. where the distance between myosin filaments of pork LD was shown to be about 46 nm in muscle samples which were buffered to pH 7.2 [98]. This was considered comparable to the conditions in the resting muscle. After 3–6 h, the pH has fallen to 5.2–5.5, and the muscle has gone into *rigor mortis*. This was accompanied by a decline of the myosin filament separation to 41–42 nm, hence a reduction of 4–5 nm. Similar results were reported using electron microscopy [99]. These observations and further studies [96, 100, 101] indicate that the main source of exudate (drip loss) in pork meat are the myofilament lattice and the sarcoplasm. Low field nuclear magnetic resonance (NMR) studies revealed that a higher proportion of water is held in the I-band than in the more dense A-band [102]. The I-band is shortening during muscle contraction and rigor (see section 2.2.1) hence the myofibrils are shortening and reducing the intramyofibrillar volume resulting in a water

flow into the extramyofibrillar space. At this point, the exudate is still contained inside the muscle bundle, but with on-going rigor, gaps between muscle bundles are forming by which purge flows from the meat [103, 104].

High DL is related to rapid pH decline [66, 70]. However, only pH_{45} values above 6.1 had a large effect on drip loss while only a small effect was found for values below 6.1 [71, 105]. This was first observed by Wismer-Pedersen [82] and confirmed by others [106, 107]. Furthermore, in a study where no samples with $\text{pH}_{45} < 6.0$ were measured, a linear relationship between pH_{45} and drip loss (bag-drip) was reported [6]. Interestingly, a relationship of $r = -0.8$ was found between drip loss and pH measured 4 h p.m. in the *longissimus thoracis* muscle of twelve veals indicating that the commonly conducted pH measurement after 45 min may not be optimal [93]. However, the number of samples in this study was too low for a final conclusion.

Besides antemortem stress, a mutation in the halothane gene is known to cause high DL by accelerating the Ca^{2+} ion release, which results in an increase in the postmortem metabolic rate of the muscle cells [108]. For instance, the Hampshire pig breed is known for its low water holding capacity (=high DL), which is the result of 70 % increase in muscle glycogen content hence a greater lactate production and a lower ultimate pH [90]. Similarly, some pig breeds with lower muscle glycogen content are known to yield meat with improved quality traits [109]. However, pH_u was shown to be only loosely related to drip loss with only 15 % explained variation [105], and even if the pH fall was faster than normal, the ultimate pH may not be below normal ranges [79]. This is in accordance with other studies, where ultimate pH accounted for only 24 % and 52 % of the variation in WHC in porcine muscles [110, 111]. In essence, the ultimate pH is not a reliable indicator for elevated drip loss.

In addition, drip loss is known to be influenced by the rate of postmortem cooling of the carcasses, i.e. faster cooling leads to lower drip loss [112]. This can be explained as the metabolic processes in the muscle are slowed down because low temperatures reduces to the enzymatic activity. A negative correlation ($r = -0.41$) between drip loss and protein content of the exudate was reported, i.e. the higher the absolute drip loss, the lower the relative amount of protein [113]. This is caused by the finite amount of water soluble protein in the muscle. However, the correlation is only moderate hence cannot be exploited to indirectly measure the drip loss.

2.2.3.3. Color

For the consumer, the color of meat is an important quality attribute as it defines the initial visual perception of the product [58, 80, 114]. The appearance of meat is influenced by internal factors such as animal genetics, ante- and postmortem conditions and muscle chemistry and by external factors such as meat processing, packing, distribution, storage, display and final preparation for consumption [115]. In this work, only fresh and unpacked meat was used. Hence, only internal factors and contact with air could have affected the color ($L^*a^*b^*$) measurements and will be discussed in the following.

The pH decline is known to lead to increased lightness of the meat [6, 116], decreased penetration depth of light and changes in the light absorption through heme (myoglobin, hemoglobin) [117]. It is well-known that increased protein denaturation caused by high temperature and low pH leads to a loss of color intensity [58]. In extreme cases, this leads to the very pale PSE deviation. The other extreme, DFD, results in a high ultimate pH which increases oxygen consuming enzyme activity. This reduces the amount of available oxygen to convert deoxymyoglobin to its red oxygenated state (oxymyoglobin). In equine muscles, muscle pH, the rate of lactic acid production and lactic acid accumulation were shown to play a major role in the metmyoglobin reduction via lactate dehydrogenase and

may also interact with myoglobin and increase its stability [118]. This is confirmed for porcine muscles as ultimate lactate level and L^* were moderately, but linearly related, i.e. higher levels of lactate resulted in increased paleness during storage [119]. The pH_u of porcine LD muscles was found to be correlated with L^* and b^* with $r = -0.81$ and -0.73 , respectively [111]. Similarly, the combined change in L^* , a^* and b^* were reported to be useful for differentiating beef meat of $pH_u < 6.1$ and > 6.1 [120]. However, contradictory correlations between the glycolytic potential and meat color were reported. On the one hand, weak correlations between GP and L^* values of porcine *M. longissimus* ($r = 0.23$ antemortem and 0.31 postmortem) [121] and of loin ($r = 0.33$) were reported [122]. On the other hand, no effect on loin color was found in another study with pork meat [89].

The color of meat is also influenced by breed [123] and muscle type [124, 125], but no differences in color between gilts and castrates within breeds were found for normal meat quality [126]. In this study, most of these variations were explained by the pigment content, myoglobin forms and internal reflectance. The effects of pre-harvest environment have received recent attention from meat researchers, e.g. pigs born and reared outdoors were shown to have redder loins than pigs born and reared indoors [127]. Accordingly, preslaughter handling and stunning methods may also influence meat color [128] and seasonal effects can alter L^* values [92, 129].

The color of meat is not solely related to muscle pigment state but also to the proportion of free water. Increased amounts of free water, which can be found in PSE meat, may lead to a higher reflective index of the muscle surfaces. Conversely, the dark color associated to DFD is caused by the increased amount of bound water which reduces the amount of reflective surfaces [58]. However, when L^* values were investigated for prediction of water-holding capacity, a moderate correlation of $R^2 = 0.37$ was reported, and brightness was stated not to be a reliable predictor of WHC [110]. This confirms former studies in which the authors stated that porcine L^* values are only loosely related to WHC [105, 130].

2.2.3.4. Shear Force

Of all meat quality traits, tenderness is considered to be the most important with regard to eating quality [131–133].

When the muscle enters the *rigor mortis* this leads to a steep increase in toughness, and the highest shear force values can be measured when the muscle is in the *rigor mortis*. Subsequently, a continuing tenderization of the muscle can be observed, which starts with the structural proteins of the Z-disks prior to any proteolysis of other myofibrillar proteins [58]. This process is known to be temperature and pH-dependent [134]. Since the 1960's, it is known that especially the rate and the extent of acidification of pork muscles have a profound effect upon meat softness [6, 73], although only moderate correlations with $r < |0.3|$ were found between Warner-Bratzler shear force and pH in pork meat in a recent study [135]⁴.

There is still an ongoing debate in the meat science community which proteinase is the main protagonist in the tenderization process although there is an increasing consent that μ -calpain probably has the greatest proteolytic activity [136–138]. Together with m-calpain, it is known to split titin, nebulin, filamin, desmin and troponine-T hence proteins which stabilizes the structure of the myofibrils [139]. In addition, desmin and vinculin were shown to degrade within 24 h p.m. about 15 and 35 %, respectively [66]. Cathepsine proteases only play a minor role during the post-rigor tenderizing [140], but serine proteases could have a larger influence on meat toughness [141]. At the same

⁴The study revealed also low correlations between SF and drip loss, L^* , a^* and b^* .

time, post-rigor calpastatin activity has explained a high proportion of the variation of meat tenderness [142], and there is a documented link between high calpastatin activity, limited postmortem proteolysis of troponin-T and high shear force [143, 144]. While the myofibrillar protein degradation proceeds, the muscle's connective tissue is relatively stable in the postmortem period [145].

As beef tenderness is a bigger issue, most studies regarding other parameters influencing tenderness were performed with beef: Muscle temperature [146, 147] and color [148, 149] of beef have not been found to be useful predictors for tenderness. However, other studies revealed significantly better shear force values if meat was cooled to 14° C in the pre-rigor period [150] and showed the beneficial influence of level and rate of cooling during the onset of *rigor mortis* for beef tenderness [151]. Diverging results on using early postmortem pH were reported for the prediction of beef tenderness, but some authors stated that the rate of glycolysis and thus pH decline can affect changes in meat tenderness [152–154]. Similar results were found in pork [155, 156]. Here, the pH decline within the initial stages of rigor plays a major role due to the activity of pH-dependent proteases. However, the pH measured 3 h p.m. (alone) can not be used as a criterion for sorting beef carcasses into tenderness groups [157]. The same study also stated that pH_{48} can be discarded as a predictor for tenderness. Accordingly, ultimate pH was reported to be only loosely correlated with shear force with $r = -0.26$ [94]. On the other hand, tenderness of twelve bovine *M. longissimus thoracis* (LT) muscles were shown to be correlated with ultimate pH with $r = 0.83$ [93]. However, the sample sizes was very low in the latter study, hence ultimate pH may only be moderately correlated to tenderness.

2.2.4. Classification of Meat Quality

PSE and DFD meat are extreme examples of meat quality. Besides these extremes, several intermediate qualities exist. For instance, in the early 1990's, reddish, soft and exudative (RSE) meat has been described at first [158–162]. The lack of a consistent relationship between color and WHC [110] manifests in the existence of RSE pork with acceptable color but high drip loss [105] and pale meat samples with low drip loss (pale, firm, non-exudative - PFN) [110]. Furthermore, a sixth group can be found: Acid meat. This quality is characterized by a high pH_{45} but unusual low ultimate pH which results in high drip loss and low fresh meat quality [90]. It was firstly described in the Hampshire breed in France, but can also be found in pigs of other breeds with a higher than normal muscle glycogen level.

In summary, quality traits required for the quality classification discussed in literature are pH_{45} , pH_{24} , drip loss and L^* value. Therefore, a flowchart (see Fig. 2.6) for the quality classification of pork meat ($N = 156$) was developed in the framework of the cluster project „Minimal Processing“ [163]. It is based on the parameters described in the literature which are summarized in publication 3. Here, drip loss was deemed the most important quality trait followed by pH_{24} , pH_{45} and L^* value. In the flowchart, the subclasses PSE- and DFD-tendency had to be introduced due to

- 26 samples which had high drip loss and pale color but did not meet the PSE criterion of $\text{pH}_{45} < 5.8$ and
- 8 samples with low drip loss and L^* values but with a pH_{24} between 5.7 and 6.0 hence samples which did not meet the DFD criterion of $\text{pH}_{24} > 6.0$.

The DFD-tendency samples also revealed lower than normal lactate concentrations 24 h *post mortem* indicating the reduced early postmortem acidification which is typical for

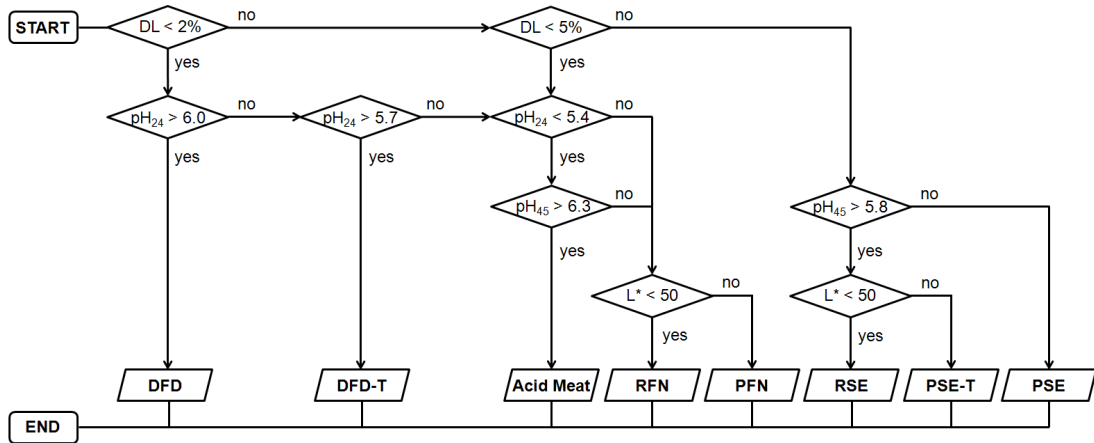


Figure 2.6.: Flowchart for the classification of meat quality based on drip loss (DL), pH_{24} , pH_{45} and L^* value.

DFD meat. The subclasses PSE- and DFD-tendency can also be found in literature as *slightly PSE* or *slightly DFD* [87].

2.2.5. Measurement of Quality Traits

In this section, the reference measurements for pH, drip loss, color ($L^*a^*b^*$) and shear force will be discussed. Firstly, the theoretical principles, the experimental designs and flaws of the standard techniques to measure the reference parameters are outlined and secondly, alternative (mostly spectroscopic) methods as well as advantages and disadvantages of those techniques are discussed.

2.2.5.1. The pH Value

The pH is a measure of the acidity or basicity of an aqueous solution and is defined as the negative decimal logarithm of the hydrogen ion activity a_{H^+} in a solution [164]:

$$\text{pH} = -\log_{10}(a_{H^+}) \quad (2.7)$$

Typically, the pH in meat is measured with puncture electrodes. In principle, the pH measurement is based on a voltage measurement of an electric potential difference between an internal reference and a glass electrode (in most cases, a pH electrode is used). As reference electrodes, a metal-ion compound such as silver/silver chloride or mercury/mercury chloride is commonly used. Its main characteristics are good reproducibility and high speed in which its equilibrium potential is adjusted.

The general technical flaws of puncture electrodes are numerous: The glass probe tip can easily break and must be kept wet at any times to avoid dehydration, the resistance of the diaphragm can deteriorate and the electrodes can oxidize which alters their conductivity. Advanced pH sensing systems minimize some of these disadvantages [165]. However, additional sources for erroneous pH measurements with puncture electrodes in meat are known such as contamination of the probe tip and diaphragm, technical malfunction of pH meters due to battery voltage, operating temperature or internal condensation on circuit components and failure to measure at sufficient or standardized depth [6]. Additionally, the meat is penetrated by the electrode which leads to sample destruction. The error of the pH measurement may be $\lesssim 0.01$ pH-units in aqueous solutions, but it is increased up to 0.05 pH-units when the ultimate pH of porcine LD

Table 2.2.: Overview of techniques for the pH measurement. Prep. = Sample preparation, NMR = nuclear magnetic resonance, VIS = visible, NIR = near-infrared, R = reflectance, A = absorption, T = transmission, FOP = fiber optical probe, HI = hyperspectral imaging, EI = electrical impedance, EC = electrical conductivity, inv. = invasive, LD = *M. longissimus dorsi*, TM = *M. teres major*, SM = *M. semimembranosus*, ST = *M. semitendinosus*, LDT = *M. longissimus dorsi thoracis*.

Method	Species (Muscle)	Samples	Prep.	R ²	RMSEC	Ref.
Electrode	Pork (LD)	34	no		<0.05 ^a	[166]
Electrode	Pork (LD)	296	no		0.05 ^b	[167]
³¹ P-NMR	Erythrocytes		yes			[168]
³¹ P-NMR	Pork (LD)	15	yes			[169]
¹ H-NMR	Pork (LD)	98	yes	0.21–0.49		[170]
NMR	Beef (LD) ^c	22	no			[172]
VIS-R	Pork (LD)	25+25	no	0.53–0.55		[174]
NIR-A	Beef (LD) ^c	12	no	0.07–0.53		[175]
NIR	Beef (LD) ^c	22	no			[172]
NIR	Pork (Duodenum)	6	<i>in vivo</i>	0.89–0.90	0.04–0.05	[173]
VIS-NIR	Pork (LD)	121+175	yes/no	0.59–0.71	0.08–0.09	[167]
NIR-R	Beef (6 muscles)	11	no	0.74	0.05	[94]
NIR-R	Rabbit (TM)	5	<i>in vivo</i>	0.98	0.02	[176]
NIR-R	Pork (LD, SM)	46	no/yes	0.14–0.63	0.08–0.12	[177]
NIR-T	Beef (6 muscles)	11	no	0.58	0.07	[94]
NIR-FOP	Beef (6 muscles)	11	no	0.61	0.06	[94]
NIR-HI	Lamb (ST, SM, LD)	42	no	0.72	0.08	[179]
NIR-HI	Pork (LD)	80	no	0.28–0.30 ^d	0.07	[180]
NIR-HI	Pork (LD)	75	no	0.87–0.91	0.08–0.10	[111]
L*a*b*	Beef (LDT)	31	no			[120]
EI+EC	Beef (LD)	47	inv.	<0.34		[182]

^a Averaged standard deviation (SD) for 3 ultimate pH measurements at the same slice

^b Within-sample SD of ultimate pH measurement

^c Early postmortem spectra

^d Cross-validation

muscle is measured [166, 167] and is even larger in early postmortem pork meat. Due to the numerous flaws of puncture electrodes, pH measurements are rarely performed in abattoirs.

Therefore, several spectroscopic techniques were investigated to (non-invasively) measure the pH *in situ* or *in vivo* such as nuclear magnetic resonance (NMR), near-infrared (NIR) and visible (VIS) spectroscopy and hyperspectral NIR imaging. In Tab. 2.2, an overview of the presented techniques is provided. In 1973, pulsed Fourier transform ³¹P-

NMR spectroscopy was shown to be able to determine intracellular pH in erythrocytes by using the chemical shifts of 2,3-diphosphoglycerate and inorganic phosphate [168]. Although the authors stated an accurate determination of the intracellular pH, no R^2 was provided. However, the samples had to be treated with carbon monoxide, and the integration time varied from several minutes to one hour. Other authors studied post-mortem changes in pig muscles ($N = 15$) achieving good agreement between ^{31}P -NMR and electrochemical pH values above pH 6.2, but below pH 6.2 they observed a systematic discrepancy [169]. Again, sample preparation was necessary: The muscles were dipped in paraffin oil and put into 10-mm NMR tubes. Using ^1H -NMR spectroscopy and preprocessed porcine LD muscles ($N = 98$), correlations with $r = 0.7$, $r = 0.69$ and $r = 0.46$ were found for pH_{30} , pH_{60} and pH_u , respectively [170]. A quantitative statistical discussion of the application of ^{31}P -NMR for *in vivo* pH measurements in breast carcinoma tissue showed errors of 0.04 pH-units due to baseline effects, whereas calibration uncertainties caused variations between 0.05 and 0.1 pH-units [171]. Using NMR measurements of the T_2 relaxation time of the water protons in early postmortem bovine LD muscle, a relatively clear separation between slow, medium and fast pH fall was observed in PCA score plots [172].

In the same study, VIS-NIR measurements (400–2498 nm) revealed only little variation and no consequent relation to pH. On the other hand, more promising correlations with NIR spectroscopy were achieved using partial least-square regression (PLSR) to predict the pH measured in the duodenum of six pigs during hemorrhagic shock [173]. The authors reported $R^2 = 0.90$ during ischemia (anaerobic metabolism) and $R^2 = 0.89$ during reperfusion (aerobic). However, to compensate for systematic discrepancies between different animals, subject-specific offsets had to be applied. By this means, an averaged root mean squared deviation of 0.042 and 0.045 pH-units was calculated for ischemia and reperfusion, respectively. With VIS-NIR spectra in the range from 400–2500 nm, pH_{24} was predicted with RMSECV's between 0.09 and 0.11 pH-units using a calibration and validation set of 121 and 175 intact and minced porcine LD muscles, respectively [167]. These predictions are promising considering the within-sample standard deviation of 0.05 pH-units. Comparing different techniques of near-infrared spectroscopy (reflectance, transmittance, fiber optics (FOP)), best correlation with pH ($r = 0.74$) was achieved using reflectance spectra [94]. However, the study used six different muscles from only eleven steers. Using a fiber optic probe, the reflectance spectra between 600 and 700 nm and 25 normal and 25 PSE porcine LD muscles revealed a moderate correlation with pH_{24} of R^2 between 0.53 and 0.55 [174]. Likewise, a moderate correlation coefficient of $r = -0.27$ to -0.73 was reported between pH_{45} and the absorbance of different wavelengths in the near-infrared (700–1000 nm) by bovine LD muscles [175]. Investigations with five *teres major* (TM) muscles from rabbits during ischemia and reperfusion showed a close correlation ($R^2 = 0.98$) between near-infrared reflectance spectra and muscle pH in the range 6.4–7.1 [176]. More closely related to this thesis, an attempt to predict the pH of intact and minced porcine LD ($N = 46$) and SM ($N = 46$) muscles using reflectance spectra in the visible and near-infrared region yielded R^2 of 0.14–0.63 and RMSEC of 0.08–0.12 pH-units [177]. Astonishingly, no difference between intact and minced samples was found. However, no validation was performed.

In neither of these studies investigating near-infrared spectroscopy, the accuracy of the pH measurements was satisfying when applied to (pork) meat. Also, no detailed information were given what spectral features were used for the pH prediction or how differences in the pH value were reflected in the NIR spectra. That is explained by two major flaws of NIR spectroscopy:

1. The measurement of (N)IR spectra of biological matter is complicated by its high

water content. In general, the water molecule reveals vibrational transitions, which give rise to the increasing absorption from the visible to the mid-IR region. Especially the μ -band around $6.3\ \mu\text{m}$ ($1650\ \text{cm}^{-1}$) produces a broad absorbance across the fingerprint region between 500 and $1800\ \text{cm}^{-1}$ [178].

2. The overtones of fundamental molecular vibration modes are measured, which are often overlapped to yield broad bands that do not provide high resolution spectroscopic fingerprints. This limits the accuracy of the biochemical profiling of biological tissue – especially of meat – with NIR spectroscopy [48].

The traditional NIR systems have another disadvantage of measuring relatively small spots hence requiring several measurements to obtain an averaged result that may still be not truly representative. Furthermore, samples exhibiting variation within the assessed region regarding their composition of meat, fat and connective tissue can affect the results according to the location of the measurement. Therefore, hyperspectral NIR imaging was developed which is capable of scanning the whole sample in the NIR wavelength range. A study investigating the application of this technique (900–1700 nm) for the prediction of pH in lamb meat ($N = 42$) showed good correlations with $R_{cv}^2 = 0.65$ and $RMSECV = 0.09$ pH-units [179], but the pH variance was achieved by using samples of *semitendinosus* (ST), SM and LD muscles. This experimental flaw was avoided in a study using the same technique and 80 pork meat samples. With six selected wavelengths, only inferior results were achieved with coefficients of determination $R_{cv}^2 = 0.28 - 0.30$ and $RMSECV = 0.15 - 0.21$ pH-units [180]. Better correlations were recently reported with ultimate pH of porcine LD muscles ($N = 75$) with R^2 between 0.88 and 0.91 and RMSEC below 0.1 pH-units using different preprocessing methods for the NIR images and subsequent wavelength reduction [111]. These results have only slightly deteriorated under cross-validation ($R_{cv}^2 = 0.84 - 0.87$, $RMSECV = 0.10 - 0.11$ pH-units). However, it is unlikely that hyperspectral imaging will be implemented in on-line industrial application due to time constraints in image acquisition and pre- and post-processing routines of the image [181]. On the other hand, as the studies have shown, only 5–7 spectral channels were necessary to achieve similar results in comparison to models relying on the complete spectral range. In future, this could be used to design a much simpler instrument which may rapidly and non-invasively measure the pH in meat.

Using electrical impedance (EI) and conductivity (EC) measurements in the time frame from 7 hours to 7 days, low coefficients of correlation with $r < |0.58|$ were achieved using bovine LD muscle and pH values which were measured with a puncture electrode 2, 5 and 7 hours after slaughter [182].

To this point, no studies were published investigating the applicability of *in-situ* Raman spectroscopy for the measurement of pH in meat or any biological tissue.

2.2.5.2. Drip Loss

Five methods to measure the drip of post-rigor meat are known and used: (1) the press-drip method [183], (2) the capillary volumeter method [184], (3) the filter paper method [185] and (4) the direct measurement by bag drip [6] or (5) by suspending the meat sample in a box [186]. The last method was firstly described by Honikel and was used for the reference analysis in this work. Thereby, the drip loss is expressed as percentage weight loss. The error for the drip loss measurement using the plastic bag method was reported between 0.3 and 1.3 % [166] and 24 and 48 h p.m., an error of 1.1 and 1.3 % was found, respectively [167]. Using the box method, the reference error was 0.75 % [187].

Table 2.3.: Overview of techniques for the measurement of drip loss. Prep. = Sample preparation, inv. = invasive, NMR = nuclear magnetic resonance, VIS = visible, (N)IR = (near-)infrared, R = reflectance, A = absorption, T = transmission, FOP = fiber optical probe, HI = hyperspectral imaging, R-SF = reflectance spectrofluorometer, EI = electrical impedance, EC = electrical conductivity, LD = *M. longissimus dorsi*, ST = *M. semitendinosus*, SM = *M. semimembranosus*.

Method	Species (Muscle)	Samples	Prep.	R ²	RMSEC / %	Ref.
bag drip	Pork (LD)	34	inv.		0.3-1.3 ^a	[166]
bag drip	Pork (LD)	296	inv.		1.1-1.3 ^a	[167]
box drip	Pork (LD)		inv.		0.8 ^a	[187]
¹ H-NMR	Pork (LD, ST)	39	yes		2.0-2.1	[189]
IR	Pork (LD) ^c	41+66	no	0.79-0.89	0.9-1.4 ^b	[7]
NIR	Pork (LD)	312	yes		2.2-2.6 ^b	[188]
NIR	Pork (LD)	121+175	y+n	0.49-0.81	1.3-2.5	[167]
NIR	Pork (LD, ST)	39	no		2.4	[189]
NIR	Pork (LD) ^c	99	inv.	0.71	1.8	[190]
NIR	Pork (LD)	96	no	0.55	1.0	[135]
NIR-R	Beef (LD)	173/176	no	0.51-0.54 ^b	0.8-0.9 ^b	[191]
NIR-T	Beef (LD)	166/167	no	0.38-0.40 ^b	1.0 ^b	[191]
NIR-HI	Lamb (LD, SM, ST)	42	no	0.84	0.2	[179]
NIR-HI	Beef (LD, PM, ST)	27	no	0.89-0.92	0.2-0.3	[181]
NIR-HI	Pork (LD)	80	no	0.61 ^b	1.1-1.2	[180]
NIR-HI	Pork (LD)	75	no	0.86-0.91	0.6-1.0	[111]
VIS-R	Pork (LD, ST)	39	no		2.1	[189]
FOP	Pork (LD, ST)	39	inv.		2.5	[189]
R-SF	Pork (LD, ST)	39	no		2.3	[189]
EI+EC	Beef (LD)	47	inv.	0.11-0.23		[182]
EI	Pork (LD) ^c	99	inv.	0.5	2.5	[190]
Raman	Pork (LD) ^c	14	no	0.96	0.3 ^b	[7]

^a Averaged standard deviation from repeated DL measurements at the same slice

^b Cross-validation

^c Early postmortem spectra were used for the prediction

The drip loss measurement is time-consuming, invasive and can only be conducted some days (dependent on method) after slaughter. Therefore, several techniques were tested to replace the standard methods (see Tab. 2.3). Investigating the predictability of drip loss of minced porcine LD ($N = 312$), RMSECV's between 2.2 and 2.6% were achieved using near-infrared spectra and different chemometric approaches [188]. Compared to the reference error of 0.3-1.3% and the standard deviation in the data set of 3.1% the prediction accuracy was unsatisfactory. Similar prediction results were

achieved with NIR spectroscopy ($RMSECV = 1.6 - 2.6\%$) [167], a fiber optical probe (FOP, $RMSEC = 2.5\%$), a visual (VIS-R, 2.1%) and near-infrared (NIR, 2.4%) reflectance spectrophotometer, a reflectance spectrofluorometer (R-SF, 2.3%) and a low-field ^1H nuclear magnetic resonance instrument ($^1\text{H-NMR}$, $2.0-2.1\%$) [189].

Another study using fresh pork ($N = 99$) reported better results with $R^2 = 0.71$ and $RMSEC = 1.8\%$. Here, near-infrared reflectance measurements in the spectral range from 900 to 1800 nm were used which were obtained – early postmortem – 30 min p.m. [190]. However, the fiber optic probe used to obtain the NIR spectra was inserted in the LD muscle, it took 30 s to acquire a useful spectrum with this instrument and the accuracy of this method was still too low. Another study using near-infrared reflectance spectroscopy achieved better correlations with $R^2 = 0.55$ and $RMSECV = 1.1\%$ [135]. Drip loss values and NIR-R spectra were obtained 2 days p.m. using 96 porcine LD muscles and were correlated using stepwise multiple linear regression and partial least squares regression. Using bovine LD ($N = 189$) and near-infrared reflectance and transmission spectra (935–2327 nm) measured at day 2 after slaughter, promising results were reported with $RMSECV = 0.9\%$ and 1.0% , respectively [191]. However, as the authors stated, with R_{cv}^2 in the range from 0.38 to 0.54, the accuracy of the predictive models under cross-validation seemed too low. Hence, in case of drip loss, the predictive power of classic NIR measurements is limited.

Using three muscles of lamb, a very good correlation ($R_{cv}^2 = 0.78$, $RMSECV = 0.3\%$) between drip loss and hyperspectral NIR images was reported [179]. Similar results were reported by the same group with bovine LD, *M. psoas major* (PM) and ST muscles [181]. However, as different muscles were included in a single PLSR model to increase the variance in DL, it seems reasonable to assume that the different color of the muscles was exploited by the PLSR model to indirectly “predict” the DL. Another perspective is provided by a third study in which the same technique was investigated, but here, the authors used only porcine LD muscles ($N = 80$). Good correlations ($RMSEC = 1.1-1.2\%$, $R_{cv}^2 = 0.61$) were achieved with six selected wavelengths, but the $RMSECV = 2.3 - 2.6\%$ seems, again, too high [180]. Better results were reported using also porcine LD muscle with $R^2 = 0.86-0.91$ and $RMSECV = 0.7-1.1\%$ evaluating different image preprocessing methods and using wavelength selection [111]. To this point, due to the contradictory results, it is difficult to evaluate the potential of this technique to predict the drip loss of meat, but, as stated above, it is unlikely that NIR hyperspectral imaging will be applied at the slaughterline due to the long acquisition times of the NIR images.

The drip loss was shown to be only weakly correlated with electrical impedance and conductivity measurements [182]. Accordingly, impedance measurements in another study were shown to have limited predictive power yielding a correlation of $r = 0.5$ and $RMSEC = 2.5\%$ with 24 h drip loss [190].

A study closely related to this thesis was published in 2003, investigating the early prediction of WHC in porcine LD muscle ($N = 41$) by infrared absorption and Raman spectroscopy [7]. Preliminary studies revealed a good correlation between early post-mortem IR spectra ($600-4000\text{ cm}^{-1}$) and drip loss ($r = 0.89$) which was later confirmed under industrial conditions with 66 pigs ($r = 0.79$). Interestingly, Raman spectra were additionally obtained during the preliminary study 10–30 min after slaughter from the same muscle ($N = 14$). PLSR correlation yielded $r = 0.98$ and $RMSECV = 0.3\%$ using spectra from 500 to 3200 cm^{-1} . As the authors stated, such an extraordinary good PLSR model is perhaps unrealistic due to overfitting, which seems reasonable considering the low number of meat samples. However, it was also stated, that “it certainly deserves further attention in future studies”, but no further studies investigating the potential of Raman spectroscopy to measure or predict WHC or drip loss were published after

this. In the same study, several reference spectra of essential energy metabolites were presented and showed that the authors intended to work on the understanding of the early postmortem Raman spectra, but the use of a borrowed LabRam Raman microscope limited the number of samples to 14. Also, Raman spectra with only 2 repetitions and 60s integration time were measured with a 632 nm laser diode with only 5 mW reaching the sample. Hence, no detailed understanding of the early postmortem Raman spectra of (pork) meat was achieved in this study.

2.2.5.3. Color

In general, color can be expressed as a point in a three-dimensional color space such as the $L^*a^*b^*$ color space. Here, L^* represents the lightness, a^* represents red and green while b^* represents blue and yellow (see Fig. 2.7). Besides the CIE $L^*a^*b^*$, the CIE XYZ (see below) and the Hunter Lab color space are widely used.

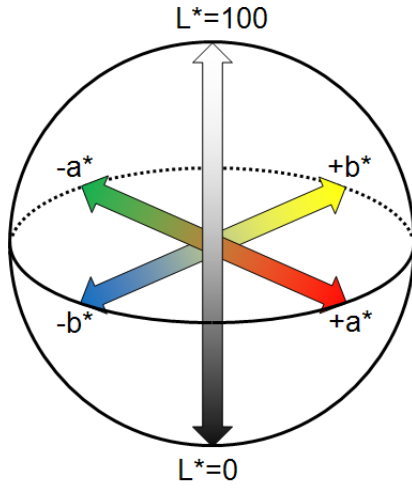


Figure 2.7.: Representation of the CIE $L^*a^*b^*$ color space.

The CIE $L^*a^*b^*$ values are defined via the color matching functions $\bar{x}(\lambda)$, $\bar{y}(\lambda)$ and $\bar{z}(\lambda)$, which are the numerical description of the chromatic response of the human observer and were experimentally determined in the late 1920's [192, 193]. On the one hand, these functions depend on the sensitivity of the human cone cells (see Fig. 2.8 left). On the other hand, due to the distribution of the cone cells in the eye, these functions also depend on the observer's field of view. Therefore, the color matching functions differ slightly from the cone sensitivity function as can be seen in Fig. 2.8 on the right-hand side. During the first experiments to determine the color matching functions, only the chromatic response within a 2° arc inside the fovea was measured which is why the name

CIE 1931 2° Standard Observer has become established. This angle was chosen due to the belief that the color-sensitive cone cells reside within a 2° arc of the fovea. In later years, 10° experiments were also conducted but these functions are less commonly used.

With $\bar{x}(\lambda)$, $\bar{y}(\lambda)$ and $\bar{z}(\lambda)$ and the spectral power distribution $I(\lambda)$ of the light source, the so-called tristimulus X , Y and Z values can be calculated:

$$X = \int_{380}^{780} I(\lambda)\bar{x}(\lambda)d\lambda \quad (2.8)$$

$$Y = \int_{380}^{780} I(\lambda)\bar{y}(\lambda)d\lambda \quad (2.9)$$

$$Z = \int_{380}^{780} I(\lambda)\bar{z}(\lambda)d\lambda \quad (2.10)$$

which span the CIE XYZ color space and are used to define the $L^*a^*b^*$ values:

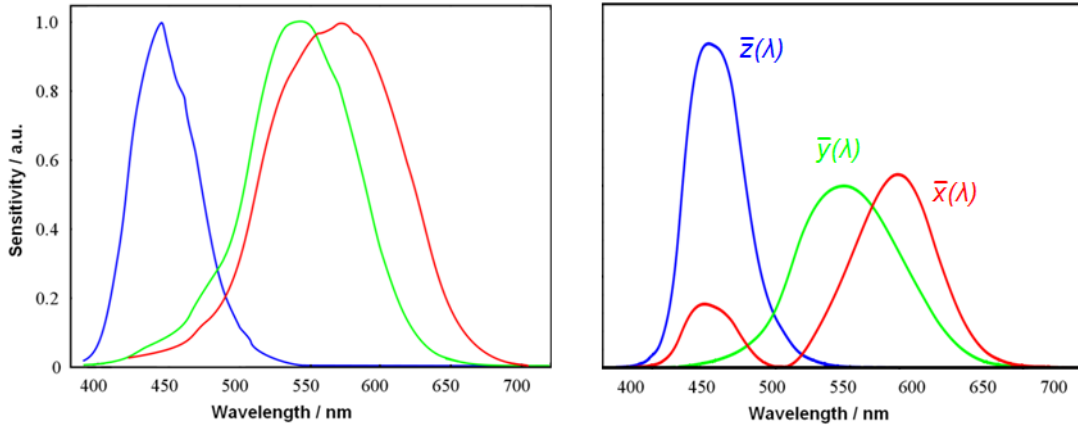


Figure 2.8.: (*left*) The sensitivity of human eye cone cells for short (blue), middle (green) and long (blue) wavelengths (based on data from [194]) and (*right*) the color matching functions $\bar{x}(\lambda)$, $\bar{y}(\lambda)$ and $\bar{z}(\lambda)$ of the CIE 1931 2° Standard Observer.

$$L^* = 116 f\left(\frac{Y}{Y_n}\right) - 16 \quad (2.11)$$

$$a^* = 500 \left[f\left(\frac{X}{X_n}\right) - f\left(\frac{Y}{Y_n}\right) \right] \quad (2.12)$$

$$b^* = 200 \left[f\left(\frac{Y}{Y_n}\right) - f\left(\frac{Z}{Z_n}\right) \right] \quad (2.13)$$

where

$$f(t) = \begin{cases} t^{1/3} & \text{if } t > \left(\frac{6}{29}\right)^3 \\ \frac{1}{3} \left(\frac{6}{29}\right)^2 t + \frac{4}{29} & \text{otherwise} \end{cases} \quad (2.14)$$

and where X_n , Y_n and Z_n are the normalized tristimulus values of a specified white object. Y_n is defined as 100 whereas X_n and Z_n are tabulated for different illuminants. The some-what odd definition for the L^* , a^* and b^* values is intended to mimic the nonlinear response of the human eye. Furthermore, uniform changes of components in the $L^*a^*b^*$ color space aim to correspond to uniform changes in the perceived color. The division of the domain of $f(t)$ into two parts was included to prevent an infinite slope at $t = 0$. As a small value of $\left(\frac{6}{29}\right)^3 \approx 0.009$ is arbitrarily chosen, the slope of the line must be equal to $\frac{1}{3} \left(\frac{6}{29}\right)^2$ to ensure differentiability in the domain of the function $f(t)$ while the intercept of $\frac{4}{29}$ must be chosen to ensure $L^*(0) = 0$. Finally, the scaling values 500 and 200 in equation 2.12 and 2.13 are included to increase the a^* and b^* values to the same order of magnitude as L^* (which is between 0 and 100).

Several different instrumental color measures are available which are not comparable due to different color spaces, illuminants, standard observers and aperture sizes [195]. In addition, it was stated that the blooming time prior to the color measurement with meat affected a^* and b^* (but not L^*) and therefore has to be considered if one intend to make comparisons. The error of the $L^*a^*b^*$ measurement was reported to be 3.1 for L^* , 1.0 for a^* and 0.9 for b^* [167] (see Tab. 2.4).

Table 2.4.: Overview of techniques for the L*a*b* measurement. Prep. = Sample preparation, VIS = visible, (N)IR = (near-)infrared, R = reflectance, T = transmission, HI = hyperspectral imaging, EI = electrical impedance, EC = electrical conductivity, LD = *M. longissimus dorsi*, SL = strip loin.

Method	Species (Muscle)	Samples	Prep.	R ²	RMSEC	Ref.
L*	Pork (LD)	296	no		3.1 ^a	[167]
Panel	Pork (LD)	21	yes	<0.1		[197]
NIR	Pork (LD)	121+175	yes+no	0.37–0.65	2.2–2.8	[167]
VIS-NIR	Beef (SL)	24	no	0.78–0.90		[199]
NIR-R	Beef (LD)	170/179	no	0.83–0.85 ^b	1.5–1.6 ^b	[191]
NIR-T	Beef (LD)	169/167	no	0.64–0.68 ^b	2.2–2.4 ^b	[191]
NIR-HI	Pork (LD)	80	no	0.62–0.74 ^b	1.8–2.1	[180]
NIR-HI	Pork (LD)	75	no	0.89–0.94	1.2–1.7	[111]
EI+EC	Beef (LD)	47	no	0.10–0.12		[182]
a*	Pork (LD)	296	no		1.0 ^a	[167]
NIR	Pork (LD)	121+175	yes+no	0.55–0.89	0.6–1.2	[167]
VIS-NIR	Beef (SL)	24	no	0.78–0.90		[199]
NIR-R	Beef (LD)	171/179	no	0.39–0.49 ^b	1.2–2.0 ^b	[191]
NIR-T	Beef (LD)	170/168	no	0.19–0.35 ^b	1.2–2.5 ^b	[191]
NIR-HI	Pork (LD)	75	no	0.82–0.86	0.4–0.5	[111]
EI+EC	Beef (LD)	47	no	0.10–0.14		[182]
b*	Pork (LD)	296	no		0.9 ^a	[167]
NIR	Pork (LD)	121+175	yes+no	0.58–0.77	0.8–1.1	[167]
VIS-NIR	Beef (SL)	24	no	0.78–0.90		[199]
NIR-R	Beef (LD)	171/178	no	0.73–0.75 ^b	0.8–1.0 ^b	[191]
NIR-T	Beef (LD)	170/168	no	0.44–0.56 ^b	1.1–1.5 ^b	[191]
NIR-HI	Pork (LD)	75	no	0.90–0.92	0.4–0.5	[111]
EI+EC	Beef (LD)	47	no	0.10–0.23		[182]

^a Within-sample standard deviation of L*, a* or b* measurement

^b Cross-validation

In contrast to pH and drip loss, the L*a*b* measurement is non-invasive, fast and the technique is robust, although the meat color early postmortem is not indicative for the ultimate color values 24 h p.m. [196]. Hence, rather few studies evaluated surrogate methods and techniques to measure meat color (see Tab. 2.4). For instance, panelists can be trained to evaluate meat color in the L*a*b* color space. Interestingly, the assessment of b* was difficult for the panelists whereas L* and a* were perceptible [197]. Using digital camera images may have distinct advantages over the traditional L*a*b* measurement such as representative assessment, accountability for surface variation in myoglobin redox state and convertibility in different color spaces. In addition to L*a*b*-values, sensory color scores of trained panelists can be predicted from digital

images with use of multilayer neural networks ($r = 0.75$) and a partial least squares method ($r = 0.52$) [198].

Good results were achieved with near-infrared spectroscopy for the assessment of $L^*a^*b^*$ values of intact and minced porcine LD muscles (calibration set: $N = 121$, validation set: $N = 175$) [167]. The authors reported minimal RMSECV of 2.4 for L^* , 0.8 for a^* and 0.9 for b^* in the calibration set and comparable results for the validation set [167]. Using near infrared reflectance (NIR) and visible spectroscopy, Hunter Lab values of beef meat (strip loins, SL) were predicted with good correlations ($R^2 = 0.78 - 0.90$) accounting for 55–90 % of the variability [199]. Likewise, good correlations between NIR-R and NIR-T spectra and L^* ($R_{cv}^2 = 0.85$) and b^* ($R_{cv}^2 = 0.75$) were reported [191]. Promising results were also achieved with R_{cv}^2 of 0.62–0.74 and RMSECV of 3.2–3.9 using hyperspectral NIR imaging to predict L^* values of pork meat [180]. The results were even improved recently and the potential of this method to measure a^* and b^* values was also shown [111]. In essence, NIR spectroscopy can accurately measure the current meat color, but, to date, no study investigating the predictability of $L^*a^*b^*$ values from early postmortem NIR spectra was published.

Likewise, no studies are yet published investigating the application of Raman spectroscopy to measure or predict meat color.

2.2.5.4. Shear Force

Tenderness is a complex quality trait because the objective measurement is complicated due to its multicausal nature [58]. Tenderness is influenced by several interacting factors such as the age of the animal, breed, collagen and fat content, cut, muscle fiber composition, pre- and post-slaughter handling, proteolytic enzyme activity, ageing and, of course, cooking time and temperature [58, 200]. Therefore, tenderness cannot be objectively measured by one method or technique. As a matter of fact, human panelists are usually the ultimate measure for tenderness. Due to the high costs of trained panelists, mechanical methods were developed of which the Warner-Bratzler shear force (WBSF) test is the most widely used and accepted objective parameter if tenderness is evaluated. On the one hand, it yields high correlations with sensory panel scores for tenderness [147, 157], but on the other hand, the mechanically determined shear force was also reported to be poorly correlated ($R^2 = 0.15$) with tenderness in another study [46]. The method is destructive, time-consuming and has a high margin of error (see Tab. 2.5).

Alternative methods to replace the classic WBSF measurement are summarized in Tab. 2.5. Many of these studies used beef cuts because tenderness is an issue in bovine muscles but less important in pork. Using a visible near-infrared spectrometer (400–2500 nm) and different subprimals ($N = 100$) from beef carcasses, only a low correlation was found between the observed and predicted shear force which indicated that the VIS-IR system did not predict specific tenderness values [201]. VIS-NIR spectra were measured at 2 d p.m. while WBSF was obtained 14 d after slaughter.

Numerous studies using near-infrared reflectance spectroscopy were published investigating its potential to predict WBSF. The first study in this field was published in 1991 [94]. High correlation coefficients were obtained for WBSF of beef cuts with $r = 0.80 - 0.83$ using three different techniques of near-infrared spectroscopy (reflectance, transmittance, fiber optic probe). However, six different muscles were combined in this study, which leaves the question whether the prediction of WBSF would be equally promising if only one muscle was used. In a second study, reflectance and transmission mode were compared using ten bovine LD muscles [202]. Principal component regression (PCR) yielded correlation coefficients in the range from $r = 0.54 - 0.89$ and $RMSECV = 6 - 10$ N for the reflectance spectra. The predictive ability of the transmit-

Table 2.5.: Overview of techniques for the shear force measurement. Prep. = Sample preparation, WBSF = Warner-Bratzler shear force, VIS = visible, (N)IR = (near-)infrared, R = reflectance, T = transmission, . FOP = fiber optic probe, HI = hyperspectral imaging, USE = ultrasonic elastogram, EI = electrical impedance, EC = electrical conductivity, SM = *M. semimembranosus*, LD = *M. longissimus dorsi*, LL = *M. longissimus lumborum*, LDL = *M. longissimus thoracis et lumborum*.

Method	Species (Muscle)	Samples	Prep.	R ²	RMSEC / N	Ref.
WBSF	Pork (SM)	64–156	yes		4–5	^a
VIS-IR	Beef (Rib eye)	100	no	low ^b		[201]
NIR-R	Beef (6 muscles)	11	no	0.83	6.2	[94]
NIR-R	Beef (LD)	10	no	0.29–0.79	5.7–10.4 ^c	[202]
NIR-R	Beef (LD)	70	no	0.37–0.67		[203]
NIR-R	Beef (LD)	119	no	0.67	12.0	[204]
NIR-R	Beef	48	no	0.52–0.83		[205]
NIR-R	Beef (LD, SM)	75	no	0.26 (LD)		[206]
NIR-R	Beef (LD) ^d	127	no	0.47–0.55	14.9–18.1 ^c	[207]
NIR-R	Pork (LD)	96	no	0.20	7.0	[135]
NIR-R	Beef (LD)	172–174	no	0.12–0.25 ^c	7.7–11.2 ^c	[191]
NIR-R	Beef (LL)	768	no	^b		[208]
NIR-R	Beef (LD)	146+146	no	0.22–0.38		[210]
NIR-T	Beef (LD)	167–170	no	0.15–0.41 ^c	8.0–9.6 ^c	[191]
NIR-T	Beef (6 muscles)	11	no	0.80	6.8	[94]
NIR-T	Beef (LD)	10	no	low ^b		[202]
NIR-FOP	Beef (6 muscles)	11	no	0.80	6.8	[94]
NIR-HI	Beef (2 muscles)	44+17	no	0.45		[211]
USE	Beef	?	no	0.72–0.95		[212]
EI+EC	Beef (LD)	47	no	0.42–0.46		[182]
EI	Lamb (LL)	6	no	0.23/0.97		[213]
Raman	Beef	52	yes	0.75	6.3 ^c	[46]
Raman	Pork (LD)	54	yes+no	0.77	10.8–11.0 ^c	[44]
Raman	Sheep (LDL)	70+70	yes	0.79–0.83	2.4–3.0	[45]

^a This work

^b No r or R^2 values were provided

^c Cross-validation

^d Early postmortem spectra

tance spectra was poor due to a small wavelength range (850–1050 nm). Similar results were achieved using 70 heifers with the same spectroscopic (750–1098 nm) and chemometric approach with r between 0.61 and 0.82 for the correlation with WBSF [203]. By expanding the spectral range to 1100–2498 nm, good results were reported for PLSR

($R^2 = 0.67$, $RMSEC = 12$ N) and MLR ($R^2 = 0.67$) calibration models using *M. longissimus thoracis* (LT) of beef ($N = 119$). Equally good PLSR validation results ($R^2 = 0.63$, $RMSEP = 13$ N) were reported using bovine LD muscles [204], which is also comparable to a later study in which prediction models from NIR spectra yielded coefficients of determination of 0.52–0.83 [205]. Contrary to those findings, only a moderate correlation with $r = 0.51$ was found for bovine LD muscles and no useful prediction was achieved for the SM muscle [206]. Another study using NIR spectroscopy (1100–2500 nm) found that the spectral changes during *rigor mortis* were not related to the ageing potential of the individual beef loin samples ($N = 127$) [207]. Accordingly, the authors reported only low correlation coefficients from 0.47 to 0.55. In newer studies, *no correlation* between WBSF and NIR reflectance spectra was found using pork meat [135]. Accordingly, with bovine LD muscles ($N = 189$) low coefficients of determination during cross-validation (R_{cv}^2) of 0.12–0.25 and 0.15–0.41 were reported using near-infrared reflectance and transmission spectra, respectively [191]. In the same study, the prediction of WBSF measured at day 8 after slaughter from NIR-R and NIR-T spectra from day 2 yielded only low correlations with $R_{cv}^2 = 0.19$ and 0.15, respectively. In summary, NIR spectra revealed good correlations with WBSF in some cases but, in general, this technique lacks the required accuracy.

Nevertheless, portable NIR-R instrumentation was developed [208] and is commercially available for the classification of beef carcasses [209, 210]. In a large study using 768 bovine *longissimus lumborum* (LL) muscles, the NIR system was able to sort tough from tender LL samples to 70 % certification levels [208]. Shackelford et al. have developed a commercially available tenderness prediction system based on visible and near-infrared reflectance spectroscopy that could be used on-line to identify carcasses that excel in longissimus tenderness [209, 210].

Another approach has shown that extracting wavelet textural features from ultrasonic elastogram (USE) images can predict WBSF scores after aging for 2, 14, 28 and 42 days with promising R^2 's between 0.72 and 0.95 [212]. In contrast, electrical impedance and conductivity measurements were only moderately correlated with WBSF of bovine LD muscle ($N = 47$) yielding $r = 0.68$ and -0.65 , respectively [182]. More recently, high resolution impedance spectroscopy was reported to be used to screen meat into tender or tough categories at 1 day p.m. ($R^2 = 0.97$), but in the same study, no significant correlation ($R^2 = 0.23$) with 5-day shear force was found [213].

In this very active field, Raman spectroscopy already proved its usefulness in a preliminary study with roasted beef silversides, which were measured on a rotating stage using a 785 nm laser source [46]. As the spectra were obtained, the sample rotated with the long axis of the myofibrils perpendicular to the incident beam. PLSR correlations were promising with $R^2 = 0.75$ and $RMSECV = 6.3$ N while the standard deviation of the SF data was 9.5 N. The same group reported similar results using raw and cooked porcine LD muscles ($N = 54$) [44]. Using the hand-held device described by Schmidt et al. [3], the shear force values of 140 *longissimus thoracis et lumborum* samples from two sheep flocks were correlated with Raman spectra [45]. Prior to the Raman measurements, the samples were aged for five days, deep frozen and thawed. Good correlation models were derived with $R^2 = 0.79$ and 0.83 for the separate data sets of the two flocks. A joint model performed less good ($R^2 = 0.72$) due to the different origins of the sheep. In summary, promising results were achieved in three studies with use of Raman spectroscopy and meat samples which were roasted, aged or frozen and thawed, but the predictive potential for WBSF of *early postmortem* Raman spectra from *untreated* meat samples is yet to be investigated.

3. Material & Methods

This chapter provides an overview of the conducted reference measurements, describes the portable Raman system and the relevant features of the self-written control software, which were both developed in the framework of this thesis, and introduces the means of data analysis applied in this work.

“Facts have to be discovered by observation, not by reasoning.”

Bertrand Russell

3.1. Meat Samples and Reference Measurements

In this work, porcine *M. semimembranosus* (SM) was used for the experiments which is colloquially referred to as topside.

Drip loss measurements were performed as follows: A sample of 100–200 g was cut from the muscle which was stored for 24 h p.m., its mass was measured and subsequently, it was suspended in a box. For additional 48 h, the sample was stored at 4° C. The final measurement was conducted after 72 h p.m. by weighing the sample again. Finally, the drip loss was expressed as percentage weight loss.

For color measurements, a Minolta CR400 (Konika Minolta, Japan) was used in this work, which can directly measure X , Y and Z (see equations 2.8 - 2.10) by illuminating the meat with a lamp with known spectral power distribution $I(\lambda)$. The light reflected by the meat surface passes through red, green and blue glass filters which simulate the color matching functions $\bar{x}(\lambda)$, $\bar{y}(\lambda)$ and $\bar{z}(\lambda)$. A photo-detector behind the filter detects the transmitted light. This gives the X , Y and Z values which can be converted into the $L^*a^*b^*$ color space.

Shear force values were determined in this work after 24 h, 72 h and 7 days using a Warner-Bratzler system (Instron Series 5564, Instron Deutschland GmbH, Pfungstadt). The samples were frozen immediately after removal from the muscle. 24 h prior to the shear force measurement, the samples were thawed at 2° C and afterwards, the mechanical shear force measurement was conducted as follows [214]: The meat samples were cut into 6x6 cm² sub-samples, vacuum-packed and subsequently cooked for 2 h at 85° C. Other methods exist in which the samples are cooked to an internal temperature of 72 or only 65° C [58]. Afterwards, they were unpacked and cut along the direction of the fiber into six 1x1 cm² sub-samples per sample. Using a V-shaped blade, the force necessary to shear through the meat (perpendicular to the muscle fibers) is measured in Newton. The maximum shear force is used as the Warner-Bratzler shear force. This measurement was repeated six times per sample, and only the mean value was used for further analysis.

3.2. Raman Setup

The experimental setup used for this work is schematically presented in Fig. 3.1. The *optode* contains the laser and the optical components in a modular design which allows the exchange or adaptation of all system components. All precision mechanical parts were manufactured in the workshop of the University of Bayreuth. Its concept was inspired by

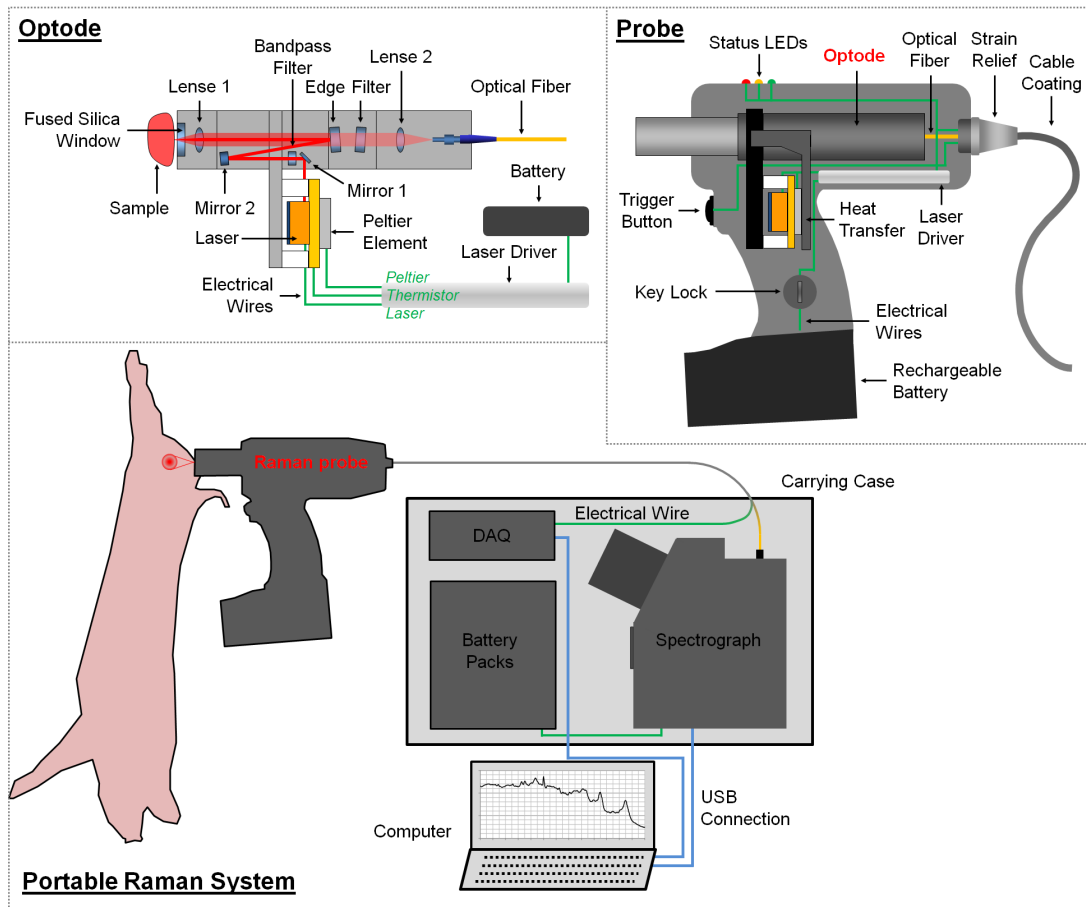


Figure 3.1.: Schematic diagram of the Raman optode, probe and portable system.

a SERS optode developed for *in situ* chemical detection in seawater [215] and its design was adapted to allow measurements with meat [3]. To this end, a 671 nm diode laser module was implemented [216, 217]. The unusual excitation wavelength was chosen to minimize the absorption by meat as (oxy-)myoglobin and oxy-hemoglobin, the main muscle pigments, reveal minimal absorption in this wavelength area [218, 219]. The injection current and the temperature (via a Peltier element) of the laser module are controlled by an OEM laser driver (RGB Lasersysteme GmbH, Kelheim, Germany). The temperature is measured using a thermocouple which is placed between the diode laser and the Peltier element. When the temperature of the laser unit is reaching its pre-set window, the operator is alerted by a green LED light on top of the housing. The collimated beam of the laser is spectrally cleaned by a bandpass filter (671 nm, Transmittance >90 %, half width 10 nm) and folded onto the optical axis of the optode by two broadband dielectric mirrors and a Raman edge filter (laser wavelength 676 nm). The beam is focused by a lens with a focal length of 10 mm through a fused silica window (thickness 3 mm) onto the sample. This results in a laser spot of about 50 μm diameter which is comparable to the diameter of the myofibrils. As the light is scattered partially back from the sample into the probe, the same lens is used to collect the back-scattered radiation. In the detection path, the Rayleigh scattered radiation is blocked by a Raman edge filter which is tilted against the optical axis. The misalignment of the beam induced by this tilt is corrected by the second edge filter. Using a lens with focal length

“Necessity is the mother of invention.”

Unknown

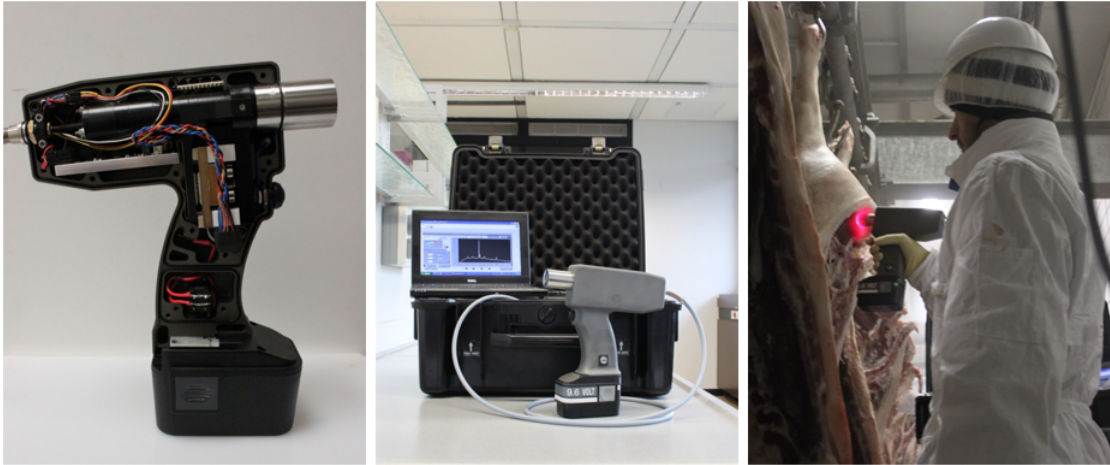


Figure 3.2.: (*left*) Raman probe with visible laser module, optode and laser driver, (*middle*) Raman system contained in a carrying case and (*right*) Raman measurements with the mobile system in the chiller of an abattoir.

of 16 mm, the Raman signal is launched into a single 105/125 μm optical fiber.

The optical ensemble was integrated into a robust housing shown in Fig. 3.1 on the right and in Fig. 3.2 on the left-hand side. In the following, this hand-held device is referred to as Raman *probe*. The housing comprises two hard anodized aluminum halves which were also manufactured in the workshop of the University of Bayreuth. Both halves are sealed by O-rings to protect the inside of the probe against dust and moisture. To keep it independent from external power supply, a rechargeable and exchangeable NiMH battery pack with a capacity of 3000mAh was chosen. The power supply is controlled by a key lock and indicated by a yellow LED light on top of the housing of the class 3B device. A Raman measurement can be started by pushing the trigger button and is indicated by a red LED light. Electrical wires and the optical fiber are protected against water, dust or physical stress by an armored cable with silicone coating which is connected to the housing via a strain relief.

In the framework of this thesis, the Raman probe was integrated into a portable system, which was developed to measure Raman spectra under conditions found in abattoirs. To this end, the hand-held Raman sensor head was connected by an optical fiber with a miniature spectrograph (HORIBA Jobin-Yvon, Longjumeau, France) with an optical resolution of 8 cm^{-1} and thermoelectrically cooled CCD detector operating at -10°C . The 671 nm diode laser is controlled by the OEM laser driver. The laser power can be adjusted in the range from 0 to 130 mW by varying the input voltage between 0 and 5 V at the laser driver. This voltage is generated by a digital data acquisition unit, DAQ (NI-USB 6008, National Instruments, Austin, TX, USA), which is connected via USB to a laptop computer. The system is controlled with a self-written LabVIEW (National Instruments, Austin, TX, USA) program which also captures and stores the Raman spectra. The trigger button is also connected to the DAQ unit and to the red LED light which indicates laser operation. The latter is recommended for laser systems in the amendment of the BGV B2 §7 II (German accident prevention regulation “Laser radiation”). For mobile usage, rechargeable battery packs with a capacity of 25 Ah were integrated to power the miniature spectrograph. The portable Raman system is depicted in Fig. 3.2, and it was successfully tested in commercial abattoirs under conditions with high humidity, low temperature and fluorescent light illumination.

Test Measurements

As the long-term stability of the calibration of the Raman system is of interest regarding the applicability of Raman spectroscopy, the peak position for the 999 cm^{-1} signal was calculated from polystyrene spectra over a period of 18 month. This was done by fitting the Raman peak with a Voigt profile $V(x)$, which is the convolution of a Gaussian $G(x)$ and Lorentzian profile $L(x)$:

$$V(x) = G(x)L(x) = \frac{1}{\sigma\sqrt{2\pi}} e^{-\frac{(x-x^*)^2}{2\sigma^2}} \cdot \frac{\gamma}{\pi((x-x^*)^2 + \gamma^2)} \quad (3.1)$$

$$= N \cdot e^{-\frac{(x-x^*)^2}{2\sigma^2}} \cdot ((x-x^*)^2 + \gamma^2)^{-1} \quad (3.2)$$

In equation 3.2, the normalization constants were combined into a single constant N . The Gaussian profile is included because the laser's beam profile is a normal distribution caused by Doppler broadening, while the Lorentz profile describes the natural shape of spectral lines. The typical shape of the Raman bands is described by a Voigt profile. By altering the peak position x^* , the width of the gaussian profile σ , the width of the Lorentzian profile γ and the normalization constant N of the Voigt profile, the root mean squared error (RMSE) between measured and fitted intensity was minimized. The fitted peak position x^* monitored over a period of 18 month is presented in Fig. 3.3. The peak position in the 18 month period scattered around an average peak position of 998.5 cm^{-1} with a standard deviation of 0.2 cm^{-1} . With an averaged wavenumber difference between two adjacent pixels of the CCD of 1.7 cm^{-1} and an optical resolution of the miniature spectrograph of about 8 cm^{-1} , this variance is small.

On the secondary axis of Fig. 3.3, the laser power of the Raman system is plotted. While it was adjusted to 80 mW , it was altering between 34 and 87 mW in this period. The variance was identified as the misalignment of a trim potentiometer of the laser driver electronics. This element is scaling the incoming electric voltage to the outgoing

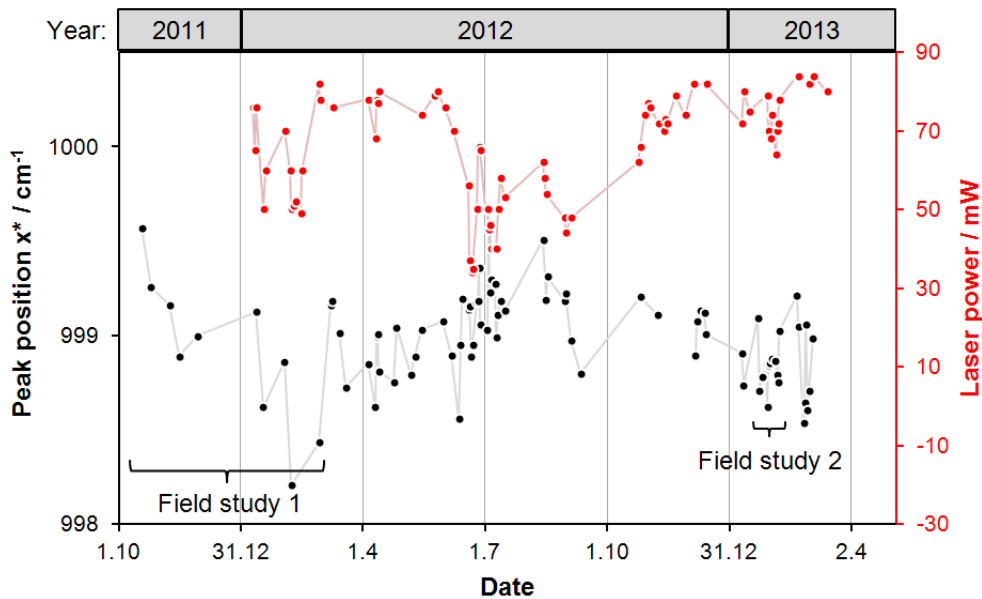


Figure 3.3.: Peak position of the 999 cm^{-1} peak of polystyrene (black dots) and the laser power (red) over an 18-month period. See section 4.3 for details regarding field study 1 and 2.

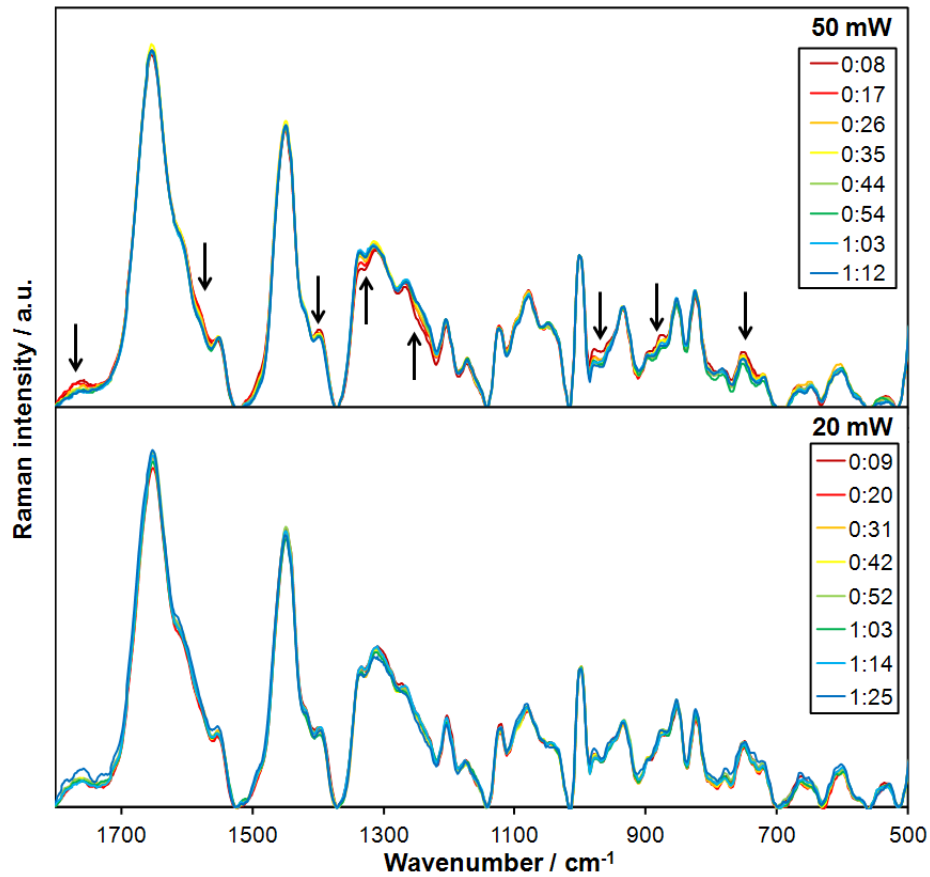


Figure 3.4.: Two Raman kinetics of pork meat with 50 and 20 mW laser power in continuous wave mode. Significant spectral changes due to exposure to laser radiation are marked with arrows.

laser current. Repeated cycles of warming and cooling may have caused this misalignment. This was solved by fixing the trim potentiometer with sealing wax. However, no correlation was observed between peak position and laser power.

In the beginning of this work, it was interesting to investigate whether the laser radiation would change the meat structure and the Raman spectra. This investigation also answers the question whether the position of the laser spot on the meat surface could be held constant or had to be changed between Raman measurements. Thus, Raman spectra from post-rigor pork meat were measured with different laser power settings and constant exposure to the laser radiation (continuous wave mode) to find the maximum laser power which does not alter the meat spectra. To this end, single Raman spectra with an integration time of X seconds were obtained every $(X + 5)$ s until 200 spectra were measured. X was increased with lower laser power to use the dynamic range of the CCD. The laser power was adjusted between 50 and 20 mW in 5 mW steps. For the presentation in Fig. 3.4, 25 spectra with an integration time of 10 and 20 s with a laser power of 50 and 20 mW were averaged and baseline-corrected (polynomial with mesh points), respectively. Apparently, the spectra measured with 50 mW laser power exhibit spectral alterations in the wavenumber range from 700 to 1800 cm^{-1} . These changes are different from cooking-induced changes reported in [47]. However, the reported changes in the amid III region (1225–1275 cm^{-1}) can also be observed in these spectra. These changes diminish with decreasing laser power, but they only vanish if the laser power is

reduced to 20 mW or below.

In a second experiment, Raman kinetics from early postmortem pork were measured with 20 mW laser power (not shown). To this end, Raman spectra of two excised, porcine *semimembranosus* muscles in the time frame 0.5–8 h p.m. were measured with constant position on the meat surface and compared to those kinetics in which the measuring position was constantly changed. With constant exposure, no spectral changes were observed. Apparently, even the reduced laser power of 20 mW inhibits the enzymatic activity in the muscle cells. Therefore, the position on the meat surface had to be constantly changed during the Raman measurements, and the laser power was adjusted to 80 mW. Due to the size of the laser spot of 10^{-8} – 10^{-9} m² in comparison to the meat sample of 10^{-2} – 10^{-3} m², it is very unlikely to hit a position again. Hence, the Raman spectra are mainly measured at metabolic intact spots of the meat surface.

3.3. Software

As the proprietary software provided by the manufacturer of the miniature spectrograph included only a limited range of functions, the software to control the spectrograph and the Raman probe was self-written in LabVIEW 9.0f3 (32-bit, Professional Version). The software's interface is depicted in Fig. 3.5.

“We are stuck with technology when what we really want is just stuff that works.”

Douglas Adams

As the program is started, a designated folder is created in the program's sub-directory named *yyyy-mm-dd* in which the current date is used for year (*yyyy*), month (*mm*) and day (*dd*). The Raman and dark spectra are saved as ASCII data in separate sub-directories as txt-files. The Raman spectra are saved in files named *file_name.txt* while the dark spectra are saved in files named *dark hh-mm-ss.txt* where the current time of day is used for hours (*hh*), minutes (*mm*) and seconds (*ss*). Additionally to the Raman spectra, a header comprising the current name, integration time, number of accumula-

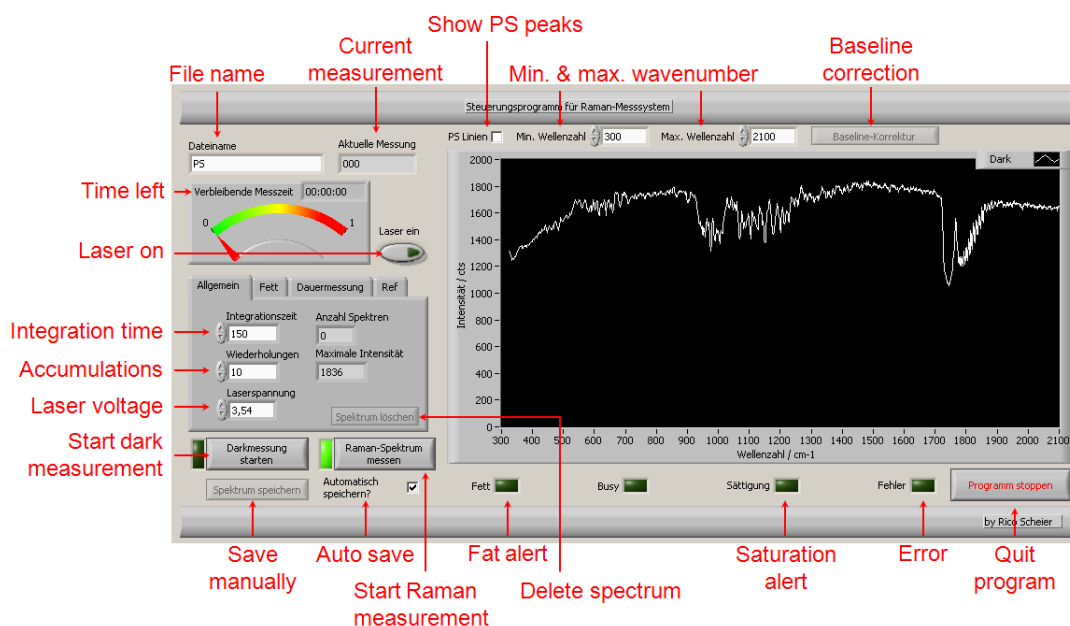


Figure 3.5.: Interface of the control software of the portable Raman system.

tions, date and time of day is saved in the txt-files. In case of dark spectra, only the integration time and the number of accumulations is saved. Each spectrum is automatically saved unless the “auto save” function is turned off. In this case, the Raman spectra can be manually saved¹. Unless the file name is altered, new Raman spectra will be saved as new columns in the same txt-file divided by tab stops. If the laser voltage, hence the laser power is changed, the time is saved in a separate file.

Polystyrene (PS) was measured as a calibration standard at the beginning of each day. Therefore, the strongest Raman signals of PS at 620, 999, 1154, 1447 and 1600 cm^{-1} can be superimposed to the current spectrum as red bars which serves as a rapid check of the calibration. In case of Raman spectra with very high fluorescence background, an automated baseline correction is already implemented in the software. The algorithm, which is described in section 3.4.1, can be applied to the currently measured Raman spectrum. Thereby, a polynomial is fitted to the Raman spectrum but only in the range defined by the minimum and maximum wavenumber, which also defines the section of the spectrum that is displayed.

The program was adapted to ease the work for untrained operators. For instance, measurements can be started by pushing the trigger button at the sensor head. This is done with use of the DAQ unit by measuring the voltage at the trigger button. In addition, continuative measurements can also be conducted with this program. To this end, a given number of Raman spectra can automatically be measured at predetermined time intervals. To reduce photo bleaching, the laser can be automatically turned of between Raman measurements.

An automated routine is implemented for the detection of saturated spectra. The CCD has a dynamic range of $2^{16} - 1 = 65535$ counts. Therefore, the software checks the *first* spectrum whether the intensity equals 65535 for any spectral channel. If so, the operator is warned by a lamp in the interface and an alert sound. In this case, the spectrum is not automatically saved. Only the first spectrum is checked as in most Raman spectra of biological samples which suffer from fluorescence background, this fluorescence can be reduced by bleaching upon laser radiation. Therefore, the first spectrum of a series of Raman spectra at one specific spot usually contains the highest background.

Likewise, an automated routine is implemented for the detection of fat based on the evaluation of the Raman spectra using a loading from a principle component analysis (see section 3.4.2). To this end, spectra of meat and fat of a series of measurements with pork muscle were used for a principal component analysis (PCA). The spectra were preprocessed with a 2nd derivative and 2nd polynomial Savitzky-Golay filter with a width of 15 channels [220] and then mean-centered. In Fig. 3.6, the fat pattern is identified as loading 1 based on the typical lipid signals [29–31], while loading 2 consists mainly of Raman signals assigned to meat proteins [18, 22–28]. As in section 3.4.2 discussed, the score value is the projection of the spectrum to a principle component. Hence, the score value the degree of the agreement between spectrum and loading. Therefore, the score values of loading 1 are correlated with the quantity of fat being detected by the measuring spots on the meat surface, while the score values of loading 2 indicate the agreement with the meat pattern. Thus, the dense cluster of data points near the y-axis of Fig. 3.7 represents the meat spectra while the fat spectra are located on the left-hand side. To determine a threshold which discriminates between meat and fat spectra, Raman spectra from the left-hand side are discarded and a new PCA is performed using the remaining spectra. The threshold is lowered until the fat pattern cannot be recognized within the first five loadings.

Accordingly, the software’s routine to detect fat is performing the following steps with

¹Raman spectra can be manually deleted at any time.

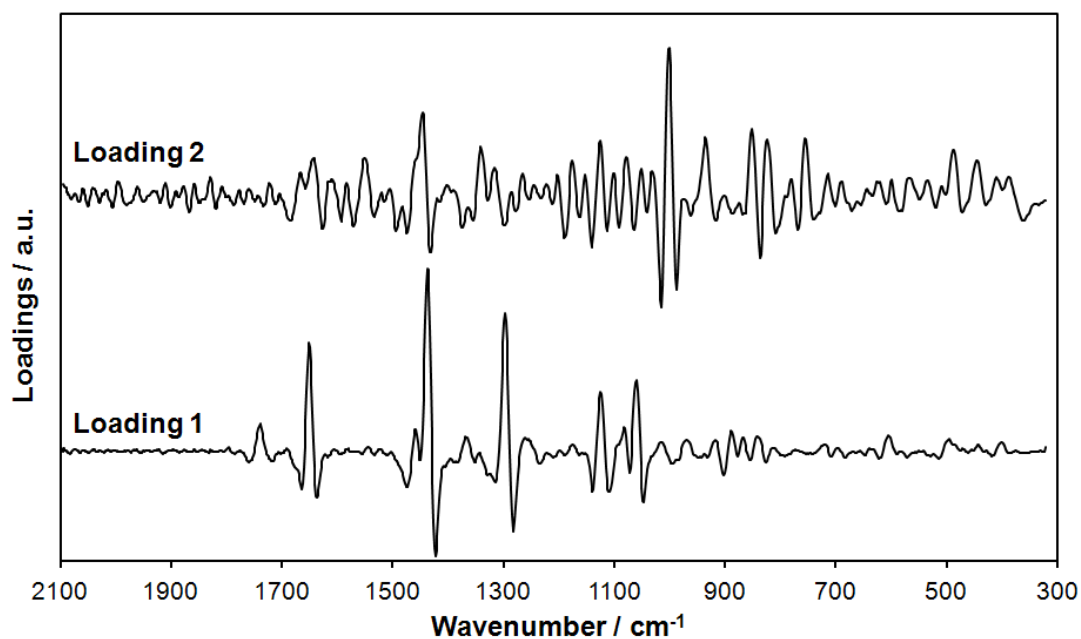


Figure 3.6.: The first two loadings of a principle component analysis with meat and fat Raman spectra.

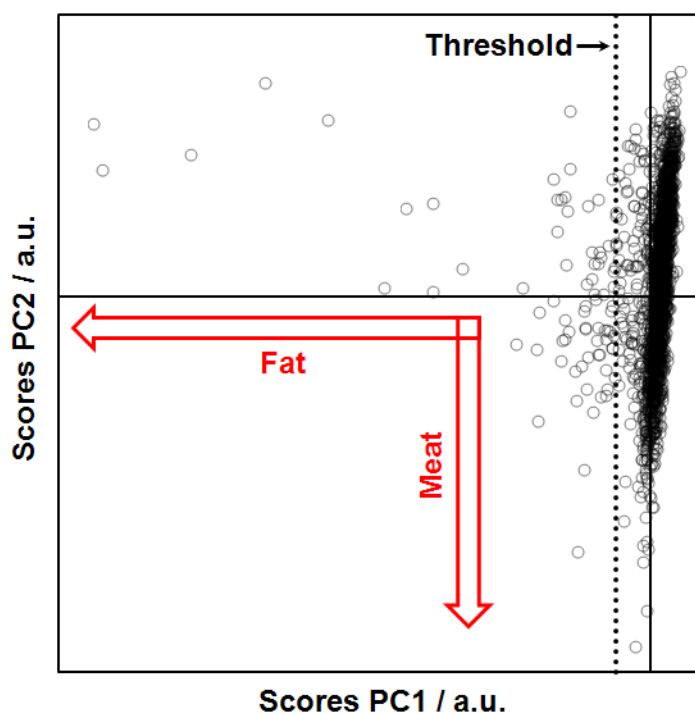


Figure 3.7.: Scores of PC1 vs. PC2 of the principal component analysis (PCA) used for Fig. 3.6 and the judiciously chosen threshold (dotted line) to differentiate between meat or fat spectra.

a newly measured Raman spectrum:

1. Savitzky-Golay filtering,
2. subtracting the stored mean spectrum,
3. calculating the dot-product with the stored fat loading and
4. comparing the result with the stored threshold value.

Depending on step 4, the spectrum is either saved as meat or as fat². Additionally, a warning sound is created and the fat alert lamp is turned on in the interface of the software.

3.4. Data Analysis

One of the challenges of using Raman spectroscopy for biological applications is the inherent fluorescence background typically caused by biological tissues that superimposes the measured Raman spectrum. The fluorescence can sometimes be several orders of magnitude more intense than the weak Raman signal and its presence must be minimized in order to analyze the Raman spectrum. Different methods to compensate or subtract the fluorescence background were applied in this work and will be briefly discussed in the following section. Besides, the spectroscopic data in this work consists of Raman spectra with 1024 channels and a large number of spectra was acquired to overcome the intrinsic heterogeneity of the biological samples. Hence, large quantities of data had to be analyzed. To this end, several chemometric methods are available of which two, principle component analysis and partial least squares regression, were applied and will be discussed in the following sections.

3.4.1. Baseline Correction

In general, the background curvature of a Raman spectrum can be estimated using a low-order polynomial. The most common way to define the polynomial is by mesh points, which are located in selected minima between the Raman bands. This is illustrated for a 5th-order polynomial with seven mesh points for the Raman spectrum of pork meat in Fig. 3.8A. To correct this spectrum, the polynomial is subtracted from the Raman spectrum. Although the procedure seems straightforward, it requires experience as the position of the mesh points have to be judiciously chosen by the user. A sufficient set of points is found if the corrected Raman spectrum consists only of positive numbers.

As the method requires user input, it is not suited for an automated baseline correction. Nevertheless, its basic principle is appealing. Therefore, an iterative polynomial baseline correction was used to automatically find the mesh points. This method is related to the algorithm presented in [221]. In the first iteration, a polynomial of n -th order is calculated to fit the spectrum in a defined wavenumber range. For instance, the 5th-order polynomial in Fig. 3.8B was calculated using the complete spectral range. Apparently, this function does not represent the background very well as it cuts through Raman bands. In the next step, the spectral channels with higher intensity than the polynomial are excluded from the data set. Then, the procedure is repeated with the reduced spectral data set. The following two iterations are also presented in Fig. 3.8B. With each step, the polynomial fits the background better. This is repeated until the number N of spectral channels being left in the spectral data set was $N \leq 25$. The method was

²All fat spectra are automatically saved in a separate sub-directory.

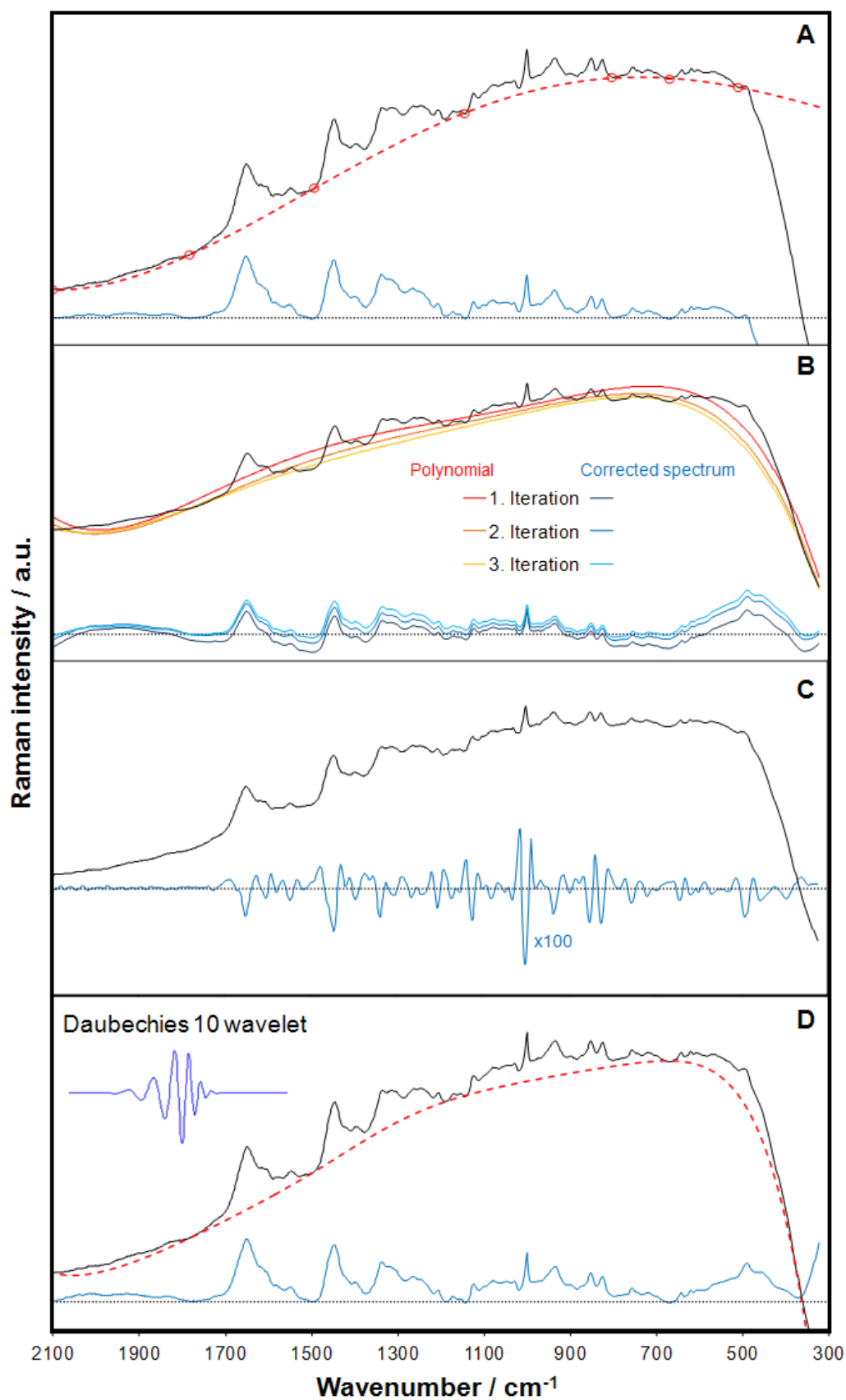


Figure 3.8.: Methods of baseline correction applied to a typical Raman spectrum of pork (black line) using (A) a polynomial with mesh points, (B) the iterative polynomial method, (C) Savitzky-Golay filtering and (D) wavelet and Fourier transforms (COBRA).

implemented in the control software presented in section 3.3 for the evaluation of Raman spectra with high fluorescence background.

A simpler way to remove background from spectral data is performed by calculating the 2nd derivative of the spectra using the parameters presented by Savitzky and Golay [220]. To this end, the dot product of the spectrum and the tabulated parameters is calculated and scaled with a normalization factor. In this work, the parameters of the 2nd polynomial and 2nd derivative order were used with a filter width of 15 spectral channels. In this case, the filtering for the x_n -th spectral channel is performed as follows:

$$y_{SavGol}(x_n) = \left(\sum_{i=1}^{15} a_i \cdot y(x_{n-8+i}) \right) / A \quad (3.3)$$

where a_i and A are the tabulated Savitzky-Golay parameters [220, 222]. The 2nd derivative Raman spectrum is illustrated in Fig. 3.8C. The main advantage of this method is its simple application. However, the spectra are more noisy and the interpretation of the spectra is complicated. Therefore, this method was only applied as a preprocessing step during the automated detection of fat spectra in the control software of the portable Raman system described in section 3.3.

Baseline correction can also be performed by wavelet transform. This method is often compared to Fourier transform in which the signals are represented by sums of sinusoids. Similarly, the signal is represented by wavelets in case of wavelet transform. The Daubechies 10 wavelet is presented in Fig. 3.8D. In the Fourier or frequency domain, a wavelet has the shape of a band pass filter. This is relevant because a typical Raman spectrum contains three frequency regimes: high frequency noise, medium frequency signal peaks and a low frequency background of which only the medium band is of interest. In this work, the baseline correction and smoothing was performed with the MATLAB based application COBRA [223]. Its main feature is an iterative algorithm based on wavelet transforms to remove backgrounds of spectroscopic signals. The algorithm works similar to the iterative polynomial baseline correction described above. In the first step, a discrete wavelet transform (DWT) decomposition is calculated using the complete spectrum which yields a first background fit. The original signal is then modified by taking all points above the fit and setting them equal to it. Subsequently, the DWT decomposition is repeated until the fit converges and it is yielding a fit very close to the real (physical) background. In this work, the Daubechies 10 wavelet was applied as it provided satisfactory results with Raman spectra of meat. The wavelet background fit is presented in Fig. 3.8D. For additional smoothing, the program comprises the fast Fourier transform algorithm, which transforms the Raman spectrum to the frequency domain in which low and high-pass filter are applied to further reduce background and noise. Subsequently, the spectrum is transformed back into the time domain. The COBRA program was used for the presentation of the Raman spectra in publication 3 (see section 4.3.1).

3.4.2. Principle Component Analysis

Principle component analysis (PCA) was invented in 1901 by Karl Pearson [224]. In essence, it aims for data reduction in high-dimensional data sets by extracting single patterns called principle components (PC), which provide as much information (maximal variance) about the data set as possible.

In multivariate data sets in which multicollinearity is present, the number of variables

“While it is easy to lie with statistics, it is even easier to lie without them.”

Attributed to Frederick Mosteller

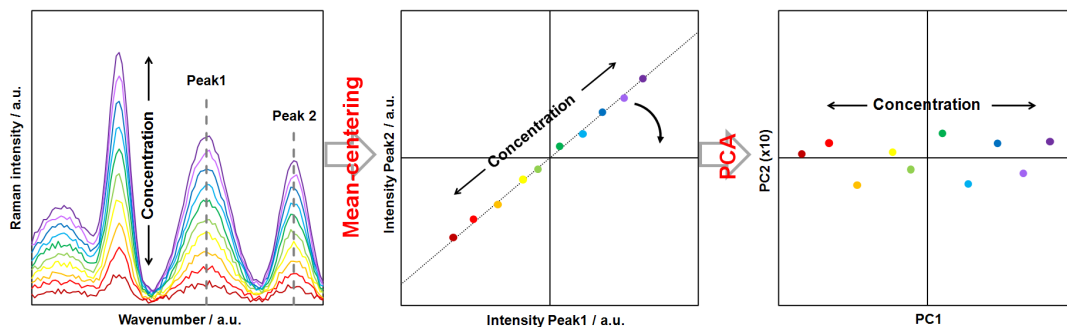


Figure 3.9.: Two dimensional visualization of the principle of PCA. (left) Simulated spectra of a calibration experiment, (middle) intensity of peak 2 vs. peak 1 after mean centering and (right) PC2 versus PC1 after PCA.

can be reduced without loss of *important* information. This is done by a transformation of the coordinate system. For Raman spectra, the original coordinate system is defined by the wavenumber and the intensity axis. Suppose the following example: In a calibration experiment Raman spectra of ten concentrations of a pure chemical are measured in aqueous solution. This gives the same pattern, the Raman spectrum of the chemical, but with varying intensities according to the concentration (see Fig. 3.9). For each concentration, a Raman spectrum with 1024 values is stored. PCA is providing a matrix which rotates the original coordinate system into a new one in a way that the first axis of coordinates possesses the highest variance. This axis is called the first *loading*. In the example, the loading is identical to the Raman spectrum of the pure chemical³. Accordingly, the coordinates of this axis are the concentrations of the chemical. The coordinates are called *scores*, which can be obtained by calculating the dot product of the spectrum and the loading. In the general case, the first axis is the loading with the highest variance and the scores are the projection on that loadings. Thereby, the score is a measure of the agreement between the spectrum and the loading.

In mathematical terms, PCA can be reduced to three steps. Firstly, the covariance of each combination of variables is calculated:

$$\text{Cov}(x, y) = \frac{\sum_{i=1}^N (x_i - \bar{x})(y_i - \bar{y})}{N - 1} \quad (3.4)$$

$$= \text{E}[(x - \text{E}[x])(y - \text{E}[y])] \quad (3.5)$$

Here, \bar{x} (or $\text{E}[x]$) and \bar{y} (or $\text{E}[y]$) are the mean (or expected) values of x and y . In case of Raman spectra, x and y are two data sets of Raman intensities of two, not necessarily different, wavenumbers and N is the total number of spectra. The calculation can be simplified as follows:

$$\text{Cov}(x, y) = \text{E}[(x - \text{E}[x])(y - \text{E}[y])] \quad (3.6)$$

$$= \text{E}[xy - x\text{E}[y] - \text{E}[x]y + \text{E}[x]\text{E}[y]] \quad (3.7)$$

$$= \text{E}[xy] - \text{E}[x]\text{E}[y] - \text{E}[x]\text{E}[y] + \text{E}[x]\text{E}[y] \quad (3.8)$$

$$= \text{E}[xy] - \text{E}[x]\text{E}[y] \quad (3.9)$$

However, the last equation is prone to catastrophic cancellation, i.e. when it is computed with floating point arithmetic it can yield $\text{E}[xy] \approx \text{E}[x]\text{E}[y]$ which yields $\text{Cov}(x, y) = 0$.

³The remaining 1023 loadings would only contain spectral noise and therefore could be discarded without loss of important information.

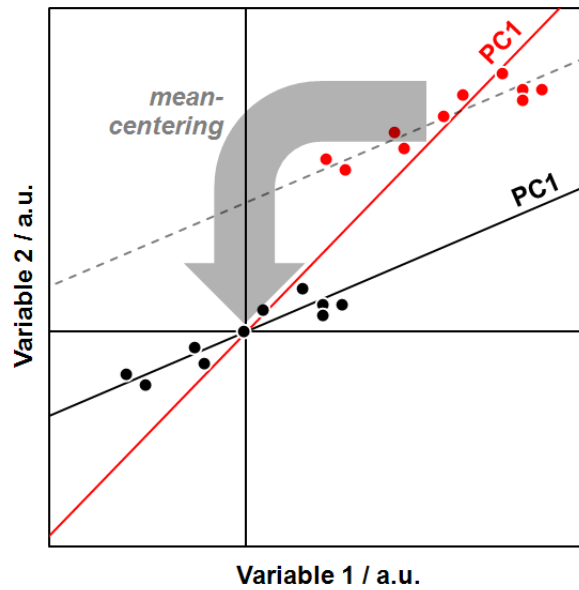


Figure 3.10.: The effect of mean-centering on PC1.

This can be avoided by mean-centering of the data, i.e. $x_i - \bar{x}$ is calculated for each x_i and repeated for each variable x , which yields $E[x] = E[y] = 0$. Mean-centering has another benefit which is illustrated in Fig. 3.10. Without mean-centering, PCA will yield misaligned principle components which do not contain the maximum variance. Therefore, it is considered mandatory for PCA and, in principle, for every multivariate statistical analysis.

In the second step of the PCA, the covariances are grouped as follows:

$$C^{n \times n} = \begin{pmatrix} \text{Cov}(x_1, x_1) & \text{Cov}(x_1, x_2) & \cdots & \text{Cov}(x_1, x_n) \\ \text{Cov}(x_2, x_1) & \text{Cov}(x_2, x_2) & & \vdots \\ \vdots & & \ddots & \vdots \\ \text{Cov}(x_n, x_1) & \cdots & \cdots & \text{Cov}(x_n, x_n) \end{pmatrix} \quad (3.10)$$

where x_j stands for the j -th spectral channel and n for the total number of spectral channels. This matrix is called the covariance matrix. As for $x = y$, the covariance $\text{Cov}(x, y)$ is equal to the variance $\text{Var}(x)$, the main diagonal of the covariance matrix comprises the variances of each spectral channel.

In the last step, the eigenvectors and eigenvalues of the covariance matrix are calculated. The eigenvectors of this matrix are the loadings while the eigenvalues are correlated with the variance of the loading, i.e. the eigenvector with the highest eigenvalue exhibits the highest variance.

In this work, PCA was performed using a self-written analysis software in LabVIEW (National Instruments, Austin, TX, USA). To this end, standard sub-VI's (virtual instrument) of the libraries *NI_Gmath.lvlib* and *NI_AALPro.lvlib* were used to calculate the covariance matrix and to solve the eigenvector and -value problem. Using this program, the loadings and scores can be conveniently visualized and be saved in txt-files for further analysis.

3.4.3. Partial Least Squares Regression

The origins of partial least squares regression can be traced back to the non-linear iterative partial least squares (NIPALS) algorithm by Herman Wold which was originally

developed to linearize models [225]. Later, this algorithm was adapted to overcome the overdetermined regression problem in which the number of variables is larger than the number of equations. That extension was termed *partial least squares* [226]. An alternative term for PLS (and more correct) is *projection to latent structures* [227], but the term partial least squares is still dominant in many areas.

In case of spectroscopic data, the number of spectral channels exceeds the number of measurements. Hence, methods like multiple linear regression (MLR) cannot be applied. Using principle component regression (PCR) or PLSR, predictors which are mostly one-dimensional or univariate data⁴, e.g. pH values can be correlated with the predictor variables which are multidimensional or multivariate data, e.g. Raman spectra. Although the methods aim at the same goal, their approach is different: While PCR attempts to capture the largest amount of variance in the predictor variables \mathbf{X} , MLR seeks a single vector which best correlates the predicted variables with the predictor \mathbf{Y} . This is why the latter cannot be applied if the number of predictor variables exceeds the number of measurements; it would result in over-determination. Hence, a perfect (but useless) correlation between predictor and predicted variables would always be calculated. PLSR is related to both PCR and MLR and can be thought of as occupying a middle ground between them. It attempts to find factors (latent variables) that maximize the amount of variation explained in \mathbf{X} that is relevant for predicting \mathbf{Y} . Hence, factors which contain variance and achieve correlation. Therefore, PLSR maximizes the *covariance*.

“Essentially, all models are wrong, but some are useful.”

Attributed to George E. P. Box

There are several ways to calculate PLSR model parameters [228]. Here, the NIPALS algorithm will be presented. It calculates scores \mathbf{t} , loadings \mathbf{p} (similar to those used in PCA, but the PLSR loadings are not orthogonal) and an additional set of vectors called weights \mathbf{w} (with the same dimensionality as the loadings \mathbf{p}). The weights are included to maintain orthogonal scores. This algorithm can handle multiple Y-variables. In such cases, scores (\mathbf{u}) and loadings (\mathbf{q}) are also calculated for the Y-data. The calculation is performed sequentially and started by choosing the column of \mathbf{Y} with the greatest variance as the starting estimated of \mathbf{u}_1 . The weights \mathbf{w} and scores \mathbf{t} of the X-data block are calculated as follows [229]:

$$\mathbf{w}_1 = \frac{\mathbf{X}^T \mathbf{u}_1}{\|\mathbf{X}^T \mathbf{u}_1\|} \quad (3.11)$$

$$\mathbf{t}_1 = \mathbf{X} \mathbf{w}_1 \quad (3.12)$$

Accordingly, in the Y-data block:

$$\mathbf{q}_1 = \frac{\mathbf{Y}^T \mathbf{t}_1}{\|\mathbf{Y}^T \mathbf{t}_1\|} \quad (3.13)$$

$$\mathbf{u}_1 = \mathbf{X} \mathbf{q}_1 \quad (3.14)$$

Now, \mathbf{t}_1 is compared with the value from the previous iteration. If they are equal within rounding errors, the algorithm proceeds with the next equation, otherwise it returns to the first equation using the \mathbf{u}_1 obtained in the current step. This is repeated until convergence is achieved, i.e. $\|t_n - t_{n+1}\| / \|t_{n+1}\| < \varepsilon$ where ε is between 10^{-6} and 10^{-8}

⁴PLSR can also handle multidimensional data.

[227]. Subsequently, the X-data block loading \mathbf{p}_1 is calculated and scaled:

$$\mathbf{p}_1 = \frac{\mathbf{X}^T \mathbf{t}_1}{\|\mathbf{t}_1^T \mathbf{t}_1\|} \quad (3.15)$$

$$\mathbf{p}_1^* = \frac{\mathbf{p}_1}{\|\mathbf{p}_1\|} \quad (3.16)$$

The scores and weights are rescaled accordingly:

$$\mathbf{t}_1^* = \mathbf{t}_1 \|\mathbf{p}_1\| \quad (3.17)$$

$$\mathbf{w}_1^* = \mathbf{w}_1 \|\mathbf{p}_1\| \quad (3.18)$$

In the next step, the regression coefficient b for the inner relation between X- and Y-data is calculated⁵:

$$b_1 = \frac{\mathbf{u}_1^T \mathbf{t}_1}{\mathbf{t}_1^T \mathbf{t}_1} \quad (3.19)$$

After the scores and loadings have been calculated for the first latent variable, the last step of the first iteration is reached. The X- and Y-block residuals are calculated:

$$\mathbf{E}_1 = \mathbf{X} - \mathbf{t}_1 \mathbf{p}_1^T \quad (3.20)$$

$$\mathbf{F}_1 = \mathbf{Y} - b_1 \mathbf{t}_1 \mathbf{q}_1^T \quad (3.21)$$

The entire procedure is now repeated using \mathbf{E}_1 for \mathbf{X} in equation 3.11, 3.12, 3.14 and 3.15 and \mathbf{F}_1 for \mathbf{Y} in equation 3.13 while all subscripts are incremented by one.

In this work, PLSR was performed with MATLAB 7.9.0 R2009b software (The Mathworks Inc., Natick, MA, USA) and PLS toolbox 6.2 (Eigenvector Research Inc., Wenatchee, WA, USA) which by default uses the SIMPLS algorithm which gives the exact same result as NIPALS for univariate, but a slightly different solution for multivariate, Y-data. As only PLSR correlations with univariate data were calculated in this work, SIMPLS is not presented. A detailed description of the algorithm can be found in [228].

To this point, it is still not obvious why this method is called *partial least squares* regression. The *least squares* is explained as each model parameter is iteratively estimated as the slope of a simple bivariate regression (least squares) between a matrix column or row of \mathbf{Y} and another parameter vector in \mathbf{X} . So, for instance, the PLSR weights \mathbf{w} are iteratively re-estimated as $\mathbf{X}^T \mathbf{u}_i / \|\mathbf{X}^T \mathbf{u}_i\|$ in the first step of the NIPALS algorithm. The *partial* in PLS indicates that this is a partial regression since \mathbf{u} is considered as fixed in the estimation in the second part of the NIPALS algorithm [227].

Note that the scores and loadings calculated in PLSR are not the same as those calculated in PCA or PCR, but can be considered as PCA scores and loadings that have been rotated to better predict \mathbf{Y} . As in PCR, the PLSR model converges to the MLR solution if the maximum possible number of latent variables is retained in the model. Hence, a criterion has to be found which defines the optimal number of latent variables for the PLSR model. This is usually done by cross-validation. In this work, the methods *leave-one out*, *contiguous blocks* and *random blocks* were applied. The difference is how the data splitting is handled (see Fig. 3.11). The contiguous blocks methods divides the X- and Y-block data, which contains N subsets, into s equally sized segments without altering the data's order. In case of the leave-one-out method, the segment size is 1 and $s = N$. In case of the random block method, the data's order is firstly randomized and subsequently split into s segments. Independently of the cross-validation method, a PLSR model is built using all but one of the segments, i.e. $(s - 1)/s$ of the available

⁵For simplicity in the following equations: $p_1^* = p_1$ and $t_1^* = t_1$.

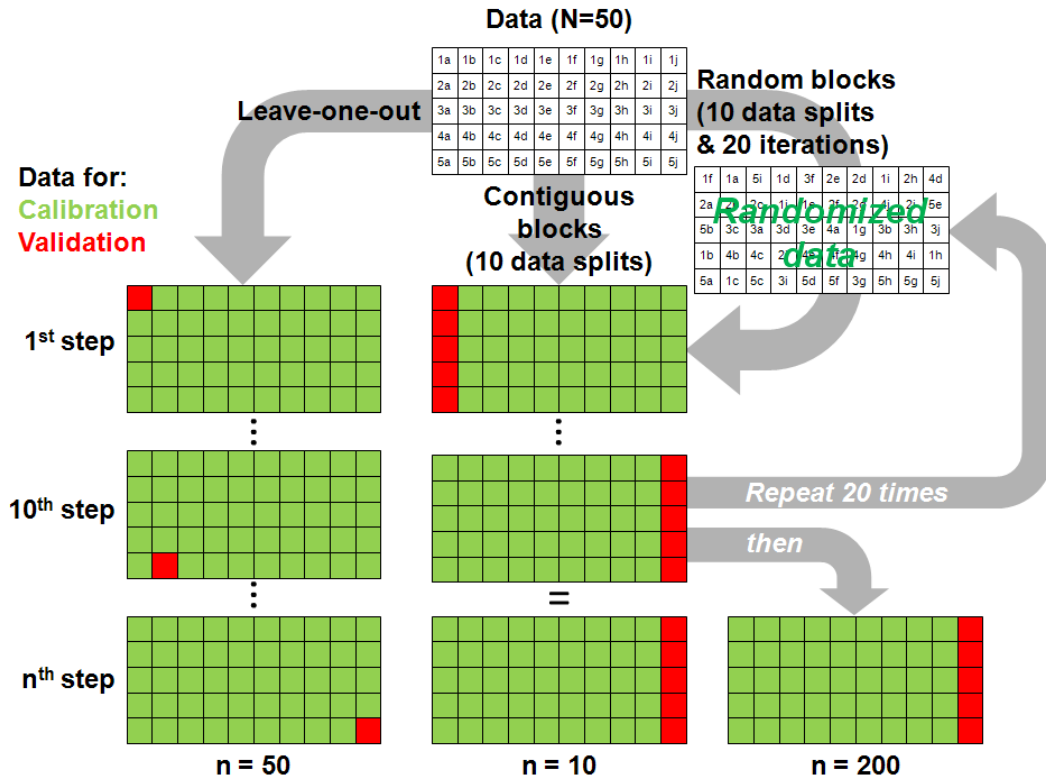


Figure 3.11.: Scheme of the data splitting for different cross-validation methods.

data. This data is called the training or calibration data set. The remaining segment is used to test the model. To this end, the predictions of X-block data calculated from the PLSR model (Y^{pred}) are compared to the Y-block data (Y) by calculation the root mean square error (RMSE) of the s -th segment:

$$RMSE_s = \sqrt{\sum_{i=1}^{N^*} (Y_i^{pred} - Y_i)^2} \quad (3.22)$$

Here, N^* is the number of data sets in the remaining segment. This is repeated for s segments and the root mean square error of cross-validation (RMSECV) is calculated:

$$RMSECV = \frac{1}{s} \sum_{i=1}^s RMSE_i \quad (3.23)$$

Hence, the RMSECV is defined as the average of the root of the squared difference between predicted and measured Y-block data. It is a measure of the predictive power of the PLSR model as it is solely derived from data which is not contained in the training data set. The minimum RMSECV is most commonly applied as the criterion to choose the number of latent variables. However, different CV methods yield different RMSECV's. The choice is dependent on the number of subsets and/or the internal structure of the data set. The leave-one-out method is mostly applied for small data sets with 20–40 subsets because in larger data sets, this method yields too optimistic results. The contiguous blocks method yields more realistic RMSECV's, but an internal structure in the data set may bias the result. Therefore, it is advisable to randomize the order of the subsets in the X- and Y-block data prior to the cross-validation. Hence, the random blocks method with the number of iterations equal or larger than 20 yield the

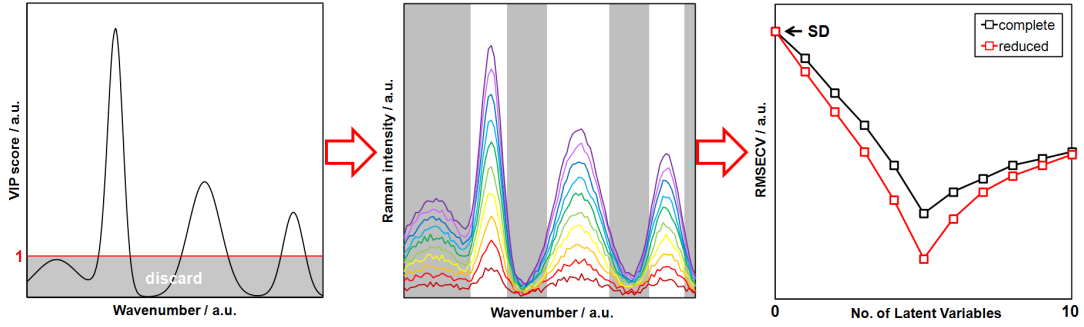


Figure 3.12.: Principle of VIP reduction and its effect on RMSECV. Step 1: Calculation of the VIP plot, Step 2: Discard spectral channels with $VIP < 1$, Step 3: Calculation of a new PLSR model.

least biased and most trustworthy results. But at the same time, this method requires much more computing time due to the number of iterations and the randomization prior to the data splitting. In this work, $s = 10$ was chosen, i.e. the data set was split into ten segments. This is a reasonable compromise because:

1. For $s \rightarrow N$, the method converges to the leave-one-out method, and the RMSECVs will become unrealistically optimistic due to the decreasing number of subsets used for the validation.
2. For $s \rightarrow 2$, the number of subsets used for the calibration is continuously decreasing. In case of data sets with large variance but relatively small number of subsets, this may lead to unrealistically poor RMSECV's because data, important to build the calibration model, is used for validation.

An important question in this context is: Which predictor variables (spectral channels) are most relevant for the correlation with the predictor (reference parameter)? Several methods to answer this question are known such as stepwise regression, selectivity ratio or variable importance in projection (VIP). In this work, VIP was chosen due to its good performance when multicollinearity is present in the data set (which is the case for Raman spectra) and when applied for variable reduction (see below). The VIP for the j -th variable (spectral channel) is calculated as follows [230]:

$$VIP_j = \sqrt{p \sum_{k=1}^h (b_k^2 t_k^T t_k (w_{jk} / \|w_k\|))^2} / \sqrt{\sum_{k=1}^h b_k^2 t_k^T t_k} \quad (3.24)$$

where p is the number of variables, h the number of retained latent variables, t the scores of the X-data, w the weights and b the regression coefficient of the inner relation between X- and Y-data. Thus, each spectral channel is evaluated regarding its importance for the prediction with a single value, the VIP score.

To improve the predictive power of the PLSR models, the number of spectral channels was iteratively reduced to exclude spectral regions carrying few or no spectral information for the prediction of a reference value [231]. The main steps of this algorithm are illustrated in Fig. 3.12. In the first step, a PLSR model and its VIP plot are calculated. Then, spectral channels with $VIP < 1$ are discarded in the X-block data. The threshold was applied as recommended in literature and is generally used as a criterion for variable selection because the average of squared VIP scores is equal to 1 [230]. Using the reduced X-block data, the procedure is repeated until a global minimum for RMSECV is reached.

4. Results & Discussion

This chapter introduces the three publications collected in Part II and a field study which is not yet published elsewhere. The publications and the unpublished work comprise studies of fresh pork meat using Raman spectroscopy to investigate early postmortem changes in the Raman spectra and whether these can be exploited to measure or predict meat quality traits.

“It is not knowledge but the act of learning, not possession but the act of getting there, which grants the greatest enjoyment.”
Carl Friedrich Gauß

Publication 1 investigates the relationship between Raman spectra and the pH value of meat. Here, in a series of measurements conducted in the laboratory, Raman, pH and lactate kinetics of excised pork samples were measured early postmortem. The relationship between pH value and lactate concentration, the early postmortem Raman spectra and three approaches to calculate the pH value from the spectra are discussed.

In publication 2, the spectral differences in the early postmortem Raman spectra of normal and PSE-like porcine SM muscles are discussed in detail. Difference spectra of pure chemicals are used to explain spectral differences in the pre-rigor (1–2 h p.m.) and rigor (2–8 h p.m.) time frame. By this means, the most distinctive alterations in the Raman spectra are assigned to important compounds of the energy metabolism. Thereby, a deeper understanding of the Raman spectra of early postmortem meat is achieved.

Publication 3 presents the results obtained during a series of measurements (field study 1) in the cooling room of a commercial abattoir with the portable Raman system. Here, in a production process, early postmortem Raman spectra were measured and correlated with quality traits such as pH, color, drip loss and shear force. The potential of Raman spectroscopy to predict important quality traits of pork meat is shown under real-life conditions.

In the last section of this chapter, a second series of measurements (field study 2) is described, which was conducted to validate the results of publication 3 and to work closer to the production process directly at the slaughterline.

4.1. Spectroscopic Measurement of the pH Value

Publication 1 investigates the measurement of the pH value in early postmortem pork meat by means of Raman spectroscopy. For the experiment, ten excised samples of porcine SM muscle were used. This muscle was chosen because it is accessible at the carcasses in abattoirs and is used for pH measurements in ham. Raman, pH and lactate measurements began 25–40 min after slaughter and were performed with three separate sub-samples. The three kinetics were measured until constant pH was reached which occurred between 7 and 11 h *post mortem*. At this point, the ATP driven metabolic activity in the muscle cells comes to halt due to the depletion of the energy stores of phosphocreatine and glycogen, and the muscle enters the *rigor mortis*.

Of the ten muscles, seven revealed normal pH₄₅, normal pH₂₄ and a rate of lactate production of 7 mmol/kg, hence were classified as normal. Two showed elevated metabolic

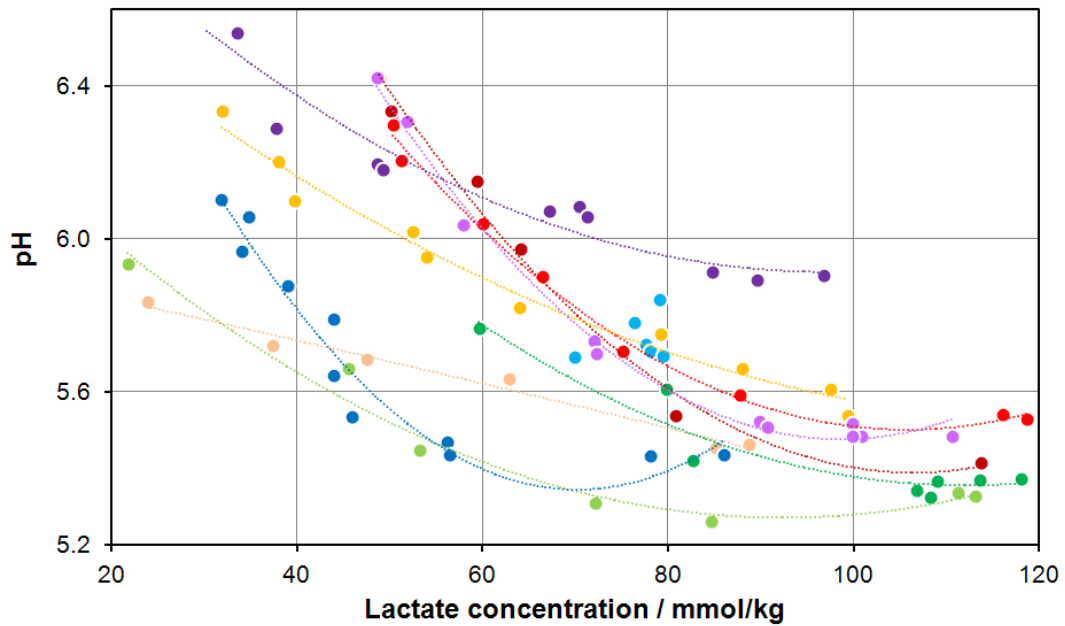


Figure 4.1.: pH value vs. lactate concentration for ten porcine SM samples measured in the time from 0.5 to 10 h.

activity indicated by a $\text{pH}_{45} < 6.0$ and a rate of lactate production above $12 \text{ mmol/kg}\cdot\text{h}$. These samples were considered as PSE-tendency but the samples did not fulfill the PSE criterion of $\text{pH}_{45} < 5.8$. However, the samples showed significantly faster acidification and lactate production than the normal samples. As the number of PSE-tendency samples was only $N = 2$, the experiment was repeated with a total of 30 muscles by the end of this thesis. During these experiments, no further PSE-tendency samples were identified. One atypical sample was measured with almost no pH fall and lactate production during the experiment although the initial lactate concentration was 79 mmol/kg . This sample must have produced its lactate concentration prior to the first measurement which points to a very rapid postmortem metabolism. This would normally cause the PSE condition but in this case no further lactate accumulation could be measured. Hence, this muscle must have had very limited glycogen storage which inhibited further lactate production. This normally points to DFD meat but as this sample exhibited DFD *and* PSE characteristics, it was classified as atypical and discarded from further analysis.

A low curvilinear correlation ($R^2 = 0.49$) between pH value and lactate concentration was observed for the different animals (see Fig. 4.1). On the other hand, a high correlation of $R^2 = 0.97$ was found, if the correlation coefficient was calculated separately for every sample and then averaged for all RFN and PSE-tendency samples. This can be explained by a distinctive biological variation between different animals.

When the lactate formation rate was correlated with pH_{45} values, a negative correlation was found below pH 6.0. Above this pH, no useful relationship was found. In normal samples, $7\text{--}9 \text{ mmol/kg}$ per hour of lactate were formed while in PSE-tendency samples over 12 mmol/kg were metabolized. Due to the low number of deviating samples, these findings have only limited significance and require further work to be validated.

As the lactate concentration revealed only a low correlation with the pH value, the initial goal to use the lactate concentration to predict the pH value had to be discarded. However, the Raman spectra are directly correlated with pH, which was exploited in three different ways to predict the pH value. Firstly, two phosphate peaks were used

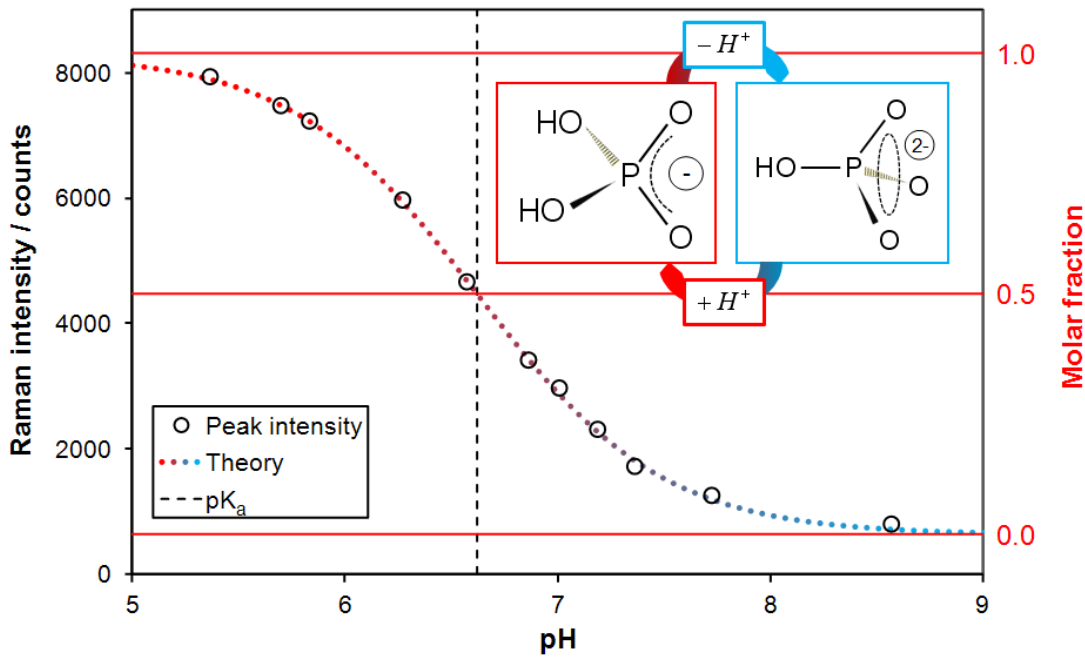


Figure 4.2.: Raman net intensity of the $\nu_s(\text{PO}_2^-)$ peak at 1074 cm^{-1} of inorganic phosphate versus the pH value. Theoretical curve (dotted) calculated with the Henderson-Hasselbalch equation and $pK_a = 6.62$ (dashed). Protonation and deprotonation of both species are presented schematically.

for the pH prediction. In reference measurements with phosphoric acid in aqueous solution, three pH-dependent peaks were observed at 875 , 987 and 1074 cm^{-1} . These peaks are assigned to the symmetric stretching vibrations $\nu_s P(\text{OH})_2$, $\nu_s(\text{PO}_3^{2-})$ and $\nu_s(\text{PO}_2^-)$, respectively. The peaks indicate the transformation of hydrogen phosphate (HPO_4^{2-}) to dihydrogen phosphate (H_2PO_4^-) with decreasing pH which is described by the Henderson-Hasselbalch equation:

$$pH = pK_a + \log_{10} \left(\frac{A^-}{HA} \right) \quad (4.1)$$

Here, A^- and HA represent the concentration of the base and the acid, respectively. The dissociation constant pK_a is a matter constant and equals the pH if the concentrations of the base and the acid are equal. For the calculation from the Raman spectra, the specific Raman scattering intensities for each vibration are required. These constants define the expected Raman intensity per molar concentration (counts/mM) for a given set-up. Hence, the Henderson-Hasselbalch equation must be rewritten as:

$$pH = pK_a + \log_{10} \left(\frac{A^-}{HA} \cdot \frac{\sigma_{HA}}{\sigma_{A^-}} \right) \quad (4.2)$$

Here, σ_{A^-} and σ_{HA} are the Raman intensities of the peak which is assigned to the basic and the acid compound, respectively. They can be easily obtained from normalized¹ Raman spectra of solutions with high or low pH value, i.e. $pH = pK_a \pm 2 - 3$ pH-units. For instance, for low pH values, the acidic component has a concentration of 100% hence the constants can be directly read off the Raman spectrum from the acidic peaks. This is illustrated in Fig. 4.2. In case of P_i , a ratio of $\sigma_{A^-}/\sigma_{HA} = 2.4$ was determined. Using

¹In this context, this means normalized to the concentration (mmol/l or mM).

this value and $pK_a = 6.62$, the pH of phosphoric acid in aqueous solution was very accurately ($R^2 = 0.996$) calculated from the Raman spectra.

Besides inorganic phosphate, several other phosphorylated metabolites can be found in the early postmortem muscle (see Fig. 2.3 on page 18) which may contribute intensity to the signals at 987 and 1074 cm^{-1} . The phosphate group is bound to a sugar (e.g. ribose, glucose) or another compound (e.g. creatine), which alters the pK_a values in the range from below 6 to beyond 7 [36]. The symmetric stretching vibration $\nu_s P(OH)_2$ disappears due to the bonding with the compound. Instead, the stretching vibration νPOH can be observed at lower wavenumbers between 815 and 825 cm^{-1} . Due to a strong signal of creatine at 826 cm^{-1} , the contribution of the phosphorylated compounds to this peak is difficult to quantify in meat spectra hence only the vibrations $\nu_s (PO_3^{2-})$ and $\nu_s (PO_2^-)$ are used for the pH determination. In comparison to P_i , the peaks are slightly shifted to 980 and 1078 cm^{-1} and their respective Raman intensities are also altered [41].

In the spectra of meat, the signals of the phosphorylated metabolites are superimposed, but it is still possible to calculate the pH via the sum bands. To this end, the pK_a was fitted to the data set consisting of 564 Raman spectra and pH values using only the ratio of the net peak intensity of the acid and base peaks. As result, an adjusted pK_a^* of 7.0 was obtained. This adjustment is taking into account the pK_a variations of the different phosphorylated metabolites and it also corrects the deviation of the specific Raman intensity ratio σ_{A^-}/σ_{HA} . This can be understood if the Henderson-Hasselbalch equation 4.2 is rewritten as:

$$pH = pK_a + \log_{10} \left(\frac{\sigma_{A^-}}{\sigma_{HA}} \right) + \log_{10} \left(\frac{A^-}{HA} \right) \quad (4.3)$$

Using

$$pK_a^* = pK_a + \log_{10} \left(\frac{\sigma_{A^-}}{\sigma_{HA}} \right) \quad (4.4)$$

equation 4.3 can be rewritten as:

$$pH = pK_a^* + \log_{10} \left(\frac{A^-}{HA} \right) \quad (4.5)$$

Hence, only the parameter pK_a^* has to be adjusted. By this means, the pH value calculated from the Raman spectra was correlated with the pH value measured with the puncture electrode. The correlation yielded an average correlation coefficient of $R^2 = 0.71$ and $RMSEC = 0.3$ pH-units. Again, the linearity was good for the single muscles, but the correlation also revealed systematic differences between the meat samples which is caused by a position effect. This is mainly attributed to the inhomogeneity of the muscle consisting of fast and slow glycolysing fibers. To quantify the inhomogeneity, an additional experiment was performed in which the pH was repeatedly measured at nine different positions in three excised SM muscles. The variation increased from an initial value of 0.08 pH-units to a maximum value of 0.18 after 5–6 h after slaughter. Subsequently, the variation decreased until a minimum of <0.03 pH-units was reached after 9–10 h. These findings also confirm that a larger reference error has to be expected for the pH_{45} than the pH_{24} measurement. A smaller contribution to the error is added by the simplification of equation 4.1 in which the activity coefficients were neglected in the \log_{10} -term. The activity coefficients are modulated by the ionic strength and the charge of the ions in the solution which alter the pH but not the concentration of the acid and base. Hence, there is a difference between the pH value provided by the puncture electrode, which measures the thermodynamic pH, and the pH value calculated from the

Raman spectra, which only depends on the ratio of the acid/base pair. This difference can be accounted for with the pK_a^* value in equation 4.5, but variances in the ion composition within the muscle cells of different animals result in subject-specific pK_a^* values. Despite the discrepancies between the different samples, the calculations demonstrated that the pH value of meat can be calculated from the Raman spectra, in principle, using only two signals from phosphate.

For a more robust pH prediction, a multiple linear regression (MLR) was performed using the net intensities of eleven peaks ($S(\nu_i)$) and one offset value (A):

$$pH_{MLR} = A + \sum_{i=1}^{11} a_i \cdot S(\nu_i) \quad (4.6)$$

For $S(\nu_i)$, signals from lactate (535, 855, 1305, 1350 and 1414 cm^{-1}), creatine² (827 cm^{-1}), phosphate (980 and 1078 cm^{-1}), the carbonyl bond (1714 cm^{-1}), ATP (1578 cm^{-1}) and IMP (1552 cm^{-1}) were selected due to their significance in the early postmortem Raman spectra. Then, the net intensities of these Raman peaks were calculated. By adjusting the coefficients a_i and the offset A , the following RMSEC was minimized:

$$RMSEC = \sqrt{\left(\sum_{i=1}^{564} (pH_{meas} - pH_{MLR})^2 \right)} \quad (4.7)$$

The MLR model yielded a correlation with $R^2 = 0.78$ and $RMSEC = 0.14$ pH-units. The root mean square error of cross-validation (RMSECV) is calculated with the leave-one-out method and yields 0.22 pH-units. To this end, the spectra of nine different samples were used to compute a model and to test the prediction with the spectra of the residual sample which was repeated for all permutations.

The last approach was a PLSR model. Using baseline-corrected Raman spectra (polynomial with mesh points) in the range from 500–1800 cm^{-1} , a model based on nine latent variables with $R^2 = 0.94$ and a $RMSEC = 0.07$ pH-units was calculated. With the described leave-one-out method, an average $R_{cv}^2 = 0.87$ and $RMSECV = 0.22$ pH-units were calculated.

As expected, the coefficient of determination was improved with increasing number of spectral channels used by the method. While the calculation based on the peak ratio of two phosphate peaks only required six spectral channels (2 for the peak and 2 mesh points per peak), the MLR model requires 33 and the PLSR model 726 spectral channels. Accordingly, the RMSEC is markedly reduced from 0.3 (phosphate peak ratio) to 0.14 (MLR) to 0.07 pH-units (PLSR). However, all models exhibit a similar offset for the different samples which is caused by a distinctive position effect within the muscle.

These results demonstrate that the pH of meat can be determined from the Raman spectra by using only two pH-dependent phosphate peaks, eleven selected signals from significant metabolites or the whole spectral range from 500 to 1800 cm^{-1} . In comparison, the accuracy of the pH measurement based on Raman spectra from the *early postmortem* time phase is higher than the results with NMR and NIR spectroscopy and comparable to hyperspectral NIR imaging in which *post-rigor* meat was used (see Tab. 2.2). As for the ubiquity of phosphorylated compounds in biological tissue, the Raman spectroscopic pH measurement based on the phosphate group could also be useful in other foods or biological matter.

²In publication 1, this peak was tentatively assigned to lactic acid although it is mainly attributed to a change of the creatine concentration and pH-induced changes of the stretching vibration νPOH of phosphorylated sugars.

4.2. Early Postmortem Changes in Raman Spectra

Publication 1 was focused on the quantification of the lactate concentration and the pH value. However, in the Raman kinetics, several alterations besides lactate and pH-induced signals were observed. Therefore, publication 2 was focused on the assignment of these spectral alterations which were found in the early postmortem Raman kinetics of pork. For this study, the same experimental data as for publication 1 was used.

To show the changes of the Raman spectral patterns for normal meat, difference spectra of the seven RFN samples were calculated. To this end, two time frames were chosen: *pre-rigor* and *rigor* phase. The first includes very early postmortem changes in the metabolism of the muscle cell between <1 and 2 h after slaughter, while the latter includes metabolic changes which occur along with the onset of *rigor mortis* between 2 and 8.5 h *post mortem*.

In the pre-rigor phase, the averaged pH values of the meat samples were 6.2 and 6.0 for the <1 h period and after 2 h, respectively. To show the changes in the Raman spectra, ten spectra measured 2 h p.m. were averaged and subtracted from the average of the first ten spectra measured before 1 h p.m. This was repeated for the seven RFN samples and the averaged spectrum was used for further analysis and presentation. Thereby, this difference spectrum represents an accumulative integration time of almost 5 hours. As this difference spectrum is far too complex to be discussed on the basis of individual bands, changes of signal difference patterns due to a number of individual metabolic reactions were considered. These can be understood as material balance equations. In the difference spectra, only the turnover is revealed because the constant parts of the spectrum cancel each other out. The accumulated metabolites are revealed by positive signals while the depleted metabolites are indicated by negative signals. By subtracting the scaled Raman spectra of the pure compounds, the situation in the muscle is reproduced. To this end, the spectra have to be scaled according to the integration and laser power settings of the measurements with the meat samples. In the last step, the conversion rate is judiciously chosen in accordance to concentrations measured as reference or found in the literature.

The early postmortem metabolism in muscle cells is well-known. In the pre-rigor phase, the muscle regenerates ATP to maintain its relaxed state by metabolizing phosphocreatine and glycogen. Thus, the ATP concentration remains relative constant in this time frame. According to literature, a conversion rate of 2 mmol/kg from PCr to Cr and 0.5 mmol/kg from ATP to IMP can be expected [64, 66, 69]. As two molecules lactate are formed during glycolysis, the conversion rate from glycogen to lactate is different: 9 mmol/kg glycogen are metabolized to 18 mmol/kg lactate in the pre-rigor phase. The latter value was obtained from the lactate reference measurements. Additionally, the concentration of inorganic phosphate (P_i) can be expected to be increased by 6 mmol/kg [169, 232]. In parallel, the muscle's pH decreased from 6.2 to 6.0. Therefore, the spectrum of P_i is changed: The base peak at 987 cm^{-1} decreases while the acid peaks at 875 and 1074 cm^{-1} gain intensity. The same holds for the phosphorylated metabolites of the glycolysis, ATP and IMP. Hence, for the difference spectra of the pure compounds only spectra with the mean measured pH of the time slot were used. Besides concentration and pH-induced changes, oxidative processes also alter the Raman spectra. Here, the reduction of oxy-(oxy-Mb) to deoxymyoglobin (deoxy-Mb) play a major role. When the sample was cut from the SM muscle, the meat surface was exposed to oxygen which led to the formation of oxy-Mb. During the Raman measurements the

“What I cannot create, I do not understand.”

Richard P. Feynman

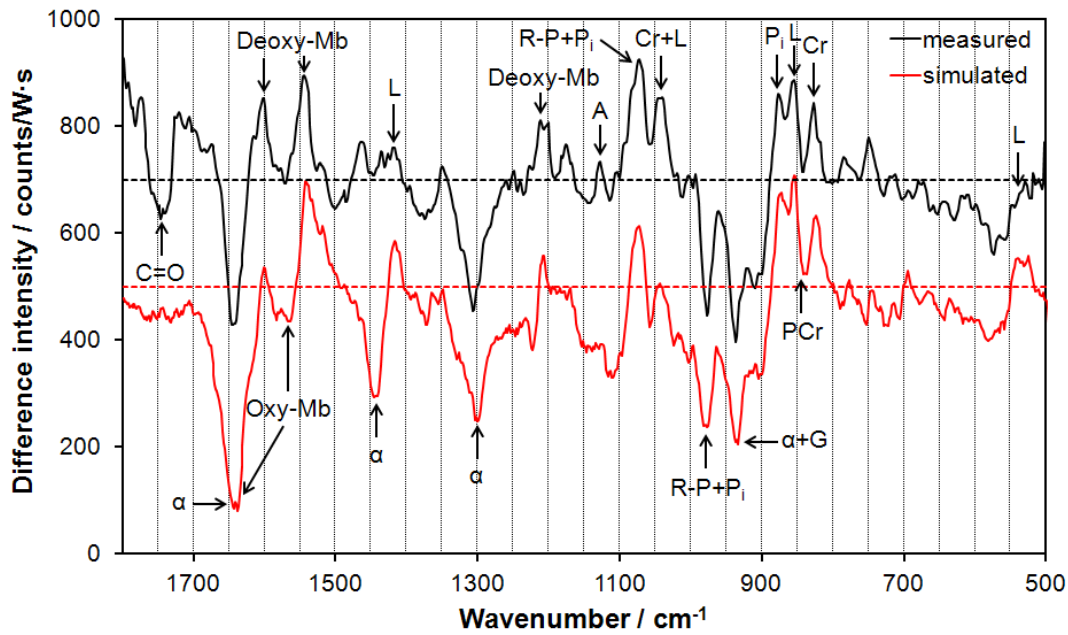


Figure 4.3.: Measured difference spectrum 2 h minus <1 h p.m. (offset = 0.7 counts/mW · s) and the simulated spectrum (0.5) based on the difference spectra creatine (Cr) minus phosphocreatine (PCr), lactate (L) minus glycogen (G), deoxy- (deoxy-Mb) minus oxymyoglobin (Oxy-Mb) and the Raman spectrum of α -helical proteins (α). Raman signals of ATP (A), phosphorylated metabolites (R-P), inorganic phosphate (P_i) and the carbonyl band (C=O) are marked with arrows.

exposure to air was reduced by the sensor head and deoxy-Mb is formed because, early postmortem, the muscle cell's mitochondria still consume oxygen. Hence, the difference spectrum *deoxy- minus oxymyoglobin* reflects the situation in very early postmortem meat. Not surprisingly, indication for a decrease of signals of α -helical proteins was observed with peaks at 901, 935, 1309, 1448 and 1645 cm^{-1} as such a decrease was reported upon storage of meat. However, the loss of signals from the α -helical secondary structure in the amid I or III region is not understood. The origin of this decline of α -helical signals is unknown but may partly be explained by changing alignments of the meat samples relative to the laser's polarization during the experiments which would have caused altering intensities of the α -helical signals.

The difference spectra of the metabolites were calculated and scaled as described above, while the difference spectrum deoxy- minus oxymyoglobin and the spectrum of α -helical proteins were judiciously scaled for best agreement between measured and calculated difference spectrum. Then, the difference spectra were summed up and compared with the measured difference spectrum (see Fig. 4.3). Evidently, there is very good agreement between the simulation and the measured spectrum especially in the wavenumber area from 800 to 1150 cm^{-1} leaving only a few peaks unassigned. Namely, the CH-deformation band at 1450 cm^{-1} and a peak at 1740 cm^{-1} are not well explained and may belong to a compound not included in the simulation. The latter peak can be assigned to C=O stretching vibrations of carbonyl groups of saturated esters or ketones in five-membered rings [233].

In the rigor phase, the muscle's energy storage is exhausted and the muscle enters the

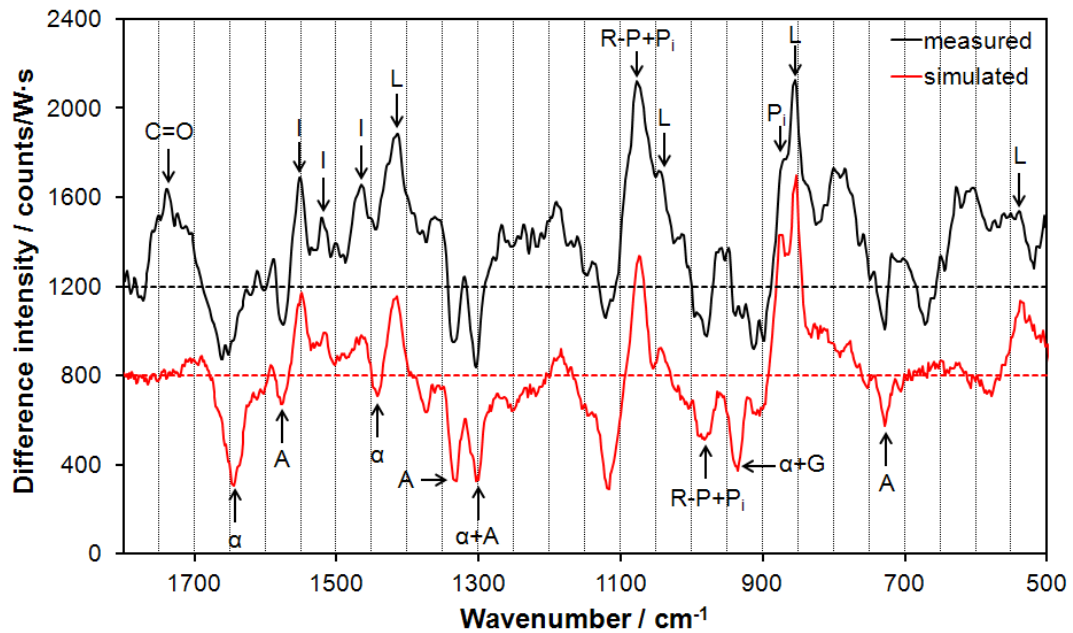


Figure 4.4.: Measured difference spectrum 8.5 h minus 2 h p.m. (offset = 1 counts/mW · s) and the simulated spectrum (0.6) based on the difference spectra of inosine monophosphate (I) minus adenosine triphosphate (A), lactate (L) minus glycogen (G), phosphoric acid (P_i) at pH 5.6 minus pH 6.0, glucose 6-phosphate at pH 5.6 minus pH 6.0 and the Raman spectrum of α -helical proteins (α). Raman signals of phosphorylated metabolites (R-P) and the carbonyl band (C=O) are marked with arrows.

rigor mortis. At the beginning of this phase 2 h p.m., the phosphocreatine storage is depleted and the muscle's energy metabolism has to essentially rely on the energy production via glycolysis [60]. Thus, between 2 and 8.5 h p.m. an average of 22 mmol/kg glycogen is metabolized to 44 mmol/kg lactate [61, 64, 66]. Thereby, the pH dropped from 6.0 to 5.6 which is close to the ultimate pH. At the same time, ATP is also regenerated via the adenylate kinase (AK) reaction from two ADP molecules. In this reaction, AMP is produced which is rapidly deaminized to IMP. Using only the AK reaction and glycolysis, the muscle is not able to maintain constant ATP concentration. Thus, a conversion rate of ATP to IMP of 3.1 mmol/kg is observed in the rigor phase. P_i is accumulated as the end product of the ATP degradation. Thus, its concentration increases from 26 to 34 mmol/kg [169, 232]. Furthermore, the pH-induced changes of P_i and the phosphorylated metabolites of the glycolysis have to be accounted for. In the simulation, this was done by using Raman spectra which were obtained at $pH = 5.6$ and 6.0 and, as a proxy for the phosphorylated metabolites, by using the spectrum of glucose 6-phosphate. The latter is justified as G6P is the phosphorylated metabolite with the highest concentration of up to 8 mmol/kg [61]. This concentration is reached after 2 h p.m. and remains almost constant for at least 12 h. Finally, loss of intensity or degradation of α -helical proteins was also observed in this time frame at a much higher level compared to the pre-rigor time frame.

Again, the sum of the difference spectra was calculated (see Fig. 4.4). In accordance to the pre-rigor phase, very good results were also achieved for the rigor phase. Excellent agreement was found between 1050 and 1700 cm^{-1} , while minor deviations between simulation and measurement can be found below 700 cm^{-1} , between 770 and 800 cm^{-1}

and again in the carbonyl region around 1740 cm^{-1} .

In the next step, the spectra of normal samples were compared with the two PSE-tendency samples. Although the number of animals is small, the spectral data set comprises 700 and 200 spectra of normal and deviating meat which represent an accumulative integration time of 4.9 and 1.4 hours, respectively. Hence, there is a sound spectroscopic basis and the difference spectra of the PSE-like samples can be reasonably compared to the spectra of the RFN samples in the pre-rigor and rigor phase.

In the *pre-rigor phase*, the PSE-tendency samples revealed elevated metabolic activity which is indicated by a lower pH_{45} and a higher rate of lactate formation. Accordingly, the pH at the beginning of the pre-rigor phase was 5.8 and it decreased to 5.6 within 2 h. In the Raman difference spectra, the accelerated metabolism was revealed by signals of ATP at 1576 cm^{-1} and IMP at 1551 cm^{-1} . In normal meat, a difference between these peaks of 190 counts/Ws was found while PSE-like meat revealed a difference of 250 counts/Ws. Hence, in PSE-like meat, more ATP was metabolized to IMP in the pre-rigor phase which is in accordance to the literature [169, 234]. The quantitative determination of this ratio could be very useful because the ratio ATP/IMP was reported to be an excellent predictor for deviating metabolism hence meat qualities [63, 234]. At the same time, a lower intensity of the pH-dependent triphosphate signal (mainly ATP) at 1119 cm^{-1} points to a lower absolute concentration in PSE-like samples. Also, formation of P_i is higher as indicated by the signal at 875 cm^{-1} . Due to the rapid exhaustion of the PCr pool in PSE meat no further formation of Cr after 1 h p.m. was reported in literature [61, 64, 66, 169] hence no spectral indication was found in the pre-rigor phase spectrum of PSE-like meat.

In the *rigor phase* most of the differences are equalized between RFN and PSE-tendency meat. In both qualities, ATP is degraded and the final concentrations of lactate and P_i as well as the ultimate pH are reached. These parameters do not differ significantly between RFN and PSE meat. However, the more rapid metabolism in the PSE-tendency samples has left its spectral traces. The most obvious difference is the higher loss of α -helical signal intensity, which points at the known denaturation of proteins in PSE meat, which eventually leads to lower water holding capacity and higher drip loss. As in the excised samples, the temperature within in the meat decreased faster than in the complete carcass, the well-known degradation of the muscle proteins is minimized, which normally would occur when low pH and high temperature are combined. Therefore, a stronger effect can be expected in intact PSE carcasses.

In summary, this study could follow and visualize the metabolic changes in pork meat with Raman difference spectra in the pre-rigor and rigor phase. The observed changes were successfully simulated using Raman spectra of the pure metabolites of appropriate pH and concentrations taken from own measurements or from the literature. By this means, excellent agreement between measured and simulated difference meat spectra was achieved. The comparison between RFN and PSE-tendency meat indicated higher conversion rate of ATP to IMP, lower concentration of ATP, a faster formation of P_i and a lack of Cr formation for the PSE-tendency meat in the pre-rigor phase and a significantly higher loss of signals from α -helical proteins in the rigor phase. Hence, the potential of portable Raman spectroscopy to follow the early postmortem metabolism in pork meat was demonstrated. The Raman spectra were shown to give a deeper insight into the metabolic conditions than the pH measurements and they provide the information non-invasively and faster than classic reference methods.

4.3. Prediction of Quality Traits from Early Postmortem Raman Spectra

To this point, Raman spectroscopy was shown to measure the pH value early postmortem of excised porcine SM muscle in the laboratory. Moreover, essential energy metabolites were identified in the spectra of pork meat. As the early postmortem metabolism determines quality traits like pH_{24} , drip loss, color and shear force, it was interesting to investigate whether these parameters can be predicted from Raman spectra measured in abattoirs. To this end, two field studies were performed in two different commercial abattoirs. In the first study, the Raman spectra were obtained in the chiller 1–2 h p.m., while the spectra in second study were measured at the slaughterline between 30 and 60 min p.m.. The results of the first study are described in publication 3 and summarized in the following section. The second, unpublished field study is presented in section 4.3.2.

“Truth is what stands the test of experience.”
Albert Einstein

4.3.1. Field Study in the Chiller

In this experiment, Raman and reference measurements were performed as part of a larger study with the left topside (SM) of 96 pigs representing a random sample of typical pig breeds slaughtered in Germany. The Raman spectra were obtained using the portable Raman system described in section 3.2. In the cooling room of an abattoir, ten Raman spectra were recorded with an integration time of 2.5 s at the freshly cut surface of each muscle between 60 and 120 min after slaughter. Prior to these measurements, pH_{45} was measured in duplicate using a puncture electrode. After 24 h, the pH measurement was repeated and $L^*a^*b^*$ values were determined in triplicate. Shear force values were measured 24 and again 72 h p.m. using a Warner-Bratzler system. Additionally, drip loss was determined 72 h after slaughter. The reference measurements were performed by researchers of the Max Rubner-Institut in Kulmbach, Germany.

Using the flow chart introduced in section 2.2.4, the meat samples were sorted in eight quality groups. To show differences in the Raman spectra between normal and PSE meat, the difference spectrum *RFN minus PSE* was calculated. RFN was chosen because it is the reference quality, while PSE was selected because it is the most problematic quality deviation. The data set contained 31 RFN and 6 PSE samples. The difference spectrum revealed the different metabolic states of the two meat qualities (see Fig. 4.5). For instance, the advanced metabolic state of PSE compared to RFN meat is reflected by negative creatine signals at 826 and 1040 cm^{-1} in the difference spectrum which indicates a faster decay of phosphocreatine in PSE meat. At the same time, higher concentrations of PCr in RFN meat are indicated by positive signals at 849 and 976 cm^{-1} . The latter is superimposed by further phosphorylated metabolites which add intensity to this peak. Similar observations can be made for the metabolic pairs glycogen/lactate and ATP/IMP. The accelerated metabolism in PSE meat leads to a faster acidification, which is reflected in the Raman difference spectrum by the pH-dependent signals of inorganic phosphate and the terminal phosphate moiety at 872, 976 and 1077 cm^{-1} . The signal at 976 cm^{-1} is stronger under less acidic conditions and indicates the higher pH in RFN meat. On the other hand, the signals at 872 and 1077 cm^{-1} are increased under more acidic conditions in PSE meat. This is confirmed by the reference measurements which yielded $pH_{45} = 6.4$ for RFN and 5.5 for PSE meat. Also, signals of α -helical proteins were more pronounced in RFN meat. These observations confirm the earlier findings in the laboratory as described in the previous section and in publication 2.

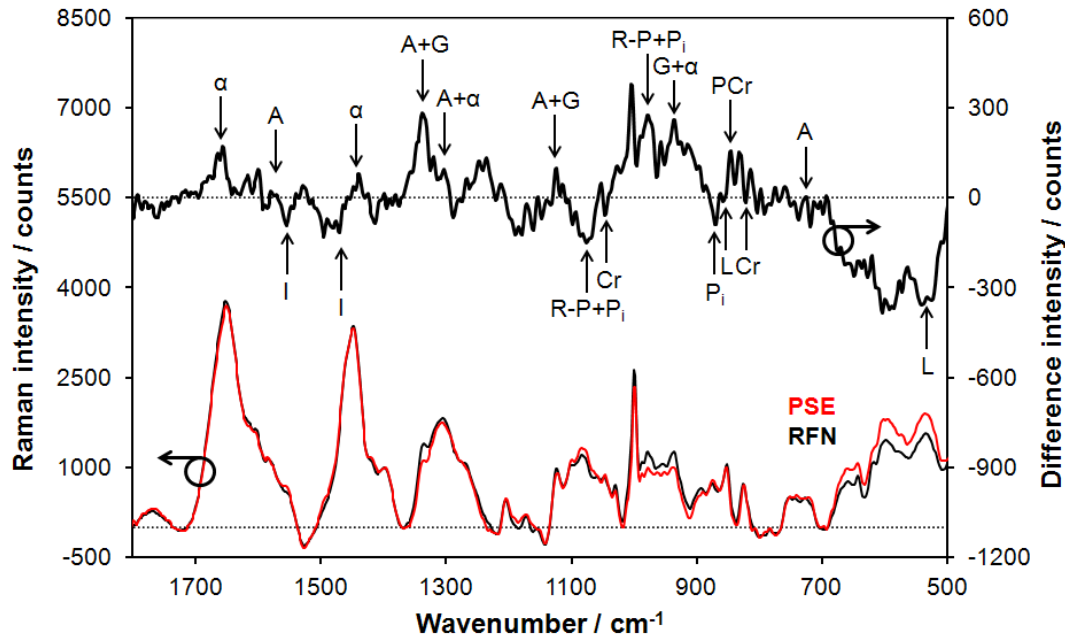


Figure 4.5.: Averaged spectra of 6 PSE samples (red line), 31 RFN samples (black) and the difference spectrum RFN minus PSE (black bold). Indicated by arrows: adenosine triphosphate (A), inosine monophosphate (I), glycogen (G), lactate (L), inorganic phosphate (P_i), phosphorylated metabolites (R-P), creatine (Cr), phosphocreatine (PCr) and α -helical proteins (α).

The Raman spectra were shown to indicate the metabolic state of the *semimembranosus* muscle and it is reasonable to evaluate to what extent the spectral information can be used to predict meat quality traits. Firstly, the Raman spectra were correlated with the pH_{45} values. Here, the VIP based reduction of spectral channels was used as described in section 3.4.3 to calculate optimized PLSR models. Using this procedure, the RMSECV could be reduced by up to 35% in this work. The coefficients of determination were promising with $R^2 = 0.82$ and $R_{cv}^2 = 0.65$ for pH_{45} . The model yielded $RMSEC = 0.11$ and $RMSECV = 0.17$ pH-units which comes close to the estimated error of the pH measurement of 0.06–0.14 pH-units. However, as the pH values were measured 45 min p.m., while the Raman measurements started between 60 and 120 min p.m., some deviation between measured and predicted pH has to be expected. Furthermore, the pH was measured inside the SM while the Raman spectra were obtained from the meat surface which adds some deviation.

The Raman signals which provided relevant information for the prediction of the pH_{45} are highlighted in the VIP plot of the PLSR model. The most important signal can be assigned to the symmetric stretching PO_3^{2-} vibration of the terminal phosphate moiety at 976 cm^{-1} which acts as an indicator for pH. Secondly, a broad wavenumber region around the peak at 928 cm^{-1} is weighted. Additional peaks at 1300 and 1455 cm^{-1} point to α -helical protein signals. Furthermore, peaks of lactate, ATP, creatine and phosphocreatine are utilized to predict pH_{45} .

To this point, the results confirm the findings of publication 1: The early postmortem Raman spectra of pork can be used to determine the current pH. To investigate the potential of Raman spectroscopy to predict further quality traits, PLSR correlations with pH_{24} , color, drip loss and shear force were calculated.

A good correlation was found between the Raman spectra and the pH_{24} . The PLSR

model yielded $R^2 = 0.84$ and $R_{cv}^2 = 0.68$ and prediction errors of $RMSEC = 0.06$ and $RMSECV = 0.09$ pH-units. The good predictability of pH_{24} from Raman spectra obtained 1–2 h p.m. can partly be explained by the smaller variance of the ultimate pH of 0.01–0.05 pH-units. On the other hand, this is a result of the early postmortem energy metabolism of meat and its correlation with ultimate pH. The concentration of glycogen is limiting the final concentration of lactate and H^+ ions hence the ultimate pH. Besides signals of glycogen, the Raman spectra contain signals of lactate, PCr, Cr, ATP, ADP, IMP and P_i which provide further information about the metabolic conditions within the muscle cells and which indicate the ultimate pH of the muscle.

The VIP plot of the pH_{24} model is quite different from the VIP plot for the correlation with pH_{45} . Here, the prediction is mainly based on energy metabolites but not on the peaks which indicate the current pH. The strongest peak in the VIP plot can be found at 1109 cm^{-1} which is assigned to ADP. A smaller peak at 1120 cm^{-1} is assigned to the triphosphate ATP. Apparently, the PLSR model utilizes different concentrations of ADP and ATP to predict the final pH values. In literature, this is known for ATP in pork muscle in which a difference of 3 mmol/kg of ATP was found between RFN and DFD (high pH_{24}) in the time frame from 30 to 120 min after slaughter [169]. Additionally, a 17 mmol/kg higher concentration of P_i in DFD and a four times higher concentration of phosphocreatine in RFN were reported in this study. This is also reflected in the VIP plot: Three distinct signals at 875, 978 and 1078 cm^{-1} indicate the influence of the concentration of P_i , while signals at 826, 855, 978 and 1037 cm^{-1} indicate the conversion of PCr to Cr. As DFD meat has much lower content of glycogen than RFN meat [64], signals from glycogen and lactate are used. Additional peaks at 1455 cm^{-1} (CH, CH_2 and CH_3 deformation modes) and between 1630 and 1690 cm^{-1} (Amid I) were also weighted in the VIP plot although their correlation with ultimate pH and their origin in metabolic compounds or structural features is unknown. Interestingly, a broad band at 1740 cm^{-1} ($\text{C}=\text{O}$ stretching vibration of the carbonyl group) is weighted but its origin remains also unclear.

The color of the meat is important for the buying decision of the consumer but, to date, the color can only be determined 24 h after slaughter. Its prediction from early postmortem Raman spectra could be beneficial for the meat industry. The prediction of the L^* values from the early postmortem Raman spectra was promising. The PLSR model yielded good correlations ($R^2 = 0.95$ and $R_{cv}^2 = 0.64$) and prediction errors ($RMSEC = 0.7$ and $RMSECV = 1.9$) considering the reference error of the measurement of 0.9 using the Minolta CR400 device. The PLSR models for a^* and b^* values performed very differently. For a^* , only a moderate correlation ($R^2 = 0.46$) was found while b^* was highly correlated ($R^2 = 0.9$) with the early postmortem Raman spectra. The PLSR model for b^* yielded $RMSEC = 0.4$ and $RMSECV = 0.6$ which are comparable to the reference error of 0.3.

Meat color is mainly determined by the concentration of oxymyoglobin, deoxymyoglobin and metmyoglobin of which oxy- and deoxymyoglobin were shown to contribute to the early postmortem pork spectra. However, meat color 45 min p.m. was reported not to be indicative for ultimate color in porcine SM and LD muscles [196]. Thus, the $L^*a^*b^*$ values have to be predicted indirectly from the Raman spectra. It is known that the early conditions after death such as rate of glycolysis, pH and temperature play a major role in determining the meat color [116, 117]. For instance, high temperature in combination with low pH_{45} in the muscle leads to denaturation of proteins which influences light scattering. Furthermore, a high pH_{45} was associated with a decreased L^* values in LD and SM pork meat [196]. As the present data show only a weak correlation between pH_{45} and L^* ($r = -0.27$) it is concluded that the correlation is not indirectly

based on the pH information of the spectra. This is confirmed by the VIP plot of the L* model, which weights signals of glycogen and α -helical proteins but not the indicative signals of phosphate. On the other hand, the pH₂₄ does correlate with the L* with a coefficient of $r = -0.6$. This is in keeping with the known relationship between ultimate pH and L* value [235]. The model for a* relies mainly on signals of α -helical proteins but also strongly weighs peaks at 999 and 1038 cm⁻¹, presumably attributed to phenylalanine and creatine/lactate, respectively. The VIP plot of the b* model is a combination of the plot of L* and a*.

In contrast to color, the relationship between early postmortem metabolism and *drip loss* is well-known [66, 95, 107]. In general, perimortem stress leads to high drip loss while antemortem exhaustion of the glycogen reservoir leads to very low drip loss. Thus, the energy compounds indicating the metabolic state of the muscle can be used to predict drip loss. As was shown in publication 2, the early postmortem spectra comprise the Raman signals of these components. Accordingly, the PLSR model to predict DL from Raman spectra yields good results: $R^2 = 0.9$ and $R_{cv}^2 = 0.73$, $RMSEC = 0.6\%$ and $RMSECV = 1.0\%$. In comparison to the overall variation of drip loss of 0.7–9.2% and the error of the reference method of 0.3–1.3%, the PLSR prediction is very accurate.

The VIP plot indicates the influence of signals from lactate, glycogen, ADP, adenine, creatine, the terminal phosphate groups and the carbonyl group which is in accordance to the above statement: The prediction of drip loss is mostly based on Raman signals which indicate the state of the energy metabolism of the muscle.

The rate of postmortem pH decline is known to influence the rate of tenderization [155, 156]. Interestingly, the *shear force* values measured 24 and 72 h p.m. revealed only a moderate correlation of $R^2 = 0.35$. Accordingly, the PLSR correlations of the Raman spectra and the shear force data performed very differently: While only a moderate relationship was found for SF 24 h p.m. with $R^2 = 0.37$ and $RMSECV = 7.8\text{ N}$, a much better model was obtained for SF 72 h p.m. with $R^2 = 0.95$ and $RMSECV = 4.0\text{ N}$. The latter cross-validation error is comparable to the estimated reference error of 4.6 N. The good predictability of the shear force value measured after 72 h p.m. is surprising when the relatively small variance of the SF data of 6.9 N is considered. Here, the ratio of the standard deviation to the reference error is below 1.5. However, the Raman spectra reflect the rate of early postmortem metabolism and it is reasonable to assume that this relationship is the reason for the good prediction of SF 72 h *post mortem*. On the other hand, the shear force values 24 h p.m. are not very reliable as no tenderization took place after only one day of ageing. Therefore, effects such as the shortening of the sarcomers during *rigor mortis* or its duration may interfere with the SF measurement 24 h after slaughter and may disturb the SF24 prediction from the early postmortem Raman spectra.

In summary, the portable Raman system described in section 3.2 was tested in a series of Raman measurements in a commercial abattoir. PLSR models yielded promising correlations ($0.8 < R^2 < 0.9$) for pH₄₅ and pH₂₄ and even better correlations ($R^2 > 0.9$) for drip loss, L*, b* and shear force 72 h p.m. Only moderate correlation were found for shear force 24 h p.m. ($R^2 = 0.37$) and the a* value ($R^2 = 0.48$). Using difference spectra between PSE and RFN meat, the results of publication 2 were confirmed: Raman spectra are a reliable indicator for the state of the early postmortem metabolism. The metabolites glycogen/lactate, ATP/IMP, creatine/phosphocreatine and the phosphate group were identified in the difference spectra. The signals of these metabolites were, amongst others, used by the PLSR models to predict the reference parameters of which especially drip loss and shear force are presently only available via time consuming and

invasive reference analyses. In this study, the feasibility to apply Raman spectroscopy to predict six important quality traits was proven using a portable Raman system and spectra with only 2.5 s integration time and ten repetitions during early postmortem *in-situ* measurements under real-life conditions.

4.3.2. Field Study at the Slaughterline

A second field study was performed to confirm the promising results of study 1. However, the time of measurement of study 1 is impractical for an application in an industrial slaughtering process. Hence, in study 2 the first attempt was made to perform the Raman measurements directly at the slaughterline in the time slot from 30 to 60 min *post mortem*. This study and its results are not yet presented or published elsewhere.

“Anything worth doing is worth doing twice, the first time quick and dirty and the second time the best way you can.”

Arthur L. Schawlow

Experimental

Raman and reference measurements were performed as part of a larger study with 151 porcine SM muscles which represent a random sample of pig breeds slaughtered in Switzerland. Early postmortem Raman and pH measurements were performed along the slaughterline during the normal operation of the abattoir. To this end, 3–5 carcasses at a time were moved from the main slaughterline to the veterinarian line (see Fig. 4.6). Then, 3–6 pH measurements were conducted 25–40 min *p.m.* using a puncture electrode (Portamess 913 X pH, Fa. Knick, Berlin). Subsequently, seven Raman spectra of meat were obtained from the freshly cut surface of the SM muscle. The integration time was set to 2.5 s and six accumulations were measured at each spot. The spectra for each muscle were averaged for further analysis. Due to the accidental occurrence of fat spectra, the measurement time per carcass altered between 1.5 and 6 min. In comparison to field study 1, the number of accumulations was increased from 1 to 5 and the same integration time of 2.5 s, but the number of repetitions at different spots on the meat surface was reduced from 10 to 7. The main difference to study 1 is that the spectra were measured 30 min earlier and the time slot for the Raman measurements was reduced to 30 min. The experimental settings of both field studies are summarized in Tab. 4.1.



Figure 4.6.: Measurements at the veterinarian line with the portable Raman system during field study 2.

After 24 h, the SM muscles were excised. During the deboning process, 15 SM samples

Table 4.1.: Comparison of experimental characteristics between field study 1 and 2.

Parameter		Field study 1	Field study 2
General	Location	Germany	Switzerland
	Samples	Cooling room 96	Veterinarian line 151
Raman	Measuring time p.m. / min	60–120	30–60
	Integration time / s	2.5	2.5
	Accumulations	1	6
	Repetitions	10	7
	Integration time per sample / s	25	105
Reference	Early postmortem pH / min	45	25–40
	Ultimate pH / h	24	24
	Color / h	24	24
	Drip loss / h	72	72
	Shear force / d	3	7

were lost, which reduced the number of samples for the subsequent analysis to 136. In the laboratory, two pH values were obtained using the same puncture electrode that was used in the abattoir. Additionally, L^* measurements with a Minolta Chromameter CM-2500d (Konica Minolta Sensing Europe B.V., Swiss Branch Dietikon) were conducted in duplicate, but not at day 1. This reduced the number of L^* values to 96. Then, a slice of the muscle was weighted, suspended in a box and stored for 48 h. After 72 h, the samples were reweighted and the difference between initial and ultimate weight was expressed as percentage weight loss. In both studies, Warner-Bratzler systems with a V-shaped blade were used to perform the shear force measurements and the samples were sliced, vacuum packaged and deep-frozen at day 1. In study 2, the samples were thawed at day 7 in a water bath at 20°C for two hours and subsequently cooked in a water bath at 72°C for 45 min. After cooling under running tap water for 10 min, the shear force was measured on six cores per slice sheared perpendicular to the direction of the muscle fibers with a cross section of 1x1 cm² using a TA.HDplus Texture Analyzer (Stable Micro Systems Ltd, Surrey, UK).

In conclusion, the reference measurements were performed very similar to field study 1 except the point in time of the shear force measurement. For further analysis, the averaged pH, L^* , DL and SF values were used per sample.

Results – Reference Measurements

An overview of the results of the reference measurements of both field studies is given in Tab. 4.2. The early pH measurement in study 2 was performed ten minutes earlier in average than in study 1 which partly explains the higher average pH of 6.58. However, the difference of 0.3 pH-units is too high to be simply explained by the time difference. The main reason is that in field study 1 samples with (on average) elevated metabolism, hence faster acidification, were measured. Accordingly, the first data set comprises six PSE samples while the second data set is missing this quality. This results in a two times higher standard deviation in the first data set. The error of the reference method was

Table 4.2.: Overview of the reference results of both field studies (values of field study 1 in brackets) with number of samples, mean, minimum and maximum value, standard deviation (SD), error of the reference method (Ref. error) and the ratio SD/Ref. error.

Parameter	pH ₃₅ (pH ₄₅)	pH ₂₄	L*	DL / %	SF7(3) / N
Samples	151 (96)	136 (96)	96 (96)	136 (81)	136 (64)
Mean	6.58 (6.29)	5.42 (5.53)	50.0 (48.8)	2.8 (4.1)	35 (49)
Min	6.09 (5.41)	5.30 (5.28)	42.5 (41.0)	0.9 (0.7)	24 (36)
Max	6.94 (6.80)	5.65 (6.13)	56.2 (55.1)	5.1 (9.2)	67 (69)
SD	0.14 (0.29)	0.06 (0.15)	2.4 (3.1)	0.9 (1.9)	6 (7)
Ref. error	0.08 (0.06–0.14)	0.02 (0.04)	1.3 (0.9)	0.3–1.3 ^a	4 (5)
SD/Ref. error	1.8 (2.1–4.8)	3.0 (3.8)	1.8 (3.5)	0.7–3.0 (1.5–6.3)	1.5 (1.4)

^a from [166]

comparable in both studies. In study 2, the error of the pH₄₅ measurement was calculated from the within-sample standard deviation. Due to the higher standard deviation the ratio between SD and reference error is higher in study 1. This ratio is a measure of the precision of the reference method and of the utmost importance for the calculation of regression models. A ratio below 2 cannot give a relevant prediction, between 2.0 and 3.0 it is regarded adequate for rough screening and above 3.0 as satisfactory for screening [236]³. With only 1.8, the ratio of the early postmortem pH in study 2 is rather low.

Similar to the early postmortem pH, the ultimate pH values also reveal distinct differences between the two studies. While the averaged and minimum pH₂₄ values are comparable, the maximum values differ by about 0.5 pH-units. Data set 1 comprises three DFD and five DFD-tendency samples while data set 2 is missing these qualities. This leads to a more than two times higher standard deviation in study 1. As described in section 4.1, the heterogeneity inside the SM muscle is increasing between slaughtering and 5–6 h p.m. while it is decreasing afterwards, until the minimum variance is reached after 24 h. This is reflected by the reference error which is mainly caused by the intrinsic heterogeneity of the SM muscle. While the error of the early pH measurement is high but comparable between both studies, the pH₂₄ error is low but two times higher in study 1. This may be explained by the higher overall variance in this data set. However, both studies reveal a sufficient variance with a low reference error as indicated by the ratio SD/Ref. error of 3.8 and 3.0, respectively.

Interestingly, the distinct pH differences are only partly reflected by the L* values. Mean, minimum and maximum value are shifted by 1–1.5 between the studies indicating slightly paler meat in study 2. The standard deviation of field study 1 of 3.1 is slightly increased in comparison to 2.4 in study 2. The reference error is higher in study 2 because only duplicate measurements were performed in opposite to triplicate measurements in study 1. Therefore, the ratio of the standard deviation to the reference error is decreased from 3.5 in study 1 to 1.8 in study 2. Hence, a better correlation with the Raman spectra can be expected in study 1.

The difference in the distribution of meat quality between both data sets is confirmed

³The authors also stated that only values of 5 and upward are suitable for quality control analysis.

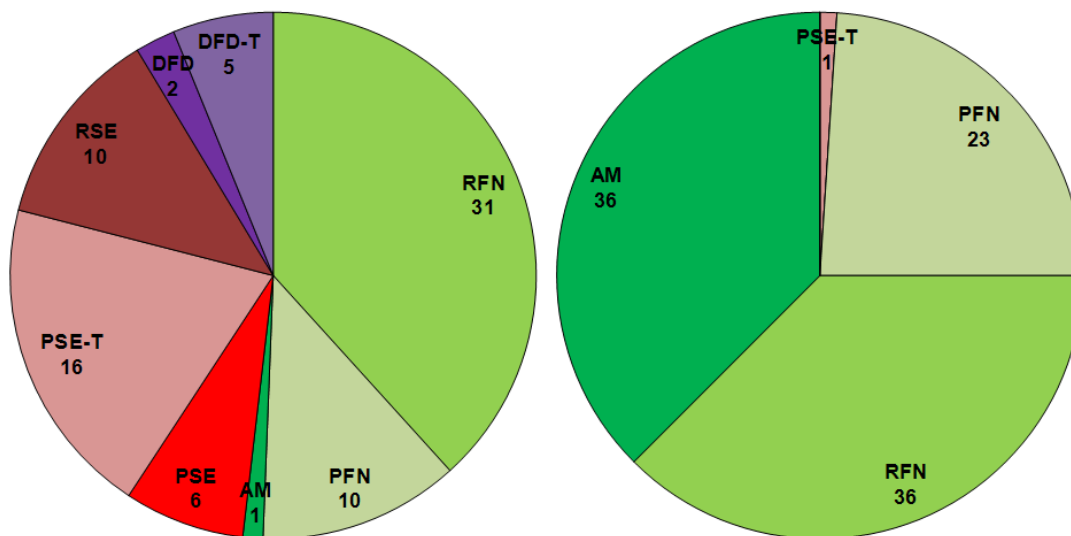


Figure 4.7.: Comparison of meat qualities of field study 1 (*left*) and 2 (*right*).

by the drip loss. While the mean DL of data set 1 is 4.1%, the average drip loss in data set 2 was 2.8%. Accordingly, with a maximum value of 5.1%, data set 2 contains only one sample with drip loss above 5%, while almost 40% of the samples of data set 1 revealed elevated drip loss. The maximum value in this data set was 9.2% which is in agreement with the occurrence of PSE. Correspondingly, the standard deviation was more than two times higher in data set 1. As the drip loss measurement was conducted only once per sample, the reference error of 0.3–1.3% was obtained from the literature [166]. Due to the margin of 1%, the ratio SD/Ref. error range from 1.5 to 6.3 in study 1 and from 0.7 to 3.0 in study 2.

As the tenderness of the muscle increases with time [68], the shear force values in study 1 are higher because they were obtained after 3 days while the SF measurements in study 2 were conducted after 7 days. Interestingly, this is reflected by the minimum, but not by the maximum SF value. Both, the standard deviations and the reference errors of the Warner-Bratzler method were comparable. However, the ratio SD/Ref. error of 1.5 and 1.4 indicate poor preconditions for the calculation of regression models.

In conclusion, data set 2 consists of more homogeneous samples indicated by lower standard deviations for the measured reference parameters. Also, data set 2 comprises higher quality samples regarding early postmortem pH, ultimate pH and drip loss. L^* measurements performed comparable. The time difference of the shear force measurements is resulting in higher SF values in study 1. The error of the reference methods used to measure pH, L^* , drip loss and shear force were comparable.

The difference in quality is also reflected in Fig. 4.7 in which both field studies are compared regarding their quality distribution. Here, the flowchart presented in section 2.2.4 was applied to classify the meat samples of both studies. Apparently, study 1 comprises almost 50% deviating meat qualities namely DFD, DFD-tendency, PSE, PSE-tendency and RSE while study 2 contains only one PSE-tendency sample. The high amount of acid meat in study 2 is surprising but the oftenly reported high drip loss of this quality could not be observed in this data set [90]. Here, the AM, PFN and RFN samples revealed an averaged drip loss of 3.1, 2.7 and 2.6%, respectively.

Results – Raman Spectra

Data analysis was performed as in field study 1 to assure comparability between both studies. However, the times of measurement of the early postmortem Raman spectra were different and the post-slaughter treatment was different between the German and Swiss abattoir. Therefore, the Raman spectra and the PLSR models can be compared, but the Raman spectra of study 2 cannot be utilized as a validation of the PLSR models of study 1.

The PLSR correlation of the Raman spectra and the pH_{35} values yielded good coefficients of determination with $R^2 = 0.75$ and $R_{cv}^2 = 0.55$ (see also Tab. 4.3 and Fig. 4.8). In Fig. 4.8, the PLSR predictions of the pH_{35} values which were derived during the calibration (cal) and the cross-validation (cv) are depicted separately. In this model, excellent $RMSEC$ and $RMSECV$ were calculated with 0.07 and 0.09 pH-units, which is in accordance to the error of the reference measurement of 0.08 pH-units using a puncture electrode. In principle, the reference error limits the predictive ability of regression models. In comparison to field study 1, the prediction of the early postmortem pH was improved from $RMSEC = 0.11$ to 0.07 pH-units and from $RMSECV = 0.17$ to 0.09 pH-units. The coefficients of determination deteriorated slightly due to the 50% smaller standard deviation in data set 2. The PLSR model of study 2 performed better due to:

1. More than four times higher integration time per sample ($7 \times 6 \times 2.5\text{s} = 105\text{s}$ versus $10 \times 2.5\text{s} = 25\text{s}$) leading to an improvement of the signal to noise ratio by a factor 2,
2. a shorter offset between pH and Raman measurement (5–15 min versus 15–75),
3. a 50% shorter period in which the Raman measurements were conducted (30 versus 60 min) and
4. a higher number of pH measurements per sample (3–6 versus 2).

The last point influences the PLSR prediction because the reference error is decreased if the number of measurements per sample is increased.

Table 4.3.: Number of latent variables (LVs), number of spectral channels (NSC) and figures of merit of the PLSR correlations with the corresponding parameters of both field studies (field study 1 in brackets). For comparison, standard deviation (SD) of the reference data set and error of the reference method (Ref. error) are presented.

Parameter	pH_{35} (pH_{45})	pH_{24}	L^*	DL / %	SF7(3) / N
LVs	8 (8)	9 (6)	1 (9)	9 (7)	1 (10)
NSC	183 (123)	130 (99)	1024 (261)	122 (87)	1024 (95)
R^2	0.75 (0.82)	0.58 (0.85)	<0.1 (0.95)	0.83 (0.90)	<0.1 (0.95)
R_{cv}^2	0.55 (0.65)	0.31 (0.68)	<0.1 (0.64)	0.52 (0.73)	<0.1 (0.70)
RMSEC	0.07 (0.11)	0.04 (0.06)	2.3 (0.7)	0.4 (0.6)	6 (1.4)
RMSECV	0.09 (0.17)	0.05 (0.09)	2.4 (1.9)	0.6 (1.0)	6 (4)
SD	0.14 (0.29)	0.06 (0.15)	2.4 (3.1)	0.9 (1.9)	6 (7)
Ref. error	0.08 (0.06–0.14)	0.02 (0.04)	1.3 (0.9)	0.3–1.3 ^a	4 (5)

^a from [166]

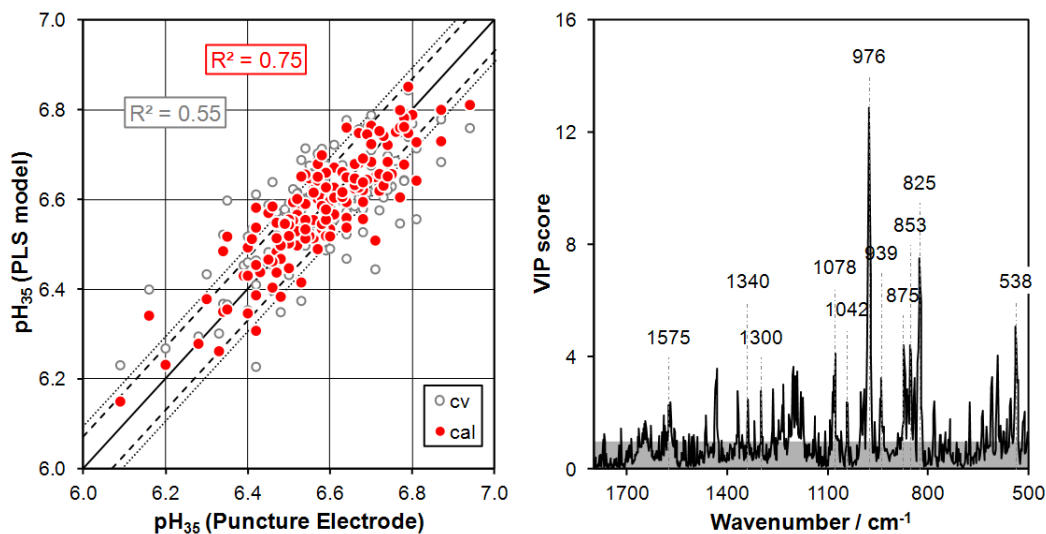


Figure 4.8.: (left) Correlation of pH_{35} predicted from Raman spectra (cv = cross-validation, cal = calibration) with PLSR versus pH_{35} measured with the puncture electrode. (right) VIP plot calculated from PLSR model, exclusion band with VIP score < 1 (gray) and relevant Raman signals marked by their wavenumbers.

As in study 1, VIP plots are used to determine which Raman signals are relevant for the prediction of a given reference parameter (see Fig. 4.8). In case of pH_{35} , the VIP plot reveals a strong influence of the phosphate vibration at 976 cm^{-1} which is in accordance to field study 1. Unlike study 1, the associated phosphate vibration at 1078 cm^{-1} is also weighted. Peaks at 538 , 853 and 1042 cm^{-1} are assigned to lactate, while the peaks at 939 and 1340 cm^{-1} are related to glycogen. Besides the signal at 1340 cm^{-1} , these signals were also weighted in the PLSR model of field study 1. The signal at 1042 cm^{-1} in the Raman spectra is only partly explained by lactate but mostly by creatine, which has a second strong signal at 825 cm^{-1} (with a small contribution to this signal by sugar phosphates). The signal at 825 cm^{-1} is weighted as the second strongest signal in the VIP plot indicating a strong influence of the creatine concentration for the pH_{35} model. This is explained by the higher conversion rate of phosphocreatine to creatine in the earlier time frame from 30 to 60 min compared to the later time frame of study 1 from 60 to 120 min *post mortem* [61, 64, 66]. Signals of phosphocreatine can be found at 849 and 978 cm^{-1} . The first is superimposed by the strong lactate vibration at 855 cm^{-1} . The partial cancellation of these signals may be the reason for the rather weak VIP score at 853 cm^{-1} . The latter adds intensity to the phosphate signal at 976 cm^{-1} . Besides the small VIP scores at 1300 and 1575 cm^{-1} , no indication for an influence of the ATP concentration can be found in this VIP plot which is in contrast to field study 1. This may be explained by the different time frames in which the Raman spectra were obtained. The ATP concentration was shown to be nearly constant in the first hour after slaughter [61]. Thus, the ATP signals are relatively constant and cannot be utilized as an indicator for the metabolic activity. The time difference may also explain why signals of α -helical proteins were weighted in field study 1 but not in study 2.

In field study 1, the pH_{24} could be predicted from the early postmortem Raman spectra with high accuracy ($RMSECV = 0.09$ pH-units). It was interesting to evaluate whether this could be repeated in field study 2. The PLSR model is presented in Fig. 4.9 and yields $R^2 = 0.58$ and $R_{cv}^2 = 0.31$. This is rather poor in comparison to the results

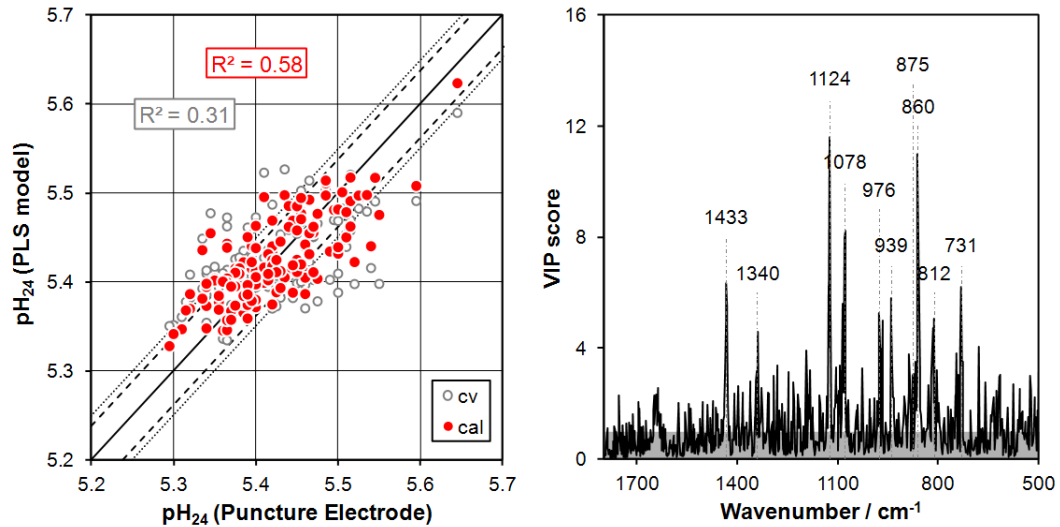


Figure 4.9.: (left) Correlation of pH_{24} predicted from the Raman spectra (cv = cross-validation, cal = calibration) with PLSR versus pH_{24} measured with the puncture electrode. (right) VIP plot calculated from PLSR model, exclusion band with VIP score < 1 (gray) and relevant Raman signals assigned marked by their wavenumbers.

of field study 1 with $R^2 = 0.84$ and $R_{cv}^2 = 0.68$. However, this is partly explained by the more than two times smaller standard deviation in data set 2. Due to the small variance in the pH_{24} , the model performs seemingly inferior but when the $RMSECV$'s are compared, the higher predictive power of model 2 is revealed. With the data of study 2, the PLSR model yields $RMSEC = 0.04$ and $RMSECV = 0.05$ pH-units. The improved performance can be explained by the higher integration time, the shorter time frame in which the spectra were measured and the smaller reference error of the pH_{24} measurement in field study 2.

Again, the VIP plot is used to reveal the most relevant Raman peaks for the pH_{24} prediction (see Fig. 4.9). In contrast to field study 1, the model does not rely on the ADP peak at 1109, but on the ATP peak at 1124 cm^{-1} . Additional ATP signals can be found at 731 and 1340 cm^{-1} . Besides, the strong signal at 860 cm^{-1} may be assigned to lactate and the signal at 939 cm^{-1} to glycogen although the wavenumbers are slightly shifted from 855 and 937 cm^{-1} , respectively. The PLSR utilizes these metabolites because the lactate and glycogen concentrations are closely related, and the amount of glycogen defines the ability of the muscle for acidification hence the ultimate pH. In accordance to study 1, inorganic phosphate signals are weighted at 875, 976 and 1078 cm^{-1} . Besides 976 cm^{-1} , no further signals of PCr and Cr can be found in the VIP score plot which is in conflict with study 1. In addition, two signals at 812 and 1433 cm^{-1} , which are not yet assigned, were not weighted in the VIP plot of study 1.

The color of the meat is an important parameter in the consumer's perception. Hence, its predictability from early postmortem Raman spectra is of high interest. In field study 1, the PLSR model for the prediction of L^* and b^* value yielded very good results with $R^2 > 0.9$, while the correlation between early postmortem Raman spectra and a^* value was only moderate ($R^2 = 0.48$). In field study 2, only L^* values were measured as color parameters. The PLSR model yielded a very poor correlation with coefficients of determination below 0.1 while $RMSEC$ and $RMSECV$ were comparable to the standard deviation in the data set. This PLSR model has no predictive power and is not presented

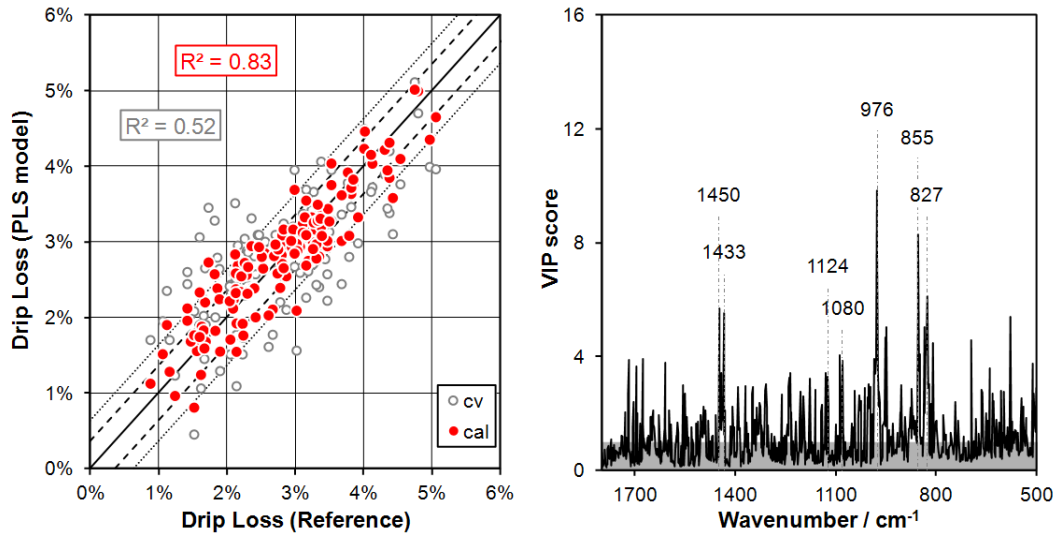


Figure 4.10.: (left) Correlation of drip loss predicted from the Raman spectra (cv = cross-validation, cal = calibration) with PLSR versus drip loss measured with the box method. (right) VIP plot calculated from PLSR model, exclusion band with VIP score < 1 (gray) and relevant Raman signals assigned with its respective wavenumbers.

for that reason. This may partly be explained by the low ratio of the standard deviation to the reference error of 1.8 in this data set. In data set 1, this ratio was almost twice as high with 3.5. On the other hand, a good model was achieved using the pH₃₅ data in field study 2 with an equally low ratio of 1.8 and in field study 1, a promising model could also be calculated for shear force data 72 h p.m. with an even lower ratio of 1.4. Due to the contradictory results in both studies, no conclusive statement can be provided to this point regarding the ability of early postmortem Raman spectra to predict the L* value, except that the time of measurement is important.

The good prediction of the drip loss measured after 72 h from the early postmortem Raman spectra in field study 1 is even excelled in study 2 (see Fig. 4.10). Here, the PLSR model for the prediction of drip loss yielded $R^2 = 0.83$ and $R_{cv}^2 = 0.52$. Due to the small variance of the DL data (0.9%) compared to study 1 (1.9%) the coefficients of determination are slightly inferior in this model. However, with $RMSEC = 0.4\%$ and $RMSECV = 0.6\%$, its predictive power is considerably higher than in study 1 with $RMSEC = 0.6\%$ and $RMSECV = 1.0\%$. This is again explained by the higher integration time per sample and the shorter period of the Raman measurements.

The VIP plot reveals strong influence of the phosphate concentration and the current pH value with the two phosphate signals at 976 and 1080 cm⁻¹ (see Fig. 4.10). Besides, signals at 855 and 1450 cm⁻¹ assigned to lactate and at 827 cm⁻¹ assigned to creatine and phosphorylated sugars are weighted in the PLSR model. To this point, the weighted peaks are in good accordance to the PLSR model calculated in field study 1. However, the VIP plot in field study 2 indicates influence of the signal at 1124 cm⁻¹ assigned to the triphosphate moiety of ATP. On the other hand, signals of ADP, IMP and PCr, which were used in the model of field study 1, are not weighted in this PLSR correlation. In conclusion, both models performed promising, but the VIP plots of study 1 and 2 reveal distinct differences which Raman signals are the basis for these predictions. This may be explained by the different measuring time (60–120 min vs. 30–60 min p.m.) and location (cooling room vs. slaughterline) in both studies.

The correlation between early postmortem Raman spectra and shear force measured 7 d p.m. yielded only very low coefficients of determination with $R^2 < 0.1$ and $R_{cv}^2 < 0.1$ and prediction errors equal to the standard deviation of the data set. This may be caused by the low ratio of the standard deviation and the reference error of 1.5⁴. Another reason may be the late determination of the shear force. As the SF values obtained at day 1 in field study 1 could not be predicted, the ability of the early postmortem Raman spectra to predict SF is contradictory. A possible interpretation is that the early postmortem metabolism partly determines the velocity of the tenderization process. This could explain the lack of predictability of day 1 and 7 SF values. At day 1, tenderization has not yet started and at day 7 the process is too far advanced. Another explanation is that the early postmortem Raman spectra in field study 2 were measured too early to allow for a prediction of SF.

Summary

The second data set comprises meat of higher quality as indicated by higher early postmortem pH, lower pH₂₄ and lower drip loss. The L* values of both data sets are comparable while the shear force values in study 2 are lower on average due to the later measurement 7 days after slaughter. The PLSR correlations between the early postmortem Raman spectra and pH₃₅, pH₂₄ and drip loss yielded 40–50 % lower RMSECVs in field study 2. In fact, the prediction errors were nearly equal to the reference errors. This is mainly the result of four differences between both studies: Higher integration time, smaller time difference between pH and Raman measurement, shorter time frame in which the Raman measurements were conducted and a lower reference error in case of pH₃₅ and pH₂₄. Due to different post-slaughter handling in both abattoirs and different time frame and location of the Raman measurements in both studies, the data of study 2 could not be used to validate the models of study 1. Nevertheless, the PLSR correlations mainly rely on the same energy metabolites which were also identified in field study 1. In both studies glycogen, lactate, creatine, phosphocreatine, ATP, ADP and the phosphate group were identified as key factors for the prediction of pH₃₅, pH₂₄ and drip loss. The differences between the VIP plots are explained by the different time frames of the Raman measurements in both studies. The good predictability of L* value and shear force in study 1 could not be confirmed in study 2, which may be explained by the high reference error of these quality traits. The ratio SD/Ref. error was only 1.8 and 1.5 in case of L* and shear force, respectively. In addition, the very poor correlation in this study may be explained by a too early time frame in which the Raman measurements were conducted.

In conclusion, the second field study confirms the good predictability of pH₃₅/pH₄₅, ultimate pH and drip loss, but more research has to be done to evaluate the potential of early postmortem Raman spectra to predict color and shear force of pork meat.

At this point, it is interesting to evaluate the predictive performance of Raman spectroscopy in both field studies in comparison to other spectroscopic techniques. However, a comparison between the field studies and the literature studies presented in section 2.2.5 is very complicated due to differences in animal species, muscle, sample number, time of spectroscopic and reference measurements, variability of the reference parameters, data preprocessing and data analysis:

- The pH₄₅ has never been successfully predicted from spectral data before. Attempts using NMR spectroscopy revealed, in fact, a relatively clear separation

⁴Although, a promising correlation was found with an even lower ratio of 1.4 in field study 1.

between slow, medium and fast pH fall [172], but just as for NIR spectra, no quantitative relationship between spectra and pH in meat was found [172, 175]. Hence, Raman spectroscopy was proven to be an new spectroscopic technique for the non-invasive assessment of this important quality trait.

- In case of pH_{24} , predictions from early postmortem spectra could not be found in the literature. In comparison to spectroscopic measurements after 24 h p.m., Raman spectroscopy performed better than NMR [169, 170] and NIR spectroscopy [167, 177] and similar to hyperspectral NIR imaging [111, 179, 180].
- No successful prediction of meat *color* from early postmortem data is yet published. In comparison to post-rigor measurements, Raman spectroscopy yielded better coefficients of determination and lower prediction errors in case of L^* and b^* values but inferior results in case of a^* in field study 1 than NIR spectroscopy [167] or hyperspectral NIR imaging [111, 180]. As the good results for L^* could not be repeated in field study 2, no conclusive statement regarding the performance of Raman spectroscopy can be provided in this thesis.
- *Drip loss* was predicted from early postmortem measurements using IR [7] and NIR spectroscopy [190], but Raman spectroscopy performed slightly better in field study 1 and much better in field study 2. In comparison to post-rigor measurements, Raman spectroscopy yielded comparable results to NIR [135, 167, 191] and hyperspectral NIR imaging [111, 179–181] in field study 1 and better results in field study 2.
- To date, *shear force* (beef) was only correlated with early postmortem NIR spectra [207], but the SF predictions using the Raman spectra of field study 1 yielded better results. Using different NIR techniques and post-rigor muscles, comparable or inferior results were achieved with pork and beef samples [135, 191, 204, 207, 208, 210]. As the SF correlations in study 2 were poor, no conclusive statement can be made under which conditions early postmortem Raman spectra can predict shear force of pork meat.

In summary, Raman spectroscopy was shown to provide at least three (pH_{45} , pH_{24} , DL) and up to six important quality traits (L^* , b^* , SF) via a fast, non-invasive and early postmortem measurement with a similar or even higher accuracy than other spectroscopic techniques which mostly used post-rigor measurements. In fact, in case of the early postmortem pH, ultimate pH and drip loss after 72 h p.m., the accuracy of the predictions from the Raman spectra was even comparable to the error of the reference methods.

5. Conclusion & Outlook

As proven in this thesis, Raman spectroscopy can rapidly and non-invasively provide information about the metabolic and structural composition of pork meat early postmortem. Using the first semi-quantitative description of the spectral changes in the early postmortem Raman spectra of meat, signals of important metabolites such as glycogen, lactate, phosphocreatine, creatine, ATP and IMP were shown to contribute to the Raman difference spectra of the pre-rigor and rigor phase. Hence, the early postmortem metabolism in meat can be monitored using this technique. In parallel, the pH value can be measured directly by exploiting the vibrations of terminal phosphate moieties and inorganic phosphate at 980 and 1080 cm^{-1} using the elementary relationship between the concentration ratio of the acid/base pair and the pH provided by the Henderson-Hasselbalch equation. Contrary to the expectations, the lactate signals can not solely be used to predict the pH value due to numerous signals of other metabolites superimposing the lactate peaks. Nevertheless, the pH prediction becomes more accurate if signals of lactate and additional metabolites are included in the regression models. As a result of the pH and lactate investigations in the laboratory, a distinct position effect within porcine *semimembranosus* muscles was observed which reflects the intrinsic heterogeneity of biological matter. The variability is mainly caused by altering muscle fiber composition, enzymatic activity and temperature profile within the muscle/carcass. With respect to these findings, two field studies in the abattoir were performed using a portable Raman system realized in this thesis. In the first study, pH, color, drip loss and shear force were closely correlated with the early postmortem Raman spectra using partial least squares regression of which pH_{45} , pH_{24} , L^* , b^* , drip loss and shear force after 72 h yielded good correlations with $0.80 \leq R^2 \leq 0.95$. In the second field study, this was confirmed and even excelled for pH_{35} , pH_{24} and drip loss. The prediction of L^* and shear force could not be repeated in the second data set due to lower variance, higher reference errors and the very early time of the Raman measurements. In comparison to other spectroscopic techniques, the accuracy of the Raman predictions of the early postmortem pH, pH_{24} and drip loss after 72 h p.m. was similar or even higher and came close to the reference error in both field studies. The improved performance in field study 2 is caused by a combination of higher integration time, shorter time frame in which the spectra were measured, smaller reference error of the pH measurements and smaller delay between Raman and pH measurements. While the last three parameters can hardly be improved due to handling and time constraints of the Raman and pH measurements, the optimization of the integration time deserves further attention in future experiments. Due to inconsistent results in the field studies, future investigations have also to reveal whether the color and the shear force can be accurately predicted from early postmortem Raman spectra. Both studies confirmed that the PLS regression models are mainly weighting Raman signals of the terminal phosphate moiety, energy metabolites and α -helical proteins. Hence, the actual pH value, the metabolic fingerprint and structural information are extracted from the Raman spectra to predict quality traits, which are usually obtainable not until 1 to 3 days *after* the early postmortem, spectroscopic measurements and require labor-intensive, time-consuming

“A great deal more is known than has been proved.”

Richard P. Feynman

and invasive reference analyses.

Thus, this work revealed, for the first time, the principal ability and the feasibility of Raman spectroscopy to provide important quality traits of pork meat by a rapid, accurate, non-invasive and *early postmortem* measurement. In field study 1, Raman spectra were obtained from ten different spots of the meat surface with an integration time of only 2.5s hence one carcass could be analyzed in about one minute. However, a modern abattoir can accommodate an average of 1000–1200 pigs/h per slaughterline [237] and even small abattoirs can handle hundreds of carcasses per hour. Therefore, to be useful for an industrial process, the quality assessment has to be finished in less than five seconds. In future, a Raman system capable of measuring much faster than the current portable system has to be developed to match these requirements. Prior to the commercial application, the following milestones have to be achieved:

- The regression models have to be validated.
- As a result of the validation, the *actual* prediction errors (RMSEP) has to be determined and, if necessary, be improved to meet with the demands of modern abattoirs or meat processing plants.
- The long-term stability of the Raman system has to be evaluated.
- It has to be proven that the prediction models can be transferred between different Raman systems without loss of predictive power.
- The susceptibility of the system to changes within the abattoir has to be investigated, i.e. whether the system has to be newly calibrated each time the handling of the carcasses, the muscle, the cooling regime or similar properties are changed.

Although some obstacles must be overcome until Raman spectroscopy can be commonly applied in abattoirs, use of this promising technique with its unique potential to measure and/or predict several quality traits with only one device could minimize losses to meat producers and processors and help to improve the meat quality for the consumer. As the Raman spectra provide a detailed fingerprint of the postmortem metabolism of the muscle, this technique can probably be extended to additional technological or sensory meat quality traits and should also be applicable to other muscles types and animal species.

Besides the meat industry, Raman spectroscopy could be useful in other fields in which fast and non-invasive measurements are required. As for the ubiquity of phosphorylated compounds in biological matter, Raman spectroscopy could be applied to measure the pH value in other foods and biological tissues. In principle, this technique even enables to non-invasively measure the energy metabolism of living and dying cells. This could establish novel fields of application for Raman spectroscopy in biology or medicine. However, technological improvements, especially in the field of CCD detectors, must be achieved to ensure reasonable measuring times. Nevertheless, Raman spectroscopy is a very promising analytical technique whose potential is far from being fully explored.

Abbreviations

ADP	Adenosine Diphosphate
AMP	Adenosine Monophosphate
ATP	Adenosine Triphosphate
deoxy-Mb	Deoxymyoglobin
DFD	Dark, Firm, Dry
DL	Drip Loss
EC	Electric Conductivity
EI	Electric Impedance
GP	Glycolytic Potential
LD	<i>Musculus longissimus dorsi</i> (coll.: Loin)
LDT	<i>Musculus longissimus dorsi thoracis</i>
LT	<i>Musculus longissimus thoracis</i>
MLR	Multiple Linear Regression
mM	mmol/l
NIR-A	Near-infrared Spectroscopy (Absorbance Mode)
NIR-FOP	Near-infrared Spectroscopy (Fiber Optic Probe)
NIR-HI	Near-infrared Hyperspectral Imaging
NIR-R	Near-infrared Spectroscopy (Reflectance Mode)
NIR-T	Near-infrared Spectroscopy (Transmittance Mode)
NMR	Nuclear Magnetic Resonance Spectroscopy
oxy-Mb	Oxymyoglobin
p.m.	<i>post mortem</i> (Latin: After Death)
PM	<i>Musculus psoas major</i>
PC	Principle Component
PCA	Principle Component Analysis
PCr	Phosphocreatine
PCR	Principle Component Regression
pH ₂₄	pH measured 24 h p.m.
pH ₄₅	pH measured 45 min p.m.
pH _u	Ultimate pH
P _i	Inorganic Phosphate
PLS(R)	Partial Least Squares (Regression)
PSE	Pale, Soft, Exudative
RMSEC	Root Mean Square Error of Calibration
RMSECV	Root Mean Square Error of Cross-Validation
RMSEP	Root Mean Square Error of Prediction
RSE	Reddish, Firm, Non-exudative
SF	Shear Force
SM	<i>Musculus semimembranosus</i> (coll.: Topside)
ST	<i>Musculus semitendinosus</i>
VIP	Variance in Projection
WBSF	Warner-Bratzler Shear Force
WHC	Water-Holding Capacity

Bibliography

- [1] C. V. Raman, K. S. Krishnan (1928) *A new type of secondary radiation*. Nature 121:501–502.
- [2] K. Carron, R. Cox (2010) *Qualitative Analysis and the Answer Box: A Perspective on Portable Raman Spectroscopy*. Analytical Chemistry, 82:3419–3425.
- [3] H. Schmidt, K. Sowoidnich, H.-D. Kronfeldt (2010) *A prototype hand-held Raman sensor for the in-situ characterization of meat quality*. Applied Spectroscopy 64:888–894.
- [4] K. Sowoidnich, H. Schmidt, H.-D. Kronfeldt, F. Schwägele (2012) *A portable 671 nm Raman sensor system for rapid meat spoilage identification*. Vibrational Spectroscopy 62:70–76.
- [5] G. Eikelenboom (1987). In *Evaluation and Control of Meat Quality in Pigs*. Martinus Nijhoff Publishers, Dordrecht, The Netherlands, pp. 479–481.
- [6] J. R. Bendall, H. J. Swatland (1988) *A review of the relationships of pH with physical aspects of pork quality*. Meat Science 24:85–126.
- [7] D. K. Pedersen, S. Morel, H. J. Andersen, S. B. Engelsen (2003) *Early prediction of water-holding capacity in meat by multivariate vibrational spectroscopy*. Meat Science 65:581–592.
- [8] A. G. Smekal (1923) *Zur Quantentheorie der Dispersion*. Die Naturwissenschaften 11:873–875.
- [9] G. Landsberg, L. Mandelstam (1928) *Eine neue Erscheinung bei der Lichtzerstreuung in Krystallen*. Die Naturwissenschaften 16:557–558.
- [10] D. A. Long (2002) In *The Raman Effect: A Unified Treatment of the Theory of Raman Scattering by Molecules*. John Wiley and Sons, Chichester, NY, USA.
- [11] B. Schrader (1995) In *Infrared and Raman Spectroscopy*. VCH Verlagsgesellschaft, Weinheim, NY, USA.
- [12] W. R. Fenner, H. A. Hyatt, J. M. Kellam, S. P. S. Porto (1975) *Raman cross section of some simple gases*. Journal of the Optical Society of America 63:73–77.
- [13] K. Kneipp (2007) *Surface-enhanced Raman scattering*. Physics Today 60(11):40–46.
- [14] M. Snee, W. Ubachs (2005) *Direct measurement of the Rayleigh scattering cross section in various gases*. Journal of Quantitative Spectroscopy and Radiative Transfer 92:293–310.
- [15] K. R. Spring, M. W. Davidson (2013) *Concepts in Digital Imaging Technology – Quantum Efficiency*. Downloaded from <http://learn.hamamatsu.com/articles/quantumefficiency.html> (15 August 2013).

- [16] T. J. Fellers, M. W. Davidson (2013) *Concepts in Digital Imaging Technology – CCD Noise Sources and Signal-to-Noise Ratio*. Downloaded from <http://learn.hamamatsu.com/articles/ccdsnr.html> (15 August 2013).
- [17] B. G. Frushour, J. L. Koenig (1975) In *Advances in Infrared and Raman Spectroscopy – Raman spectroscopy of proteins*. Heyden, London, UK.
- [18] T. G. Spiro, B. P. Gaber (1977) *Laser Raman Scattering as a Probe of Protein Structure*. Annual Reviews of Biochemistry 46:553–569.
- [19] M. Berjot, J. Marx, A. J. P. Alix (1987) *Determination of the secondary structure of proteins from the Raman amide I band: The reference intensity profiles method*. Journal of Raman Spectroscopy 18:289–300.
- [20] M. Pézolet, M. Pigeon-Gosselin, J.-P. Caillé (1978) *Laser raman investigation of intact single muscle fibers: Protein conformations*. Biochimica et Biophysica Acta 533:263–269.
- [21] M. Pézolet, M. Pigeon, D. Ménard, J.-P. Caillé (1988) *Raman spectroscopy of cytoplasmic muscle fiber proteins. Orientational order*. Biophysical Journal 53:319–325.
- [22] E. B. Carew, I. M. Asher, H. E. Stanley (1975) *Laser Raman Spectroscopy - New Probe of Myosin Substructure*. Science 188:933–936.
- [23] T. W. Barrett, W. L. Peticolas, R. M. Robson (1978) *Laser Raman Light-Scattering Observations of Conformational Changes in Myosin Induced by Inorganic Salts*. Biophysical Journal 23:349–358.
- [24] M. Careche, A. M. Herrero, A. Rodriguez-Casado, M. L. Del Mazo, P. Carmona (1999) *Structural changes of hake (Merluccius merluccius L.) fillets: effects of freezing and frozen storage*. Journal of Agricultural and Food Chemistry 47:952–959.
- [25] J. Brøndum, D. V. Byrne, L. S. Bak, G. Bertelsen, S. B. Engelsen (2000) *Warmed-over flavour in porcine meat - a combined spectroscopic, sensory and chemometric study*. Meat Science 54:83–95.
- [26] M. Harz, C. L. Bockmeyer, P. Rösch, R. A. Claus, J. Popp (2007) *UV-Resonance Raman spectroscopic investigation of human plasma for medical diagnosis*. Medical Laser Applications 22:87–93.
- [27] U. Böcker, R. Ofstad, Z. Wu, H. C. Bertram, G. D. Sockalingum, M. Manfait, B. Egelandsdal, A. Kohler (2007) *Revealing covariance structures in Fourier transform infrared and Raman microspectroscopy spectra: a study on pork muscle fiber tissue subjected to different processing parameters*. Applied Spectroscopy 61:1032–1039.
- [28] A. M. Herrero (2008) *Raman Spectroscopy for monitoring protein structure in muscle food systems*. Critical Reviews in Food Science and Nutrition 48:512–523.
- [29] N. K. Howell, H. Herman, E. C. Y. Li-Chan (2001) *Elucidation of Protein-Lipid Interactions in a Lysozyme-Corn Oil System by Fourier Transform Raman Spectroscopy*. Journal of Agricultural and Food Chemistry 49:1529–1533.
- [30] J. W. Chan, D. Motton, J. C. Rutledge, N. L. Keim, T. Huber (2005) *Raman Spectroscopic Analysis of Biochemical Changes in Individual Triglyceride-Rich Lipoproteins in the Pre- and Postprandial State*. Analytical Chemistry 77:5870–5876.

- [31] J. R. Beattie, S. E. J. Bell, C. B. W. Moss (2004) *A Critical Evaluation of Raman Spectroscopy for the Analysis of Lipids: Fatty Acid Methyl Esters*. *Lipids* 39:407–419.
- [32] J. R. Beattie, S. E. J. Bell, C. Borggaard, A. Fearon, B. W. Moss (2006) *Prediction of Adipose Tissue Composition Using Raman Spectroscopy: Average Properties and Individual Fatty Acids*. *Lipids* 41:287–294.
- [33] L. B. Lyndgaard, K. M. Sørensen, F. van den Berg, S. B. Engelsen (2012) *Depth profiling of porcine adipose tissue by Raman spectroscopy*. *Journal of Raman Spectroscopy* 43:482–489.
- [34] E. F. Olsen, C. Baustad, B. Egelanddal, E. O. Rukke, T. Isaksson (2010) *Long-term stability of a Raman instrument determining iodine value in pork adipose tissue*. *Meat Science* 85:1–6.
- [35] S. P. Verma, D. F. H. Wallach (1977) *Raman Spectra of some Saturated, Unsaturated and Deuterated C18 Fatty Acids in the HCH-Deformation and CH-Stretching Regions*. *Biochimica et Biophysica Acta* 486:217–227.
- [36] R. M. C. Dawson, D. C. Elliott, W. H. Elliott, K. M. Jones (1989) In *Data for Biochemical Research*. Oxford University Press, Oxford, UK.
- [37] J. G. Mesu, T. Visser, F. Soulimani, B. M. Weckhuysen (2005) *Infrared and Raman spectroscopic study of pH-induced structural changes of l-histidine in aqueous environment*. *Vibrational Spectroscopy* 39:114–125.
- [38] T.-J. Yu, J. L. Lippert, W. L. Peticolas (1973) *Laser Raman studies of conformational variations of poly-L-lysine*. *Biopolymers* 12:2161–2176.
- [39] J. L. Koenig, B. Frushour (1972) *Raman studies of the helix-to-coil transition in poly-L-glutamic acid and poly-L-ornithine*. *Biopolymers* 11:1871–1892.
- [40] K. T. Yue, M. Lee, J. Zheng, R. Callender (1991) *The determination of the pK_a of histidine residues in proteins by Raman difference spectroscopy*. *Biochimica et Biophysica Acta* 1078:296–302.
- [41] L. Rimai, T. Cole, J. L. Parsons, J. T. Hickmott Jr, E. B. Carew (1969) *Studies of Raman spectra of water solutions of adenosine tri-, di-, and monophosphates and some related compounds*. *Biophysical Journal* 9:320–329.
- [42] Y. Xie, Y. Jiang, D. Ben-Amotz (2005) *Detection of amino acid and peptide phosphate protonation using Raman spectroscopy*. *Analytical Biochemistry* 343:223–230.
- [43] M. E. Heyde, L. Rimai, (1971) *A Raman Spectroscopic Study of the Interaction of Ca^{2+} and Mg^{2+} with the Triphosphate Moiety of Adenosine Triphosphate in Aqueous Solution*. *Biochemistry* 10:1121–1128.
- [44] J. R. Beattie, S. E. J. Bell, C. Borggaard, B. W. Moss (2008) *Preliminary investigations on the effects of ageing and cooking on the Raman spectra of porcine longissimus dorsi*. *Meat Science* 80:1205–1211.
- [45] H. Schmidt, R. Scheier, D. Hopkins (2013) *Preliminary investigation on the relationship of Raman spectra of sheep meat with shear force and cooking loss*. *Meat Science* 93:138–143.

- [46] R. J. Beattie, S. J. Bell, L. J. Farmer, B. W. Moss, D. Patterson (2004) *Preliminary investigation of the application of Raman spectroscopy to the prediction of the sensory quality of beef silverside*. Meat Science 66:903–913.
- [47] D. T. Berhe, M. S. Hviid, S. B. Engelsen, R. Lametsch (2013) *Use of Raman Spectroscopy To Study Effect of Cooking Temperature and Time on Meat Proteins*. Proceedings of the 59th International Congress of Meat Science and Technology.
- [48] Q. Wang, S. M. Lonergan, C. Yu (2012) *Rapid determination of pork sensory quality using Raman spectroscopy*. Meat Science 91:232–239.
- [49] *Leitsätze für Fleisch und Fleischerzeugnisse des Deutschen Lebensmittelbuchs* from 27./28. November 1974.
- [50] R. A. Lawrie, D. A. Ledward (2006) In *Lawrie's meat science*. (7th edition) Woodhead Publishing Limited, Abington Hall, Abington, Cambridge, UK.
- [51] W. Baltes (2007) In *Lebensmittelchemie*. (6th edition) Springer-Verlag, Berlin, Germany.
- [52] H.-D. Belitz, W. Grosch, P. Schieberle (2008) In *Lehrbuch der Lebensmittelchemie*. Springer-Verlag, Berlin, Germany.
- [53] F. Hill, F. M. O'Carroll (1962) *The Chemical Composition of Pig Carcasses at Pork, Bacon, and Manufacturing Weights*. Irish Journal of Agricultural Research 1:115–130.
- [54] K. O. Honikel: *Zusammensetzung von Schweinefleisch* (Internal paper: Composition of pork meat), Bundesanstalt für Fleischforschung Kulmbach.
- [55] P. G. Williams (2007) *Nutritional composition of red meat*. Nutrition & Dietetics 64:113–119.
- [56] P. Tonino, C. T. Pappas, B. D. Hudson, S. Labeit, C. C. Gregorio, H. Granzier (2010) *Reduced myofibrillar connectivity and increased Z-disk width in nebulin-deficient skeletal muscle*. Journal of Cell Science 123:384–391.
- [57] R. G. Taylor, G. H. Geesink, V. F. Thompson, M. Koohmaraie, D. E. Goll (1995) *Is Z-disk degradation responsible for postmortem tenderization?* Journal of Animal Sciences 73:1351–1367.
- [58] C. R. Kerth (2013) In *The Science of Meat Quality*. (1st edition) Wiley-Blackwell (John Wiley & Sons, Inc.), Ames, IA, USA.
- [59] R. L. Lieber (2002) In *Skeletal Muscle Structure, Function, and Plasticity: The Physiological Basis of Rehabilitation*. Lippincott Williams & Wilkins, Baltimore, MD, USA.
- [60] T. L. Scheffler, S. Park, D. E. Gerrard (2011) *Lessons to learn about postmortem metabolism using the AMPK γ 3^{R200Q} mutation in the pig*. Meat Science 89:244–250.
- [61] L. L. Kastenschmidt, W. G. Hoekstra, E. J. Briskey (1968) *Glycolytic Intermediates and Co-Factors in "Fast-" and "Slow-Glycolyzing" Muscles of the Pig*. Journal of Food Science 33:151–158.

- [62] R. Tsai, R. G. Cassens, E. J. Briskey, M. L. Greaser (1972) *Studies on nucleotide metabolism in porcine longissimus muscle postmortem*. Journal of Food Science 37(4):612–617.
- [63] N. Batlle, M.-C. Aristoy, F. Toldrá (2000) *Early Postmortem Detection of Exudative Pork Meat Based on Nucleotide Content*. Journal of Food Science 65:413–416.
- [64] P. Henckel, A. Karlsson, M. T. Jensen, N. Oksbjerg, J. S. Petersen (2002) *Metabolic conditions in Porcine longissimus muscle immediately pre-slaughter and its influence on peri- and post mortem energy metabolism*. Meat Science 62:145–155.
- [65] R. A. Meyer, J. M. Foley (1996) In *Handbook of physiology – Cellular processes integrating the metabolic response to exercise*. Comprehensive Physiology 841–869.
- [66] A. Schäfer, K. Rosenvold, P. P. Purslow, H. J. Andersen, P. Henckel (2002) *Physiological and structural events post mortem of importance for drip loss in pork*. Meat Science 61:355–366.
- [67] T. L. Copenhafer, B. T. Richert, A. P. Schinckel, A. L. Grant, D. E. Gerrard (2006) *Augmented postmortem glycolysis does not occur early postmortem in AMPK3-mutated porcine muscle of halothane positive pigs*. Meat Science 73:590–599.
- [68] E. Dransfield, R. C. Jones, H. J. Macfie (1981) *Tenderising in M. longissimus dorsi of beef, veal, rabbit, lamb and pork*. Meat Science 5:139–147.
- [69] N. Batlle, M.-C. Aristoy, F. Toldrá (2001) *ATP Metabolites During Aging of Exudative and Nonexudative Pork Meats*. Journal of Food Science 66:68–71.
- [70] F. Adzitey, H. Nurul (2011) *Pale soft exudative (PSE) and dark firm dry (DFD) meats: causes and measures to reduce these incidences - a mini review*. International Food Research Journal 18:11–20.
- [71] G. Offer (1991) *Modelling of the Formation of Pale, Soft and Exudative Meat: Effects of Chilling Regime and Rate and Extent of Glycolysis*. Meat Sciences 30:157–184.
- [72] U. Küchenmeister, K. Nürnberg, I. Fiedler, G. Kuhn, G. Nürnberg, K. Ender (1999) *Cell injury and meat quality of pig in the time period post mortem from two genotypes susceptible or resistant to malignant hyperthermia*. European Food Research and Technology 209:97–103.
- [73] E. J. Briskey (1964) *Etiological status and associated studies of pale, exudative porcine musculature*. Advances in Food Research 13:89–178.
- [74] D. J. O'Neill, P. B. Lynch, D. J. Troy, D. J. Buckley, J. P. Kerry (2003) *Effects of PSE on the quality of cooked hams*. Meat Science 64:113–118.
- [75] C. Bernard (1877) In *Leçons sur la diabète et la glycogénèse animal*. Baillière et fils, Paris, France, p. 329.
- [76] P. D. Warriss (2000) In *Meat science: An introductory text*. CAB-International, Wallingford, UK.
- [77] K. G. Newton, C. O. Gill (1981) *The microbiology of DFD fresh meats: A review*. Meat Science 5:223–232.

- [78] Y. C. Ryu, B. C. Kim (2006) *Comparison of histochemical characteristics in various pork groups categorized by postmortem metabolic rate and pork quality*. Journal of Animal Science 84:894–901.
- [79] K. Rosenvold, H. J. Andersen (2003) *Factors of significance for pork quality – a review*. Meat Science 64:219–237.
- [80] E. Risvik (1994) *Sensory properties and preferences*. Meat Science 36:67–77.
- [81] G. Monin (1998) *Recent methods for predicting quality of whole meat*. Meat Science 49(S1):S231–S234.
- [82] J. Wismer-Pedersen (1959) *Quality of pork in relation to rate of pH change post-mortem*. Journal of Food Science 24:711–727.
- [83] A. McM. Taylor (1966) *The incidence of watery muscle in commercial British pigs*. International Journal of Food Science & Technology 1:193–199.
- [84] J. R. Bendall, A. Cuthbertson, D. P. Gatherum (1966) *A survey of pH_1 and ultimate pH values of British progeny-test pigs*. International Journal of Food Science & Technology 1:201–214.
- [85] F. Schmitt, K. H. Schepers, A. Festerling, B. Huebbers, U. Reul (1983) *Beurteilung der Schweinefleischbeschaffenheit in der Schlachtkette*. Schweinezucht und Schweinemast 31:418–421.
- [86] A. J. Kempster, D. G. Evans, J. P. Chadwick (1984) *The effects of source population feeding regimen sex and day of slaughter on the muscle quality characteristics of british crossbred pigs*. Animal Production 39:455–464.
- [87] M. D. Garrido, S. Bañón, J. Pedauy, J. Laencina (1994) *Objective Meat Quality Measurements of Ham: A Practical Classification Method on the Slaughterline*. Meat Science 37:421–428.
- [88] J. R. Bendall (1979) *Relations between muscle pH and important biochemical parameters during post-mortem changes in mammalian muscles*. Meat Sciences 3:143–157.
- [89] D. N. Hamilton, M. Ellis, M. D. Hemann, F. K. McKeith, K. D. Miller, K. W. Purser (2002) *The impact of Longissimus glycolytic potential and short-term feeding of magnesium sulfate heptahydrate prior to slaughter on carcass characteristics and pork quality*. Journal of Animal Science 80:1586–1592.
- [90] G. Monin, P. Sellier (1985) *Pork of low technological quality with a normal rate of muscle pH fall in the immediate post-mortem period – the case of the hampshire breed*. Meat Science 13:49–63.
- [91] K. Immonen, E. Puolanne (2000) *Variation of residual glycogen-glucose concentration at ultimate pH values below 5.75*. Meat Science 55:279–283.
- [92] D. J. O'Neill, P. B. Lynch, D. J. Troy, D. J. Buckley, J. P. Kerry (2003) *Influence of the time of year on the incidence of PSE and DFD in Irish pigmeat*. Meat Science 64:105–111.
- [93] F. Guignot, C. Touraille, A. Ouali, M. Renerre, G. Monin (1994) *Relationships between Post-mortem pH Changes and Some Traits of Sensory Quality in Veal*. Meat Science 37:315–325.

- [94] M. Mitsumoto, S. Maeda, T. Mitsuhashi, S. Ozawa (1991) *Near infrared spectroscopy determination of physical and chemical characteristics in beef cuts*. Journal of Food Science 56:1493–1496.
- [95] E. Huff-Lonergan, S. M. Lonergan (2005) *Mechanisms of water-holding capacity of meat: The role of postmortem biochemical and structural changes*. Meat Science 71:194–204.
- [96] G. Offer, P. Knight (1988) In *Developments in meat science – The structural basis of water-holding capacity in meat. Part 2: drip losses*. (4th edition) Elsevier Science Publications, London, UK, pp. 173–243.
- [97] O. R. Fennema (1985) In *Food chemistry – Water and ice*. Marcel Dekker Inc., New York, NY, USA.
- [98] L. Diesbourg, H. J. Swatland, B. M. Millman (1988) *X-ray- diffraction measurements of postmortem changes in the myofilament lattice of pork*. Journal of Animal Science 66:1048–1054.
- [99] H. J. Swatland, S. Belfry (1985) *Post mortem changes in the shape and size of myofibrils from skeletal muscle of pigs*. Mikroskopie 42:26–34.
- [100] R. T. Pearson, I. D. Duff, W. Derbyshire, J. M. Blanshard (1974) *An NMR investigation of rigor in porcine muscle*. Biochimica et Biophysica Acta 362:188–200.
- [101] T. C. Irving, H. J. Swatland, B. M. Millman, (1989) *X-ray diffraction measurements of myofilament lattice spacing and optical measurements of reflectance and sarcomere length in commercial pork loins*. Journal of Animal Science 67: 152–156.
- [102] H. C. Bertram, P. P. Purslow, H. J. Andersen (2002) *Relationship between meat structure, water mobility, and distribution: a lowfield nuclear magnetic resonance study*. Journal of Agricultural and Food Chemistry 50:824–829.
- [103] G. Offer, P. Knight, R. Jeacocke, R. Almond, T. Cousins, J. Elsey, N. Parsons, A. Sharp, R. Starr, P. Purslow (1989) *The structural basis of the water-holding, appearance and toughness of meat and meat-products*. Food Microstructure 8:151–170.
- [104] G. Offer, T. Cousins (1992) *The mechanism of drip production – formation of 2 compartments of extracellular-space in muscle postmortem*. Journal of the Science of Food and Agriculture 58:107–116.
- [105] P. D. Warriss, S. N. Brown (1987) *The relationships between initial pH, reflectance and exudation in pig muscle*. Meat Sciences 20:65–74.
- [106] I. F. Penny (1977) *The effect of temperature on the drip, denaturation and extracellular space of pork longissimus dorsi muscle*. Journal of the Sciences of Food and Agriculture 28:329–338.
- [107] P. D. Warriss (1982) *The relationship between pH_{4.5} and drip in pig muscle*. International Journal of Food Science & Technology 17:573–578.
- [108] J. Fujii, K. Otsu, F. Zorzato, S. Deleon, V. K. Khanna, J. E. Weiler, P. J. O'Brien, D. H. MacLennan (1991) *Identification of a mutation in porcine ryanodine receptor associated with malignant hyperthermia*. Science 253:448–451.

- [109] D. C. Ciobanu, J. Bastiaansen, S. M. Lonergan, H. Thomsen, J. C. M. Dekkers, G. S. Plastow, M. F. Rothschild (2004) *New alleles in calpastatin gene are associated with meat quality traits in pigs*. Journal of Animal Science 82:2829–2839.
- [110] R. L. J. M. van Laack, R. G. Kauffman, W. Sybesma, F. J. M. Smulders, G. Eikelenboom, J. C. Pinheiro (1994) *Is Colour Brightness (L-Value) a Reliable Indicator of Water-Holding Capacity in Porcine Muscle?* Meat Science 38:193–201.
- [111] D. F. Barbin, G. ElMasry, D.-W. Sun, P. Allen (2012) *Predicting quality and sensory attributes of pork using near-infrared hyperspectral imaging*. Analytica Chimica Acta 719:30–42.
- [112] A. A. Taylor, S. J. Dant (1971) *Influence of carcass cooling rate on drip loss in pig meat*. Journal of Food Sciences & Technology 6:131–139.
- [113] A. W. J. Savage, P. D. Warriss, P. D. Jolley (1990) *The Amount and Composition of the Proteins in Drip from Stored Pig Meat*. Meat Science 27:289–303.
- [114] C. E. Carpenter, D. P. Cornforth, D. Whittier (2001) *Consumer preferences for beef color and packaging did not affect eating satisfaction*. Meat Science 57:359–363.
- [115] R. A. Mancini, M. C. Hunt (2005) *Current research in meat color*. Meat Science 71:100–121.
- [116] S. T. Joo, R. G. Kauffmann, B. C. Kim, G. B. Park (1999) *The relationship of sarcoplasmic and myofibrillar protein solubility to color and water-holding capacity in porcine longissimus muscle*. Meat Science 52:291–297.
- [117] F. Feldhusen (1994) *Einflüsse auf die postmortale Farbveränderung der Oberfläche von Schweinemuskulatur*. Fleischwirtschaft 74:989–991.
- [118] R. A. Mancini, R. Ramanathan (2007) *Sodium lactate influences myoglobin redox stability in vitro*. Meat Science 78:529–532.
- [119] D. Juncher, B. Ronn, E. T. Mortensen, P. Henckel, A. Karlsson, L. H. Skibsted (2001) *Effect of pre-slaughter physiological conditions on the oxidative stability of color and lipid during chill storage of pork*. Meat Science 58:347–357.
- [120] M. Abril, M. M. Campo, A. Onenc, C. Sanudo, P. Alberti, A. L. Negueruela (2001) *Beef color evolution as a function of ultimate pH*. Meat Science 58:69–78.
- [121] D. N. Hamilton, K. D. Miller, M. Ellis, F. K. McKeith, E. R. Wilson (2003) *Relationships between longissimus glycolytic potential and swine growth performance, carcass traits, and pork quality*. Journal of Animal Science 81:2206–2212.
- [122] S. J. Moeller, T. J. Baas, T. D. Leeds, R. S. Emnett, K. M. Irvin (2003) *Rendement Napole gene effects and a comparison of glycolytic potential and DNA genotyping for classification of Rendement Napole status in Hampshire-sired pigs*. Journal of Animal Science 81:402–410.
- [123] P. D. Warriss, S. N. Brown, S. J. M. Adams, D. B. Lowe (1990) *Variation in haem pigment concentration and color in meat from British pigs*. Meat Science 28:321–329.
- [124] G. R. Beecher, R. G. Cassens, W. G. Hoekstra, E. J. Briskey (1965) *Red and white fiber content and associated post-mortem properties of seven porcine muscles*. Journal of Food Science 30:969–976.

- [125] G. R. Beecher, L. L. Kastenschmidt, W. G. Hoekstra, R. G. Cassens, E. J. Briskey (1969) *Energy metabolites in red and white striated muscles of the pig*. Journal of Agricultural and Food Chemistry 17:29–33.
- [126] G. Lindahl, K. Lundström, E. Tornberg (2001) *Contribution of pigment content, myoglobin forms and internal reflectance to the color of pork loin and ham from pure breed pigs*. Meat Science 59:141–151.
- [127] J. G. Gentry, J. J. McGlone, M. F. Miller, J. R. Blanton Jr (2004) *Environmental effects on pig performance, meat quality, and muscle characteristics*. Journal of Animal Science 82:209–217.
- [128] H. A. Channon, A. M. Payne, R. D. Warner (2000) *Halothane genotype, pre-slaughter handling and stunning method all influence pork quality*. Meat Science 56:291–299.
- [129] U. Küchenmeister, G. Kuhn, E. Ender (2000) *Seasonal effects on Ca^{2+} transport of sarcoplasmic reticulum and on meat quality of pigs with different malignant hyperthermia status*. Meat Science 55:239–245.
- [130] H. J. Swatland (1987) In *Evaluation and Control of Meat Quality in Pigs*. Kluwer Academic Publishers Group, Dordrecht, The Netherlands, p. 143.
- [131] M. F. Miller, M. A. Carr, C. B. Ramsey, K. L. Crockett, L. C. Hoover (2001) *Consumer thresholds for establishing the value of beef tenderness*. Journal of Animal Science 79:3062–3068.
- [132] J. D. Wood, M. Enser, A. V. Fisher, G. R. Nute, P. R. Sheard, R. I. Richardson, S. I. Hughes, F. M. Whittington (2008) *Fat deposition, fatty acid composition and meat quality: A review*. Meat Science 78:343–358.
- [133] J.-L. Damez, S. Clerjon (2008) *Meat quality assessment using biophysical methods related to meat structure*. Meat Science 80:132–149.
- [134] D. J. Etherington, M. A. J. Taylor, D. K. Wakefield, A. Cousins, E. Dransfield (1990) *Proteinase (Cathepsin B, D, L and Calpains) Levels and Conditioning Rates in Normal, Electrically Stimulated and High-Ultimate-pH Chicken Muscle*. Meat Science 28:99–109.
- [135] G. H. Geesink, F. H. Schreutelkamp, R. Frankhuizen, H. W. Vedder, N. M. Faber, R. W. Kranen, M. A. Gerritzen (2003) *Prediction of pork quality attributes from near infrared reflectance spectra*. Meat Science 65:661–668.
- [136] A. Ducastaing, C. Valin, J. Schollmeyer, R. Cross (1985) *Effects of electrical stimulation on post-mortem changes in the activities of two Ca dependent neutral proteinases and their inhibitor in beef muscle*. Meat Science 15:193–202.
- [137] G. H. Geesink, M. Koohmaraie (1999) *Effect of Calpastatin on Degradation of Myofibrillar Proteins by μ -Calpain Under Postmortem Conditions*. Journal of Animal Science 77:2685–2692.
- [138] G. H. Geesink, S. Kuchay, A. H. Chishti, M. Koohmaraie (2006) *μ -Calpain is essential for postmortem proteolysis of muscle proteins*. Journal of Animal Science 84:2834–2840.

- [139] E. Huff-Lonergan, T. Mitsuhashi, D. D. Beekman, F. C. Parrish Jr., D. G. Olson, R. M. Robson (1996) *Proteolysis of Specific Muscle Structural Proteins by m-Calpain at Low pH and Temperature Is Similar to Degradation in Postmortem Bovine Muscle*. Journal of Animal Science 74:993–1008.
- [140] D. L. Hopkins, J. M. Thompson (2002) *Factors contributing to proteolysis and disruption of myofibrillar proteins and the impact on tenderisation in beef and sheep meat*. Australian Journal of Agricultural Research 53:146–166.
- [141] F. Zamora, L. Aubry, T. Sayd, J. Lepetit, A. Lebert, M. A. Sentandreu, A. Ouali (2005) *Serine peptidase inhibitors, the best predictor of beef ageing amongst a large set of quantitative variables*. Meat Science 71:730–742.
- [142] G. Whipple, M. Koohmaraie, M. E. Dikeman, J. D. Crouse, M. C. Hunt, R. D. Klemm (1990) *Evaluation of attributes that affect longissimus muscle tenderness in bos taurus and bos indicus cattle*. Journal of Animal Science 68:2716–2724.
- [143] M. Koohmaraie (1992) *Effect of pH, temperature, and inhibitors on autolysis and catalytic activity of bovine skeletal muscle mu-calpain*. Journal of Animal Science 70:3071–3080.
- [144] S. M. Lonergan, E. Huff-Lonergan, B. R. Wiegand, L. A. Kriese-Anderson (2001) *Postmortem proteolysis and tenderization of top loin steaks from brangus cattle*. Journal of Muscle Foods 12:121–136.
- [145] R. J. McCormick (1994) *The flexibility of the collagen compartment of muscle*. Meat Science 36:79–91.
- [146] J. V. Lochner, R. G. Kauffman, B. B. Marsh (1980) *Early-post-mortem cooling rate and beef tenderness*. Meat Science 4:227–241.
- [147] S. G. May, H. G. Dolezal, D. R. Gill, F. K. Ray, D. S. Buchanan (1992) *Effects of Day Fed, Carcass Grade Traits, and Sub-cutaneous Fat Removal on Post-mortem Muscle Characteristics and Beef Palatability*. Journal of Animal Science 70:444–453.
- [148] L. E. Jeremiah, A. K. W. Tong, L. L. Gibson (1991) *The usefulness of muscle color and pH for segregating beef carcasses into tenderness groups*. Meat Science 30:97–114.
- [149] D. M. Wulf, S. F. O'Connor, J. D. Tatum, G. C. Smith (1997) *Using objective measures of muscle color to predict beef longissimus tenderness*. Journal of Animal Science 75:684–692.
- [150] M. P. Rees, G. R. Trout, R. D. Warner (2003) *The influence of the rate of pH decline on the rate of ageing for pork. II: Interaction with chilling temperature*. Meat Science 65:805–818.
- [151] R. H. Locker, C. J. Hagyard (1963) *A cold shortening effect in beef muscles*. Journal of the Science of Food and Agriculture 14:787–793.
- [152] B. K. Jones, J. D. Tatum (1994) *Predictors of beef tenderness among carcasses produced under commercial conditions*. Journal of Animal Science 72:1492–1501.

- [153] G. R. O'Halloran, D. J. Troy, D. J. Buckley, W. J. Reville (1997) *The role of endogenous proteases in the tenderisation of fast glycolysing muscle*. Meat Science 47:187–210.
- [154] A. P. White, A. O'Sullivan, E. E. O'Neill, D. J. Troy (2004) *Manipulation of pre-rigor glycolytic behaviors to produce consistent beef tenderness*. Proceedings of the 50th International Congress of Meat Science and Technology 62–63.
- [155] G. Bee, A. L. Anderson, S. M. Lonergan, E. Huff-Lonergan (2007) *Rate and extent of pH decline affect proteolysis of cytoskeletal proteins and water-holding capacity in pork*. Meat Science 76:359–365.
- [156] J. L. Melody, S. M. Lonergan, L. J. Rowe, T. W. Huiatt, M. S. Mayes, E. Huff-Lonergan (2004) *Early postmortem biochemical factors influence tenderness and water-holding capacity of three porcine muscles*. Journal of Animal Science 82:1195–1205.
- [157] S. D. Shackelford, M. Koohmaraie, J. W. Savell (1994) *Evaluation of Longissimus dorsi Muscle pH at Three Hours Post Mortem as a Predictor of Beef Tenderness*. Meat Science 37:195–204.
- [158] S. T. Joo, R. G. Kauffman, B. C. Kim, C. J. Kim (1995) *The relationship between color and water-holding capacity in post-rigor porcine longissimus muscle*. Journal of Muscle Foods 6:211–226.
- [159] R. G. Kauffman, R. G. Cassens, A. Scherer, D. L. Meeker (1992) In *Variation in pork quality*. National Pork Producers Council Publication, Des Moines, IA, USA.
- [160] R. D. Warner, R. G. Kauffman, R. L. Russell (1993) *Quality attributes of major porcine muscles: A comparison with longissimus lumborum*. Meat Science, 33:359–372.
- [161] R. D. Warner, R. G. Kauffman, M. L. Greaser (1997) *Muscle protein changes post mortem in relation to pork quality traits*. Meat Science 45:339–352.
- [162] R. L. J. M. van Laack, M. B. Solomon, R. D. Warner, R. G. Kauffman (1996) *A comparison of procedures for measurement of pigment concentration in pork*. Journal of Muscle Foods 7:149–63.
- [163] A. Petzet, R. Scheier, A. Octoviani, A. Bauer, A. Hammon, H. Diepolder, H. Schmidt, F. Schwägele (2013) *Entwicklung von Analysemethoden zur Etablierung einer online-fähigen Beurteilung der Fleischqualität*. Fleischwirtschaft 93:84–87.
- [164] A. K. Covington, R. G. Bates, R. A. Durst (1985) *Definitions of pH scales, standard reference values, measurement of pH, and related terminology*. Pure and Applied Chemistry 57:531–542.
- [165] J. Frisby, D. Raftery, J. P. Kerry, D. Diamond (2005) *Development of an autonomous, wireless pH and temperature sensing system for monitoring pig meat quality*. Meat Science 70:329–336.
- [166] L. B. Christensen (2003) *Drip loss sampling in porcine m. longissimus dorsi*. Meat Science 63:469–477.

- [167] M. Čandek-Potokar, M. Prevolnik, M. Škrlep (2006) *Ability of near infrared spectroscopy to predict pork technological traits*. Journal of Near Infrared Spectroscopy 14:269–277.
- [168] R. B. Moon, J. H. Richards (1973) *Determination of intracellular pH by ^{31}P magnetic resonance*. Journal of Biological Chemistry 248:7276–7278.
- [169] A. Miri, A. Talmant, J. P. Renou, G. Monin (1992) *^{31}P NMR study of post mortem changes in pig muscle*. Meat Science 31:165–173.
- [170] J. P. Renou, G. Monin (1985) *Nuclear Magnetic Resonance Measurements on Pork of Various Qualities*. Meat Science 15:225–233.
- [171] A. Madden, M.O. Leach, J.C. Sharp, D.J. Collins, D. Easton (1991) *A quantitative analysis of the accuracy of In Vivo pH measurements with ^{31}P NMR spectroscopy: Assessment of pH measurement methodology*. NMR in Biomedicine 4:1–11.
- [172] E. Tornberg, M. Wahlgren, J. Brøndum, S. B. Engelsen (2000) *Pre-rigor conditions in beef under varying temperature- and pH-falls studied with rigormeter, NMR and NIR*. Food Chemistry 69:407–418.
- [173] J. C. Puyana, B. R. Soller, S. Zhang, S. O. Heard Continuous (1999) *Measurement of Gut pH with Near-Infrared Spectroscopy during Hemorrhagic Shock*. The Journal of Trauma: Injury, Infection, and Critical Care 46:9–15.
- [174] H. J. Swatland (1986) *Color measurements on pork and veal carcasses by fiber optic spectrophotometry*. Canadian Institute of Food Science and Technology 19:170–173.
- [175] H. J. Swatland (1983) *Infrared fiber optic spectrophotometry of meat*. Journal of Animal Science 56:1329–1333.
- [176] B. R. Soller, R. H. Micheels, J. Coen, B. Parikh, L. Chu, C. Hsi (1996) *Feasibility of non-invasive measurement of tissue pH using near-infrared reflectance spectroscopy*. Journal of Clinical Monitoring 12:387–395.
- [177] J. R. Andersen, C. Borggaard, A. J. Rasmussen, L. P. Houmøller (1999) *Optical measurements of pH in meat*. Meat Science 53:135–141.
- [178] J. E. Bertie, Z. Lan (1996) *Infrared Intensities of Liquids XX: The Intensity of the OH Stretching Band of Liquid Water Revisited, and the Best Current Values of the Optical Constants of $\text{H}_2\text{O}(l)$ at 25°C between 15,000 and 1 cm^{-1}* . Applied Spectroscopy 50:1047–1057.
- [179] M. Kamruzzaman, G. ElMasry, D.-W. Sun, P. Allen (2012) *Prediction of some quality attributes of lamb meat using near-infrared hyperspectral imaging and multivariate analysis*. Analytica Chimica Acta 714:57–67.
- [180] J. Qiao, N. Wang, M. O. Ngadi, A. Gunenc, M. Monroy, C. Gariépy, S. O. Prasher (2006) *Prediction of drip-loss, pH, and color for pork using a hyperspectral imaging technique*. Meat Science 76:1–8.
- [181] G. ElMasry, D.-W. Suna, P. Allen (2011) *Non-destructive determination of water-holding capacity in fresh beef by using NIR hyperspectral imaging*. Food Research International 44:2624–2633.

- [182] C. E. Byrne, D. J. Troy, D. J. Buckley (2000) *Postmortem changes in muscle electrical properties of bovine M. longissimus dorsi and their relationship to meat quality attributes and pH fall*. Meat Science 54:23–34.
- [183] R. Grau, R. Hamm, (1956) *Die Bestimmung der Wasserbindung des Fleisches mittels der Preßsaftmethode*. Fleischwirtschaft 12:733–736.
- [184] K. Hofmann (1975) *Ein neues Gerät zur Bestimmung der Wasserbindung des Fleisches: Das "Kapillar-Volumeter"*. Fleischwirtschaft 55:25–30.
- [185] R. G. Kauffman, G. Eikelenboom, P. G. van der Wal, G. Merkus, M. Zaar (1986) *The use of filter paper to estimate drip loss of porcine musculature*. Meat Science 18:191–200.
- [186] K. O. Honikel (1998) *Reference Methods for the Assessment of Physical Characteristics of Meat*. Meat Sciences 49:447–457.
- [187] M. Scheeder (2013) *personal communication*.
- [188] M. Prevolnika, M. Čandek-Potokar, M. Novič, D. Škorjanc (2009) *An attempt to predict pork drip loss from pH and color measurements or near infrared spectra using artificial neural networks*. Meat Science 83:405–411.
- [189] J. Brøndum, L. Munck, P. Henckel, A. Karlsson, E. Tornberg, S. B. Engelsen (2000) *Prediction of waterholding capacity and composition of porcine meat by comparative spectroscopy*. Meat Science 55:177–185.
- [190] J. C. Forrest, M. T. Morgan, C. Borggaard, A. J. Rasmussen, B. L. Jespersen, J. R. Andersen (2000) *Development of technology for the early post mortem prediction of water holding capacity and drip loss in fresh pork*. Meat Science 55:115–122.
- [191] B. Leroy, S. Lambotte, O. Dotreppe, H. Lecocq, L. Istasse, A. Clinquart (2003) *Prediction of technological and organoleptic properties of beef Longissimus thoracis from near-infrared reflectance and transmission spectra*. Meat Science 66:45–54.
- [192] W. D. Wright (1928) *A re-determination of the trichromatic coefficients of the spectral colours*. Transactions of the Optical Society 30:141–164.
- [193] J. Guild (1932) *The colorimetric properties of the spectrum*. Philosophical Transactions of the Royal Society of London. Series A, Containing Papers of a Mathematical or Physical Character 230:149–187.
- [194] A. Stockman, D. I. A. MacLeod, N. E. Johnson (1993) *Spectral sensitivities of the human cones*. Journal of the Optical Society of America A 10:2491–2521.
- [195] M.S Brewer, L. G. Zhu, B. Bidner, D. J. Meisinger, F. K. McKeith (2001) *Measuring pork color: Effects of bloom time, muscle, pH and relationship to instrumental parameters*. Meat Science 57:169–176.
- [196] Y. Duan, L. Huang, J. Xie, K. Yang, F. Yuan, H. L. Bruce, G. S. Plastow, J. Ma, L. Huang (2013) *Effect of temperature and pH on postmortem color development of porcine M. longissimus dorsi and M. semimembranosus*. Journal of the Sciences of Food and Agriculture 93:1206–1210.

- [197] M. G. O'Sullivan, D. V. Byrne, H. Martens, G. H. Gidskehaug, H. J. Andersen, M. Martens (2003) *Evaluation of pork color: Prediction of visual sensory quality of meat from instrumental and computer vision methods of color analysis*. Meat Science 65:909–918.
- [198] J. Lu, J. Tan, P. Shatadal, D. E. Gerrard (2000) *Evaluation of pork color by using computer vision*. Meat Science 56:57–60.
- [199] Y. Liu, B. G. Lyon, W. R. Windham, C. E. Realini, T. D. Pringle, S. Duckett (2003) *Prediction of color, texture and sensory characteristics of beef steaks by visible and near infrared reflectance spectroscopy. A feasibility study*. Meat Science 65:1107–1115.
- [200] C. Maltin, D. Balcerzak, R. Tilley, M. Delday (2003) *Determinants of meat quality: tenderness*. Proceedings of the Nutrition Society 62:337–347.
- [201] D. M. Price, G. G. Hilton, D. L. VanOverbeke, J. B. Morgan (2008) *Using the near-infrared system to sort various beef middle and end muscle cuts into tenderness categories*. Journal of Animal Science 86:413–418.
- [202] K. I. Hildrum, B. N. Nilsen, M. Mielnik, T. Næs (1994) *Prediction of sensory characteristics of beef by near-infrared spectroscopy*. Meat Science 38:67–80.
- [203] C. E. Byrne, G. Downey, D. J. Troy, D. J. Buckley (1998). *Non-destructive prediction of selected quality attributes of beef by nearinfrared reflectance spectroscopy between 750 and 1098 nm*. Meat Science 49:399–409.
- [204] B. Park, Y. R. Chen, W. R. Hruschka, S. D. Shackelford, M. Koohmaraie (1998) *Near-infrared Reflectance analysis for predicting beef longissimus tenderness*. Journal of Animal Science 76:2115–2120.
- [205] R. Rødbotten, B. H. Mevik, K. I. Hildrum (2001) *Prediction and classification of tenderness in beef from non-invasive diode array detected NIR spectra*. Journal of Near Infrared Spectroscopy 9:199–210.
- [206] C. Venel, A. M. Mullen, G. Downey, D. J. Troy (2001) *Prediction of tenderness and other quality attributes of beef by near infrared reflectance spectroscopy between 750 and 1100 nm; further studies*. Journal of Near Infrared Spectroscopy 9:185–198.
- [207] R. Rødbotten, B. N. Nilsen, K. I. Hildrum (2000) *Prediction of beef quality attributes from early post mortem near infrared reflectance spectra*. Food Chemistry 69:427–436.
- [208] S. R. Rust, D. M. Price, J. Subbiah, G. Kranzler, G. G. Hilton, D. L. Vanoverbeke, J. B. Morgan (2008) *Predicting beef tenderness using near-infrared spectroscopy*. Journal of Animal Science 86:211–219.
- [209] S. D. Shackelford, T. L. Wheeler, M. Koohmaraie (2004) *Development of optimal protocol for visible and near-infrared reflectance spectroscopic evaluation of meat quality*. Meat Science 68:371–381.
- [210] S. D. Shackelford, T. L. Wheeler, M. Koohmaraie (2005) *Online classification of U.S. Select beef carcasses for longissimus tenderness using visible and near-infrared reflectance spectroscopy*. Meat Science 69:409–415.

- [211] K. Cluff, G. K. Naganathan, J. Subbiah, R. Lu, C. R. Calkins, A. Samal (2008) *Optical scattering in beef steak to predict tenderness using hyperspectral imaging in the VIS-NIR region*. Sensing and Instrumentation for Food Quality and Safety 2:189–196.
- [212] Y. Huang, R. E. Lacey, L. L. Moore, R. K. Miller, A. D. Whittaker, J. Ophir (1997) *Wavelet textural features from ultrasonic elastograms for meat quality prediction*. Transactions of the American Society of Agricultural Engineers 40:1741–1748.
- [213] D. L. Hopkins, D. Wang (2012) *Preliminary investigation of high resolution impedance spectroscopy for measuring shear force*. 58th International Congress of Meat Science and Technology B-27:1–4.
- [214] S. D. Shackelford, T. L. Wheeler, M. Koohmaraie (1999) *Tenderness classification of beef: Design and analysis of a system to measure beef longissimus shear force under commercial processing conditions*. Journal of Animal Science 77:1474–1481.
- [215] H. Schmidt, T. Murphy, S. Lucht, H.-D. Kronfeldt (1999) *Development of a SERS optode for the in-situ detection of chemicals in sea water*. SPIE Proceedings 3853, Environmental Monitoring and Remediation Technologies II.
- [216] M. Maiwald, A. Ginolas, A. Müller, A. Sahm, B. Sumpf, G. Erbert, G. Tränkle (2008) *Wavelength-Stabilized Compact Diode Laser System on a Microoptical Bench With 1.5- W Optical Output Power at 671 nm*. IEEE Photonics Technology Letters 20:1627–1629.
- [217] B. Sumpf, H. Schmidt, M. Maiwald, A. Müller, G. Erbert, H.-D. Kronfeldt, G. Tränkle (2009) *Microsystem technology based diode lasers and Raman sensors for in situ food quality control*. SPIE Proceedings 7315, Sensing for Agriculture and Food Quality and Safety.
- [218] W. J. Bowen (1949) *The absorption spectra and extinction coefficients of myoglobin*. The Journal of Biological Chemistry 179:235–245.
- [219] D. J. Faber, M. C. G. Aalders, E. G. Mik, B. A. Hooper, M. J. C. van Gemert, T. G. van Leeuwen (2004) *Oxygen Saturation-Dependent Absorption and Scattering of Blood*. Physical Review Letters 93:028102-1–028102-4.
- [220] A. Savitzky, M. J. E. Golay (1964) *Smoothing and Differentiation of Data by Simplified Least Squares Procedures*. Analytical Chemistry 36:1627–1639.
- [221] H. G. Schulze, R. B. Foist, K. Okuda, A. Ivanov, R. F. B. Turner (2011) *A Model-Free, Fully Automated Baseline-Removal Method for Raman Spectra*. Applied Spectroscopy 65:75–84.
- [222] Anonymous (1972) *Comments on Smoothing and Differentiation of Data by Simplified Least Square Procedure*. Analytical Chemistry 44:1906–1909.
- [223] C. M. Galloway, E. C. Le Ru, P. G. Etchegoin (2009) *An Iterative Algorithm for Background Removal in Spectroscopy by Wavelet Transforms*. Applied Spectroscopy 63:1370–1376.
- [224] K. Pearson (1901) *On lines and planes of closest fit to systems of points in space*. Philosophical Magazine 2:559–572.

- [225] H. Wold (1966) In *Multivariate Analysis – Estimation of principal components and related models by iterative least squares*. Academic Press, New York, USA, pp.391–420.
- [226] S. Wold, H. Martens, H. Wold (1983) In *Matrix Pencils – The multivariate calibration problem in chemistry solved by the PLS method*. Springer, Heidelberg, Germany, pp. 286–298.
- [227] S. Wold, M. Sjöström, L. Eriksson (2001) *PLS-regression: a basic tool of chemometrics*. Chemometrics and Intelligent Laboratory Systems 58:109–130.
- [228] S. de Jong (1993) *SIMPLS: an alternative approach to partial least squares regression*. Chemometrics and Intelligent Laboratory Systems 18:251–263.
- [229] B. M. Wise, J. M. Shaver, N. B. Gallagher, W. Windig, R. Bro, R. S. Koch (2006) In *Chemometrics Tutorial for PLS_Toolbox and Solo*. Eigenvector Research, Inc., Wenatchee, WA, USA, pp. 147–149.
- [230] I.-G. Chong, C.-H. Jun (2005) *Performance of some variable selection methods when multicollinearity is present*. Chemometrics and Intelligent Laboratory Systems 78:103–112.
- [231] S. Osborne, R. Jordan, R. Kunnemeyer (1997) *Methods of wavelength selection for partial least squares*. Analyst 122:1531–1537.
- [232] H. C. Bertram, S. Dønstrup, A. H. Karlsson, H. J. Andersen, H. Stødtkilde-Jørgensen (2001) *Post mortem energy metabolism and pH development in porcine M. longissimus dorsi as affected by two different cooling regimes. A ³¹P-NMR spectroscopic study*. Magnetic Resonance Imaging 19:993–1000.
- [233] D. Lin-Vien, N. B. Colthup, W. G. Fateley, J. G. Grasselli (1991) *The Handbook of Infrared and Raman Characteristic Frequencies of Organic Molecules*, Academic Press, Boston, MA, USA.
- [234] K. O. Honikel, C. Fischer (1977) *A rapid method for the detection of PSE and DFD porcine muscles*. Journal of Food Science 42:1633–1636.
- [235] M. S. Brewer, J. Novakofski, K. Freise (2006) *Instrumental evaluation of pH effects on ability of pork chops to bloom*. Meat Science 72:596–602.
- [236] H. Baillères, F. Davrieux, F. Ham-Pichavan (2002) *Near infrared analysis as a tool for rapid screening of some major wood characteristics in a eucalyptus breeding program*. Annals of Forest Science 59:479–490.
- [237] S. Barbut (2014) *Review: Automation and meat quality-global challenges*. Meat Science 96:335–345.

Acknowledgement

This thesis would have never been possible without the support of many people. Here is the place to appreciate their help. In particular, I want to thank...

... my supervisors, *Heinar Schmidt* and *Jürgen Köhler*, for their support, advice, help, ideas and patience and for giving me the opportunity to earn my PhD in their work groups,

... *Heinz-Detlef Kronfeldt* from the TU Berlin, for his generous support with the prototype handheld Raman device at the beginning of this thesis,

... the technicians of the workshop of the University of Bayreuth, especially *Heinz Krejtschi* and *Frank Neumann* for the realization of the portable Raman system,

... the staff of the abattoir in Kulmbach, Germany, especially *Dirk Grünh*, for excellent cooperation and for generously providing the pork samples used for the experiments described in publication 1 and 2,

... the staff of the abattoirs in Bayreuth, Germany and Bazenhaid, Switzerland, for excellent cooperation and access to their plants where the field studies were conducted,

... our cooperation partners, *Anja Petzet*, *Manfred Spindler*, *Sabine Wiedel*, *Anneliese Bittermann* and *Sybill Nordhausen* of the Max Rubner-Institut in Kulmbach, Germany, for their help with the reference analyses in field study 1,

... *Martin Scheeder* of the School of Agricultural, Forest and Food Sciences HAFL in Zollikhofen, Switzerland, for his help with the reference analyses in field study 2,

... my team colleagues, *Thomas Kador*, *Natalja Agarkov*, *Stefanie Hofmann* and *Alexandra Bauer*, for their assistance with Raman and reference measurements and all members of the Research Centre of Food Quality, for the friendly atmosphere in the work group, the many fruitful and entertaining discussions, the delicious cakes and the “alcofrolic” evenings,

... and, of course, my family and friends, for their support during all ups and downs over the past four years.

Additionally, I want to thank the “Emergency fund for doctoral candidates at the University of Bayreuth” for the start-up funding of this work. Later, this work was financially supported by the German research foundation DFG (Deutsche Forschungsgemeinschaft, Schm2724/1-1) and the German Federation of Industrial Research Associations AiF (Arbeitsgemeinschaft industrieller Forschungsvereinigungen “Otto von Guericke” e.V., 16692 N II) in the framework of the cluster project “Minimal Processing” of the Research Association of the German Food Industry (FEI).

List of Publications

Publications (peer review):

1. R. Scheier, H. Schmidt (2013) *Measurement of the pH value in pork meat early postmortem by Raman spectroscopy*. Applied Physics B 111:289–297.
2. R. Scheier, J. Köhler, H. Schmidt (2014) *Identification of the early postmortem metabolic state of porcine M. semimembranosus using Raman spectroscopy*. Vibrational Spectroscopy 70:12–17.
3. R. Scheier, A. Bauer, H. Schmidt (2014) *Early postmortem prediction of meat quality traits of porcine semimembranosus muscles using a portable Raman system*. Food and Bioprocess Technology, In Press, DOI: 10.1007/s11947-013-1240-3.

Further publications (non-peer review):

1. R. Scheier, H. Schmidt (2012) *Non-invasive pH measurement early postmortem in porcine M. semimembranosus using Raman spectroscopy*. 58th International Congress of Meat Science and Technology, Paper 157:1–4.
2. R. Scheier, M. Nache, N. Agarkov, B. Hitzmann, H. Schmidt (2013) *Raman-Sensorik zur automatisierbaren Beurteilung der Fleischqualität*. Fleischwirtschaft 93:170–174.
3. R. Scheier, A. Petzet, A. Bauer, H. Schmidt (2013) *Hand-held Raman system for an early postmortem detection of pH and drip loss of pork meat*. 59th International Congress of Meat Science and Technology, Paper O-20:1–5.

Erklärung

Hiermit erkläre ich an Eides statt, dass ich die vorliegende Arbeit selbstständig verfasst und keine anderen als die angegebenen Quellen und Hilfsmittel benutzt habe. Die Arbeit wurde in gleicher oder ähnlicher Form keiner anderen Prüfungsbehörde zur Erlangung eines akademischen Grades vorgelegt. Desweiteren erkläre ich hiermit, dass ich bisher keinen anderweitigen Promotionsversuch unternommen habe.

Rico Scheier
Kulmbach, den 20. Januar 2014

Part II.

Publications

Publikation 1

Measurement of the pH value in pork meat early postmortem by Raman spectroscopy

R. Scheier and H. Schmidt

Applied Physics B **111**

p. 289–297 (2013)

© Springer 2013

DOI 10.1007/s00340-012-5332-y

available at:

http:

[//link.springer.com/article/10.1007%2Fs00340-012-5332-y](http://link.springer.com/article/10.1007%2Fs00340-012-5332-y)

**Reprinted with permission from Springer
(License number 3421260595091)**

Measurement of the pH value in pork meat early postmortem by Raman spectroscopy

R. Scheier · H. Schmidt

Received: 24 September 2012 / Accepted: 28 December 2012 / Published online: 2 February 2013
© Springer-Verlag Berlin Heidelberg 2013

Abstract The pH of a muscle is an accepted parameter to identify normal and deviating meat qualities. In this work, Raman spectroscopy is shown to be suitable for the non-invasive measurement of the early postmortem pH of meat. Raman spectra of ten pork *semimembranosus* muscles were recorded with a portable handheld device 0.5–24 h postmortem. The spectra were correlated with pH and lactate kinetics measured in parallel. Seven of the muscles were normal, two exhibited accelerated glycolysis and one showed absence of acidification. The pH decline with time could be calculated from the Raman spectra with the Henderson–Hasselbalch equation using only two signals of phosphate vibrations at 980 and 1,080 cm^{-1} with a close correlation for each muscle, but larger variations between animals. More robust and better correlations for all muscles were obtained with a linear model based on 11 signals from lactate, lactic acid, phosphate, a carbonyl band and nucleotides resulting in $R^2 = 0.78$ and $\text{RMSECV} = 0.2$ or a partial least-square model using the complete spectrum ($R^2 = 0.94$ and $\text{RMSECV} = 0.2$). These results show the potential of Raman spectroscopy for an online detection of the pH and thus meat qualities during meat processing.

1 Introduction

Velocity and extent of the early postmortem energy metabolism are essential factors for the development of meat quality. On the one hand, accelerated anaerobic glycolysis leads to pale, soft and exudative (PSE) meat. On the

other hand, strongly reduced glycolysis due to a depletion of the glycogen reserves in the muscle leads to dark, firm and dry (DFD) meat [1, 2]. Both qualities are unwanted by breeders, processors, retailers and consumers. To distinguish these deviating qualities from the desired reddish, firm and non-exudative (RFN) meat quality, two pH measurements are required 45 min (pH_{45}) and 24 h (pH_{24}) postmortem. PSE meat is characterized by a $\text{pH}_{45} < 5.8$, whereas DFD meat exhibits a $\text{pH}_{24} > 6.0$ [3]. Presently, monitoring the pH is the standard method when both qualities are to be discriminated from normal meat. However, this pH measurement has to be performed with glass electrodes which have to puncture the muscle. This is time-consuming and susceptible to operational faults such as contamination or break, not to speak of the injury of the meat. Therefore, pH measurements are performed in abattoirs or during processing only when absolutely required. A fast and non-invasive technique to reliably determine pH_{45} and pH_{24} would be beneficial for meat processing. In the present paper, the feasibility of using Raman spectroscopy for the non-invasive measurement of the pH of meat early postmortem will be shown.

Raman spectroscopy was chosen as a non-destructive and contactless method which is based on inelastic scattering of light providing information of molecular vibrations of the probed material. With this feature, pH-induced changes can be detected on a molecular level. Another driving force for this development is the progress of laser and Raman technology enabling the construction of small, robust and energy-efficient portable devices, such as the recently developed handheld Raman probe for the characterization of meat quality and spoilage [4].

Raman spectroscopy is a sensitive probe of the secondary structure of proteins with the amide I and III modes as well as the carbon–carbon stretching modes of the

R. Scheier · H. Schmidt (✉)
Research Centre of Food Quality, University Bayreuth,
E.-C.-Baumannstraße 20, 95326 Kulmbach, Germany
e-mail: heinar.schmidt@uni-bayreuth.de

protein backbone as important indicators [5–7]. Thus, pH-induced conformational changes of poly-amino acids have been observed in aqueous solutions with Raman spectroscopy [8, 9]. These conformational changes are a consequence of the protonation/deprotonation of the amino acid side chains which are characterized by their pK_a values indicating the pH at which both species of the corresponding acid/base pair have the same concentration. In the pH range from 7 to 5, the basic amino acids do not change, but aspartic acid ($pK_a = 3.86$) and glutamic acid ($pK_a = 4.25$) show some effect of protonation upon lowering the pH to 5 [10]. However, to be useful as pH indicator, the pK_a should be in the considered measuring range. Here, histidine with a $pK_a = 6.08$ has been studied for pH-induced structural changes of the free amino acid [11] and in the protein transferrin [12]. In the Raman difference spectra, the basic form showed signals at 1,575 and 1,312 cm^{-1} , while in the acidic form signals occurred at 1,210, 1,490 and 1,630 cm^{-1} . A variation of the pK_a of histidine was attributed to different histidine sites resulting in an average pK_a in the protein of 6.56 [12].

With pK_a values around 7 inorganic phosphate and terminal phosphate groups of the organic esters show pH-induced changes between pH 5.5 and 8 [10]. In the Raman spectra this can be recognized amongst others by means of two strong vibrations: the symmetric PO_3^{2-} stretching vibration of the basic form at 980 cm^{-1} and the symmetric PO_2^- stretching vibration of the acidic form at 1,082 cm^{-1} [13]. Note that all intermediates of the glycolysis from glucose 6-phosphate to phosphoenolpyruvate are phosphorylated and that the sugar phosphates [14] have pK_a values between 6.1 and 6.3. Raman spectra of phosphorylated proteins have been used to determine the pK_a values of phosphoserine and phosphothreonine in aqueous solution [15]. The Raman spectra of the energy-rich adenosine di- and triphosphates exhibit different band positions due to coupling of the polyphosphate chain [13, 16]. For adenosine triphosphate in the pH range from 6 to 7 a peak shift was observed from 1,125 to 1,112 cm^{-1} for the symmetric PO_2^- stretching mode of the polyphosphate moiety [13].

The pH can be measured in situ or in vivo using other techniques such as nuclear magnetic resonance (NMR), near-infrared or near-infrared reflectance spectroscopy. Pulsed Fourier transform ^{31}P -NMR spectroscopy was shown to be able to determine intracellular pH in erythrocytes by using the chemical shifts of 2,3-diphosphoglycerate and inorganic phosphate [17]. An accurate determination of intracellular pH was reported, but no R^2 was given. However, the samples had to be treated with carbon monoxide and the integration time varied from several minutes to 1 h. Other authors studied postmortem changes in pork muscles ($n = 15$) achieving good agreement between NMR and electrochemical pH value above

pH 6.2, but below pH 6.2 they observed a systematic discrepancy [18]. Again, sample preparation was necessary (muscles were dipped in paraffin oil and put into 10-mm NMR tubes). A quantitative statistical discussion of the application of ^{31}P -NMR for in vivo pH measurements in breast carcinoma tissue [19] showed errors of 0.04 pH units due to baseline effects, whereas calibration uncertainties caused variations between 0.05 and 0.1 pH units.

With near-infrared spectroscopy [20], promising correlations using partial least-square regression (PLSR) were achieved to predict the pH measured in the duodenum of six pigs during hemorrhagic shock ($R^2 = 0.90$ during ischemia and $R^2 = 0.89$ during reperfusion). To compensate for systematic discrepancies between different animals, subject-specific offsets had to be applied. By this means, an averaged root mean squared deviation of 0.042 and 0.045 pH units was calculated for ischemia and reperfusion, respectively. No detailed information was given on what spectral features were used for pH prediction or how differences in the pH value are reflected in the spectra. Investigations with five rabbit muscles during ischemia and reperfusion [21] showed a close correlation between near-infrared reflectance spectra and muscle pH in the range 6.4–7.1. Again, no detailed information was provided regarding the cause of these changes.

To our knowledge, no studies have yet been carried out to measure the pH of meat in situ with Raman spectroscopy. The above studies essentially showed principal feasibility but not applicable techniques which require non-invasiveness, rapidity and suitable instrumentation. Therefore, the aim of this study was to identify pH-dependent changes in Raman spectra of pork meat early postmortem and to link them to cellular components allowing for a pH measurement with a view to a practical application.

2 Materials and methods

For the experiments, the *semimembranosus* muscle (SM or topside) of pork was chosen because this muscle is accessible at the carcasses and used for pH measurements of ham. The meat samples (approx. 500 g) were removed 20–30 min postmortem from 10 pigs which were slaughtered in a local commercial abattoir. In the laboratory, the samples were divided into three parts for pH, lactate and Raman measurements which began immediately, i.e., 25–40 min postmortem. Due to the decreasing production of lactate with time, pH values were taken in increasing intervals with a pH electrode (Mettler Toledo, SevenGo pro, Giessen, Germany) until constant pH was reached over three consecutive measurements. The ultimate pH was measured after 24 h. In parallel, about 7 lactate concentrations were determined per muscle in the time 0.5–9 h

postmortem and the ultimate concentration after 24 h. To this end, 5 g of each muscle were homogenized with 20 ml 1 M perchloric acid for 3 min on ice. Subsequently, the pH was adjusted to 10 with potassium hydroxide solution. After 20 min of storage at +4 °C the homogenate was filtered with Whatman GF/A filters. Finally, the lactate content of the filtrate was measured photometrically using an enzymatic test assay and the absorbance of NADH at 340 nm (Megazyme International Ireland Ltd., Wicklow, Ireland) [22]. Raman spectra were acquired with a 671 nm handheld Raman probe [23] coupled to a miniature spectrograph (HORIBA Jobin-Yvon, Longjumeau, France) controlled by a self-written LabVIEW program (National Instruments, Austin, TX, USA) [24]. The Raman spectra were recorded from 0.5 to 10 h postmortem at a laser power of 100 mW with 5 s integration time and 5 accumulations at each spot. For further analysis five of these spectra were averaged. The time intervals between each set of spectra were increased from 5 to 10 s during the first 1–2 h to 15–30 min during the last 2 h of the measurement.

To evaluate the variation of pH measurement within a muscle, pH measurements were recorded in three additional topsides at 9 different positions with 4 cm spacing between each spot covering the whole SM. The measurements were performed in intervals of 30 min during the first 5 h postmortem and of 1 h until 10 h postmortem. Reference spectra of phosphoric acid, glucose 6-phosphate, fructose 6-phosphate, phosphoenolpyruvate, inosine monophosphate and adenosine triphosphate were measured at 50 mM concentrations in the pH range from 4.5 to 7.2 using hydrochloric acid and potassium hydroxide solutions for the pH adjustment. The Raman spectra were recorded with 25 s integration time and 10 accumulations.

For further analysis, Raman spectra were baseline corrected with a fifth order polynomial. Subsequently, all

spectra were smoothed by Savitzky–Golay filter [25] using a width of 15 pixel and second polynomial order. Finally, the spectra were normalized to the net peak intensity of phenylalanine at 1,000 cm^{-1} to compensate for differences in the intensity. Partial least square regression (PLSR) was performed with MATLAB 7.9.0 R2009b software (The Mathworks Inc., Natick, MA, USA) and PLS toolbox 6.2 (Eigenvector Research Inc., Wenatchee, WA, USA). For cross-validation the contiguous blocks method with ten data splits was applied.

3 Results and discussion

3.1 Lactate and pH

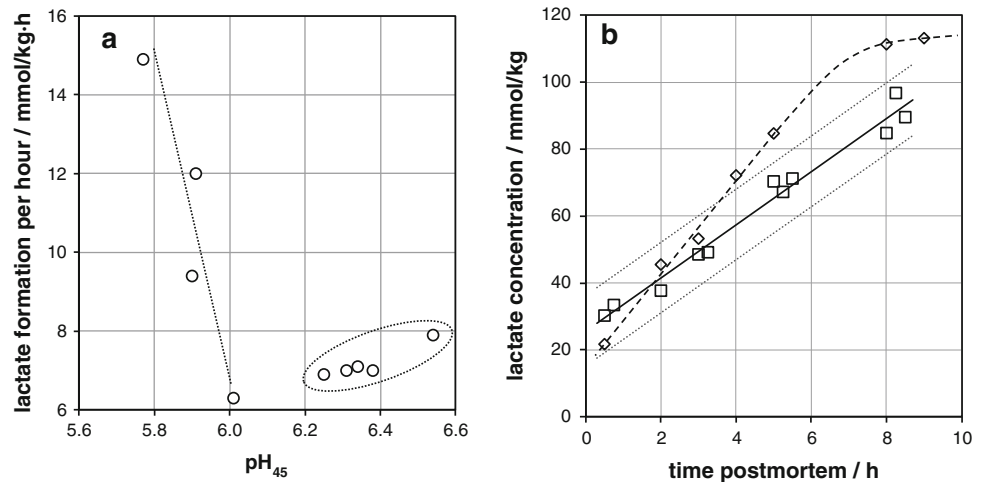
An overview of the pH and lactate concentrations of the samples is given in Table 1 with the samples sorted according to their rate of lactate formation. The pH_{45} of the samples varied from 6.54 to 5.77, the latter indicating PSE-tendency for sample 10. The ultimate pH (pH_{24}) scattered around 5.51 with a standard deviation (SD) of 0.13. These values are in accordance with former studies on pork SM muscles [26]. The lactate content increased by 50–90 mmol kg^{-1} , except for sample 1 with no increase at all. The lack of glycolysis and the low lactate content of this sample points at meat which is neither DFD nor PSE. The final pH value of 5.7 is still rather normal but the low initial pH points at PSE meat, i.e., this sample cannot be classified in the common system of three categories. Samples 9 and 10 showed accelerated glycolysis and also the lowest pH_{24} values in this series.

As the acidification is caused by glycolysis and fermentation, there is a close correlation between the rate of lactate formation and the pH_{45} (Fig. 1a). Samples of RFN quality

Table 1 pH values measured 45 min and 24 h postmortem, lactate concentrations (initial = 30 min, final = 24 h postmortem) and rate of lactation before rigor mortis

#	pH		Lactate			Meat quality
	pH_{45}	pH_{24}	Initial/ mmol kg^{-1}	Final/ mmol kg^{-1}	Rate/ $\text{mmol kg}^{-1} \text{ h}^{-1}$	
1	5.87	5.70	79	70	<0.5	Atypical
2	6.01	5.44	32	86	6.3	RFN
3	6.25	5.53	50	119	6.9	RFN
4	6.31	5.50	49	100	7.0	RFN
5	6.38	5.40	49	114	7.0	RFN
6	6.34	5.51	32	99	7.1	RFN
7	6.54	5.80	30	90	7.9	RFN
8	5.90	5.47	24	89	9.4	RFN
9	5.91	5.35	22	113	12.0	PSE-tendency
10	5.77	5.38	60	118	14.9	PSE-tendency
\bar{x}	6.13 ± 0.25	5.51 ± 0.13	43 ± 17	100 ± 15	8.7 ± 2.7	

Fig. 1 a Correlation of lactate formation rate with pH_{45} for 9 pork samples. **b** Lactate concentrations measured between 0.5 and 10 h postmortem for RFN meat (square), for meat with PSE-tendency (diamond) and margin of error based on lactate measurements with 7 RFN samples (dotted line)



produced 7–9 mmol kg^{-1} per h of lactate under these conditions, whereas meat with PSE-tendency metabolized over 12 mmol kg^{-1} of lactate per hour (Fig. 1b). Again, sample 1 did not fit into the picture. This sample must have had strong glycolysis at the time of death, but subsequently exhausted glycogen reserves prevented further lactate formation. Therefore, sample 1 was not included in Fig. 1b. The excised topsides were cooling faster to room temperature (24 °C) compared to the muscles in the intact carcasses. Therefore, metabolism is slowed down and the above rates are lower than in the carcass.

We found a rather low curvilinear correlation between pH value and lactate concentration with $R^2 = 0.49$ for the different animals which is low compared to the literature [27]. This could be due to the fact that pH, lactate and Raman measurements were not conducted on the very same segment of the muscle and that the segments did not cool to ambient temperature at exactly the same rate. In an additional experiment to evaluate the pH variation in the SM, a distinctive position effect was observed. This is mainly attributed to the inhomogeneity of the muscle consisting of fast and slow glycolysing fibers. The reference pH measurements varied considerably according to the site and time. As depicted in Fig. 2, within the first 6 h postmortem the SD of a pH measurement in each muscle sample exceeded 0.06 pH units with a maximum of 0.18 pH units about 5–6 h postmortem.

3.2 Raman spectra

The Raman kinetics recorded during acidification of the muscle showed intensity changes virtually in the entire spectrum, except for sample 1 which showed almost no spectral changes (therefore not shown). Figure 3 illustrates these spectral changes on the example of pork meat with RFN quality observed 40 min and 9 h postmortem Raman

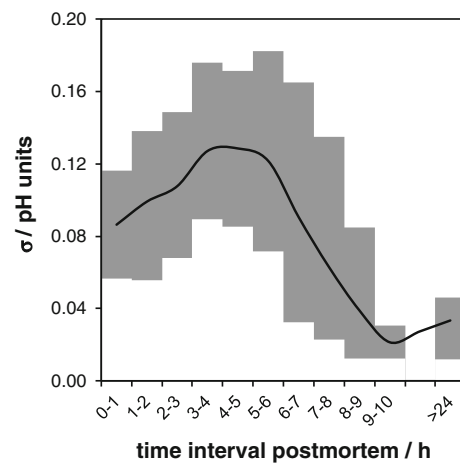
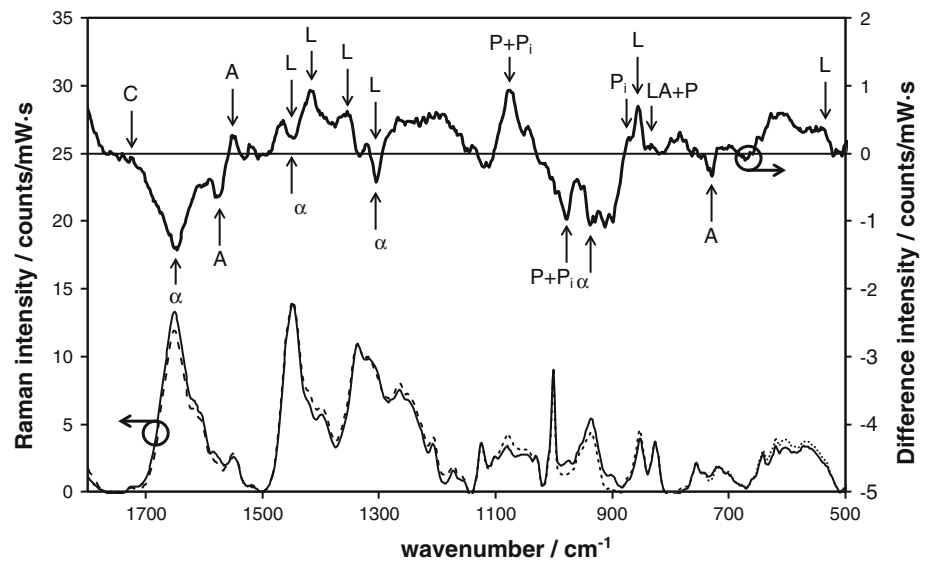


Fig. 2 Averaged standard deviation of pH measurements with puncture electrode for 9 positions during time interval from 1 to 9 h and after 24 h postmortem (black line) as well as minimal and maximal values observed for standard deviations (grey bars)

bands of lactate (with intensities in brackets) occur at 535 (s), 853 (vs), 1,305 (m), 1,352 (m), 1,414 (s) and 1,452 cm^{-1} (s) and they are marked with L. Not all bands do reflect the expected increasing concentration of lactate in the pork muscle, some even decrease in intensity which is understood as overcompensation by other signals. The most prominent peak at 853 cm^{-1} assigned to the stretching C–C vibration of the single bond adjacent to the carboxylate function [28] is overlaid by the tyrosine doublet and interferes with signals of glycogen [29], glucose [29], creatine phosphate [30] and creatine [30]. The content of creatine phosphate, glycogen and glucose decrease postmortem, thus compensating to some extent the signal intensity of lactate at 853 cm^{-1} , but the summed up increase of lactate is stronger. Similarly, the signals at 535, 1,352 and 1,414 cm^{-1} show a positive intensity balance although to a lesser extent than expected. Only the signal at 1,352 cm^{-1} matches the expected intensity increase. The 1,414 cm^{-1} peak represents the symmetric

Fig. 3 Raman spectra of RFN pork meat 0.7 h (solid line) and 9 h (dotted line) postmortem and difference spectrum 9 h minus 0.7 h (bold line). Indicated by arrows lactate (L), lactic acid (LA), terminal phosphate group (P), inorganic phosphate (P_i), carbonyl (C), heteroaromatics (A) and α -helical protein (α)



CO_2^- stretching vibration and therefore other components containing carboxylate groups may contribute to this signal as well. The lactate peaks at 1,305 and 1,452 cm^{-1} are overcompensated mainly by the amide III mode and the sum of the CH, CH_2 and CH_3 bending modes of the α -helix (marked with α). We observe a strong decrease of the intensity of α -helix signals during the first hours postmortem which can be also recognized at 1,650 cm^{-1} (amide I) and 935 cm^{-1} (C–C skeletal) modes [31, 32].

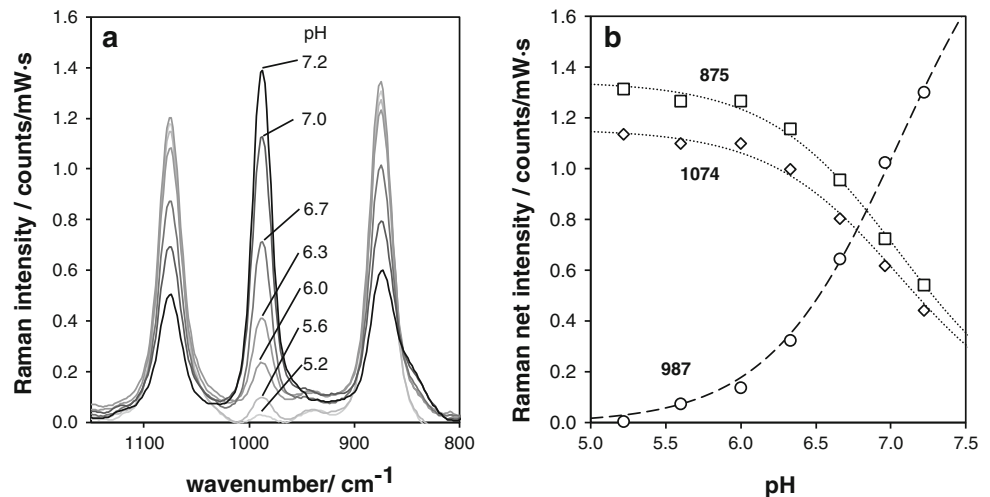
Two further peaks with diametric tendency are observed in the Raman difference spectrum (Fig. 3) at 1,552 and 1,578 cm^{-1} . They are typical for asymmetric ring stretching vibrations of heteroaromatic compounds and marked with A [33, 34]. The former corresponds very well with the strongest signal of inosine and inosine monophosphate which is reported to be at 1,553 cm^{-1} [35]. The latter can be attributed to adenosine triphosphate [13, 16]. Inosine monophosphate is a degradation product of adenosine monophosphate and guanosine monophosphate. Hence, both peaks are indicating the decay of the energy-rich phosphates. In pork meat an increase of the inosine monophosphate concentration of 7 mmol kg^{-1} after 8 h was reported and an increase of inosine content by 1 mmol kg^{-1} after 24 h [36, 37]. The decrease of the 729 cm^{-1} peak of the purine bases also confirms this assignment as our reference measurements with ATP and IMP in aqueous solution revealed an intensity ratio ATP/IMP for this band of 5/3.

While the content of lactate increases with proceeding glycolysis, the muscle acidifies to pH values of 5.6–5.2 and due to its $\text{p}K_a$ value of 3.86, formation of 2–5 % of lactic acid (LA) is calculated according to the Henderson–Hasselbalch equation. The slight increase of the net intensity at 827 cm^{-1} observed in the difference spectrum can therefore be partly assigned to the C–C stretching vibration

adjacent to the carboxylic acid of lactic acid. Another contribution comes from the O–P–O stretching vibration of protonated phosphate groups of sugar phosphates at 825–833 cm^{-1} [29, 38, 39]. Hence, a quantitative analysis based on the two signals at 853 and 827 cm^{-1} is virtually impossible due to co-location with the tyrosine doublet and with a number of intermediates of the energy metabolism. However, the aforementioned protonation of carboxylate groups at low pH can be detected by means of the C=O stretching vibration (carbonyl band, C) in the 1,705–1,730 cm^{-1} range [40] which is less biased by other Raman signals. As the small content of lactic acid alone cannot account for the intensity change observed in the difference spectrum, this band has to be regarded as the sum band of all carbonyl group(s) adding intensity to this peak.

The two Raman signals at 980 and 1,080 cm^{-1} marked with P + P_i in Fig. 3 are assigned to phosphate groups. Both peaks show diametric behavior. While the peak of the symmetric PO_3^{2-} stretching vibration at 980 cm^{-1} decreases with acidification of the muscle, the peak of the symmetric stretching vibration PO_2^- at 1,080 cm^{-1} increases. This holds for terminal phosphate groups [15] and with slightly shifted peak positions at 987 and 1,075 cm^{-1} also for inorganic phosphate. The protonation of hydrogenphosphate to dihydrogenphosphate is shown in Fig. 4a with a series of Raman spectra of phosphoric acid in the pH range from 7.2 to 5.2. The third peak at 875 cm^{-1} corresponds to the symmetric $\text{P}(\text{OH})_2$ stretching vibration of dihydrogenphosphate. This peak is also observed in the Raman difference spectrum in Fig. 3 and can be assigned to inorganic phosphate (P_i) which is released in quantities of up to 40 mmol kg^{-1} during glycolysis and fermentation in porcine *M. longissimus dorsi* [18, 41].

Fig. 4 a Raman spectra of 50 mM phosphoric acid in the pH range from 5.2 to 7.2. **b** Raman net intensities versus pH at 875 cm^{-1} (square), 987 cm^{-1} (circle) and 1,074 cm^{-1} (diamond) and theoretical curves calculated with the Henderson–Hasselbalch equation for basic (dashed line) and acidic (dotted lines) species



3.3 Correlation of Raman spectra with pH

The Henderson–Hasselbalch equation describes the correlation between the pH value and the concentrations of base (A^-) and acid (HA):

$$\text{pH} = \text{p}K_a + \log_{10} \left(\frac{A^-}{HA} \right) \quad (1)$$

The measured Raman intensities shown in Fig. 4b were in very good accordance ($R^2 = 0.996$) with the theoretical curves (broken lines) calculated for phosphoric acid with $\text{p}K_a = 7.2$.

Conversely, the pH can be calculated for an acid–base pair with the Henderson–Hasselbalch equation from the intensity ratio of this acid–base pair, provided that the $\text{p}K_a$ is known. In meat, the situation is more complicated because several compounds with varying $\text{p}K_a$ and Raman scattering cross sections contribute to both signals. To this end, we have compared the ratio of the specific Raman intensities of the acidic and basic species for a number of phosphates. This ratio is used to convert the Raman intensities into concentrations. The ratio varied from 1.4 (phosphoenolpyruvate) to 4.3 (inosine monophosphate) with ratios of 2.2 and 2.7 for the sugar phosphates fructose 6-phosphate and glucose 6-phosphate, respectively. Similarly, the $\text{p}K_a$ values varied from 6.1 to 7.2. For the calculations we chose $\text{p}K_a$ (7.2) and ratio (2.4) of phosphoric acid as starting point. In a second step, the $\text{p}K_a$ was fitted to the data set consisting of 564 Raman spectra and pH values using only the peak intensity ratio of the measurements. As result, an adjusted $\text{p}K_a$ for phosphate in meat of $\text{p}K_a = 7.0$ was obtained which is close to the value of phosphoric acid. This adjustment is taking into account the $\text{p}K_a$ variations of the involved phosphate groups and it also corrects the deviation of the specific Raman intensity ratio from 2.4. For example, the difference in the ratio of phosphoric acid

and a sugar phosphate would account for a difference of 0.03–0.04 pH units. The model yields an averaged correlation coefficient of calibration of $R^2 = 0.71$ and $\text{RMSEC} = 0.30$. The linearity is good for the single muscles, but the correlation also reveals systematic differences between the meat samples (see Fig. 5a) which might have their reason in a position effect as mentioned earlier. Note that the pH change can only be indicated down to $\text{pH} = 5.5$ because at this pH nearly all phosphate groups are protonated and the intensity of the base is approaching zero. Despite of the discrepancies between the different samples, the calculations demonstrates that the pH of meat can be calculated from the Raman spectra in principle using only two signals from phosphate.

For a more robust prediction of the pH from the Raman spectra, a multiple linear regression (MLR) was performed using the net intensities of 11 peaks and one offset value. These signals were selected from the peaks marked in Fig. 3 according to their significance and they comprise lactate (535, 855, 1,305, 1,350 and 1,414 cm^{-1}), lactic acid (827 cm^{-1}), the phosphate group (980 and 1,078 cm^{-1}), the carbonyl double bond (1,714 cm^{-1}) and the two peaks ascribed to inosine monophosphate and adenosine triphosphate (1,552 and 1,578 cm^{-1}). All other signals were disregarded. The MLR model yields a correlation with $R^2 = 0.78$ and $\text{RMSEC} = 0.14$ pH units (Fig. 5b). The root mean square error of cross-validation (RMSECV) which is a better indicator for the predictive power of the model is calculated with the leave-one-out method and yields 0.22 pH units. To this end, the spectra of nine different samples were used to compute a model and to test the prediction with the spectra of the residual sample which was repeated for all permutations.

Finally, a PLSR model was calculated to predict the pH of the meat based on baseline-corrected Raman spectra in the range from 500 to 1,800 cm^{-1} . The model with 9 latent

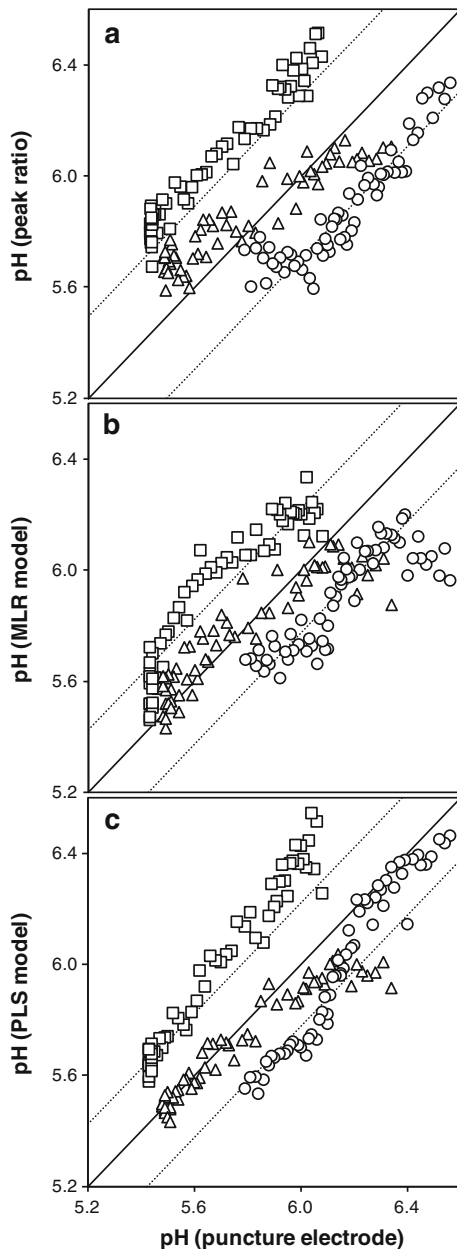


Fig. 5 Predicted pH from Raman spectra: **a** calculated from the peak intensity ratio at 980 and 1,080 cm^{-1} , **b** determined with MLR models using net intensities of 11 peaks and 1 offset and **c** determined with PLSR models using 726 spectral channels versus pH measured with an electrode. For clarity only 3 of 10 measurements are shown. Dashed lines indicate averaged RMSECV

variables resulted in $R^2 = 0.94$ and $\text{RMSEC} = 0.07$ pH units. With the described leave-one-out method an average $R_{\text{cv}}^2 = 0.87$ and a $\text{RMSECV} = 0.22$ pH units were calculated (Fig. 5c).

For comparison, Table 2 summarizes the figures of merit of the three methods to predict pH values from Raman spectra. Considering the above-described uncertainties when analyzing only the peak ratio of 980–1,080 cm^{-1} , the MLR model utilizes 33 out of 1,024 spectral channels for

Table 2 R^2 , RMSEC and RMSECV values for pH prediction using the peak intensity ratio at 980 and 1,080 cm^{-1} , multiple linear regression (MLR) and partial least-square regression (PLSR)

	Peak ratio	MLR	PLSR
R^2	0.71	0.78	0.95
RMSEC^{a}	0.30	0.14	0.07
R_{cv}^2	–	0.70	0.87
RMSECV^{a}	–	0.22	0.22
Spectral channels	2 ^b	11 + 1 ^b	726

First 2 rows give mean values for model data set; next 2 rows give mean values for cross-validation data set. Last row gives the number of spectral channels used for the calculations

^a In pH units

^b 2 mesh points used per peak

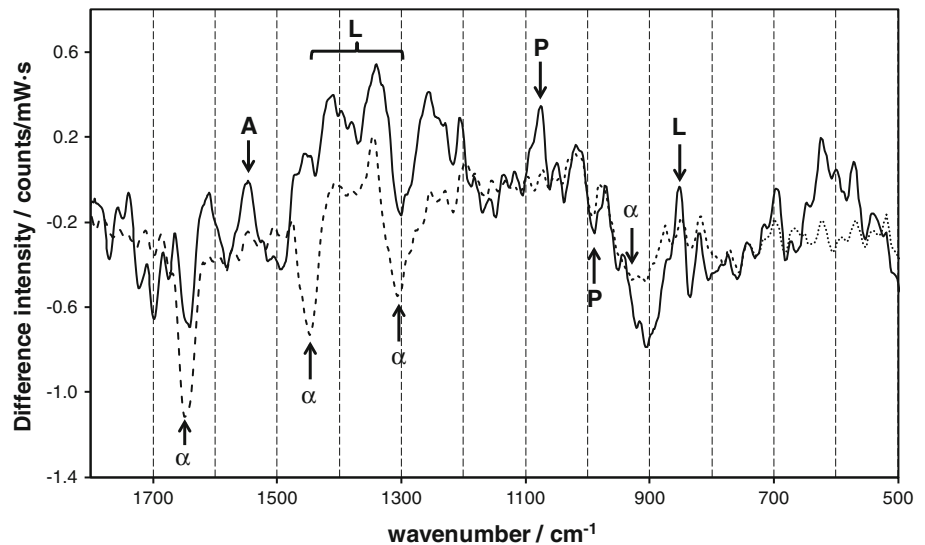
the prediction and the PLS model 726. As expected, the coefficient of determination is improved with increasing number of spectral channels used by the method and accordingly the RMSEC is markedly reduced. However, all models showed a similar offset for the different samples which may be due to a position effect within the muscle. This can also be the reason why the RMSECV did not improve in the PLS model compared with the MLR model. In view of the (biological) variance in the muscle, the pH would have to be measured at exactly the same position as the Raman measurement to obtain better correlations. The phosphate peak ratio method clearly shows that the relation between pH and the Raman intensities is logarithmic and that this is a significant pH indicator. However, the best predictions were obtained with linear regression models. Therefore, non-linear algorithms may yield more accurate predictions and should be applied in future.

3.4 Discrimination of meat quality

The measurement of pH and lactate content of meat with Raman spectroscopy was carried out with a view to the non-invasive detection of normal and deviating meat qualities. Having shown that the pH can be reasonably well detected in the Raman spectra of meat and that lactate and a number of metabolites of the energy metabolism contribute to this, it is interesting to examine whether this can be used to discriminate the exudative meat quality from RFN.

To illustrate the spectral differences between samples with RFN quality and PSE-tendency the difference spectra PSE minus RFN are shown in Fig. 6 for two particular times after 1–2 h and after 24 h. To this end, the spectra measured 1–2 h and after 24 h postmortem were each averaged. Positive peaks indicate signals which are stronger in meat with PSE-tendency, while negative peaks indicate signals which dominate in meat of RFN quality. The notation of the signals is the same as in Fig. 3.

Fig. 6 Difference spectra of PSE minus RFN meat measured 2 and 24 h postmortem, respectively (same notations as in Fig. 3)



The difference spectrum for the early postmortem phase (2 h) exhibits much stronger signals of the protonated phosphate group at $1,080\text{ cm}^{-1}$ at the expense of the base peak at 980 cm^{-1} , thus indicating the low pH value. Furthermore, lactate signals and the formation of inosine monophosphate is more pronounced in meat with PSE-tendency which is in good agreement with an accelerated metabolism. For example, in exudative pork meat, inosine and inosine monophosphate concentrations 2 h postmortem have been reported to be more than three times higher than compared with normal meat [37].

After 24 h the difference spectrum between PSE-tendency and RFN meat changed completely. The difference in the Raman signals of lactate, lactic acid, heteroaromatic compounds and phosphate groups vanished completely. Again, this is in keeping with the expectations because ultimate pH, final lactate and inosine monophosphate concentrations are not significantly different for RFN and PSE meat [37]. The main difference was a markedly reduced signal intensity of the α -helix at 935, 1,305, 1,450 and $1,650\text{ cm}^{-1}$ in PSE meat compared with RFN meat which can be explained by a stronger denaturation or damage of α -helical-structured domains caused by overheating of the muscle during the accelerated glycolysis [42, 43].

4 Conclusions

The correlation of the Raman spectra of excised topsides (*M. semimembranosus*) 0.5–10 h postmortem demonstrated that the pH of meat can be determined from the Raman spectra. This is largely based on the pH-dependency of two Raman signals of terminal phosphate groups at 980 and $1,080\text{ cm}^{-1}$. Using the net intensities of both signals the

pH can be calculated with the Henderson–Hasselbalch equation with $R^2 = 0.71$ and RMSEC = 0.30. More robust models with higher precision were obtained with a linear model consisting of 11 net peak intensities and 1 offset parameter ($R^2 = 0.78$ and RMSEC = 0.14) and a PLSR model using the whole spectral information yielding $R^2 = 0.94$ and RMSEC = 0.07. An offset between Raman and pH data set was observed which is due to a position effect reflecting a biological variance in the muscle. This heterogeneity was a limiting factor in our study and therefore, the predictability of the MLR and PLSR models were comparable (RMSECV = 0.2 pH units). Better correlations should be obtained when the pH is measured at exactly the same position where the Raman measurement is carried out.

The calculation of the pH from two phosphate signals demonstrates that significant pH information is contained solely in these two signals and that the relation between pH and the Raman intensities is logarithmic. However, the best predictions were obtained with linear regression models. Therefore, the application of non-linear algorithms is expected to be beneficial. Considering the ubiquity of phosphate, this pH detection could also be useful for other biological systems or food.

Along with the phosphate, significant changes in Raman spectra during the first hours postmortem could be assigned to lactate, lactic acid, the carbonyl group of carboxylic acids as well as vibrations of heteroaromatic compounds of the energy metabolism like adenosine triphosphate and inosine monophosphate. These spectral differences could be used to discriminate meat with accelerated metabolism (PSE-tendency) and meat with RFN quality. A clear decrease of the intensity of Raman signals originating from α -helical proteins was observed for all samples concurrent to the acidification which can be regarded as an indicator of

degradation of α -helical domains or denaturation. This effect was more pronounced for meat with PSE-tendency and finally this is the main difference in the Raman spectra of meat with RFN quality and with PSE-tendency after 24 h.

The results demonstrate the usefulness of Raman spectroscopy to observe qualitative metabolic changes in a pork muscle and to quantify the pH value between 0.5 and 24 h postmortem. The results show good promise for the early identification of (deviating) meat qualities during meat processing. As a next step, the performance of the method should be tested in a field study with a larger number of animals in an abattoir.

Acknowledgments This work was funded by the German research foundation DFG (Deutsche Forschungsgemeinschaft) in the framework of the cluster project “Minimal Processing” of the Research Association of the German Food Industry (FEI). Financial support for the Research Centre of Food Quality by the European Regional Development Fund (ERDF) is gratefully acknowledged. The authors wish to thank Dr. Heinz-Detlef Kronfeldt for generous support with the prototype handheld Raman device, Dirk Grünh for the excellent cooperation and for providing the pork samples as well as Stefanie Hofmann and Thomas Kador for assistance with lactate and Raman measurements.

References

- P. Henckel, A. Karlsson, N. Oksbjerg, J.S. Petersen, *Meat Sci.* **55**, 131–138 (2000)
- T.L. Scheffler, D.E. Gerrard, *Meat Sci.* **77**, 7–16 (2007)
- R.D. Warner, R.G. Kauffman, M.L. Greaser, *Meat Sci.* **45**(3), 339–352 (1997)
- H. Schmidt, K. Sowoidnich, M. Maiwald, B. Sumpf, H.-D. Kronfeldt, *Proc. SPIE* **73120H**, 1–8 (2009)
- B.G. Frushour, J.L. Koenig, Raman spectroscopy of proteins. in *Advances in Infrared and Raman Spectroscopy* (Heyden, London, 1975)
- T.G. Spiro, B.P. Gaber, *Annu. Rev. Biochem.* **46**, 553–572 (1977)
- M. Berjot, J. Marx, A.J.P. Alix, *J. Raman Spectrosc.* **18**, 289–300 (1987)
- T.-J. Yu, J.L. Lippert, W.L. Peticolas, *Biopolymers* **12**, 2161–2176 (1973)
- J.L. Koenig, B. Frushour, *Biopolymers* **11**, 1871–1892 (1972)
- R.M.C. Dawson, D.C. Elliott, W.H. Elliott, K.M. Jones, *Data for Biochemical Research* (Oxford University Press, Oxford, 1989)
- J.G. Mesu, T. Visser, F. Soulimani, B.M. Weckhuysen, *Vib. Spectrosc.* **39**, 114–125 (2005)
- K.T. Yue, M. Lee, J. Zheng, R. Callender, *Biochim. Biophys. Acta* **1078**, 296–302 (1991)
- L. Rimai, T. Cole, J.L. Parsons, J.T. Hickmott Jr, E.B. Carew, *Biophys. J.* **9**(3), 320–329 (1969)
- W.D. McElroy, B. Glass, *Phosphorus Metabolism*, vol. I (Johns Hopkins University Press, Baltimore, 1951)
- Y. Xie, Y. Jiang, D. Ben-Amotz, *Anal. Biochem.* **343**, 223–230 (2005)
- L. Rimai, M.E. Heyde, *Biochemistry* **10**(7), 1121–1128 (1971)
- R.B. Moon, J.H. Richards, *J. Biol. Chem.* **248**(20), 7276–7278 (1973)
- A. Miri, A. Talmant, J.P. Renou, G. Monin, *Meat Sci.* **31**, 165–173 (1992)
- A. Madden, M.O. Leach, J.C. Sharp, D.J. Collins, D. Easton, *NMR Biomed.* **4**(1), 1–11 (1991)
- J.C. Puyana, B.R. Soller, S. Zhang, S.O. Heard, *J. Trauma Issue* **46**(1), 9–15 (1999)
- B.R. Soller, R.H. Micheels, J. Coen, B. Parikh, L. Chu, C. Hsi, *J. Clin. Monit.* **12**, 387–395 (1996)
- W. Schneider, G. Hildebrandt, H.-J. Sinell, *Fleischwirtschaft* **63**, 1198–1205 (1983)
- H. Schmidt, K. Sowoidnich, H.-D. Kronfeldt, *Appl. Spectrosc.* **64**, 888–894 (2010)
- H. Schmidt, R. Scheier, D.L. Hopkins, *Meat Sci.* **93**, 138–143 (2013)
- A. Savitzky, M.J.E. Golay, *Anal. Chem.* **36**, 1627–1639 (1964)
- R. Chizzolini, E. Novelli, A. Badiani, P. Rosa, G. Delbono, *Meat Sci.* **34**, 49–77 (1993)
- J.R. Bendall, *Meat Sci.* **3**, 143–157 (1979)
- G. Cassanas, M. Morssli, E. Fabrègue, L. Bardet, *J. Raman Spectrosc.* **22**, 409–413 (1991)
- J. De Gelder, K. De Gussem, P. Vandenabeele, L. Moens, *J. Raman Spectrosc.* **38**, 1133–1147 (2007)
- D.K. Pedersen, S. Morel, H.J. Andersen, S.B. Engelsens, *Meat Sci.* **65**, 581–592 (2003)
- M. Pezolet, M. Pigeon-Gosselin, J.-P. Caille, *Biochim. Biophys. Acta* **533**, 263–269 (1978)
- M. Pézolet, M. Pigeon, D. Ménard, J.-P. Caillé, *Biophys. J.* **53**, 319–325 (1988)
- R.C. Lord, G.J. Thomas Jr, *Spectrochim. Acta A* **23**, 2551–2591 (1967)
- J.-M. Delabar, W. Guschlbauer, *Biopolymers* **18**(8), 2073–2089 (1979)
- R. Escobar, P. Carmona, A. Rodríguez-Casado, M. Molina, *Talanta* **48**, 773–780 (1999)
- A. Schäfer, K. Rosenvold, P.P. Purslow, H.J. Andersen, P. Henckel, *Meat Sci.* **61**, 355–366 (2002)
- N. Battle, M.-C. Aristoy, F. Toldrá, *J. Food Sci.* **66**(1), 68–71 (2001)
- J. Twardowski, I. Nowak, D.J. Stufkens, T.L. Snoeck, *Biochim. Biophys. Acta* **790**(1), 70–77 (1984)
- T.W. Barrett, *Spectrochim. Acta A* **37**(4), 233–239 (1981)
- D. Lin-Vien, N.B. Colthup, W.G. Fateley, J.G. Grasselli, *The Handbook of Infrared and Raman Characteristic Frequencies of Organic Molecules* (Academic Press, Boston, 1991)
- H.C. Bertram, S. Dønstrup, A.H. Karlsson, H.J. Andersen, H. Stødkelde-Jørgensen, *Magn. Reson. Imaging* **19**, 993–1000 (2001)
- R.N. Sayre, E.J. Briskey, *J. Food Sci.* **28**(6), 675–679 (1963)
- C. Lopez-Bote, P.D. Warriss, S.N. Brown, *Meat Sci.* **26**, 167–175 (1989)

Publikation 2

**Identification of the early postmortem metabolic
state of porcine *M. semimembranosus* using
Raman spectroscopy**

R. Scheier, J. Köhler and H. Schmidt

Vibrational Spectroscopy **70**
p. 12–17 (2014)

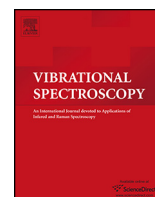
© Elsevier 2014

DOI 10.1016/j.vibspec.2013.10.001

available at:

[http://www.sciencedirect.com/science/article/pii/
S0924203113001318](http://www.sciencedirect.com/science/article/pii/S0924203113001318)

**Reprinted with permission from Elsevier
(License number 3307540432546)**



Identification of the early postmortem metabolic state of porcine *M. semimembranosus* using Raman spectroscopy



Rico Scheier^a, Jürgen Köhler^b, Heinar Schmidt^{a,*}

^a University of Bayreuth, Research Centre of Food Quality, E.-C.-Baumann Straße 20, D-95326 Kulmbach, Germany

^b University of Bayreuth, Experimental Physics IV and Bayreuth Institute for Macromolecular Research (BIMF), Universitätsstraße 30, D-95447 Bayreuth, Germany

ARTICLE INFO

Article history:

Received 10 June 2013

Received in revised form 10 October 2013

Accepted 17 October 2013

Available online 26 October 2013

Keywords:

Energy metabolism

In situ

pH

Lactate

ATP

IMP

ABSTRACT

The metabolic conditions in the early postmortem muscle determine meat quality. Raman spectroscopy is shown to follow the early postmortem metabolism (0.5–10 h) of porcine *M. semimembranosus* ($N = 10$). To this end the Raman spectra, pH and lactate kinetics were measured in the laboratory. Raman difference spectra were utilized to identify the spectral changes and to assign them to metabolic and structural alterations in the *pre-rigor* (50–120 min) and *rigor* (2–8.5 h) phases. In the Raman spectra, the decreasing pH was indicated by three signals assigned to phosphorylated metabolites and inorganic phosphate. Furthermore, the degradation of glycogen to lactate and a reduction of signal intensity of α -helical proteins were revealed. In the *pre-rigor* phase, degradation of phosphocreatine to creatine and reduction of oxy- to deoxymyoglobin was found. In the *rigor* phase, additionally, degradation of ATP to inosine monophosphate (IMP) was observed. Good agreement was achieved between measured and simulated Raman difference spectra. In the *pre-rigor* and *rigor* time frame, normal and deviating meat quality could be distinguished based on signals of phosphocreatine, ATP, IMP and α -helical proteins. This work provides a deeper understanding and the first semi-quantitative description of the early postmortem Raman spectra of meat which show potential for the non-invasive and early detection of the metabolic state of meat, and hence for the identification of deviating meat qualities.

© 2013 Elsevier B.V. All rights reserved.

1. Introduction

To date, classical reference measurements to determine the metabolic state of early postmortem meat are performed using mostly enzymatic (concentration of metabolites) or physical methods (pH) which, however, are invasive and time-consuming. Using these methods a sound understanding of the early postmortem metabolism of muscle cells was achieved. [1–4]. The vital role of adenosine triphosphate (ATP) for the cells is well known and its depletion *post mortem* causes the muscle entering the *rigor mortis*. After death of the animal, the muscle can mainly rely on three (series of) reactions to regenerate ATP (Fig. 1): (a) using the phosphocreatine (PCr) energy storage which is converted to creatine (Cr). (b) Using two ADP via the adenylate kinase reaction generating

adenosine monophosphate (AMP) which is rapidly metabolized to inosine monophosphate (IMP). (c) When 70% of the PCr pool has been depleted [5] and ATP levels decreased significantly glycogen is consumed to phosphorylate ADP in the course of the glycolysis. With interruption of the blood circulation, the end product of this process, pyruvate, is further metabolized to lactate and the H^+ ions are accumulated. This leads to an acidification of the muscle cells. In pork meat, pH 7.4 is measured *in vivo* while postmortem lactic acid production typically decreases this value below 5.7 [6]. The ATP is mainly used to maintain the relaxed state of the muscle (Fig. 1, reaction d). The hydrolysis produces ADP and inorganic phosphate (P_i) which both can reenter the glycolytic pathway. An overview of the postmortem metabolism describing the conversion from muscle to meat is given in [7].

Our approach to measure the postmortem metabolic state was to directly utilize a fast and non-invasive optical method, Raman spectroscopy, which provides information of metabolites and structural changes in meat. In principle, laser light stimulates vibrations in molecules or atomic lattices which shift the wavelength of the scattered light. The relative wavelength shifts are a vibrational spectroscopic fingerprint and they are utilized to identify and quantify chemical compounds. Raman spectroscopy is a fast and non-invasive method which has proven its usefulness as a

Abbreviations: ADP, adenosine diphosphate; AMP, adenosine monophosphate; ATP, adenosine triphosphate; Cr, creatine; IMP, inosine monophosphate; PCr, phosphocreatine; P_i , inorganic phosphate; PLSR, partial least squares regression; PSE, pale, soft, exudative; RFN, red, firm, non-exudative.

* Corresponding author. Tel.: +49 09221 8780 3103; fax: +49 0921 5584 3086.

E-mail addresses: rico.scheier@uni-bayreuth.de (R. Scheier),

juergen.koehler@uni-bayreuth.de (J. Köhler), heinar.schmidt@uni-bayreuth.de (H. Schmidt).

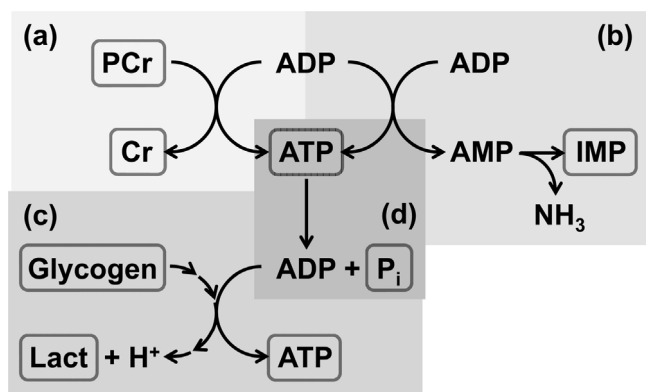


Fig. 1. Simplified overview of postmortem ATP metabolism in pork meat with (a) formation from PCr, (b) regeneration from ADP with subsequent deamination of AMP to IMP, (c) formation by degradation of glycogen to lactate (*Lact*) and H⁺ ions with consumption of ADP and P_i, (d) ATP hydrolysis to maintain muscle tension. Metabolites identified in Raman difference spectra of meat are marked by a frame.

tool for investigations of biological matter such as the detection of bacterial contamination in cell or tissue cultures [8] or of foodborne microorganisms on food surfaces [9], protein structure [10] or muscle fibers [11,12] and glucose level in aqueous humor [13] with use of different Raman techniques. Additionally, Raman spectroscopy has proven to determine the secondary structure of proteins with the amid I and III modes [14–16], to observe pH-induced conformational changes of poly-amino acids in aqueous solutions [17,18] and pH-induced structural changes of the free amino acid histidine [19] and in the protein transferrin [20]. Furthermore, the symmetric PO₃²⁻ stretching vibration of the basic form of the terminal phosphate moiety at 980 cm⁻¹ and the symmetric PO₂⁻ stretching vibration of the acidic form at 1082 cm⁻¹ were shown to be an excellent indicator for the pH [21,22].

In meat science, Raman spectroscopy came under scrutiny for the prediction of water holding capacity [23], tenderness [24–26], cooking temperature [27], sensory quality [28] and microbiological spoilage [29]. Most of this work focused on using chemometric methods to evaluate the spectra because of the complexity of the biological samples. Since the early work of Carew et al. [30] the assignment of Raman spectra of meat was almost exclusively related to *post-rigor* spectra, but rather little is known so far regarding the peak assignment of early post-mortem spectra [22,23]. One reason is that the Raman peaks of a multi-component system such as a muscle have to be regarded as a superposition of signals of structure forming components and many metabolites, some of which are only temporarily detectable [22]. Hence, the objective of this study is to assess whether Raman spectra can serve as an indicator of the metabolic state of early postmortem pork meat and to develop a deeper understanding of the Raman spectra by assigning the spectral changes to metabolic and structural changes which occur during the first ten hours postmortem.

2. Materials and methods

2.1. Meat samples

Raman and reference measurements were performed with the topside (*M. semimembranosus*) from ten pigs representing a sample of typical breeds slaughtered in Germany. The samples were selected with a view to obtain normal and deviating meat qualities. Thus, this sample does not reflect the normal distribution of meat qualities of the abattoir. The meat samples were removed 20–30 min post-slaughter in a local abattoir. After that, the samples were immediately transported to the laboratory, where they

were divided into three parts for Raman, pH and lactate measurements which started 25–40 min *post mortem* (p.m.). The allocation of the three parts to Raman, pH and lactate analysis was randomized between samples. The subsamples cooled to room temperature within 30 min.

2.2. Reference measurements

As the metabolic rates of the muscle decreased with time, pH and lactate were measured in increasing intervals. Using a puncture electrode (Mettler Toledo – SevenGo pro, Giessen, Germany), pH values were taken until constant pH was reached in three consecutive measurements. In parallel, at least seven lactate concentrations were determined per muscle in the time from 0.5 to 10 h p.m. applying the sample preparation described in [22]. The lactate concentration was finally measured photometrically using an enzymatic test assay and the absorbance of NADH at 340 nm (Megazyme International Ireland, Wicklow, Ireland) [31].

2.3. Raman measurements

Raman measurements were conducted with the handheld Raman probe presented in [32]. The sensor is connected via an optical fiber with a miniature spectrograph (HORIBA Jobin-Yvon, Longjumeau, France) with a spectral range from 689 to 769 nm and an optical resolution of <0.5 nm. The built-in CCD detector (Hamamatsu S7031-1006S) is cooled by a Peltier element. Additionally to the Raman optics and electric supply described in [32], the sensor head contains an OEM laser driver (RGB Lasersysteme GmbH, Kelheim, Germany) which controls the 671 nm external-cavity diode laser [33] and a Peltier element for temperature control. This handheld system is operated by a program written in LabVIEW (National Instruments, Austin, TX, USA).

From 0.5 to 10 h p.m., Raman spectra were obtained with an integration time of 5 s and 5 accumulations at a laser power of 100 mW at one spot of the meat surface. Subsequent measurements took place at different spots on the meat surface. Raman measurements were conducted in increasing intervals beginning with 5 s between each spectrum. These intervals were incrementally increased until 5 min between spectra after 10 h p.m. For further analysis, five consecutive Raman spectra were averaged, reduced to the wavenumber range from 500 to 1800 cm⁻¹ and subsequently baseline-corrected using MATLAB (The MathWorks, Natick, MA) with the COBRA toolbox [34].

2.4. Reference Raman spectra

Raman spectra of the energy metabolites adenosine triphosphate, inosine monophosphate, lactate, glucose 6-phosphate (G6P) glycogen (from oyster, CAS9005-79-2), creatine, phosphocreatine and phosphoric acid (P_i) were recorded as a reference using 50 mM (100 mM in case of lactate) aqueous solutions, laser power of 100 mW, integration time of 25 s and 10 accumulations. The pure chemicals were purchased from Sigma-Aldrich Chemie GmbH, Steinheim, Germany. To account for variations of the spectra due to changes of the pH [35], the Raman spectra of G6P, ATP, IMP and inorganic phosphate solutions were recorded in the range from pH 5 to 7 in steps of 0.2 pH units. The pH was adjusted by adding KOH or HCl solution.

The Raman spectrum of α -helical proteins was obtained using one day old meat samples by measuring the muscle fibers parallel and perpendicular to the laser's polarization orientation. The difference spectrum parallel-perpendicular yields the Raman spectrum of α -helical proteins according to [12]. The spectra of

Table 1

Summary of reference results for the investigated meat samples with assigned quality, number of samples (*N*), pH₄₅, pH₂₄ and lactate formation rates (mean ± standard deviation).

Quality	<i>N</i>	pH ₄₅	pH ₂₄	Lactate formation rate/mmole kg ⁻¹ h ⁻¹
RFN	7	6.25 ± 0.20	5.52 ± 0.12	7.4 ± 0.9
PSE-tendency	2	5.84 ± 0.07	5.37 ± 0.02	13.5 ± 1.5
Atypical	1	5.87	5.7	<0.5

Table 2

Measured pH values and estimated concentrations of metabolites used to calculate the difference spectra in Fig. 2S and 3S.

Time p.m.	pH	Lactate	Glycogen	PCr	ATP	IMP	P _i
~1 h	6.2	37	53	2	4.0	1.5	20
~2 h	6.0	55	44	0	3.5	2.0	26
>8 h	5.6	100	22	0	0.4	5.1	34

deoxy- and oxymyoglobin were obtained by measuring meat samples with different degrees of oxidation.

3. Results and discussion

Table 1 summarizes the results of the pH and lactate analyses which were conducted in parallel to the Raman measurements. According to pH₄₅ and lactate formation kinetics, seven out of ten samples were assigned to normal meat (red, firm, non-exudative – RFN), while two revealed increased lactate formation and showed tendency of PSE meat (pale, soft, exudative). One sample showed essentially no lactate formation over 8 h, but also no significant changes of the Raman spectra during that period and therefore, was excluded from the analysis.

In the following two sections, the changes which are observed in the Raman spectra during the *pre-rigor* phase (50 min–2 h p.m.) and during the *rigor* phase (2–8.5 h p.m.) are discussed on the basis of the difference spectra of the measured SM samples which are compared with difference spectra calculated from the reference Raman spectra to underpin the peak assignment.

3.1. Pre-rigor phase

To show the changes of the Raman spectral patterns for normal meat, difference spectra of the seven normal samples were calculated. To this end, 50 preprocessed spectra of samples measured after 2 h p.m. were averaged per sample and subtracted from an equal number of spectra measured before 1 h p.m. The averaged difference spectrum of the seven samples is presented in Fig. 2(a). Positive peaks indicate metabolites which were formed, whereas negative peaks point at degraded metabolites.

This difference spectrum is far too complex to be discussed on the basis of individual bands. Therefore, changes of signal difference patterns due to a number of metabolic reactions were considered, e.g. the Raman difference spectrum of *creatine minus phosphocreatine* is depicted in Fig. 2(b). The difference spectrum was scaled according to the integration and laser power settings of the measurements with the meat samples and an conversion rate of 2 mmol/kg of PCr to Cr in this interval which was judiciously chosen in accordance to the concentrations found in [1,2]. An overview of the concentrations of the relevant metabolites according to the literature is given in Table 3 and an overview of the concentrations which were used to scale the Raman difference spectra is given in Table 2. The averaged pH values of the meat samples were 6.2 and 6.0 for the <1 h period and after 2 h p.m., respectively (see Table 2). The pH dependency of the Raman spectra of PCr can be neglected due to its low pK_a value of 4.5 [35]. Accumulation of Cr is indicated

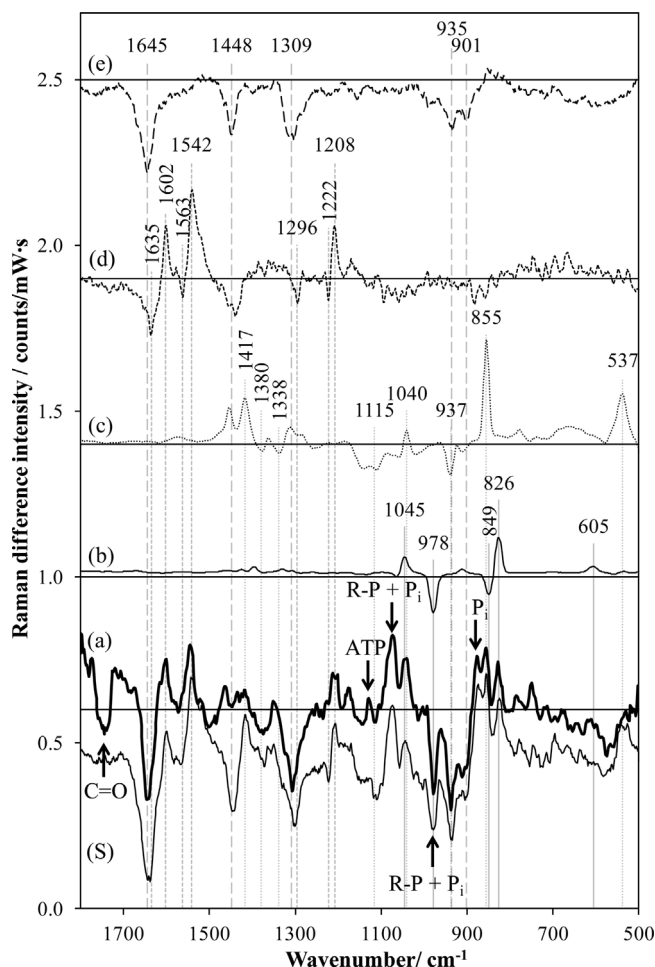


Fig. 2. Difference Raman spectra of (a) RFN meat samples measured 2 h minus <1 h p.m. and (S) simulated, (b) creatine minus phosphocreatine, (c) lactate minus glycogen, (d) deoxyMb minus oxyMb and (e) Raman spectrum of α -helical proteins. Peaks assigned to phosphorylated metabolites (R-P), inorganic phosphate (P_i) and ATP are marked with arrows.

by positive peaks at 605, 826 and 1045 cm⁻¹, while degradation of PCr can be identified by the negative peak at 978 cm⁻¹ assigned to the symmetric PO₃²⁻ stretching vibration of the phosphate moiety [21]. It is noteworthy that this latter signal is superimposed by peaks of metabolites with one terminal phosphate group which add intensity to the peak at 978 cm⁻¹ (marked with R-P + P_i in Fig. 2(a)) [36]. The signals of PCr at 846 cm⁻¹ and of Cr at 1045 cm⁻¹ are co-located with the strong peak at 855 and a smaller signal at 1040 cm⁻¹ both originating from lactate. The peak at 826 cm⁻¹ can be utilized to estimate the conversion rate of PCr to Cr in the meat spectra. The difference intensity in Fig. 2(a) would account for the formation of 2.1 mmol/kg Cr when we consider that the pH-induced change in the sugar phosphates contributes about 13% of the difference intensity at 826 cm⁻¹. This was estimated from a total content of sugar phosphates of ca. 12 mmol/kg [4], the acidification by 0.2 pH units and using G6P as example (see Fig. 3(e)).

In Fig. 2c the result of the reaction of 9 mmol/kg glycogen to 18 mmol/kg lactate is shown as difference spectrum. The conversion rate of glycogen to lactate was estimated from the lactate production measured in the RFN samples and from literature [1]. The difference spectrum reproduces the situation found in Fig. 2(a). Signals of glycogen can be expected at 937, 1115, 1338 and 1380 cm⁻¹. In the difference spectrum in Fig. 2(a), the band at 1115 and the peak at 1338 cm⁻¹ are clearly visible, while the other Raman signals are attenuated or overcompensated by peaks of

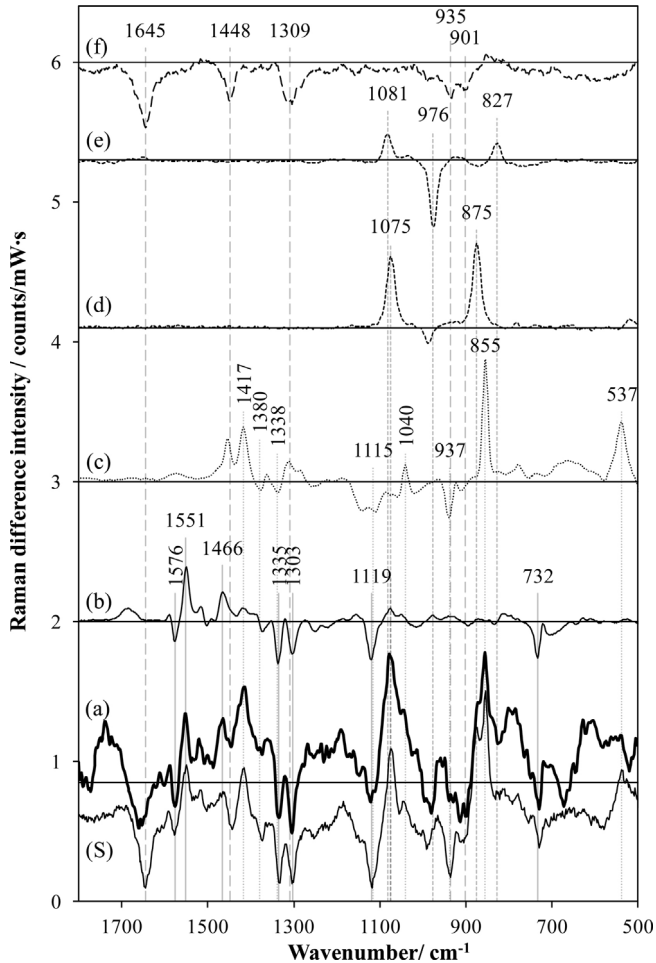


Fig. 3. Difference Raman spectra of (a) RFN meat samples measured 8.5 h minus 2 h p.m. and (S) simulated, (b) IMP at pH 5.6 minus ATP at pH 6.0, (c) lactate minus glycogen, (d) phosphoric acid at pH 5.6 minus pH 6.0, (e) G6P at pH 5.6 minus G6P at pH 6.0 and (f) Raman spectrum of α -helical proteins.

α -helical proteins at 935 and one yet unassigned signal at 1380 cm^{-1} . Two distinct signals of lactate are expected at 537 and 853 cm^{-1} [38]. Both can be found in Fig. 2(a). The latter is disturbed at low wavenumbers by an imperfect baseline correction. The smaller Raman peaks at 1040 and 1417 cm^{-1} are also found in the meat difference spectra.

Interestingly, a pronounced peak can be found at 1123 cm^{-1} which is probably caused by the increasing intensity of the pH-dependent, symmetric PO_2^- stretching mode of the triphosphate moiety in ATP [21,39]. With decreasing pH, this peak's intensity is increased. The same holds for ADP but here much lower intensities are expected due to concentrations of below 1 mmol/kg [2,4]. In case of ADP, the aforementioned pH-dependent vibration can be found at 1109 cm^{-1} and in fact, the meat difference spectrum reveals a weak shoulder at 1105 cm^{-1} . As the concentration of ADP and ATP in the *pre-rigor* phase is nearly constant, primarily these two pH-dependent peaks appear in the difference spectrum.

The Raman pattern between 1500 and 1600 cm^{-1} is mainly explained by the Raman difference spectrum *deoxy-minus oxymyoglobin* depicted in Fig. 2(d). The positive peaks at 1208, 1542 and 1602 cm^{-1} can be assigned to the formation of deoxymyoglobin (deoxy-Mb), while the negative peaks at 1296 and 1635 cm^{-1} are due to a loss of oxymyoglobin (oxy-Mb) [40]. The similarity of this pattern and the meat difference spectrum in Fig. 2(a) (above 1500 cm^{-1}) is obvious. Even two weaker signals of oxy-Mb at 1222 and 1563 cm^{-1} are recognizable in the meat. This spectral pattern

can be interpreted as a conversion from oxy- to deoxymyoglobin between 50 and 120 min p.m. When the sample was cut from the SM muscle the meat surface was exposed to oxygen which led to the formation of oxy-Mb. During the Raman measurements the exposure to air was reduced by the sensor head and deoxy-Mb is formed because early postmortem, the muscle cell's mitochondria still consume oxygen.

In addition to the discussed metabolites a decrease of the signals of α -helical proteins is observed in Fig. 2(a). The signals can be found at 901, 935, 1309, 1448 and 1645 cm^{-1} [11,12]. A spectrum of α -helical proteins is depicted in Fig. 2(e). The signals at 901, 1309 and 1645 cm^{-1} are the least perturbed signals. Additionally, the α -helix signals are responsible for Raman signals at 935 and 1448 cm^{-1} . While the peak at 935 cm^{-1} is clearly visible in the meat difference spectrum and increased by glycogen, the signal at 1448 cm^{-1} is rather weak compared to the expected intensity. The increasing lactate signal only partly compensates this signal. In general, CH-deformation modes give rise to signals in this wavenumber area and in proteins, the intensity of this band was reported to be sensitive to the hydrophilicity/hydrophobicity of the protein environment [41,42]. This could overcompensate the expected decrease. Nevertheless, the loss of signals from the α -helical secondary structure and the lack of increasing signals of beta pleated sheet or random coil structure in the amid I or III region is surprising considering the very early time frame of these Raman measurements. The origin of this decline of α -helical signals is unknown.

The simulated difference spectra presented in Fig. 2(S) was obtained by summing up the difference spectra (b–e) shown in Fig. 2. The Raman difference spectra which were measured with the pure metabolites in aqueous solution were scaled with the concentrations listed in Table 2. These values are in accordance with values found in the literature (see Table 3) or were measured such as pH and lactate concentration. The difference spectra of deoxy-minus oxy-Mb and of α -helical proteins were judiciously scaled for best agreement between measured and calculated difference spectrum. Evidently, there is very good agreement between the simulation and the measured spectrum especially in the wavenumber range from 800 to 1150 cm^{-1} leaving only a few peaks unassigned. Namely, the CH-deformation band at 1450 cm^{-1} and a peak at 1740 cm^{-1} are not well explained and belong to a compound not included in our simulation. The latter peak can be assigned to C=O stretching vibrations of carbonyl groups which is attributed to saturated esters or ketones in five-membered rings [43]. Apparently, some of these compounds are significantly degraded during the first hours *post mortem*, but at this point, its origin remains unclear.

3.2. Rigor phase

The second phase was chosen to emphasize metabolic changes when the muscle is entering the *rigor mortis*. To this end, Raman spectra from 2 h p.m. (pH 6.0) and the final (8.5 h p.m.) spectra of each series of measurement (pH 5.6) were subtracted and averaged. The difference spectrum *final minus 2 h p.m.* is presented in Fig. 3(a).

In the *rigor* phase, ATP is degraded to adenosine di-, monophosphate and finally IMP. The latter can further react to inosine, inorganic phosphate, ribose and hypoxanthine but this takes place on a longer time scale, i.e. less than 0.8 mmol/kg inosine can be determined <8 h p.m. within pork meat [3]. Hence, the important reactant is ATP while the relevant end product is IMP. Typical concentrations found in pork meat differ between 5 and 7 mmol/kg of ATP after exsanguination and once 70% of the Pcr pool has been consumed [5], its level is declining below 0.6 mmol/kg after 8 h p.m. [1–4]. IMP concentrations vary from 0.1 to 0.8 mmol/kg at time of death and rise to 4.5–6.1 mmol/kg after 8 h [1–3]. The difference spectrum *ATP at pH 6.0 minus IMP at pH 5.6* is presented in

Table 3

Overview of pH and range of concentration of energy metabolites in three time frames early postmortem for RFN meat quality according to the literature.

Time p.m.	pH	Concentration/mmol/kg					
		Lactate	Glycogen	PCr	ATP	IMP	P _i
~1 h	5.8–6.5	40–70	49–56	0.4–3.0	3.1–4.5	1.1–2.6	19–20
~2 h	5.6–6.3	50–90	39	0.2–2.6	1.9–5.0	1.0–4.1	27–28
>8 h	5.5–5.8	85–125	24–36	0.1	0.2–0.6	4.5–6.1	41
Ref.	[2,45]	[1,2,4]	[1,2,4]	[1,2,4,45]	[1–4,45]	[1–3]	[44,45]

Fig. 3(b). Besides the typical Raman signals from adenine at 732, 1303, 1335 and 1576 cm^{-1} , ATP shows a distinct triphosphate peak at 1119 cm^{-1} [21]. Strong signals assigned to vibrations of IMP can be found at 1466 and 1551 cm^{-1} . Under acidic conditions, the terminal phosphate group, $-\text{PO}_3\text{H}^-$ is only responsible for the weak signal at 1074 cm^{-1} assigned to the symmetric PO_2^- stretching vibration. In the meat difference spectrum depicted in Fig. 3(a), all peaks from ATP are clearly visible. The signal at 1303 cm^{-1} is superimposed by the signal of the α -helical proteins. Both signals of IMP can be found in meat at 1466 and 1551 cm^{-1} .

In our samples acidification and glycolysis continued until 8 to 10 h p.m. which results in strong, positive signals of lactate and negative signals of glycogen in Fig. 3(a). Again, the difference spectrum *lactate minus glycogen* is shown in Fig. 3(c). The spectrum was scaled for the conversion of 22.5 mmol/kg glycogen to 45 mmol/kg lactate. In the excised samples, lactate was formed in this phase with a nearly constant rate of 7.0 mmol/kg per hour between 2 and 8.5 h p.m. which is comparable to values found in [1].

During glycolysis, ADP and P_i are recycled (see Fig. 1). While ADP is further metabolized to IMP, P_i is accumulated in concentrations of up to 40 mmol/kg in pork meat [44,45]. In Fig. 3(d), a difference spectrum of inorganic phosphate in aqueous solution is presented. According to the concentration of P_i found in literature the spectrum at pH 5.6 was scaled with 34 mmol/kg and at pH 6.0 with 26 mmol/kg before subtraction. The aforementioned peaks in pork meat at 980 and 1080 cm^{-1} (marked with R-P+P_i in Fig. 2(a)) are assigned to the vibration of P_i and to the phosphate group in sugar phosphates such as glucose 6-phosphate (see Fig. 3(e)) and IMP. Additionally, high concentrations of the acidic form of P_i (H_2PO_4^-) yield a strong signal at 875 cm^{-1} which corresponds to the symmetric $\text{P}(\text{OH})_2$ stretching vibration (Fig. 3(d)). This band is observed in the meat difference spectra in Fig. 2(a) and in Fig. 3(a) as a shoulder.

The negative signal at 980 cm^{-1} in Fig. 3(a) cannot be explained by inorganic phosphate alone. This signal can be attributed to phosphorylated metabolites with lower pK_a values than P_i such as G6P ($\text{pK}_a = 6.1$) which is the glycolytic intermediate with the highest concentration of up to 8 mmol/kg [4,46]. This concentration is reached after 2 h p.m. and remains almost constant for at least 12 h [46]. The difference spectrum of *G6P at pH 6.0 minus G6P at pH 5.6* was calculated and then scaled with a factor of 5 for better visibility (Fig. 3(e)). In this case, the base peak at 976 cm^{-1} is apparent and due to the summed intensity of every sugar phosphate the negative signal in Fig. 3(a) can be explained. Note that the peak at 827 cm^{-1} assigned to the $\nu\text{R-PO}_3\text{H}$ vibration also adds intensity to the Cr signal in the *pre-rigor* phase (Fig. 2(a)) and to the shoulder in the meat difference spectrum in Fig. 3(a).

When comparing the Raman spectra of meat before and after *rigor mortis*, the signals of α -helical proteins decrease (Fig. 3(f)) in the meat difference spectrum and indicate, again, loss of intensity or degradation of α -helical proteins in this time frame.

Again, the sum of the difference spectra presented in Fig. 3(b)–(f) was calculated. In comparison to the *pre-rigor* phase, similar results were achieved for the *rigor* phase (see Fig. 3(S)). Excellent agreement was found between 1050 and 1700 cm^{-1} , while minor deviations between simulation and measurement can be

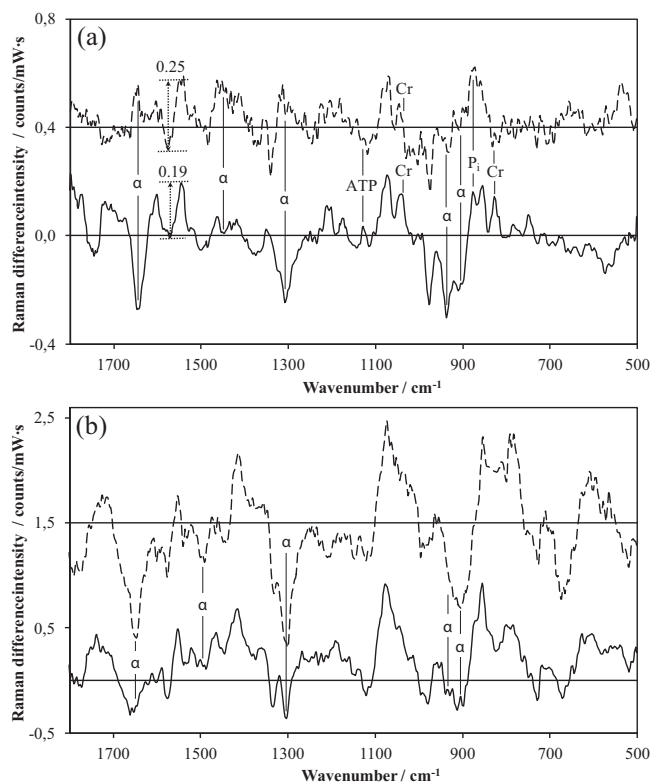


Fig. 4. Difference spectra of meat with RFN (solid) and PSE-like (dashed) quality from (a) the *pre-rigor* and (b) the *rigor* phase.

found below 700 cm^{-1} , between 770 and 800 cm^{-1} and again in the carbonyl region around 1740 cm^{-1} .

3.3. Deviating meat quality

To this point, only spectra of normal samples were discussed, but according to pH_{45} and lactate formation rates two samples revealed PSE-like behavior. Although the number of samples is low, the Raman difference spectra in Fig. 4 represent a total of 700 and 200 spectra taken at different positions for the normal and the PSE-like samples, respectively. Hence, the spectral differences have a sound spectroscopic basis and it is now interesting to compare the difference spectra of the PSE-like samples for the *pre-rigor* (Fig. 4(a)) and *rigor* phase (Fig. 4(b)). In the *pre-rigor* phase, the pH decreased from 5.8 to 5.6 in these samples. The difference spectrum of PSE-like meat shows a higher level of noise due to the lower number of spectra. However, an indication is found for a faster degradation of ATP to IMP according to the ratio of the Raman peaks at 1551 and 1576 cm^{-1} . The quantitative determination of this ratio could be very useful because the ratio ATP/IMP was reported to be an excellent predictor for deviating metabolism and hence, meat qualities [47]. At the same time, the pH-dependent ATP signal at 1119 cm^{-1} is weaker compared to normal samples. This points to a lower absolute concentration in the PSE-like samples which is in accordance to

the literature [45,47]. In the *pre-rigor* phase, formation of P_i is higher as indicated by the peak at 875 cm^{-1} . Furthermore, the Raman difference spectrum of PSE-like meat did not show the signals of Cr at 826 and 1045 cm^{-1} . This is in keeping with the rapid exhaustion of the PCr pool in PSE meat [45] where no further formation of Cr was found after 1 h.

In the *rigor* phase most of these differences are already equalized (see Fig. 4(b)): ATP is degraded and the final concentrations of lactate and P_i as well as the ultimate pH are reached. The most obvious difference in the Raman spectra of the *rigor* phase of PSE meat is the higher loss of α -helical signal intensity which points at the known denaturation of proteins in PSE meat which eventually leads to lower water holding capacity and higher drip loss [48]. Unassigned spectral differences can be found at 565 and around 785 cm^{-1} . Apart from that, the difference spectra of PSE-like samples reveal only minor differences in the *rigor* phase.

In summary, it can be stated that metabolic changes in pork meat could be followed and visualized with Raman difference spectra in the *pre-rigor* (50–120 min p.m.) and *rigor* phase (2–8.5 h p.m.). The difference signal patterns of normal meat quality (RFN) could be explained by summation of five Raman difference spectra which were measured with the pure compounds in solution of appropriate pH to show the effect of the individual reactions. Thus, in the *pre-rigor* phase conversion of phosphocreatine to creatine, glycogen to lactate and deoxygenation of myoglobin were shown to largely cause the observed changes in the meat spectra. In the *rigor* phase, further formation of lactate and inorganic phosphate, degradation of adenosine triphosphate to inosine monophosphate and the decreasing pH were revealed in the Raman difference spectra. The acidification of the muscle was indicated by the protonation of terminal phosphate moieties and inorganic phosphate. In both phases, a distinct loss of α -helical protein signals was observed. Using concentrations taken from the literature and Raman spectra of pure chemicals, excellent agreement was achieved between simulated and measured difference spectra of meat.

The comparison of the Raman difference spectra between normal and deviating (=PSE-like) meat quality indicated higher conversion rate of ATP to IMP, lower concentration of ATP, a faster formation of P_i and a lack of Cr formation in the PSE-like sample in the *pre-rigor* time frame. On the other hand, the main spectral difference in the *rigor* phase was a significantly higher loss of signals from α -helical proteins in PSE-like meat.

4. Conclusion

In this study we have demonstrated the potential of portable Raman spectroscopy to follow the early postmortem metabolism in pork meat. The spectral changes could be traced back to energy metabolites known to be indicators for the development of the meat quality. Therefore, Raman spectroscopy could be very useful for an early determination of meat quality. The Raman spectra give deeper insight into the metabolic conditions than the pH measurements and they provide this information non-invasively and much faster than classic reference methods. However, as the sample size was relatively small, these first results should be confirmed with a larger number of animals and the feasibility of using the portable Raman device in an abattoir remains to be shown.

Acknowledgements

This work was financially supported by the German research foundation DFG (Deutsche Forschungsgemeinschaft) in the framework of the cluster project “Minimal Processing” of the Research Association of the German Food Industry (FEI). The Research Center

of Food Quality is financed by the European Regional Development Fund (ERDF) which is gratefully acknowledged.

The authors wish to thank Dr. Heinz-Detlef Kronfeldt for generous support with the prototype handheld Raman device, Dirk Grünh for providing the pork samples and for the excellent cooperation as well as Thomas Kador and Stefanie Hofmann for assistance with lactate and Raman measurements.

References

- [1] P. Henckel, A. Karlsson, M.T. Jensen, N. Oksbjerg, J.S. Petersen, *Meat Sci.* 62 (2001) 145–155.
- [2] A. Schäfer, K. Rosenvold, P.P. Purslow, H.J. Andersen, P. Henckel, *Meat Sci.* 61 (2002) 355–366.
- [3] N. Batlle, M.C. Aristoy, F. Toldrà, *J. Food Sci.* 66 (2001) 68–71.
- [4] L.L. Kastenschmidt, W.G. Hoekstra, E.J. Briskey, *J. Food Sci.* 33 (1968) 151–158.
- [5] J.R. Bendall, *J. Physiol.* 114 (1951) 71–88.
- [6] E.J. Briskey, *Adv. Food Res.* 13 (1964) 89–178.
- [7] T.L. Scheffler, S. Park, D.E. Gerrard, *Meat Sci.* 89 (2011) 244–250.
- [8] C. Bolwien, G. Sulz, S. Becker, H. Thielecke, H. Mertsching, S. Koch, *Proc. SPIE* 6853, *Biomedical Optical Spectroscopy*, 2008, p. 68530F.
- [9] H. Yanga, J. Irudayaraj, *J. Mol. Struct.* 646 (2003) 35–43.
- [10] M. Bouraoui, S. Nakai, E. Li-Chan, *Food Res. Int.* 30 (1997) 65–72.
- [11] M. Pezolet, M. Pigeon-Gosselin, J.-P. Caille, *Biochim. Biophys. Acta* 533 (1978) 263–269.
- [12] M. Pézolet, M. Pigeon, D. Ménard, J.-P. Caillé, *Biophys. J.* 53 (1988) 319–325.
- [13] J.L. Lambert, J.M. Morookian, S.J. Sirk, M.S. Borchert, *J. Raman Spectrosc.* 33 (2002) 524–529.
- [14] B.G. Frushour, J.L. Koenig, *Advances in Infrared and Raman Spectroscopy*, Chap. Raman Spectroscopy of Proteins, Heyden, London, 1975.
- [15] T.G. Spiro, B.P. Gaber, *Annu. Rev. Biochem.* 46 (1977) 553–572.
- [16] M. Berjot, J. Marx, A.J.P. Alix, *J. Raman Spectrosc.* 18 (1987) 289–300.
- [17] T.-J. Yu, J.L. Lippert, W.L. Peticolas, *Biopolymers* 12 (1973) 2161–2176.
- [18] J.L. Koenig, B. Frushour, *Biopolymers* 11 (1972) 1871–1892.
- [19] J.G. Mesu, T. Visser, F. Soulimani, B.M. Weckhuysen, *Vib. Spectrosc.* 39 (2005) 114–125.
- [20] K.T. Yue, M. Lee, J. Zheng, R. Callender, *Biochim. Biophys. Acta* 1078 (1991) 296–302.
- [21] L. Rimai, T. Cole, J.L. Parsons, J.T. Hickmott Jr., E.B. Carew, *Biophys. J.* 9 (1969) 320–329.
- [22] R. Scheier, H. Schmidt, *Appl. Phys. B* 111 (2013) 289–297.
- [23] D.K. Pedersen, S. Morel, H.J. Andersen, S.B. Engelsen, *Meat Sci.* 65 (2003) 581–592.
- [24] R.J. Beattie, S.J. Bell, L.J. Farmer, B.W. Moss, D. Patterson, *Meat Sci.* 66 (2004) 903–913.
- [25] J.R. Beattie, S.E.J. Bell, C. Borggaard, B.W. Moss, *Meat Sci.* 80 (2008) 1205–1211.
- [26] H. Schmidt, R. Scheier, D. Hopkins, *Meat Sci.* 93 (2013) 138–143.
- [27] D.T. Berhe, M.S. Hviid, S.B. Engelsen, R. Lametsch, *Proc. 59th International Congress of Meat Science and Technology*, 2013.
- [28] Q. Wang, S.M. Lonergan, C. Yu, *Meat Sci.* 91 (2012) 232–239.
- [29] K. Sowoidnich, H. Schmidt, H.-D. Kronfeldt, F. Schwägele, *Vib. Spectrosc.* 62 (2012) 70–76.
- [30] E.B. Carew, I.M. Asher, H.E. Stanley, *Science* 188 (1975) 933–936.
- [31] W. Schneider, G. Hildebrandt, H.-J. Sinell, *Fleischwirtschaft* 63 (1983) 1198–1205.
- [32] H. Schmidt, K. Sowoidnich, H.-D. Kronfeldt, *Appl. Spectrosc.* 64 (2010) 888–894.
- [33] B. Sumpf, H. Schmidt, M. Maiwald, A. Müller, G. Erbert, H.-D. Kronfeldt, G. Tränkle, *Proc. SPIE* 7315, *Sensing for Agriculture and Food Quality and Safety*, 2009, p. 731508.
- [34] C.M. Galloway, E.C. Le Ru, P.G. Etchegoin, *Appl. Spectrosc.* 63 (2009) 1370–1376.
- [35] W.D. McElroy, B. Glass, *Phosphorus Metabolism*, vol. 1, Johns Hopkins University Press, Baltimore, 1951.
- [36] Y. Xie, Y. Jiang, D. Ben-Amotz, *Anal. Biochem.* 343 (2005) 223–230.
- [37] L. Rimai, M.E. Heyde, *Biochemistry* 10 (1971) 1121–1128.
- [38] G. Cassanas, M. Morssli, E. Fabrègue, L. Bardet, *J. Raman Spectrosc.* 22 (1991) 409–413.
- [39] T.G. Spiro, T.C. Streckas, *J. Am. Chem. Soc.* 96 (1974) 338–345.
- [40] M. Careche, A.M. Herrero, A. Rodriguez-Casado, M.L. Del Mazo, P. Carmona, *J. Agric. Food Chem.* 47 (1999) 952–959.
- [41] A. Herrero, P. Carmona, M.J. Careche, *J. Agric. Food Chem.* 52 (2004) 2147–2153.
- [42] D. Lin-Vien, N.B. Colthup, W.G. Fateley, J.G. Grasselli, *The Handbook of Infrared and Raman Characteristic Frequencies of Organic Molecules*, Academic Press, Boston, 1991.
- [43] H.C. Bertram, S. Dønstrup, A.H. Karlsson, H.J. Andersen, H. Stødkele-Jørgensen, *Magn. Reson. Imaging* 19 (2001) 993–1000.
- [44] M. Miri, A. Talmant, J.P. Renou, G. Monin, *Meat Sci.* 31 (1992) 165–173.
- [45] J.W. Stephens, M.E. Dikeman, J.A. Unruh, M.D. Haub, M.D. Tokach, S.S. Dritz, *J. Anim. Sci.* 86 (2008) 1669–1677.
- [46] K.O. Honikel, C. Fischer, *J. Food Sci.* 42 (1977) 1633–1636.
- [47] S.T. Joo, R.G. Kauffman, B.C. Kim, G.B. Park, *Meat Sci.* 52 (1999) 291–297.

Publikation 3

**Early postmortem prediction of meat quality
traits of porcine *semimembranosus* muscles
using a portable Raman system**

R. Scheier, A. Bauer and H. Schmidt

Food and Bioprocess Technology ???
p. ???–??? (2014)

© Springer 2014

DOI 10.1007/s11947-013-1240-3

available at:

http:

[//link.springer.com/article/10.1007%2Fs11947-013-1240-3](http://link.springer.com/article/10.1007%2Fs11947-013-1240-3)

**Reprinted with permission from Springer
(License number 3421260480702)**

Early Postmortem Prediction of Meat Quality Traits of Porcine *Semimembranosus* Muscles Using a Portable Raman System

Rico Scheier · Aneka Bauer · Heinar Schmidt

Received: 13 September 2013 / Accepted: 8 December 2013
© Springer Science+Business Media New York 2013

Abstract Modern abattoirs are lacking objective, fast, and noninvasive methods to measure or predict important meat quality traits such as pH, color, drip loss, or shear force early postmortem. In this work, a mobile Raman system was used to perform measurements under real-life conditions in the cooling room of an abattoir using pig's *semimembranosus* muscles ($N=96$), 60–120 min after exsanguination. The traits pH_{45} , pH_{24} , CIE $L^*a^*b^*$, drip loss, and shear force after 24 and 72 h were measured as reference and correlated with the Raman spectra using partial least squares regression. Strong correlations of the Raman spectra were obtained for pH_{45} ($R^2_{\text{cv}}=0.65$, $\text{RMSECV}=0.17$ pH units), pH_{24} ($R^2_{\text{cv}}=0.68$, $\text{RMSECV}=0.09$ pH units), L^* -value ($R^2_{\text{cv}}=0.64$, $\text{RMSECV}=1.9$), b^* -value ($R^2_{\text{cv}}=0.73$, $\text{RMSECV}=0.6$), drip loss ($R^2_{\text{cv}}=0.73$, $\text{RMSECV}=1.0$ %), and shear force after 72 h ($R^2_{\text{cv}}=0.7$, $\text{RMSECV}=4$ N). On the other hand, shear force after 24 h and a^* -value showed only weak correlations ($R^2_{\text{cv}}=0.22$, $\text{RMSECV}=7.8$ N and $R^2_{\text{cv}}=0.36$, $\text{RMSECV}=1.3$). The predictions can be traced back to differences in the early postmortem metabolic conditions as indicated by Raman signals of phosphocreatine, creatine, adenosine triphosphate, inosine monophosphate, glycogen, lactate, phosphorylated metabolites, and inorganic phosphate. This study demonstrates the potential of Raman spectroscopy for the early postmortem prediction of six pork quality traits which can be useful for the discrimination of meat qualities and sorting in the production chain.

Keywords pH · Drip loss · Color · Shear force · Noninvasive · In situ

R. Scheier · H. Schmidt (✉)
Research Centre of Food Quality, University Bayreuth,
E.-C.-Baumann Straße 20, 95326 Kulmbach, Germany
e-mail: heinar.schmidt@uni-bayreuth.de

A. Bauer
Department of Safety and Quality of Meat, Max Rubner Institute,
E.-C.-Baumann Straße 20, 95326 Kulmbach, Germany

Introduction

According to the United Nations' Food and Agriculture Organization, pork is the most widely eaten meat in the world accounting for over 36 % of the world meat intake in 2010 (FAO 2012). Therefore, pork meat quality is of high economical, social, and scientific interest that undergoes constant scrutiny.

Pork meat is often classified into quality groups such as reddish, firm, non-exudative (RFN); pale, soft, exudative (PSE); dark, firm, dry (DFD); pale, firm, non-exudative (PFN); and reddish, soft, exudative (RSE) (Kauffman et al. 1993; van Laack et al. 1994). The quality traits required for this classification are pH_{45} , pH_{24} , drip loss, and L^* -value (Bendall and Swatland 1988; Kauffman et al. 1993; van Laack et al. 1994; Joo et al. 1995; Warner et al. 1997; Adzitey and Nurul 2011; Petzet et al. 2013). Among these, the color (L^* -value) influences the consumer's purchasing decision more than any other quality factor (Mancini and Hunt 2005). On the other hand, tenderness is deemed the most important quality parameter in determining consumer acceptance (Damez and Clerjon 2008). However, tenderness is an inherent property which cannot be estimated visually and which is often replaced by shear force measurements as a physical method.

A wide range of methods was investigated regarding an (early postmortem) assessment of meat quality (Honikel and Fischer 1977; Toldrá and Flores 2000; Brondum et al. 2000; Hoving-Bolink et al. 2005; ElMasry et al. 2011; Kamruzzaman et al. 2012; Qiao et al. 2006). A rapid method for detection of PSE and DFD meat is based on the absorption ratio at 250 and 260 nm (Honikel and Fischer 1977). This ratio represents the concentration ratio of adenosine triphosphate (ATP) to inosine monophosphate (IMP) which is much higher in normal meat than in PSE or DFD meat. An additional pH measurement 1 h p.m. facilitated a separation of DFD and PSE. The preparation of the acidic muscle extract and the subsequent measurement of the absorbance ratio were reliable

for 97 % samples ($N=253$) (Honikel and Fischer 1977) but not suitable for the online detection of meat quality.

Using aminopeptidase and dipeptidylpeptidase activities, an early postmortem distinction between exudative (PSE and RSE) and non-exudative (RFN and DFD) meat was achieved (Toldrá and Flores 2000). The authors reported differences in enzyme activities among classes, mainly in exoproteases, which could be used as indicators or markers for postmortem quality in a broad time range. With a stepwise discriminant analysis, 2 h p.m. enzyme activity could explain 75 % of the variability of meat quality, while 24 h p.m. enzyme activity explained 71 %. The authors proposed to use the enzyme assays online. However, the sample preparation is complicated and time consuming.

For online applications, spectroscopic methods are more appropriate because they are fast and do not require sample preparation. For the prediction of drip loss of pork meat visible (VIS) and near infrared (NIR) reflectance, fluorescence and low-field ^1H nuclear magnetic resonance (NMR) spectroscopy were compared (Brondum et al. 2000). Best regression results were obtained with NMR spectra yielding $R^2=0.75$ ($N=39$) and standard error of prediction of 2 %. Also, good correlations ($R^2=0.72$, $RMSEP=2.1$ %) were reported for VIS spectra, but the prediction errors were still too high considering the expected total variance in drip loss from <1 to 10 %. Early postmortem NIRS spectra revealed no correlation with drip loss and only a low correlation with color (Hoving-Bolink et al. 2005). Similarly, when L^* -values were investigated for the prediction of water-holding capacity (WHC), low correlations were reported, and brightness was stated not to be a reliable predictor of WHC (van Laack et al. 1994). On the other hand, using hyperspectral NIR imaging (900–1,700 nm), drip loss could be predicted in three different muscles of beef ($N=27$) (ElMasry et al. 2011). Coefficient of determination in cross-validation $R^2_{cv}=0.89$ and standard error of cross-validation $RMSECV=0.26$ % revealed the potential of this technique. A continuative study of the same technique showed also good correlations for quality traits like pH ($R^2_{cv}=0.65$ and $RMSECV=0.09$), drip loss ($R^2_{cv}=0.77$ and $RMSECV=0.3$), and L^* -value ($R^2_{cv}=0.91$ and $RMSECV=1.3$) for lamb meat (Kamruzzaman et al. 2012). Slightly inferior results were achieved using the same technique to predict pH, drip loss, and color of pork meat (Qiao et al. 2006). However, in its current characteristics, hyperspectral imaging is difficult to be implemented in online industrial application due to time constraints in image acquisition and pre- and post-processing routines of the image (ElMasry et al. 2011).

As an emerging method, Raman spectroscopy has lately received increasing attention. For instance, the WHC of pork meat was predicted using Raman spectra (Pedersen et al. 2003), and the shear force (SF) was correlated with Raman spectra from lamb and beef (Beattie et al. 2004; Beattie et al. 2008; Schmidt et al. 2013). The early postmortem Raman

spectra of pork were shown to provide a metabolic fingerprint of meat revealing amongst others degradation of glycogen to lactate and ATP to IMP (Scheier et al. 2014). Under laboratory conditions, Raman spectroscopy showed its potential to non-invasively measure the pH with $R^2=0.94$ and $RMSECV=0.2$ pH units (Scheier and Schmidt 2013). Therefore, the aim of this work was to investigate the feasibility of Raman spectroscopy to measure and predict quality traits such as pH, color, drip loss, and shear force early postmortem in a field study in an abattoir.

Materials and Methods

Samples

Raman and reference measurements were performed as part of a larger study with the left topside (*m. semimembranosus*, SM) of 96 pigs representing a random sample of typical pig breeds slaughtered in Germany. Due to complete dismembering of 15 hams, only 81 SM samples were available for determination of drip loss and for shear force measurements after 24 h, and 64 samples for shear force after 72 h p.m.

Reference Measurements

The pH measurements were performed in duplicate with a puncture electrode (Portamess 913 X pH, Knick, Berlin) after 45 min in the abattoir and after 24 h in the laboratory. The CIE $L^*a^*b^*$ color was measured after 24 h p.m. with a Minolta CR400 (Konica Minolta, Japan). After a blooming period, the measurement was performed in triplicate on a freshly cut surface at different sites of the muscle. The mean values of L^* per SM were used for analysis. Drip loss was measured on a size-standardized sample of approximately 170 g between 24 and 72 h, while the sample was suspended and stored at 4 °C. The difference between initial and final weight was determined and expressed as percentage weight loss (Honikel 1998). Shear force values were determined for two aging times (24 and 72 h) on six cooked $1 \times 1 \text{ cm}^2$ subsamples (Shackelford et al. 1999) per sample and per aging time using a Warner–Bratzler system (Instron Series 5564, Instron Deutschland GmbH, Pfungstadt). For analysis, the mean values of the six subsamples per sample were used.

Raman Measurements

Raman measurements were conducted with the portable Raman system depicted in Fig. 1. This device was developed to measure Raman spectra under conditions found in abattoirs. To this end, the handheld Raman sensor head described by Schmidt et al. (2010) was connected by an optical fiber with a miniature spectrograph (HORIBA Jobin-Yvon, Longjumeau, France) with an optical resolution of 8 cm^{-1} and a

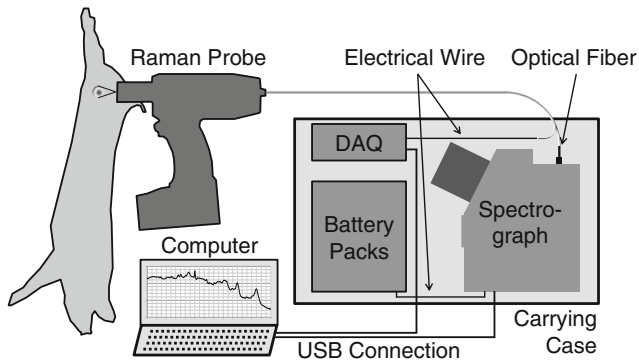


Fig. 1 Scheme of the portable Raman system in a carrying case, consisting of a handheld Raman sensor head connected to a spectrograph, a portable computer which is linked via a digital acquisition (DAQ) unit and rechargeable battery packs for mobility

thermoelectrical cooled CCD camera operating at $-10\text{ }^{\circ}\text{C}$. A laser driver (RGB Lasersysteme GmbH, Kelheim, Germany) is used to control the 671-nm micro system diode laser (Sumpf et al. 2009). The laser power can be adjusted in the range from 0 to 130 mW by varying the input voltage at the laser driver. This voltage is generated by a digital data acquisition unit (NI-USB 6008, National Instruments, Austin, TX, USA) connected via USB to a laptop computer. The system is controlled with a self-written LabVIEW program (National Instruments, Austin, TX, USA) which also captures and stores the Raman spectra. The program was adapted to ease work for (untrained) operators. For instance, measurements can be started by pushing the trigger button at the sensor head. Automated routines are implemented for the detection of fat and invalid measurements (see [Data Analysis](#)). For mobile usage, rechargeable battery packs with a capacity of 25 Ah were integrated. With this system, continuous Raman measurements can be conducted over 8 h. The system was successfully used in commercial abattoirs under conditions with high humidity, low temperature, and fluorescent light illumination.

Ten Raman spectra were recorded at the freshly cut meat surface of each SM in the cooling room between 60 and 120 min p.m. The laser power was set to 80 mW, and the integration time to 2.5 s. For further analysis, all meat spectra per sample were averaged. Occasionally, fat was detected. If this happened, additional spectra were recorded at different spots.

Data Analysis

After each measurement, the spectrum was automatically evaluated whether meat or fat was detected. The fat detection was based on a principle component analysis with meat and fat spectra providing a loading which was used to score the measured spectra. A high score value indicated high fat content at the measuring spot. Using a judiciously chosen threshold, the Raman spectra were classified either as meat or as fat (or fat with meat) and stored separately.

For further analysis, the meat spectra were limited to the wavenumber region from 500 to $1,800\text{ cm}^{-1}$. For better visibility of the Raman peaks, in [Fig. 3](#), Raman spectra were baseline corrected using MATLAB (The Mathworks Inc., Natick, MA, USA) with COBRA (Galloway et al. 2009).

Partial least square regression (PLSR) was performed with MATLAB 7.9.0 R2009b software (The Mathworks Inc., Natick, MA, USA) and PLS toolbox 6.2 (Eigenvector Research Inc., Wenatchee, WA, USA). Besides mean centering, no further preprocessing of the spectral data was applied. For cross-validation, the random blocks method with nine data splits and 20 iterations was applied. To this end, the order of the spectra was randomized, and the data set was split into nine commensurate subsets. Using eight subsets, a PLSR model was calculated. With the remaining subset, the model's predictive power was evaluated by calculating the root of the averaged, squared difference between measured and predicted reference values (RMSECV). This was repeated until every subset was used once. Subsequently, the randomization and cross-validation procedure was repeated 19 times. The resulting 20 R^2 and RMSECVs were each averaged.

To improve the predictive power of the PLSR models (i.e., minimize RMSECV), the number of spectral channels was iteratively reduced to exclude spectral regions carrying little or no spectral information for the prediction of the particular reference value (Osborne et al. 1997). To this end, variance importance in projection (VIP) plots and a threshold value of 1 were applied (Chong and Jun 2005). A PLSR model was calculated, and the number of latent variables was chosen to minimize the RMSECV. Then, the VIP plot was calculated, and the spectral channels with VIP scores lower than 1 were excluded from the data set. With the reduced data set, a new PLSR model was calculated. This was repeated until a global minimum of RMSECV was reached.

Results and Discussion

Reference Parameters

An overview of the reference parameters measured in addition to the Raman spectra is given in [Table 1](#). All traits exhibit a sufficient variance to establish correlations. At the same time, the errors of the reference methods are low compared to the variance of the trait as indicated by the SD which is essential for establishing prediction models. The error of the reference method for pH_{45} and pH_{24} was taken from a series of measurements described in Scheier and Schmidt (2013). The errors of the measurement of L^* , a^* , and b^* and shear force were calculated from the standard deviation within one

Table 1 Number of samples (*N*), mean value, minimum and maximum value, standard deviation (*SD*), and measurement error of the reference method (ref. error) for the investigated quality traits

	<i>N</i>	Mean	Min	Max	<i>SD</i>	Ref. error
pH ₄₅	96	6.29	5.41	6.8	0.29	0.06–0.14
pH ₂₄	96	5.53	5.28	6.13	0.15	0.01–0.05
L*	96	48.8	41.0	55.1	3.1	0.9
a*	96	9.1	5.9	14.2	1.6	0.4
b*	96	4.2	1.7	7.5	1.2	0.3
Drip loss/%	81	4.1	0.7	9.2	1.9	0.3–1.3 ^a
SF24/N	81	57.1	37.5	79.3	8.7	4.7
SF72/N	64	48.7	35.6	68.7	6.9	4.6

^a from Christensen (2003)

sample. The error of the drip loss measurement was taken between 0.3 and 1.3 % as reported by Christensen (2003).

The meat samples were classified according to drip loss, pH₄₅, pH₂₄, and L* using the flow chart published by Petzet et al. (2013). The sorting criteria are based on and adapted from literature values (Monin and Sellier 1985; Bendall and Swatland 1988; Kauffman et al. 1993; Joo et al. 1995; Warner et al. 1997) which are summarized in Table 2. The samples exhibited a broad distribution of qualities (see Fig. 2). About 52 % of the samples showed normal drip loss between 1 and 5 % (Fig. 2, light gray), about 39 % of the samples were exudative with drip loss over 5 % (white), and 9 % were found to be dry (drip loss below 2 %, marked dark gray in Fig. 2). The extreme samples PSE (*N*=6) and DFD (*N*=2) were scarce in the data set according to their low prevalence.

Table 2 Criteria for the meat quality classification in Fig. 2 based on drip loss, pH₂₄, pH₄₅, and L*-value

Quality	DL/%	pH ₂₄	pH ₄₅	L*
RFN	<5 ^{a, b}			<50 ^{a, c}
PFN	<5 ^b			>50 ^b
AM	<5 ^d	<5.4 ^{d, e}	>6.3 ^{d, e}	
PSE	>5 ^{a, b}		<5.8 ^f	
PSE-T	>5 ^e		>5.8 ^e	>50 ^e
RSE	>5 ^{a, b, c}		>5.8 ^a	<50 ^{a, c}
DFD	<2 ^c	>6.0 ^{a, c}		
DFD-T	<2 ^e	5.7–6.0 ^e		

^a Warner et al. (1997)

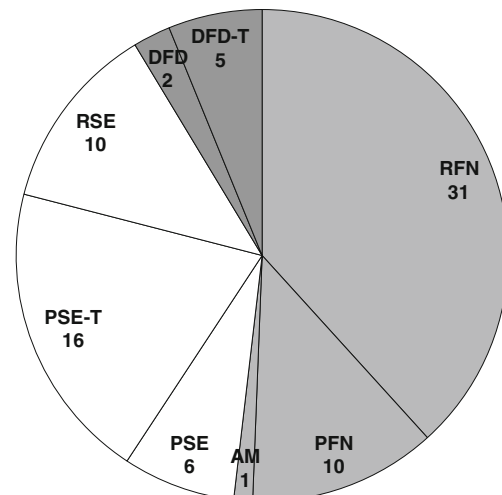
^b Kauffman et al. (1993)

^c Joo et al. (1995)

^d Monin and Sellier (1985)

^e Petzet et al. (2013)

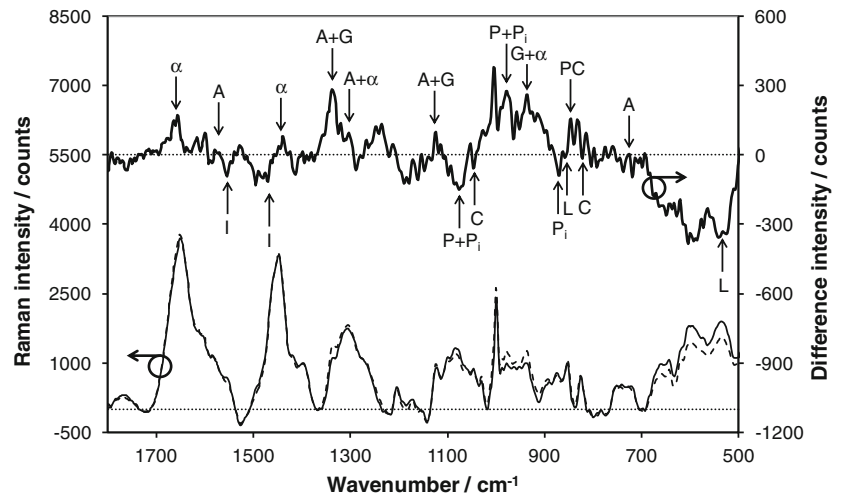
^f Bendall and Swatland (1988)

**Fig. 2** Meat quality distribution classified according to Petzet et al. (2013) for 81 of 96 hams (15 hams were completely dismembered). Normal samples (2 % < drip loss < 5 %) are marked light gray: reddish, firm, non-exudative (RFN); pale, firm, non-exudative (PFN); and acid meat (AM). Exudative samples (drip loss > 5 %) are marked white: pale, soft, exudative (PSE); PSE tendency (PSE-T); and reddish, soft, exudative (RSE). Dry samples (drip loss < 2 %) are marked dark gray: dark, firm, dry (DFD) and DFD tendency (DFD-T)

Raman Spectra of RFN and PSE Meat

To show differences in the Raman spectra between normal and PSE meat qualities, the difference spectrum RFN minus PSE was calculated. To this end, the preprocessed spectra of the 31 RFN and the six PSE samples (cf. Fig. 2) were averaged and subtracted. The difference spectrum is presented in Fig. 3. Positive signals indicate metabolites with higher concentrations in RFN than in PSE samples and vice versa. The different metabolic states of the two meat qualities are indicated by Raman peaks assigned to phosphocreatine (PC), creatine (C), glycogen (G), lactate (L), ATP (A), IMP (I), inorganic phosphate (P_i), phosphorylated metabolites (P), and α -helical proteins (α) (Scheier et al. 2014). For instance, the advanced metabolic state of PSE compared to RFN meat is reflected by negative creatine signals at 826 and 1,040 cm⁻¹ in the difference spectrum which indicates a faster decay of phosphocreatine in PSE meat. Creatine is produced from phosphocreatine for ATP regeneration. Its faster accumulation in PSE meat was shown by Henckel et al. (2001). At the same time, higher concentrations of PC in RFN meat are indicated by positive signals at 849 and 976 cm⁻¹ in Fig. 3. The latter is superimposed by further phosphorylated metabolites which add intensity to this peak. Similar observations can be made for the metabolic pairs glycogen/lactate with positive glycogen signals at 936, 1,124, and 1,337 cm⁻¹ and negative lactate signals at 535 and 855 cm⁻¹ and for the pair ATP/IMP with positive ATP signals at 732, 1,124, 1,305, 1,337, and 1,577 cm⁻¹ and negative IMP signals at 1,470 and 1,555 cm⁻¹. The accelerated metabolism in PSE meat leads

Fig. 3 Averaged spectra of six PSE samples (solid line), 31 RFN samples (dashed), and the difference spectrum RFN minus PSE (bold). Indicated by arrows: adenosine triphosphate (A), inosine monophosphate (I), glycogen (G), lactate (L), inorganic phosphate (P_i), phosphorylated metabolites (P), creatine (C), phosphocreatine (PC), and α-helical proteins (α). Circles with arrows indicate which scale applies to which curve



to a faster acidification which is reflected in the Raman difference spectrum by the pH-dependent signals of inorganic phosphate and the terminal phosphate moiety at 872, 976, and 1,077 cm⁻¹. The positive signal at 976 cm⁻¹ is assigned to the symmetric PO₃²⁻ stretching vibration which is stronger under less acidic conditions and which indicates the higher pH in RFN meat. On the other hand, the negative signals at 872 and 1,077 cm⁻¹ are increased under more acidic conditions in PSE meat. This is confirmed by the reference measurements which yielded pH₄₅=6.4 for RFN and 5.5 for PSE meat. Additionally, signals of α-helical proteins as indicated at 936, 1,305, 1,337, and 1,656 cm⁻¹ were more pronounced in RFN meat. These observations are in agreement with earlier findings in a laboratory study of the Raman and pH kinetics of excised SM muscles (Scheier et al. 2014).

Correlation with pH₄₅

The spectral differences found between RFN and PSE meat indicate difference in the metabolic states of both meat

qualities. Raman spectra have been previously shown to correlate with the pH value (Scheier and Schmidt 2013). As these results were obtained in laboratory experiments, it is interesting to evaluate to what extent the spectral information obtained in an abattoir can be used to predict the quality traits. The optimized PLSR model is presented in Fig. 4a illustrating the pH₄₅ predicted from the Raman spectra versus the pH₄₅ measured with a puncture electrode. The calibration data (black dots) represent a model comprising all samples. The model's ability to predict pH values, which are not contained in the training data set, is shown by the cross-validation where only predictions from Raman spectra are considered, which were not contained in the training data set of the PLSR model. The predictions calculated during cross-validation are represented by the gray circles in Fig. 4a. The results of the correlation models are summarized for all traits in Table 3. For the pH₄₅, the coefficients of determination are promising (R²=0.82 and R²_{cv}=0.65), and the model yields RMSEC=0.11 and RMSECV=0.17 pH units which comes close to the estimated error of the pH reference measurement

Fig. 4 a Predicted pH₄₅ (calibration=black dots, cross-validation=gray circles) from Raman spectra calculated from PLS regression model versus pH measurement with puncture electrode, RMSEC=0.11 (dashed line) and RMSECV=0.17 pH units (dotted line). **b** VIP plot calculated from PLS regression model, exclusion band with VIP score<1 (gray) and relevant Raman signals assigned with its respective wavenumbers

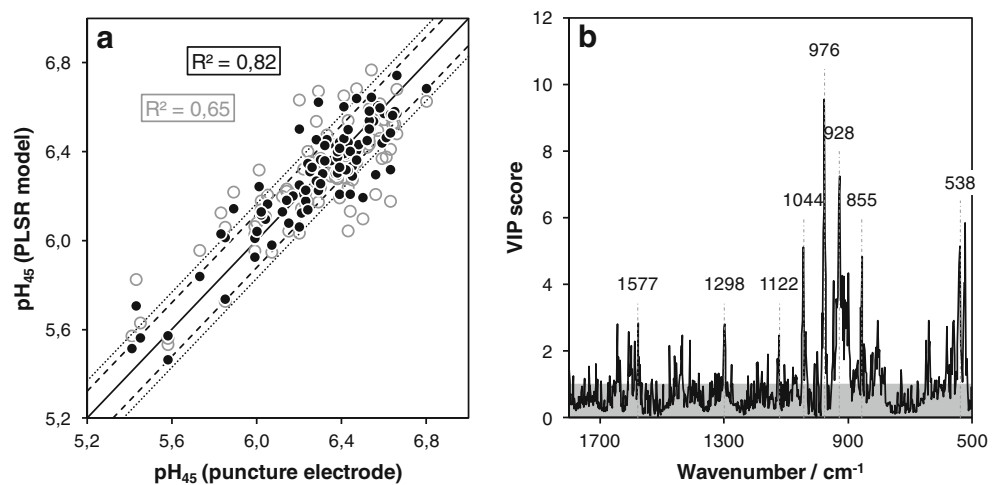


Table 3 Figures of merit for the PLS regression models of quality traits, root mean square error of calibration (RMSEC), root mean square error of cross-validation (RMSECV), and number of latent variables (LVs) and of spectral channels (NSC)

	R^2	RMSEC	R^2_{cv}	RMSECV	LVs	NSC
pH ₄₅	0.82	0.11	0.65	0.17	8	123
pH ₂₄	0.85	0.06	0.68	0.09	6	99
L*	0.95	0.7	0.64	1.9	9	261
a*	0.48	1.2	0.36	1.3	5	110
b*	0.90	0.4	0.73	0.6	9	104
Drip loss/%	0.90	0.6	0.73	1.0	7	87
SF24/N	0.37	6.9	0.22	7.8	5	99
SF72/N	0.95	1.4	0.70	4.0	10	95

of 0.06–0.14 pH units (see Table 1). The pH values were measured 45 min p.m. while the Raman measurements started between 60 and 120 min postmortem. Furthermore, the pH was measured inside the SM while the Raman spectra were obtained from the meat surface. Both effects are expected to slightly bias the predicted pH₄₅.

To highlight the Raman signals which provided relevant information for the prediction of pH₄₅, the VIP plot of the PLSR model is presented in Fig. 4b. The most important Raman signal at 976 cm⁻¹ is assigned to the basic form of the terminal phosphate moiety which acts as a pH indicator. Interestingly, the corresponding signal of the acidic form at 1,080 cm⁻¹ is not utilized by this PLSR model. This may be due to a superimposing signal from glycogen at 1,083 cm⁻¹ while the signal at 976 cm⁻¹ is relatively undisturbed by other Raman peaks. Secondly, a broad wavenumber region around the peak at 928 cm⁻¹ is weighted. Additional peaks at 1,300 and 1,455 cm⁻¹ point to α -helical protein signals (Pézolet et al. 1978; 1988). The peaks at 538 and 855 cm⁻¹ can be assigned to lactate. Furthermore, creatine and phosphocreatine signals are utilized with peaks at 1,044 cm⁻¹ and the peaks at

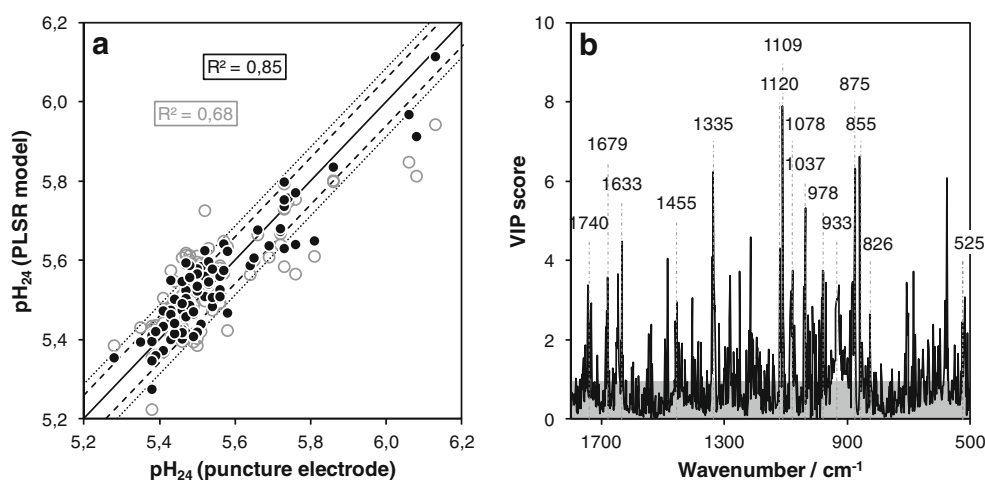
855 and 976 cm⁻¹. The signals at 1,122, 1,298, and 1,577 cm⁻¹ can be assigned to ATP. These assignments are in keeping with the difference spectra in early postmortem pork (Scheier et al. 2014).

Correlation with pH₂₄

While the correlation of the Raman spectra with pH₄₅ is largely based on a phosphate signal indicating the actual pH, it was interesting to evaluate whether the Raman measurements also can be utilized to predict the pH₂₄. The optimized PLSR model is depicted in Fig. 5a where predictions of the pH₂₄ based on calibration and cross-validation are plotted versus measurements of the pH₂₄ with a puncture electrode. The model yields $R^2=0.84$ and $R^2_{cv}=0.68$, and $RMSEC=0.06$ and $RMSECV=0.09$ pH units. This model performed better than the correlation with pH₄₅. This can be partly explained by the smaller variance of the ultimate pH value in pork meat of 0.01–0.05 pH units (Scheier and Schmidt 2013; Christensen 2003). However, only three samples were probed with pH₂₄> 6.0. The good predictability of pH₂₄ from Raman spectra obtained 1–2 h p.m. can be explained by the early postmortem energy metabolism of meat and its correlation with the ultimate pH. The low concentration of glycogen is limiting the final concentration of lactate and H⁺ ions and thereby the ultimate pH (Immonen and Puolanne 2000). Besides signals of glycogen, the Raman spectra contain signals of lactate, phosphocreatine, creatine, ATP, adenosine diphosphate (ADP), IMP, and inorganic phosphate (P_i) which provide further information about the metabolic conditions within the muscle cells and which indicate the ultimate pH of the muscle.

The VIP plot of the pH₂₄ model in Fig. 5b is different from the VIP plot for the correlation of pH₄₅ in Fig. 4b. Here, the prediction has to be based on metabolites but not on the peaks which indicate the actual pH. Accordingly, the strongest peak in this plot can be found at 1,109 cm⁻¹ which is assigned to

Fig. 5 **a** Predicted pH₂₄ from Raman spectra calculated from PLS regression model versus pH measurement with puncture electrode, $RMSEC=0.06$ and $RMSECV=0.09$ pH units. **b** VIP plot calculated from PLS regression model (presentation as in Fig. 4)



vibrations of ADP (Scheier et al. 2014; Rimai et al. 1969). The smaller peak at $1,120\text{ cm}^{-1}$ is assigned to the triphosphate ATP. Apparently, the PLSR model utilizes different concentrations of ADP and ATP to predict final pH values. In the literature, this is known for ATP in pork muscles where a difference of 3 mmol kg^{-1} of ATP was found between RFN and DFD (high pH_{24}) in the time frame from 30 to 120 min p.m. (Miri et al. 1992). Additionally, a 17-mmol kg^{-1} higher concentration of P_i in DFD and a four times higher concentration of phosphocreatine in RFN were reported in the same study. This is reflected in the VIP plot: Three distinct signals at 875 , 978 , and $1,078\text{ cm}^{-1}$ indicate the influence of the concentration of P_i , while signals at 826 , 855 , 978 , and $1,037\text{ cm}^{-1}$ indicate the conversion of phosphocreatine to creatine as shown by Scheier et al. (2014). As DFD meat has much lower content of glycogen than RFN meat (about 40 mmol kg^{-1} initial difference of glycogen content (Henckel et al. 2001)), signals from glycogen and lactate are used, notably at 855 , 933 , $1,037$, $1,078$, $1,120$, and $1,335\text{ cm}^{-1}$. Additional peaks at $1,455\text{ cm}^{-1}$ assigned to CH , CH_2 , and CH_3 deformation modes and in the Amid I region between $1,630$ and $1,690\text{ cm}^{-1}$ were also weighted in the VIP plot, as well as a broad band at $1,740\text{ cm}^{-1}$ which can be assigned to the $\text{C}=\text{O}$ stretching vibration of the carbonyl group (Lin-Vien et al. 1991). However, their assignment to metabolites or structural features is yet unknown.

Correlation with $L^*a^*b^*$ -Values

In Fig. 6, the PLS correlation of the Raman spectra and the L^* -values is presented. The prediction of L^* -values from the early postmortem Raman spectra was promising considering the reference error of the measurement of 0.9 using the Minolta

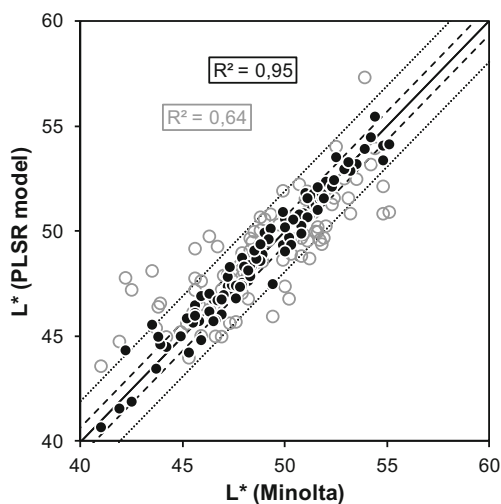


Fig. 6 Predicted L^* -value from Raman spectra calculated from PLS regression model versus L^* -value from reference measurements with Minolta CR400, $RMSEC=0.7$ and $RMSECV=1.9$ (presentation as in Fig. 4a)

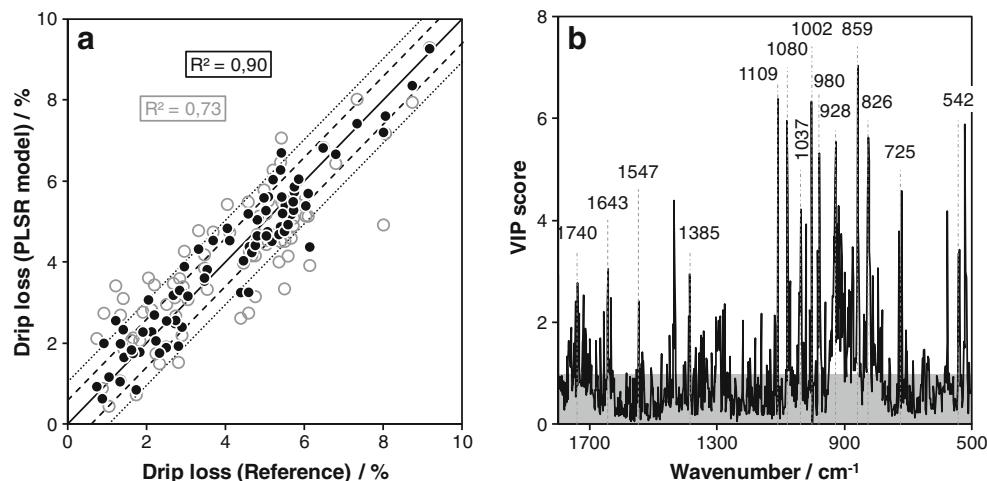
CR400. The model yielded the following figures of merit: $R^2=0.95$ and $R^2_{cv}=0.64$, and $RMSEC=0.7$ and $RMSECV=1.9$. The PLSR models for a^* and b^* performed very differently. The b^* -value was highly correlated with the early postmortem Raman spectra ($R^2=0.9$), while only a moderate correlation was found for the a^* -value ($R^2=0.46$). Meat color and L^* -value are mainly determined by the concentration of oxymyoglobin, deoxymyoglobin, and metmyoglobin (Mancini and Hunt 2005) of which oxymyoglobin and deoxymyoglobin were already shown to contribute to early postmortem pork spectra (Scheier et al. 2014). However, meat color after 45 min p.m. was reported to be not indicative for ultimate color in porcine SM and longissimus dorsi (LD) muscles (Duan et al. 2013). Thus, the $L^*a^*b^*$ -values have to be predicted indirectly from the Raman spectra. It is known that the early postmortem conditions such as rate of glycolysis, pH, and temperature play an important role in determining color (Feldhusen 1994; Joo et al. 1999). For instance, high temperature in combination with low pH_{45} in the muscle leads to denaturation of proteins which influences light scattering. Furthermore, Duan et al. (2013) found that a high pH_{45} was associated with a decreased L^* -values in LD and SM pork meat. As the present data show only a weak correlation between pH_{45} and L^* ($R=-0.27$), it is concluded that the correlation is not indirectly based on the pH information of the spectra. This is confirmed by the VIP plot of the L^* model (not shown), which weighs signals of glycogen and α -helical proteins, but not the indicative signals of phosphate. On the other hand, the pH_{24} does correlate with the L^* with a coefficient of $R=-0.6$. This is in keeping with the known relationship between ultimate pH and L^* -value (Brewer et al. 2006).

The model for a^* relies mainly on signals of α -helical proteins at 931 , $1,310$, $1,448$, and $1,649\text{ cm}^{-1}$ but also strongly weighs peaks at 999 and $1,038\text{ cm}^{-1}$, presumably attributed to phenylalanine and creatine/lactate, respectively. The VIP plot of the b^* model is a combination of the plot of L^* and a^* .

Correlation with Drip Loss

A clear and well-known relationship exists between early postmortem metabolism and drip loss (Warriss 1982; Schäfer et al. 2002; Huff-Lonergan and Lonergan 2005; Huff-Lonergan and Lonergan 2007). In general, perimortem stress leads to high drip loss while antemortem exhaustion of the glycogen reservoir leads to very low drip loss. In Fig. 7a, the PLSR prediction of the drip loss measured after 72 h is shown. The model yields the following results: $R^2=0.9$ and $R^2_{cv}=0.73$, $RMSEC=0.6\%$ and $RMSECV=1\%$, which are very accurate compared to the overall variation of drip loss from 0.7 to 9.2 % and the reference error of 0.3–1.3 % (Table 1). The results are comparable to an earlier study, where $R^2=0.79$ and $RMSECV=0.9\%$ were obtained using a Raman microscope with a 785-nm laser diode (Pedersen et al. 2003).

Fig. 7 **a** Predicted drip loss from Raman spectra calculated from PLS regression model versus drip loss from reference method, $RMSEC=0.6$ and $RMSECV=1.0\%$. **b** VIP plot calculated from PLS regression model (presentation as in Fig. 4)



The VIP plot in Fig. 7b indicates the influence of signals from lactate (542, 859, and 1037 cm^{-1}), glycogen (928 and 1385 cm^{-1}), ADP ($1,109\text{ cm}^{-1}$), adenine ($720\text{--}730\text{ cm}^{-1}$), creatine (826 and 1037 cm^{-1}), terminal phosphate groups (980 and $1,080\text{ cm}^{-1}$), and carbonyl groups ($1,740\text{ cm}^{-1}$) (Scheier et al. 2014). Hence, the PLSR prediction of drip loss is mostly based on components which indicate the energy metabolism of the muscle.

Correlation with Shear Force

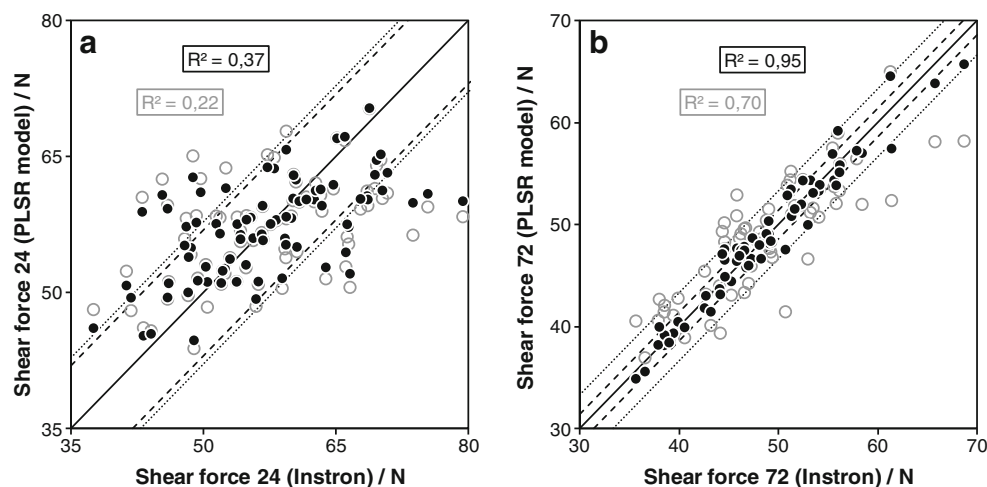
The rate of postmortem pH decline is also known to influence the rate of tenderization (Bee et al. 2007; Melody et al. 2004). Interestingly, the shear force values measured 24 and 72 h p.m. showed only a moderate correlation ($R^2=0.35$). Accordingly, the PLSR correlation of the Raman spectra and the shear force data performed very differently in our study (see Fig. 8): While only a weak relationship was found for SF 24 h p.m. with $R^2=0.37$ and $RMSECV=7.8\text{ N}$, a much better model could be calculated for SF 72 h p.m. with $R^2=0.95$ and $RMSECV=4.0\text{ N}$, which is comparable to the estimated reference error of

4.6 N. As shown above, the Raman spectra reflect the rate of early postmortem metabolism which influences proteolytic processes such as the splitting of connectin and titin filaments or the fragmentation of nebulin filaments (Huff-Lonergan et al. 2010; Takahashi 1996). Thus, it is reasonable to assume that this relationship is also the reason for the good prediction of SF 72 h postmortem. On the other hand, the shear force values 24 h p.m. are temporarily disturbed or superimposed by antagonistic effects and therefore cannot be predicted. This could be caused by the shortening of the sarcomers during rigor mortis (Tomberg 1996), or its duration may interfere with the measurement after 24 h p.m.

Conclusions

A portable Raman system was tested in a series of measurements with 96 pigs in the cooling room of an abattoir. PLS regression models were computed which yielded promising correlations ($0.6 < R^2_{cv} < 0.7$) for pH_{45} , pH_{24} , and L^* -value and even better correlations ($R^2_{cv} > 0.7$) for drip loss, b^* -value,

Fig. 8 Predicted shear force calculated from PLS regression model using Raman spectra versus drip loss from reference method measured **a** 24 h p.m. with $RMSEC=6.9$ and $RMSECV=7.8\text{ N}$ and **b** 72 h p.m. with $RMSEC=1.4$ and $RMSECV=4.0\text{ N}$ (presentation as in Fig. 4a)



and shear force 72 h p.m. Only weak correlations were found for the shear force 24 h p.m. ($R^2_{cv}=0.22$) and the a*-value ($R^2_{cv}=0.36$). As the data set comprised rather few PSE and DFD samples, future measurements should consider enlarging the sample size and pre-selecting PSE and DFD samples to account for their low prevalence. It was shown that the Raman spectra are an indicator for the state of the early postmortem metabolism of PSE and RFN meat. The metabolites glycogen/lactate, ATP/IMP, creatine/phosphocreatine, and the phosphate group were identified in the difference spectrum. The signals of these metabolites were amongst others used by the PLS regression models to predict the reference parameters. These quality traits are presently only available via five measurements requiring four different devices/methods, which are either invasive or time consuming or both. In this field study, we have shown the basic applicability of Raman spectroscopy to predict six important quality traits using a portable Raman system and spectra with only 2.5 s integration time (with ten repetitions) from early postmortem, in situ measurements performed under real-life conditions in an abattoir. The next steps will have to address the validation of these findings and to show the applicability directly at the slaughter line which is closer to the requirements of the production process.

Acknowledgments We want to thank Dr. Anja Petzet, Manfred Spindler, Sabine Wiedel, Anneliese Bittermann, and Sybille Nordhausen for their skilled help with reference measurements and Thomas Kador for his assistance with Raman measurements. The authors also thank the technicians of the workshop of the University of Bayreuth, especially Heinz Krejtschi for the realization of the portable Raman system. This work was financially supported by the German Research Foundation DFG (Deutsche Forschungsgemeinschaft) and the German Federation of Industrial Research Associations AiF (Arbeitsgemeinschaft industrieller Forschungsvereinigungen "Otto von Guericke" e.V.) in the framework of the cluster project "Minimal Processing" of the Research Association of the German Food Industry (FEI). The Research Centre of Food Quality is financed by the European Regional Development Fund (ERDF) which is gratefully acknowledged.

Disclaimers None

References

- Adzitey, F., & Nurul, H. (2011). PSE and DFD meats: causes and measured to reduce these incidences – a mini review. *International Food Research Journal*, *18*, 11–20.
- Beattie, J. R., Bell, S. J., Farmer, L. J., Moss, B. W., & Patterson, D. (2004). Preliminary investigation of the application of Raman spectroscopy to the prediction of the sensory quality of beef silverside. *Meat Science*, *66*(4), 903–913.
- Beattie, J. R., Bell, S. E., Borggaard, C., & Moss, B. W. (2008). Preliminary investigations on the effects of ageing and cooking on the Raman spectra of porcine longissimus dorsi. *Meat Science*, *80*(4), 1205–1211.
- Bee, G., Anderson, A. L., Lonergan, S. M., & Huff-Lonergan, E. (2007). Rate and extent of pH decline affect proteolysis of cytoskeletal proteins and water-holding capacity in pork. *Meat Science*, *76*, 359–365.
- Bendall, J., & Swatland, H. (1988). A review of the relationships of pH with physical aspects of pork quality. *Meat Science*, *24*, 85–126.
- Brewer, M. S., Novakofski, J., & Freise, K. (2006). Instrumental evaluation of pH effects on ability of pork chops to bloom. *Meat Science*, *72*(4), 596–602.
- Brondum, J., Munck, L., Henckel, P., Karlsson, A., Tornberg, E., & Engelsen, S. B. (2000). Prediction of water-holding capacity and composition of porcine meat by comparative spectroscopy. *Meat Science*, *55*(2), 177–185.
- Chong, I.-G., & Jun, C.-H. (2005). Performance of some variable selection methods when multicollinearity is present. *Chemometrics and Intelligent Laboratory Systems*, *78*, 103–112.
- Christensen, L. B. (2003). Drip loss sampling in porcine m. longissimus dorsi. *Meat Science*, *63*(4), 469–477.
- Damez, J.-L., & Clerjon, S. (2008). Meat quality assessment using biophysical methods related to meat structure. *Meat Science*, *80*(1), 132–149.
- Duan, Y., Huang, L., Xie, J., Yang, K., Yuan, F., Bruce, H. L., et al. (2013). Effect of temperature and pH on postmortem color development of porcine M. longissimus dorsi and M. semimembranosus. *Journal of the Sciences of Food and Agriculture*, *93*(5), 1206–1210.
- ElMasry, G., Sun, D.-W., & Allen, P. (2011). Non-destructive determination of water-holding capacity in fresh beef by using NIR hyperspectral imaging. *Food Research International*, *44*(9), 2624–2633.
- FAO (2012) Sources of meat. Rome, Italy. Available at: http://www.fao.org/ag/againfo/themes/en/meat/backgr_sources.html. Accessed 9 August 2013.
- Feldhusen, F. (1994). Einflüsse auf die postmortale Farbveränderung der Oberfläche von Schweinemuskulatur. *Fleischwirtschaft*, *74*(9), 989–991.
- Galloway, C. M., Le Ru, E. C., & Etchegoin, P. G. (2009). An iterative algorithm for background removal in spectroscopy by wavelet transforms. *Applied Spectroscopy*, *63*(12), 1370–1376.
- Henckel, P., Karlsson, A., Jensen, M. T., Oksbjerg, N., & Petersen, J. S. (2001). Metabolic conditions in porcine longissimus muscle immediately pre-slaughter and its influence on peri- and post mortem energy metabolism. *Meat Science*, *62*(2), 145–155.
- Honikel, K. O. (1998). Reference methods for the assessment of physical characteristics of meat. *Meat Science*, *49*(4), 447–457.
- Honikel, K. O., & Fischer, C. (1977). A rapid method for the detection of PSE and DFD porcine muscles. *Journal of Food Science*, *42*(6), 1633–1636.
- Hoving-Bolink, A. H., Vedder, H. W., Merks, J. W. M., de Klein, W. J. H., Reimert, H. G. M., Frankhuizen, R., et al. (2005). Perspective of NIRS measurements early post mortem for prediction of pork quality. *Meat Science*, *69*(3), 417–423.
- Huff-Lonergan, E., & Lonergan, S. M. (2005). Mechanisms of water-holding capacity of meat: the role of postmortem biochemical and structural changes. *Meat Science*, *71*, 194–204.
- Huff-Lonergan, E., & Lonergan, S. M. (2007). New frontiers in understanding drip loss in pork: recent insights on the role of postmortem muscle biochemistry. *Journal of Animal Breeding and Genetics*, *124*(S1), 19–26.
- Huff-Lonergan, E., Zhang, W., & Lonergan, S. M. (2010). Biochemistry of postmortem muscle: lessons on mechanisms of meat tenderization. *Meat Science*, *86*(1), 184–195.
- Immonen, K., & Puolanne, E. (2000). Variation of residual glycogen-glucose concentration at ultimate pH values below 5.75. *Meat Science*, *55*(3), 279–283.
- Joo, S. T., Kauffman, R., Kim, B. C., & Kim, C. J. (1995). The relationship between color and water-holding capacity in postrigor porcine longissimus muscle. *Journal of Muscle Foods*, *6*, 211–226.
- Joo, S. T., Kauffmann, R. G., Kim, B. C., & Park, G. B. (1999). The relationship of sarcoplasmic and myofibrillar protein solubility to

- colour and water-holding capacity in porcine longissimus muscle. *Meat Science*, 52, 291–297.
- Kamruzzaman, M., ElMasry, G., Sun, D.-W., & Allen, P. (2012). Prediction of some quality attributes of lamb meat using near-infrared hyperspectral imaging and multivariate analysis. *Analytica Chimica Acta*, 714, 57–67.
- Kauffman, R., Sybesma, W., Smulders, F., Eikelenboom, G., Engel, B., van Laack, R., et al. (1993). The effectiveness of examining early post-mortem musculature to predict ultimate pork quality. *Meat Science*, 34(3), 283–300.
- Lin-Vien, D., Colthup, N. B., Fateley, W. G., & Grasselli, J. G. (1991). *The handbook of infrared and Raman characteristic frequencies of organic molecules*. Boston: Academic.
- Mancini, R. A., & Hunt, M. C. (2005). Current research in meat color. *Meat Science*, 71(1), 100–121.
- Melody, J. L., Lonergan, S. M., Rowe, L. J., Huiatt, T. W., Mayes, M. S., & Huff-Lonergan, E. (2004). Early postmortem biochemical factors influence tenderness and water-holding capacity of three porcine muscles. *Journal of Animal Science*, 82, 1195–1205.
- Miri, A., Talmant, A., Renou, J. P., & Monin, G. (1992). ³¹P NMR study of post mortem changes in pig muscle. *Meat Science*, 31(2), 165–173.
- Monin, G., & Sellier, P. (1985). Pork of low technological quality with a normal rate of muscle pH fall in the immediate post-mortem period: the case of the Hampshire breed. *Meat Science*, 13, 49–63.
- Osborne, S., Jordan, R., & Kunнемeyer, R. (1997). Methods of wavelength selection for partial least squares. *Analyst*, 122, 1531–1537.
- Pedersen, D. K., Morel, S., Andersen, H. J., & Engelsen, S. B. (2003). Early prediction of water-holding capacity in meat by multivariate vibrational spectroscopy. *Meat Science*, 65, 581–592.
- Petzet, A., Scheier, R., Octoviani, A., Bauer, A., Hammon, A., Diepolder, H., et al. (2013). Entwicklung von Analysemethoden zur Etablierung einer online-fähigen Beurteilung der Fleischqualität. *Fleischwirtschaft*, 93(5), 84–87.
- Pézolet, M., Pigeon-Gosselin, M., & Caillé, J.-P. (1978). Laser Raman investigations of intact single muscle fibers. Protein conformations. *Biochimica et Biophysica Acta*, 533, 263–269.
- Pézolet, M., Pigeon, M., Ménard, D., & Caillé, J.-P. (1988). Raman spectroscopy of cytoplasmic muscle fiber proteins. Orientational order. *Biophysical Journal*, 53(3), 319–325.
- Qiao, J., Wang, N., Ngadi, M. O., Gunenc, A., Monroy, M., Gariépy, C., et al. (2006). Prediction of drip-loss, pH, and color for pork using a hyperspectral imaging technique. *Meat Science*, 76(1), 1–8.
- Rimai, L., Cole, T., Parsons, J. L., Hickmott, J. T., Jr., & Carew, E. B. (1969). Studies of Raman spectra of water solutions of adenosine Tri-, Di-, and monophosphate and some related compounds. *Biophysical Journal*, 9(3), 320–329.
- Schäfer, A., Rosenvold, K., Purslow, P. P., Andersen, H. J., & Henckel, P. (2002). Physiological and structural events post mortem of importance for drip loss in pork. *Meat Science*, 61, 355–366.
- Scheier, R., & Schmidt, H. (2013). Measurement of the pH value in pork meat early postmortem by Raman spectroscopy. *Applied Physics B*, 111, 289–297.
- Scheier, R., Köhler, J., & Schmidt, H. (2014). Identification of the early postmortem metabolic state of porcine M. semimembranosus using Raman spectroscopy. *Vibrational Spectroscopy* 70, 12–17.
- Schmidt, H., Sowoidnich, K., & Kronfeldt, H.-D. (2010). A prototype hand-held Raman sensor for the in situ detection of meat quality. *Applied Spectroscopy*, 64(8), 888–894.
- Schmidt, H., Scheier, R., & Hopkins, D. (2013). Preliminary investigation on the relationship of Raman spectra of sheep meat with shear force and cooking loss. *Meat Science*, 93(1), 138–143.
- Shackelford, S. D., Wheeler, T. L., & Koohmaraie, M. (1999). Tenderness classification of beef: Design and analysis of a system to measure beef longissimus shear force commercial processing conditions. *Journal of Animal Science*, 77, 1474–1481.
- Sumpf, B., Schmidt, H., Maiwald, M., Müller, A., Erbert, G., Kronfeldt, H.-D. & Tränkle, G. (2009). Microsystem technology based diode lasers and Raman sensors for in situ food quality control. In: SPIE Proceedings Vol. 7315, Sensing for Agriculture and Food Quality and Safety, 7-12 February 2009, Lake Buena Vista, Florida, USA.
- Takahashi, K. (1996). Structural weakening of skeletal muscle tissue during post-mortem ageing of meat: the non-enzymatic mechanism of meat tenderization. *Meat Science*, 43(S1), 67–80.
- Toldrá, F., & Flores, M. (2000). The use of muscle enzymes as predictors of pork meat quality. *Food Chemistry*, 69, 387–395.
- Tornberg, E. (1996). Biophysical aspects of meat tenderness. *Meat Science*, 43(S1), 175–191.
- van Laack, R., Kauffman, R., Sybesma, W., Smulders, F., Eikelenboom, G., & Pinheiro, J. (1994). Is colour brightness (L-value) a reliable indicator of water-holding capacity in porcine muscle. *Meat Science*, 38(2), 193–201.
- Warner, R., Kauffman, R., & Greaser, M. (1997). Muscle protein changes post mortem in relation to pork quality traits. *Meat Science*, 45, 339–352.
- Warriss, P. D. (1982). The relationship between pH45 and drip in pig muscle. *Journal of Food Technology*, 17, 573–578.